NASA/TM—2006-214226

# On the Mixing of Single and Opposed Rows of Jets With a Confined Crossflow

*James D. Holdeman*
*Glenn Research Center, Cleveland, Ohio*

*James R. Clisset*
*University of Florida, Gainesville, Florida*

*Jeffrey P. Moder*
*Glenn Research Center, Cleveland, Ohio*

*William E. Lear*
*University of Florida, Gainesville, Florida*

October 2006

# NASA STI Program . . . in Profile

Since its founding, NASA has been dedicated to the advancement of aeronautics and space science. The NASA Scientific and Technical Information (STI) program plays a key part in helping NASA maintain this important role.

The NASA STI Program operates under the auspices of the Agency Chief Information Officer. It collects, organizes, provides for archiving, and disseminates NASA's STI. The NASA STI program provides access to the NASA Aeronautics and Space Database and its public interface, the NASA Technical Reports Server, thus providing one of the largest collections of aeronautical and space science STI in the world. Results are published in both non-NASA channels and by NASA in the NASA STI Report Series, which includes the following report types:

- TECHNICAL PUBLICATION. Reports of completed research or a major significant phase of research that present the results of NASA programs and include extensive data or theoretical analysis. Includes compilations of significant scientific and technical data and information deemed to be of continuing reference value. NASA counterpart of peer-reviewed formal professional papers but has less stringent limitations on manuscript length and extent of graphic presentations.

- TECHNICAL MEMORANDUM. Scientific and technical findings that are preliminary or of specialized interest, e.g., quick release reports, working papers, and bibliographies that contain minimal annotation. Does not contain extensive analysis.

- CONTRACTOR REPORT. Scientific and technical findings by NASA-sponsored contractors and grantees.

- CONFERENCE PUBLICATION. Collected papers from scientific and technical conferences, symposia, seminars, or other meetings sponsored or cosponsored by NASA.

- SPECIAL PUBLICATION. Scientific, technical, or historical information from NASA programs, projects, and missions, often concerned with subjects having substantial public interest.

- TECHNICAL TRANSLATION. English-language translations of foreign scientific and technical material pertinent to NASA's mission.

Specialized services also include creating custom thesauri, building customized databases, organizing and publishing research results.

For more information about the NASA STI program, see the following:

- Access the NASA STI program home page at *http://www.sti.nasa.gov*

- E-mail your question via the Internet to *help@sti.nasa.gov*

- Fax your question to the NASA STI Help Desk at 301–621–0134

- Telephone the NASA STI Help Desk at 301–621–0390

- Write to:
  NASA STI Help Desk
  NASA Center for AeroSpace Information
  7121 Standard Drive
  Hanover, MD 21076–1320

NASA/TM—2006-214226

# On the Mixing of Single and Opposed Rows of Jets With a Confined Crossflow

*James D. Holdeman*
*Glenn Research Center, Cleveland, Ohio*

*James R. Clisset*
*University of Florida, Gainesville, Florida*

*Jeffrey P. Moder*
*Glenn Research Center, Cleveland, Ohio*

*William E. Lear*
*University of Florida, Gainesville, Florida*

National Aeronautics and
Space Administration

Glenn Research Center
Cleveland, Ohio 44135

October 2006

This work was sponsored by the Fundamental Aeronautics Program at the NASA Glenn Research Center.

*Level of Review*: This material has been technically reviewed by technical management.

Available from

NASA Center for Aerospace Information
7121 Standard Drive
Hanover, MD 21076–1320

National Technical Information Service
5285 Port Royal Road
Springfield, VA 22161

Available electronically at http://gltrs.grc.nasa.gov

# On the Mixing of Single and Opposed Rows of Jets With a Confined Crossflow

James D. Holdeman
National Aeronautics and Space Administration
Glenn Research Center
Cleveland, Ohio 44135

James R. Clisset
University of Florida
Gainesville, Florida 32611

Jeffrey P. Moder
National Aeronautics and Space Administration
Glenn Research Center
Cleveland, Ohio 44135

William E. Lear
University of Florida
Gainesville, Florida 32611

## Abstract

The primary objectives of this study were (1) to demonstrate that contour plots could be made using the data interface in the NASA Glenn jet-in-crossflow (JIC) spreadsheet, and (2) to investigate the suitability of using superposition for the case of opposed rows of jets with their centerlines in-line. The current report is similar to NASA/TM—2005-213137 but the "basic" effects of a confined JIC that are shown in profile plots there are shown as contour plots in this report, and profile plots for opposed rows of aligned jets are presented here using both symmetry and superposition models. Several important sections in NASA/TM—2005-213137 are not repeated in this report including (a) a listing of the correlation equations in the NASA empirical model, (b) a discussion of spreadsheet specifics (a.k.a., a user's manual), (c) several cases of confined JIC's that are typical of combustors for gas turbine engines, and (d) a suggested combustor design procedure. Although superposition was found to be suitable for most cases of opposed rows of jets with jet centerlines in-line, the calculation procedure in the JIC spreadsheet was not changed and it still uses the symmetry method for this case, as did all previous publications of the NASA empirical model. The Microsoft Excel (Microsoft Corporation) spreadsheet is included on the CD-ROM as a separate document and can also be accessed on the NASA Glenn Technical Reports Server at http://gltrs.grc.nasa.gov as TM-2006-214226-SUPPL.xls. This spreadsheet supercedes the one previously posted in NASA/TM—2005-213137.

## Nomenclature

| | |
|---|---|
| $A_J/A_M$ | jet-to-mainstream area ratio = $(\pi/4)/((S/H)(H/d)^2) = (\pi/4)/((S/d)(H/d))$ |
| $C$ | $(S/H)(\sqrt{(J)})$; same as equation (5) |

| | |
|---|---|
| $C_d$ | orifice discharge coefficient = (effective area)/(physical area) |
| $d$ | diameter of a round hole, or diameter of an equivalent-area round hole if a non-circular orifice is specified |
| $d_j$ | effective diameter = $(d)(\sqrt{(C_d)})$ |
| $DR$ | jet-to-mainstream density ratio, $\rho_J/\rho_M$ (for an incompressible flow, and for gases of the same chemical composition, this ratio is approximately equal to the mainstream-to-jet temperature ratio, $T_M/T_J$) |
| $H$ | duct height at center of row of holes (called $H_0$ in several previous publications) |
| $H/d$ | ratio of duct height to orifice diameter |
| $H_{eq}$ | effective duct height (= $H$ except in the symmetry model for opposed rows of inline jets); see equation (3) |
| $J$ | jet-to-mainstream momentum-flux ratio, $(\rho_J V_J^2)/(\rho_M U_M^2)$ $= (DR)(R)^2 = (MR)^2/DR/(C_d)^2/(A_J/A_M)^2$ |
| $m_J$ | jet mass flow |
| $m_M$ | mainstream mass flow |
| $m_T$ | total mass flow, $m_J + m_M$ |
| $m_J/m_M$ | jet-to-mainstream mass-flow ratio, $MR$ $= (\rho_J/\rho_M)(V_J/U_M)(C_d)(A_J/A_M)) = (m_J/m_T)/(1 - m_J/m_T)$ |
| $m_J/m_T$ | jet-to-total mass-flow ratio = $MR/(1 + MR)$ |
| $M$ | jet-to-mainstream mass-flux ratio, $(\rho_J V_J)/(\rho_M U_M)$; see reference 1. $= (DR)(R) = \sqrt{J * DR}$ ) |
| $MR$ | jet-to-mainstream mass-flow ratio, $m_J/m_M$ $= (M)(C_d)(A_J/A_M)$ |
| $R$ | jet-to-mainstream velocity ratio, $V_J/U_M$; see reference 1. $= \sqrt{J/DR}$ |
| S | lateral spacing between equivalent locations of adjacent orifices (e.g., between orifice centerplanes) |
| $S/d$ | ratio of orifice spacing to orifice diameter $= (S/H)(H/d)$ |
| $S/H$ | ratio of orifice spacing to duct height |
| $T$ | local scalar variable |
| $T_J$ | jet exit scalar variable |
| $T_M$ | unmixed mainstream scalar variable |
| $U$ | axial velocity |
| $U_M$ | unmixed mainstream velocity |
| $V_J$ | jet exit velocity |
| $W_{1/2}^-$ | jet half-value width on injection side of vertical distribution; i.e., for $y/H < y_c/H$, see figure 2 (note that $y = 0$ is at the top wall) |
| $W_{1/2}^+$ | jet half-value width on opposite side of vertical distribution; i.e., for $y/H > y_c/H$ , see figure 2 (note that $y = 0$ is at the top wall) |
| $x$ | downstream coordinate; $x = 0$ at center of the first row of orifices |
| $y$ | cross-stream coordinate; $y = 0$ at wall |
| $y_c$ | scalar trajectory, location of maximum scalar difference ratio, $\theta_c$ |
| $z$ | lateral coordinate; $z = 0$ at centerplane |

| | |
|---|---|
| $\theta$ | dimensionless scalar, $(T_M - T)/(T_M - T_J)$; same as equation (2) |
| $\theta_c$ | maximum scalar difference ratio, defines location of scalar trajectory, $y_c/H$ |
| $\theta_{EB}$ | equilibrium θ (called TB in ref. 16) ~ $m_J/m_T = MR/(1 + MR)$ |
| $\theta^-_{min}$ | minimum scalar difference ratio on injection side of vertical distribution; (i.e., for $y/H<y_c/H$) in figure 2 |
| $\theta^+_{min}$ | minimum scalar difference ratio on opposite side of vertical distribution; (i.e., for $y/H>y_c/H$) in figure 2 |

## Introduction

Jets in crossflow (JIC) have been extensively investigated in the literature. The large amount of previous research has provided a fairly complete description of the JIC. References to many of the studies in this field that were published prior to the summaries in references 1 to 5 can be found in their citations

The studies of multiple jets that are summarized in reference 1 were motivated by mixing of dilution jets in conventional gas turbine combustors; and the studies summarized in references 2 and 3 focused on optimizing the mixing section in the Rich burn/Quick mix/Lean burn (RQL) combustor scheme proposed for low emissions combustors for gas turbine engines. Electronic copies of most of the JIC reports and related papers that were done or funded by NASA Glenn and that were published after 1970 are posted for public availability on http://gltrs.grc.nasa.gov.

Many of the studies summarized in reference 4 were motivated by aerodynamics associated with vertical/short takeoff and landing (V/STOL) aircraft. The summary in reference 5 focused on the calculation methods that have been used previously for JIC flow fields, and the results thereof.

Although previous JIC studies have yielded insight into typical flow field characteristics, results from them may not satisfy the specific needs of diverse applications. The information obtained in any investigation is dependent on the needs of the motivating application, and this may determine such important flow field parameters as the region of interest, specifics of the orifice configuration and confinement, and the jet-to-mainstream momentum-flux and mass-flow ratios.

Most JIC research prior to 1970 focused on unconfined single jets and empirical measures of the jet trajectory, centerline decay, and shape. Although the single jet is an important component in gas turbine combustors, flows in combustion chambers are confined and interaction between jets is critical to their performance.

In the combustor dilution zone, for which the results in references 6 to 30 were from tests of, or are based on, simplified combustor mixer geometries, rapid mixing of the diluent air with the primary air stream is desired to provide a suitable temperature pattern at the turbine inlet, quench any continuing chemical reactions, and reduce combustor length.

This application was the motivation for the original development of empirical JIC models for confined flows. The experimental results from reference 7 were excerpted in references 8 and 9. From the data in reference 7, empirical models were published in references 11, 12, 14, and 16 for predicting “basic” features of the scalar field downstream of a single row of jets mixing with a confined crossflow in a rectangular duct. A journal publication is given in reference 14 showing results from the studies reported in references 7 and 11 which were funded by NASA at the Aerojet Liquid Rocket Company.

The NASA empirical model was subsequently extended to include variations typically found in gas turbine combustors; for example, double and/or opposed rows of jets with or without flow area convergence and/or a non-uniform mainstream scalar distribution. The experimental and empirical modeling results for this work are given in references 15 and 18 to 20 and the empirical model that resulted was used in reference 21 to demonstrate flow and geometric effects. CFD calculations for many of the cases in reference 14 are given in chapter 9 of reference 22. Experimental data and empirical and numerical model results are given in references 1, 23, and 24.

The mainstream duct in references 11, 12, 14, 16, and 21 has a rectangular cross section and is straight. It is neither annular or a can, nor does it curve in the flow direction as in reverse-flow combustors. By invoking assumptions, results from rectangular ducts can be applied to flow in annular and cylindrical ducts; see references 1 and 25. CFD calculations of the effects of curvature and convergence are given in references 26 and 27, and those with the extended empirical model are given in references 28 and 29. Journal publications from the work at the Garrett Turbine Engine Company (now Honeywell Engines) are given in references 1, 17, and 23 to 25.

Note that most parameters are defined the same in the current report as they were in the original studies. However, the definition and names of some parameters have changed (e.g., the momentum-flux ratio was incorrectly called the momentum ratio in early publications, and the definition of L&W for non-circular orifices is different in this report, reference 30, and most of the reports in the 1990s than it was previously) so the reader should be aware that definitions may not be the same.

The spreadsheet included with this report, and the one published with reference 30, are functionally equivalent to the BASIC program used in reference 21. The NASA JIC empirical model assumes the flows of interest will be confined and cannot be used for unconfined jet flows because the relations used therein for orifice size and spacing do not extrapolate properly as jet spacing and/or the distance to the opposite wall become large (e.g., the single unconfined JIC).

Several of the techniques suggested for modifying steady confined JICs do an excellent job of *decreasing* jet penetration, but combustor designers are usually looking for something that will *increase* penetration. So far nothing has been identified for a steady JIC that penetrates significantly farther or faster than a single, round, unbounded jet. Thus, this should be considered as the upper limit for the penetration of an array of confined JICs.

Also, the correlations in most empirical models are a “set,” so extracting individual equations and using them “out of context” is tenuous. Although empirical models had been available for several years prior to publication of reference 16, the utility of using them to provide a view of the expected mean flow field wasn’t really apparent until they were used to demonstrate expected flow and geometric effects.

The purpose of the spreadsheet is to provide an engineering tool to reduce development time and cost by allowing the researcher to quickly investigate the effects of varying flow and/or geometric parameters. There are discussions of spreadsheet specifics, several additional cases of jet mixing in a confined crossflow, a suggested design procedure, and a listing of the correlation equations in the NASA empirical model that are in reference 30 but are not repeated in this report. Thus, it is necessary to peruse the technical report that was published previously.

The spreadsheet does not output contour plots directly, but it does include an interface that can be used for that purpose. An objective of this study was to demonstrate this feature. The contour plots that are shown in figures 4 to 14 in this report were plotted with Tecplot (ref. 31)

from data calculated with the spreadsheet, and are for the cases shown in the profile plots in figures 4 to 14 in reference 30.

Another objective of this work was to investigate the appropriateness of using superposition for opposed rows of jets with their centerlines aligned (see sections on the symmetry and superposition models in the next section of this report) as using superposition would avoid the necessity of changing methods for this case. The calculation procedure in the JIC spreadsheet was not changed, and it uses symmetry as the default method for this case, as did all previous publications of the NASA empirical model. Although the changes and corrections that were made to the spreadsheet affect only the cases with non-circular orifices and cases of opposed rows of jets with their centerlines in-line, it is suggested that the spreadsheet that is on the current CD-ROM and posted with this report at http://gltrs.grc.nasa.gov/reports/2006/TM-2006-214226/TM-2006-214226-SUPPL1.xls should be used in lieu of the one previously posted with NASA/TM—2005-213137 (TM-2005-213137-SUPPL1.xls).

## Flow Field Model

Figure 1 is a schematic of the basic flow field for jets in a confined crossflow from which the empirical models were generated. The jets are shown entering the mainstream flow through orifices in the top duct wall. The primary independent geometric variables are the lateral spacing between similar locations of adjacent orifices $S$, the duct height $H$, and the orifice size $d$. These are often expressed in dimensionless form as the ratio of the orifice spacing to orifice diameter $S/d$ and the ratio of the duct height to orifice diameter $H/d$.

The ratio of these, $S/H$, was found to be a very important variable for confined JICs, and the orifice size (inversely proportional to $H/d$) is also an important variable. Thus $S/H$ and $H/d$ were chosen as independent variables, and $S/d$ (=($S/H$)($H/d$)) is calculated

Downstream distances are specified in this report, and in reference 30 and previous publications, in terms of $x/H$. The use of $x/H$ is appropriate for combustor design because the objective in this application is usually to identify orifice configurations to optimize the mixing within a given length and the downstream locations of interest are usually independent of the orifice diameter.

In the spreadsheet input for the downstream distance $x/H$ and jet spacing $S/H$ are only allowed for jets in the top front row. The user must be aware that $x/H$ and $S/H$ for other rows are dependent on, but may not be identical to, the values input in the top front row.

The ratio of the downstream distance to the orifice diameter $x/d$ is a common dimensionless parameter, particularly in unconfined or semiconfined flows where $H/d$ is large. Fortunately calculation of $x/d$ for confined flow is straight-forward, since $x/d = (x/H)(H/d)$.

A major assumption in the empirical model for the scalar field downstream of jets mixing with a confined crossflow is based on the observation that all non-dimensional vertical scalar distributions in the flow field can usually be expressed in the following form:

$$\frac{\theta-\theta_{\min}^{\pm}}{\theta_c-\theta_{\min}^{\pm}}=\exp\frac{(-\ln 2)(y/H-y_c/H)^2}{\left(W_{1/2}^{\pm}/H\right)^2} \tag{1}$$

where $$\theta = \frac{(T_M - T)}{(T_M - T_J)} \quad (2)$$

Note, $W_{1/2}^{\pm}/H$ is the half-value width on the injection or opposite side of the trajectory as appropriate. Also usually:

$$W_{1/2}^{+}/H \neq W_{1/2}^{-}/H \text{ and } \theta_{min}^{+} \neq \theta_{min}^{-}$$

Equation (1) was first applied to confined JIC data in references 11 and 12. It gives $\theta = (\theta_c + \theta_{min}^{\pm})/2$ at $|y/H - y_c/H| = W_{1/2}^{\pm}/H$, but does not guarantee that $\theta = \theta_{min}^{\pm}$ at $y = 0$ or $H$. With the Gaussian form, $\theta_{min}^{\pm}$ are the asymptotic values—the calculated θ at 0 and $H$ will deviate farther from $\theta_{min}^{\pm}$ as $y_c$ is closer to 0 or $H$. The calculation should definitely not be accepted if $y_c > H$, and probably should not be accepted if $y_c < W_{1/2}^{-}$ or $y_c > H - W_{1/2}^{+}$. An equation similar to equation (1) was applied to data for a single, unconfined JIC ($\theta_{min}^{\pm} = 0$) in references 32 to 34.

As shown in figure 2, $\theta_c$, $\theta_{min}^{+}$, $\theta_{min}^{-}$ $W_{1/2}^{+}/H$, $W_{1/2}^{-}/H$, and $y_c/H$ are scaling parameters. Note that $y = 0$ is at the top wall in figure 2, and that the trajectory $y_c/H$ defined by the maximum scalar in the profile is not the same as the trajectory defined by the maximum velocity.

A physically realistic θ should be neither <0 nor >1. Unmixed jet fluid is usually θ = 1 and unmixed mainstream fluid is θ = 0. (However, θ = 1 has been used to represent unmixed mainstream fluid so the reader should be observant). Although θ was originally formulated from temperature data, θ is dimensionless, and applies to any conserved scalar (no sources or sinks). For example, species concentration was often used in the studies summarized in references 2 and 3. Note too that although temperature is a conserved scalar in a non-reacting and incompressible flow, it is not a conserved scalar in a reacting or compressible non-reacting flow.

Correlation equations were developed for each of the scaling parameters and are given in appendix C of reference 30. For all calculations, the dimensionless flow and geometric variables that must be specified are the jet-to-mainstream density ratio *DR*, jet-to-mainstream momentum-flux ratio *J,* jet discharge coefficient $C_d$, orifice spacing-to-duct-height ratio *S/H*, duct height-to-orifice diameter ratio *H/d*, and the downstream distance *x/H*. If there is a non-uniform mainstream scalar distribution and/or flow area convergence, parameters for them must be specified too.

The correlation equations in reference 30 are written in terms of $H_{e.q}$ rather than *H*. For most cases $H_{eq} = H$, since $H_{eq}/H$ is only ≠ 1 if the symmetry model is used for opposed rows of jets with their centerlines in-line. The correlations used in the spreadsheet are the same as those included in reference 1. (Any differences are due to elimination of curvature effects, clarification, changes in nomenclature, or correction of errors.) These correlations are also the same as those in NASA TM 104412 which preceded the journal publication in reference 1.

Three-dimensional oblique plots (herein called profile plots) are the native display in the spreadsheet. The dependent variable θ is shown on the horizontal axis in the profile plots. The vertical and oblique axes are the *y* and *z* directions, which are respectively normal to and along the orifice row in an axial (constant-*x*) plane. There are 101 data points in each profile so $\Delta y/H =$

0.01. The *z*-distance shown in the plots is usually twice the orifice spacing for each configuration (4*S* is an option). There are 21 profiles in this span; thus $\Delta z/S = 0.1$ for 2*S* or $\Delta z/S = 0.2$ for 4*S*. Only six independent jet profiles are calculated. The others are generated by assuming symmetry about both centerplanes and midplanes. Twenty-one profiles are necessary because a non-uniform scalar distribution may be specified which does not assume symmetry in the span displayed.

A sheet in the JIC spreadsheet is labeled "3D" and is simply an array of the data that are plotted in the profile plots. The 3D sheet has three columns: column A is the θ distribution; column B shows *z/S*; column C shows *y/H*. This parameter (*y/H)* increases by 0.01 from 0 to 1 over every 101 rows. After 101 rows, *z/S* increases by 0.1, until reaching 2.0 (21 times). Note that θ = 0 in column A unless at least one row of jets is active or a non-uniform scalar distribution is specified.

Figure 3 shows a schematic of the several round-hole configurations for which calculations are shown in this report. The orifice configurations are in order of their round hole size (descending *H/d* first, then ascending *S/H* if *H/d* is the same). Only one identifying letter is used for configurations that differ only by a lateral shift. The configurations shown in figure 3 are often cited in the text and in figures 4 to 24 herein. The orifice configurations are the same as in reference 30 (except that the non-circular orifices there are not included).

The independent and dependent variables are identified in table 1. Not all combinations of the independent variables were tested. Note that the orifice spacing *S* was never greater that the duct height *H* in any of the previous confined JIC studies, and it is unlikely that a JIC would spread laterally farther than its penetration so *S/H* should not be greater than 1. The conditions for the cases shown in this report are given in table 2.

Although calculations can be performed for many flow and geometric conditions of interest that are not within the range of the experiments on which the empirical model is based, results will be more reliable for interpolation than extrapolation. The spreadsheet checks to determine if the inputs specified are within the range of the experiments and warns the user (but does not stop the calculation) if extrapolation is being specified. The specifics and operation of the spreadsheet (a.k.a. a user's manual), the correlations in the NASA empirical model, and the "closest" experimental data are given in reference 30.

## Symmetry Model

It was observed in reference 10 that the flow field downstream of opposed jets was similar to that downstream of a single jet injected toward an opposite wall. This was later also apparent in the experimental results in reference 18. The empirical model thus calculates profiles for opposed rows of jets with their centerlines in-line by assuming that the confining effect of opposed jets was the same as that of a wall between them.

The concept of an "equivalent" duct height was utilized in reference 13 and later in reference 35 to allow empirical correlations from single-side injection data to be applied to opposed jet injection. Opposed rows of jets with centerlines in-line were thus modeled by calculating the effective duct height $H_{eq}$ as proposed in reference 35, namely:

$$\left[H_{eq}\right]_{top} = (H)\frac{\left[\left(A_j / A_M\right)\left(\sqrt{J}\right)\right]_{top}}{\left(\left[\left(A_j / A_M\right)\left(\sqrt{J}\right)\right]_{top} + \left[\left(A_j / A_M\right)\left(\sqrt{J}\right)\right]_{bottom}\right)} \tag{3}$$

and

$$\left[H_{eq}\right]_{bottom} = H - \left[H_{eq}\right]_{top}$$

Since $(A_J/A_M)*(\sqrt{(J)}) \sim MR$ equation (3) is usually a mass-flow balance. Since this equation includes the area, it is a –flow ratio rather than a –flux ratio Alternative definitions were investigated in reference 36. The one that used $S/H$ and $\sqrt{(J)}$ agreed best with the experimental data. Equation (3) reduces appropriately for (1) the case with equal $J$'s and $H/d$'s on opposite sides, and (2) the case with different $J$'s but equal $H/d$'s on opposite sides, but not (3) the case with different $H/d$'s but equal $J$'s on opposite sides.

For the case (1) of equal $J$'s and $H/d$'s on opposite sides (fig. 19 in ref. 30), $J_{top} = J_{bottom}$ and equation (3) gives $H_{eq} = H/2$. Results for case (2) are correct too as equation (3) gives $H_{eq} = f(\sqrt{(J)})$ since the orifice configuration is the same on both sides. Results for single-side and opposed jet injection at $x/H = 0.5$ for case (2) with $H/d$=8 are shown for both experimental data and the empirical model in reference 37. The experimental data for case (3) also shows that $H_{eq} = f(\sqrt{(J)})$; but equation (3) gives $H_{eq} = f(A_J/A_M)$.

If $H_{eq}/H < 1$ the result is that profiles are calculated for a different duct height ($H_{eq}$) than the physical one ($H$) while all other parameters remain the same. Since the correlations are dimensionless, and $H_{eq}$ appears in $x/H_{eq}$, $S/H_{eq}$, and $H_{eq}/d$, all of these are changed by symmetry.

In the profiles the entire $y$-axis goes from 0 to $H$, while the top row profile is scaled to fit in $[H_{eq}]_{top}$ and the opposite row is scaled to fit in $[H_{eq}]_{bottom}$. Thus, the individual rows of jets are calculated for, and scaled to, $H_{eq}$ instead of $H$. The spreadsheet calculation is as if a (permeable) wall is placed between the two jets at $H_{eq}$ and the individual profiles are truncated there. Since several correlation equations contain $H/H_{eq}$, the results using the symmetry model may not be identical to the comparable single-side case.

## Superposition Model

The empirical profiles for superposition were obtained by combining independent calculations of the flow distributions according to the following equation:

$$\theta = \frac{\left[\theta_1 + \theta_2 - 2(\theta_1)(\theta_2)\right]}{\left[1 - (\theta_1)(\theta_2)\right]} \tag{4}$$

For opposed rows of jets with centerlines in-line, $\theta_1$ is the distribution for the top row and $\theta_2$ is the distribution for the bottom row (or vice-versa). If more than two θ's are needed, the result is used with $\theta_3$ in equation (4). This resulting formula has three θ′s. The same steps are required twice more to get a function of five θ's (a JIC spreadsheet maximum: row 1 and row 2. top and bottom plus a non-uniform mainstream scalar). All five θ's are always calculated. If any of the θ's is zero, it will drop out and not affect the final result (as a $\theta_1$ or $\theta_2$ of zero will do in eq. (4)).

Unlike in the symmetry model, superposition profiles are calculated for the actual dimensionless orifice spacing *S/H*, size *H/d*, and downstream location *x/H*. Thus the contribution of each side can be observed by deactivating the other side.

Although superposition often gives a good approximation to the experimental data, it should be realized that it is an approximation, since there may be an interaction between opposite and/or adjacent jets and cross-stream transport that is not accounted for in superimposing independently calculated distributions. In this case, superposition can give non-physical results; for example, if opposing jets approach and pass the same location, the calculated result will be as if they had penetrated through each other without having any influence.

### How to Invoke the Superposition Model

The symmetry model is the default method in the spreadsheet for opposed rows of jets with their centerlines in-line. Specifying round holes, streamlined slots, or bluff slots in rows 1 or 2, top and bottom with all orifices aligned [e.g., both sides either )-0-( or -0—0-] uses symmetry, but only if neither row of opposed jets are slanted slots. To invoke the superposition model, one must not have the same configurations on both top and bottom active in any row. The "solution" to get superposition is to activate row 1 top and row 2 bottom (or vice-versa) and to specify $S_X/H = 0$. (That is how the data plots for superposition in figs. 15 to 24 were made.) Recall that *x/H* and *S/H* must be specified in row 1 top, even if that row is not active.

## Results and Discussion

The conditions for the cases shown in figures 4 to 24 are given in table 2. Independent variables are also given in the figure titles and subtitles, and important dependent variables are often included in parentheses. As in reference 30, figures 4 and 8 to 14 show the centerplane at the edge in the plots [)-0-( in the spreadsheet] and figures 5 to 7 show the midplane at the edge [-0-0- in the spreadsheet]. Figures 15 to 24 in this report also show the midplane at the edge.

At a user-specified downstream distance *x/H* there are always 21 *z/S* profiles, with 101 *y/H* data points in each profile. The dependent variable is θ and is a function of *z/S* and *y/H*. The span of *y/H* is from 0 to 1 for all profiles, and *z/S* always includes either two or four orifices, so the physical *z*-span increases as *S/H* increases (see fig. 3 in this report and ref. 30 and fig. 8 in ref. 1). The plots for single-side injection shown in figures 4 to 14 are all contour plots, and the plots for opposed rows with jet centerlines in-line that are shown in figures 15 to 24 are all profile plots.

### Slideshow

A slideshow has been assembled as an appendix to this report to show basic flow and geometric variations and those that are typical in combustors for gas turbine engines. All are shown with profile plots. Those in sequences 4 to 10 of the slideshow show the centerplane at the edge, as do the corresponding figures in reference 30. (Figures in ref. 21 show the midplane at the edge.) The profile plots in sequences 1 to 3 and 11 to 21 show the midplane at the edge, as do the corresponding figures in references 21 and 30, and this document. Reports are primary references only if the flow and geometry conditions are identical in at least one part of the figure. Other figures (noted with see also) may be close but might differ by, for example, the orifice diameter, lateral arrangement, or downstream distance. The slideshow table of contents is given in the appendix.

## Contour Plots for One Side Injection

The primary objective of this task is not to provide new insight, but to present contour plots for the same conditions that are in the profile plots in figures 4 to 14 of reference 30. The cases shown here (and the figure numbers) are the same to facilitate comparisons of profile and contour plots. A limited comparison of profile and contour plots is shown in references 1 and 27 from numerical results for selected opposed jet configurations.

This task was motivated by pre-publication feedback on the spreadsheet which suggested that the ability to do contour plots was critical to its use. Although the spreadsheet can calculate distributions at user-specified downstream locations for other configurations, the distributions shown in figures 4 to 14 are all for one side injection from a single row of jets.

Data for the contour plots were plotted with Tecplot (ref. 31) from datasets created with the spreadsheet. The vertical and horizontal axes in the contour plots are the $y$ and $z$ directions, which are respectively normal to and along the orifice row in an axial (constant-$x$) plane. The $z$-distance shown in the plots is twice the orifice spacing for each configuration.

All contour plots in this report use the same $0 \le \theta \le 1$ color bar with $\theta = 0$ = (blue) and $\theta = 1$ = (red). Color maps for contour plots are highly subjective. It was the authors' predisposition for blue jets and a red mainstream as used in most of the NASA JIC studies in the 1990s. Perhaps our preference for the color distribution used in most of the contour plots in this report is in part because the equilibrium $\theta_{EB}$ value here is $0 < \theta_{EB} < 0.5$ and in the RQL mixers it was $0.5 < \theta_{EB} < 1$. (The jet-to-mainstream mass-flow ratio $MR$ was significantly higher in the RQL mixers.)

Figures 4 to 14 show example variations in θ contour plots as a function of the several flow and geometric variables. Typical contour plots for an optimum mixing configuration are shown in figure 4 for $J = 26.4$ and configuration F: $S/H = 0.5$, $H/d = 5.66$ as given in table 2 (the orifice configuration is shown in fig. 3).

### View Options

***Plane of symmetry***.—Different features may be apparent depending on whether the centerplane or midplane is at the edge in the distribution. As an example, compare the distribution in figure 5, where the midplane is at the edge for $J = 26.4$ and configuration F: $S/H = 0.5$, $H/d = 5.66$, with the distributions in figure 4, where the centerplane is at the edge.

**θ *definition***.—The flow also can appear quite different depending on the definition used for θ. Distributions may be shown as either 'cold' [$\theta = (T_M - T)/(T_M - T_J)$], as in figure 5, or as 'hot' [$\theta = (T - T_J)/(T_M - T_J)$], as in figure 6. In the 'cold' distribution, the numerator is the difference between the local and the undisturbed mainstream, and unmixed jet flow is $\theta = 1$ in the distribution. However, for the 'hot' θ distribution (i.e., $1 - \theta_{cold}$), the numerator is the local difference from the jets, and unmixed jet fluid is $\theta = 0$. Both figures 5 and 6 are for $J = 26.4$ and configuration F: $S/H = 0.5$, $H/d = 5.66$. The switch in colors in figure 6 results from the specification of 'hot' θ distributions as $\theta = 1$ = (red) and $\theta = 0$ = (blue) in all the contour plots.

***Injection location***.—Distributions for bottom wall injection of the jets can be created as shown in figure 7. The contour plots shown in figure 7 provide an additional view of θ distributions for $J = 26.4$ and configuration F: $S/H = 0.5$, $H/d = 5.66$. This figure shows the

midplane at the edge as do figures 5 and 6. Note that although the top front row is inactive in this case, the downstream distance and orifice spacing must be specified there and that the capability to do injection from both top and bottom walls is needed for the opposed jet cases in figures 15 to 24 in this report and in figures 19(a) and (b) in reference 30.

**"Basic" Flow and Geometry Effects for a Confined JIC**

***Downstream distance (x/H)***.—Figure 8 shows that the mixing improves with increasing *x/H*. Variation in scalar distributions with downstream distance are shown for $J = 26.4$; the downstream locations are $x/H = 0.25$, 0.5, 1.0, and 2.0, with the centerplane at the vertical edge in the contour plots (as in fig. 4). In figure 8(a) orifice configuration C is used ($S/H = 0.25$, $H/\mathrm{d} = 8$), with $J = 26.4$; and in figure 8(b) configuration I ($S/H = 1$, $H/d = 4$) is used, also with $J = 26.4$. In figure 8, the momentum-flux ratio *J* and the ratio of total orifice area to mainstream cross sectional area ($A_J/A_M$) are equal. Because *J* and $A_J/A_M$ are the same, the jet to mainstream mass-flow ratio *MR* is constant too. Thus, the range of distributions from under-penetration in figure 8(a) to over-penetration in figure 8(b) results entirely from variation in orifice spacing.

Mixing improves with increasing downstream distance whatever the configuration. If the objective is a uniform scalar distribution in a minimum *x/H*, an optimum mixer is usually best. Distributions for the optimum orifice size and spacing for this flow condition are shown in figure 4 (configuration F in fig. 3, $S/H = 0.5$, $H/d = 5.66$).

***Momentum-flux ratio (J)***.—The momentum-flux ratio *J* is the most significant flux variable. Figure 9 shows the increase in jet penetration that is expected with increasing *J* (from 6.6 to 105.6) for orifice configuration F: $S/H = 0.5$ and $H/d = 5.66$. These distributions are at a downstream distance equal to one-half of the duct height ($x/H = 0.5$). As the downstream distance is arbitrary, the same trends would be apparent for different *x/H* values. Note that the jets are under-penetrating in part (a), and over-penetrating in part (c). Since the orifice size and spacing are constant in figure 9, the jet-to-mainstream mass-flow ratio *MR* increases with increasing momentum-flux ratio *J*.

***Density ratio (DR)***.—Analyses of the experimental data in reference 7 suggested that for flows with a constant *J*, the effect of varying the density ratio *DR* was minor when *J* was constant. The range of the *DR* variation was expanded and the effects were shown in reference 1 and other papers, too. The similarity of the distributions when *DR* is varied at constant *J* is in contrast to the (1) increased penetration with increasing *DR* at constant $R = \sqrt{J/DR}$, and (2) decreased penetration with increasing *DR* at constant $M = \sqrt{J*DR}$ that are shown in figures 17 and 18 in reference 1. (If $DR = 1$; $\sqrt{(J)} = M = R$.)

The minor effect of varying the density ratio at constant *J* can be seen in figure 10. In the figure, the density ratio varies from 0.5 (less dense jets) to 1 (equal density) to 2 (more dense jets) at a downstream distance of $x/H = 0.5$. $J = 26.4$ in figure 10 and the orifice geometry is configuration F: $S/H = 0.5$ and $H/d = 5.66$ which was also used in figures 4 to 7. Note that the magnitude of θ increases slightly because the jet-to-mainstream mass-flow ratio increases as the density ratio increases. Other that this, there is not much difference between hot-jets-in-a-cold-mainstream and cold-jets-in-a-hot-mainstream at a constant momentum-flux ratio.

***Orifice spacing (S/H)***.—Figure 11 shows the effect on the distribution of decreasing the lateral spacing between orifices with $J = 26.4$ for configurations E ($S/H = 1.0$), D ($S/H = 0.5$), and C ($S/H = 0.25$) at a downstream distance equal to one-half of the duct height. ($x/H = 0.5$). The jet penetration decreases as orifice spacing $S/H$ decreases. (The maximum penetration for a given $J$ will occur for an unconfined JIC.) Note that the lateral uniformity of the distribution also increases as the orifice spacing decreases. Both this and the decreased penetration probably occur because adjacent jets are closer as $S/H$ decreases. The jet-to-mainstream mass-flow ratio increases as the spacing decreases, since the orifice size is constant ($H/d = 8$ in all cases).

***Orifice size at constant S/d***.—Figure 12 shows the increased jet penetration, and decreased lateral uniformity that result from increasing the orifice size $d$ with the orifice spacing-to-diameter ratio $S/d$ held constant for $J = 26.4$ at $x/H = 0.5$. As orifice size increases ($H/d$ decreases), the orifice spacing $S/H$ must increase to maintain a constant $S/d$ since $S/d = (S/H)*(H/d)$. In figure 12(a), $S/H = 0.125$ and $H/d = 16$ (configuration A); in figure 12(b), $S/H = 0.25$ and $H/d = 8$ (configuration C); and figure 12(c), $S/H = 0.5$ and $H/d = 4$ (configuration F). Note that since these distributions are at a constant downstream distance ($x/H = 0.5$), $x/d$ varies in proportion to $H/d$ [$x/d = (x/H)(H/d)$], so $x/d = 8$ in figure 12(a), $x/d = 4$ in figure 12(b), and $x/d = 2$ in figure 12(c). Jet penetration increases as orifice size increases ($S/H$ increases and $H/d$ decreases) at constant $S/d$. The reader should also note that the lateral uniformity decreases as the size of the hole becomes larger.

***Orifice size at constant S/H***.—In contrast to the variations seen in figure 12 for $S/d = 2$, the jet penetration in figure 13 for $S/H = 0.5$ remains very similar when the orifice diameter $d$ increases ($H/d$ decreases) at a constant $S/H$. The distributions in figures 13(a) and (b) are at downstream distances equal to one-half and two duct heights respectively. The orifice diameter doubles as $H/d$ is varied from 8 to 4, resulting in a four-fold increase in the jet-to-mainstream mass-flow ratio $MR$. The result is that the distributions shift to higher θ values, consistent with the larger jet mass flow, but the jet penetration and shape of the distributions remain similar. The obvious conclusion from figure 13 is that varying the orifice size has a secondary effect, and orifice size can be chosen to satisfy other considerations (e.g., the mass-flow ratio) provided $S/H$ is constant. Note that since $S/d = (S/H)(H/d)$ and $x/d = (x/H)(H/d)$, both $S/d$ and $x/d$ decrease as $H/d$ decreases.

***Coupled orifice spacing (S/H) and momentum-flux ratio (J)***.—Analysis of the experimental data in references 7 and 15 suggested a coupling between the momentum-flux ratio $J$ and the orifice spacing $S/H$, and led to the conclusion that for a given momentum-flux ratio there exists an orifice spacing for which the most efficient mixing occurs, independent of orifice size. Conversely, for a given orifice spacing $S/H$ there is a $J$ for which the most efficient mixing occurs. This relationship can be stated as

$$C = (S/H)\sqrt{J} \tag{5}$$

The contour plots shown in figure 14 represent optimum mixing conditions (C = 2.57) for a single row of jets, and show the inverse relationship between the orifice spacing $S/H$ and the momentum-flux ratio $J$ when they are related according to equation (5). For $J = 6.6$, $S/H = 1$ (e.g., configuration I); for $J = 26.4$, $S/H = 0.5$ (e.g., configuration F); and for $J = 105.6$,

*S/H* = 0.25 (e.g., configuration B). The contour plots in figures 14(a) and (b) are at downstream distances equal to one-half and two duct heights respectively. Here, the mass-flow ratio *MR* is constant, as the orifice size was decreased for increased *J*. Clearly, similar penetration is obtained over a range of momentum-flux ratios if *J* and *S/H* are coupled, but note also that the flow is laterally less uniform for smaller momentum-flux ratios.

The NASA Design Procedure given in reference 30 and previous publications is based on equation (5) and assigns priority to specifying the orifice spacing *S/H* for a given *J*. Equation (5) has been found to be useful in characterizing the mixing. For one-sided injection, optimum penetration is expected when C is ~2.5; under-penetration is expected if C is approximately half of the optimum value; and over-penetration is expected when C is approximately double the optimum value. Note that this procedure, which emphasizes orifice spacing, is different from the Cranfield Design Method which emphasizes the size of individual orifices. Both of these methods are described in reference 38.

As can be see from equation (5), and inferred from perusing figures 9 and 11, there is usually a trade-off between momentum-flux ratio *J* and orifice spacing *S/H*, Note that, for example, figures 9(a) and 11(c) and 9(c) and 11(a) have very similar penetration and equal C values (C = 1.28 and 5.14, respectively), but there are have significant differences in lateral uniformity.

It is evident that flows with smaller momentum-flux ratios need a larger spacing *S/H* and a greater downstream distance to achieve equivalent mixing. Increasing *J* will usually promote better optimum mixing, but often at the "cost" of a higher pressure loss. The reader should note that the optimum mixer at a given *J* may appear to give worse mixing than a non-optimum mixer at a higher momentum-flux ratio. Thus one should always examine the anticipated distributions and not base a configuration selection solely on a "mixing parameter."

## Symmetry and Superposition for Opposed Jets

The profile plots in figures 15 to 24 show $0 \leq \theta \leq 1$ with $\theta = 1$ for unmixed jets and $\theta = 0$ for an unmixed mainstream, and with the midplane at the edge in the plots [-0-0- in the spreadsheet]. Although the spreadsheet can calculate distributions for other configurations, the distributions in figures 15 to 24 are all for opposed rows of jets with centerlines in-line.

### Optimum Round Hole Configurations

Profiles calculated with the symmetry and superposition models for opposed jets with an orifice spacing, *S/H*, of 0.5 and with a momentum-flux ratio, *J*, of 6.6 are shown in figure 15 for orifice configuration D: *S/H* = 0.5, *H/d* = 8 (fig. 15(a)), configuration F: *S/H* = 0.5, *H/d* = 5.66 (fig. 15(b)), and configuration H: *S/H* = 0.5, *H/d* = 4 (fig. 15(c)). Profiles for opposed jets with an orifice spacing, *S/H*, of 0.25 and with a momentum-flux ratio, *J*, of 26.4 are shown in figure 16 for orifice configuration B: *S/H* = 0.25, *H/d* =11.32 (fig. 16(a)) and configuration C: *S/H* = 0.25, *H/d* = 8 (fig. 16(b)); and profiles for opposed jets with an orifice spacing, *S/H*, of 0.125 and with a momentum-flux ratio, *J*, of 105.6 are shown in figure 17 for orifice configuration A: *S/H* = 0.125, *H/d* =16. Calculations made using the symmetry model are in the left columns of figures 15 to 17, whereas calculations made with the superposition model are in the right columns. Figures 15 to 17 show downstream distances of *x/H* = 0.25, 0.5, and 1.0 for optimum mixing conditions (C = 1.28). There is very little difference between results from the superposition and symmetry models.

**Under-penetration**

Figures 18 and 19 show calculations using both symmetry and superposition models for under-penetrating opposed jets at downstream distances of $x/H = 0.25$, 0.5, and 1.0. Profiles with an orifice spacing, $S/H$, of 0.25 and with a momentum-flux ratio, $J$, of 6.6 are shown in figure 18 for configuration B: $S/H = 0.25$, $H/d = 11.32$ (fig. 18(a)) and configuration C: $S/H = 0.25$, $H/d = 8$ (fig. 18(b)). Profiles for opposed jets with an orifice spacing, $S/H$, of 0.125 and with a momentum-flux ratio, $J$, of 26.4 are shown in figure 19 for configuration A: $S/H = 0.125$, $H/d = 16$. C = 0.64 for all cases and the jets under-penetrate in all cases as expected. Again, there is very little difference between profiles calculated with the symmetry and superposition models.

**Over-penetration**

These configurations (C = 2.57) are usually optimum mixers for one-side injection, but they would be expected to be over-penetrating cases for opposed rows of jets with their centerlines in-line since $H_{eq}$ is usually = $H/2$. These cases are, e.g., $J = 6.6$ and $S/H = 1$ (configurations E and I), $J = 26.4$ and $S/H = 0.5$ (configurations D, F, and H), and $J = 105.6$ and $S/H = 0.25$ (configurations B and C). Results from the symmetry and superposition models may be significantly different for over-penetrating cases. Results for these cases are not shown in this report as the NASA empirical model is usually not appropriate for modeling over-penetrating cases. The assumption of Gaussian profiles is often not valid on both sides of the scalar trajectory (if $y_c > H_{eq}$ the opposite side doesn't exist in symmetry model calculations).

Furthermore, it seems like lot of jet mass flow would be "lost" by symmetry if a significant part of the profile were truncated. Superposition would not have this mass-flow problem; but with superposition individual calculations can yield profiles for jets that cross $H_{eq}$ without interacting with any opposite jet and this is not physically realistic.

**Different Mass Addition on Opposite Sides**

There are two obvious limiting cases where mass addition is different on opposing sides; they are (1) the orifice size is different on the two sides, but the momentum-flux ratio $J$ and the orifice spacing $S/H$ are the same; and (2) the momentum-flux ratio $J$ is different on opposite sides, but the orifice size and spacing ($H/d$ and $S/H$) are the same. (If $S/H$ is not the same on opposite sides then the orifice configuration is not opposed rows with jet centerlines in-line.) Experimental data for both cases 1 and 2 is shown in reference 35.

A non-physical discontinuity will appear in θ calculations at $H_{eq}$ using the symmetry model when the $\theta^{+}_{\min}$ values from the top and bottom are not equal. This will only occur if the mass addition is different on opposite sides (as will most likely be the case if the geometry and/or flow conditions are different on opposite sides). A partial "fix" is to average the two $\theta^{+}_{\min}$ as suggested in reference 13. The centerplane $\theta^{+}_{\min}$ values are averaged in the version of the empirical model included herein. Averaging the centerplane $\theta^{-}_{\min}$ values does not completely smooth out the plots as the $\theta^{+}_{\min}$ is not the physical value of θ at $y = H$. Also, off-centerplane $\theta^{+}_{\min.z} / \theta_{c.z} = \theta^{+}_{\min} / \theta_c$ so even when the centerplane $\theta^{+}_{\min}$ values are averaged, the plots will have a discontinuity if the $\theta_c$ values differ for the two sides. Because of the expected discontinuity, and because the $\theta^{+}_{\min}$ values were not averaged, there is no figure in reference 30, comparable to figure 16 in reference 21 (which appears to be wrong). No discontinuity will occur

with superposition. That method can give non-physical results also, and this is most apparent if $y_c > H_{eq}$. The results from the empirical model should not be accepted if this is apparent.

***Different orifice sizes***.—For this case either the opposed-jet configuration or the single-side configuration can be optimum, but not both. If the opposed-jet configuration is optimum, the jets in the single-side case will under-penetrate; and if the single-side case is optimum, the jets in the opposed-row configuration will over-penetrate.

Both symmetry and superposition results at $x/H = 0.5$ for $J = 6.6$ and $S/H = 0.5$ are shown in figures 20(a) and (b) and profiles for $J = 26.4$ and $S/H = 0.25$ are shown in figure 21. The top row is an optimum configuration for opposed jets with their centerlines in-line and the bottom row is the configuration for an equal-area, single side (bottom) injection case with the same orifice spacing. The middle row is an intermediate configuration with the same total area and spacing. Note that figures 20 and 21 are optimum configurations for opposed jets (C = 1.28).

The single-side optimum orifice spacing for the flow conditions in figures 20 and 21 are shown in figure 22 (i.e., for $J = 6.6$ it is $S/H = 1$; for $J = 26.4$ the single-side optimum is $S/H = 0.5$). The appropriate orifice spacing for optimum opposed jets with centerlines in-line is half that for the corresponding single-side injection case. Since there are twice the number of rows for opposed jets and also twice as many jets in each row, the orifice diameter for single-side injection needs to be doubled to get the same total orifice area for single-side configurations as for opposed rows with centerlines in-line.

The experimental data for the case of opposed rows of jets with $H/d$ different on opposite sides in reference 36 shows that $H_{eq} = f(\sqrt{(J)})$; unfortunately equation (3) gives $H_{eq} = f(A_J/A_M)$. Thus superposition gives more realistic results for the case of different orifice sizes on opposite sides.

***Different momentum-flux ratios***.—Equation (3) for $H_{eq}$ is correct for this case since the orifices are the same on top and bottom so $H_{eq} = f(\sqrt{(J)})$. Results from the empirical model for a case with different $J$'s on opposite sides of the duct is shown in figure 23 for $J_{top} = 58.4$ and $J_{botttom} = 6.5$ for configurations B: $S/H = 0.25$, $H/d = 11.32$ (fig. 23(a)) and C: $S/H = 0.25$, $H/d = 8$ (fig. 23(b)) at downstream distances of $x/H = 0.25$, 0.5, and 1. Experimental results for this case are shown in test 34 in reference 18.

The transition from opposed jets with equal momentum-flux ratios on opposite sides to one side injection is shown at $x/H = 0.5$ in figures 24(a) and (b) using the symmetry (fig. 24(a)) and superposition (fig. 24(b)) models. Note that both the opposed rows and single side cases can be optimum for equal orifice areas. Empirical model results using the symmetry model and experimental data for this case are given in reference 37.

For most cases, both the symmetry and superposition models give satisfactory results for opposed rows of jets with centerlines in-line. There are differences in appearance though, as superposition profiles have a smooth first derivative, and symmetry profiles often do not. The similarity of the profiles suggests that if any future revisions are made to the spreadsheet, it may not be necessary to change to symmetry for this case.

## Conclusions

An interactive computer code, written with a spreadsheet is used which displays three-dimensional oblique plots of the distributions of a conserved scalar downstream of jets mixing with a confined crossflow and provides data for other plotting programs.

Contours calculated with data from the JIC spreadsheet, which was published in NASA/TM—2005-213137, are presented for variations of the "basic" flow and geometry parameters to show their effects on the mixing. The primary purpose of this section is not to provide new insight, but to present contour plots for the same conditions that are in the profile plots in figures 4 to 14 of NASA/TM—2005-213137. The contour plots in figures 4 to 14 demonstrate the suitability of the data array in the spreadsheet for generating them, and, of course, lead to the same conclusions reached previously from profile plots.

Profiles for opposed rows of jets with their centerlines in-line can be calculated using either a symmetry or superposition model. Superposition results show that that method is quite satisfactory for most cases of opposed rows with jet centerlines in-line. As shown in figures 15 to 19, both the symmetry and superposition models give very similar results for under- and optimum-penetrating cases. However, they can be significantly different for over-penetrating cases. Actually, the empirical model results are uncertain for over-penetrating cases anyway (particularly if the scalar trajectory approaches or exceeds the equivalent duct height) as the assumption of Gaussian profiles may not be appropriate for these cases. For opposed jets cases with different mass addition on opposite sides the superposition model is superior to the symmetry model in that results from superposition are in better agreement with experimental data than are the symmetry results.

The spreadsheet used herein is capable of calculating flow fields which are physically unrealistic, and/or represent large extrapolations from the test conditions in the data base on which the model is based. Since one would have more confidence in results obtained for conditions that are within the range of the generating experiments, extrapolations are flagged in the spreadsheet with warnings, but they are not stopped. Also, as with previous versions of the NASA empirical model, symmetry is the default method for opposed jets, but if any future revisions are made to the spreadsheet, it may not be necessary to change to symmetry for the case of opposed rows with jet centerlines in-line.

# Appendix A

# Profiles for the Mixing of Jets With a Confined Crossflow in a Rectangular Duct—Slideshow

# Slideshow Table of Contents — Slide 1 of 159

Sequence 1

**Variations in scalar distributions with Increasing downstream distance**

*x/H=0.25, 0.375, 0.5, 0.75, 1, 1.5, 2*

*DR=2.2, J=26.4. S/H= 0.5, H/d=5.66, $C_d$=0.64*

(cf. figure 5 in NASA/TM—2005-213137, and figure 2 in NASA TM–87294); see also figure 4 in NASA/TM—2005-213137 and figure 3 in NASA TM–83457)

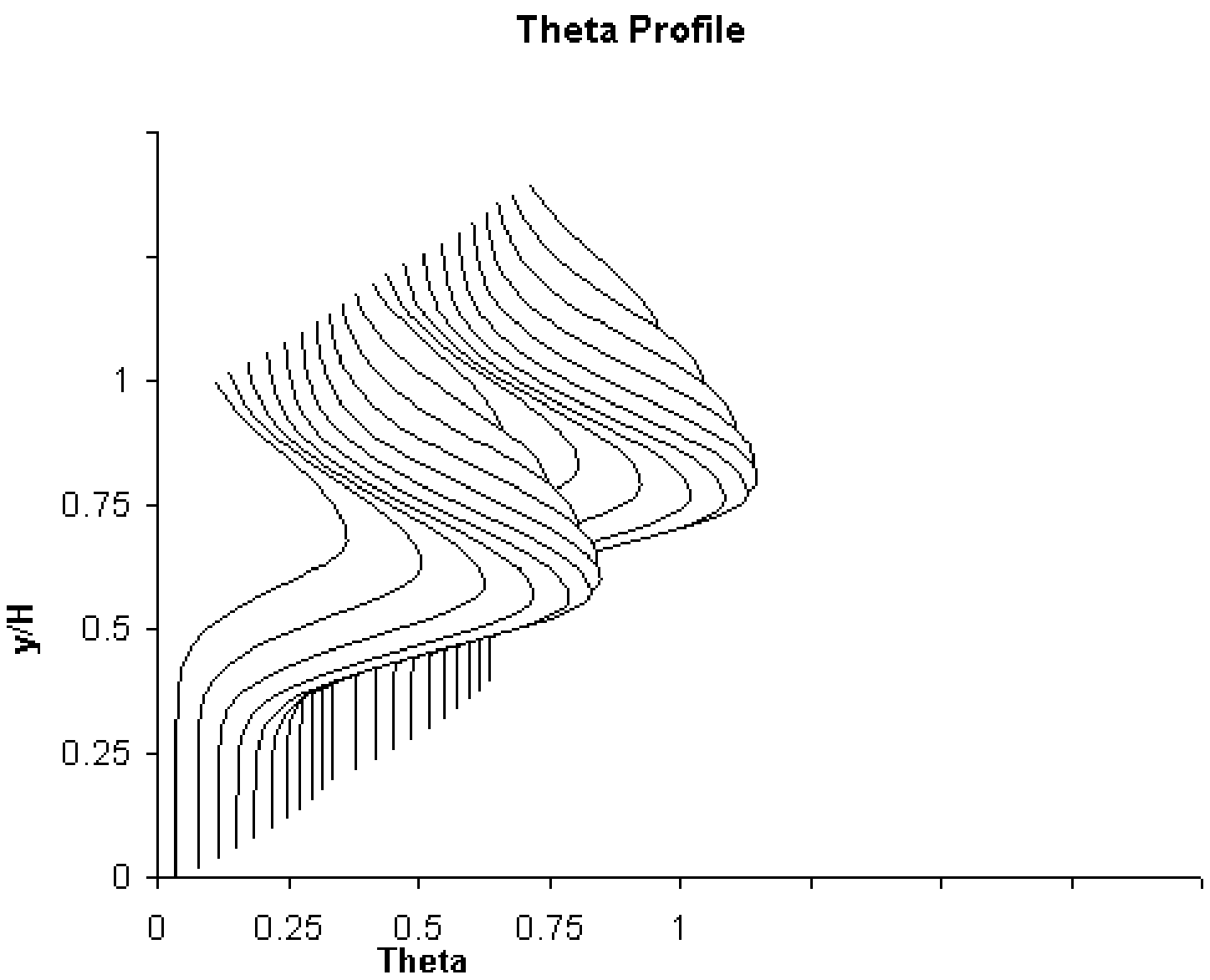


*x/H=0.25 (x/d=1.42)*

*J=26.4, S/H= 0.5, H/d=5.66, (S/d=2.83)*

## Theta Profile

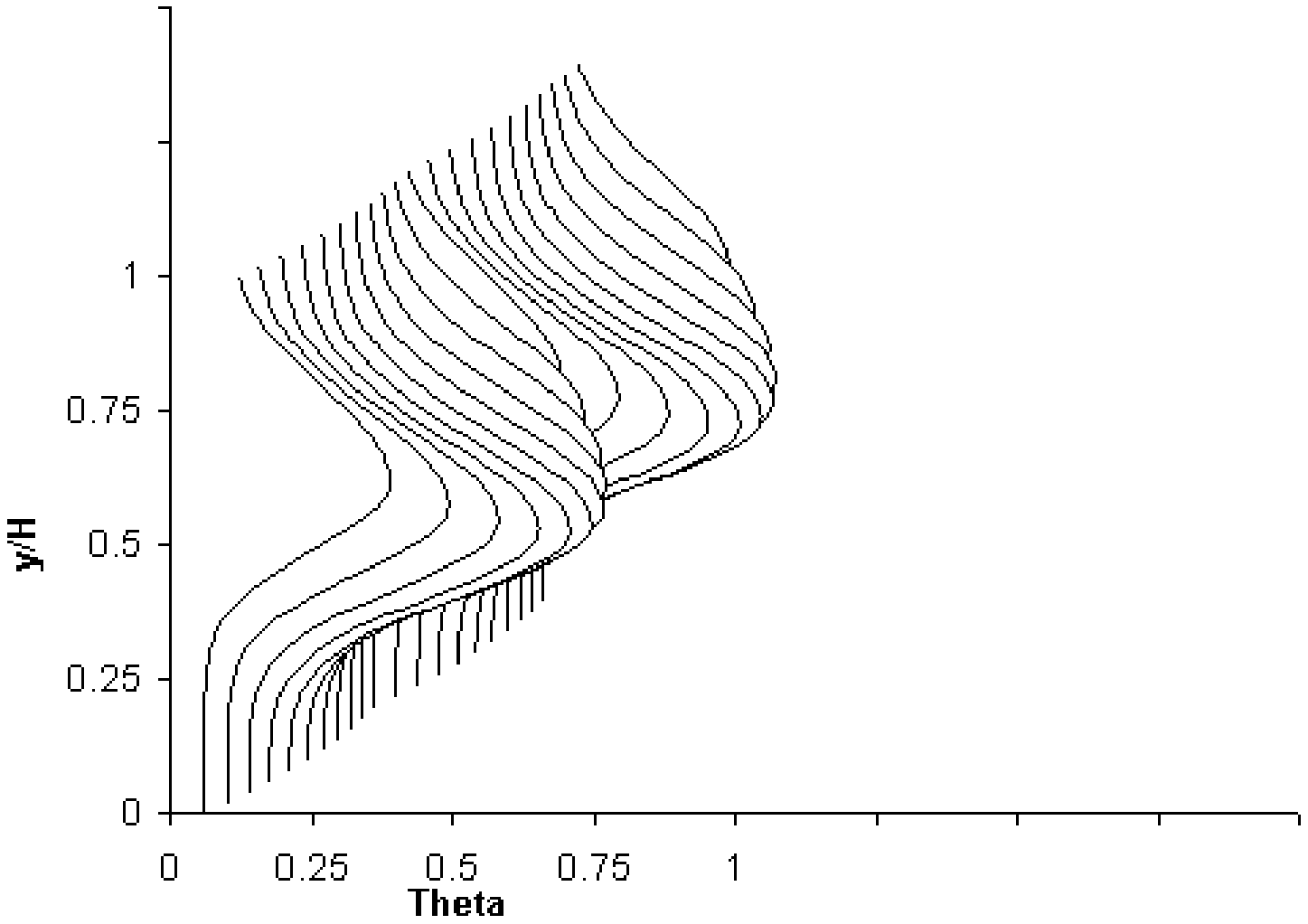


*x/H=0.375 (x/d=2.12)*

*J=26.4, S/H= 0.5, H/d=5.66, (S/d=2.83)*

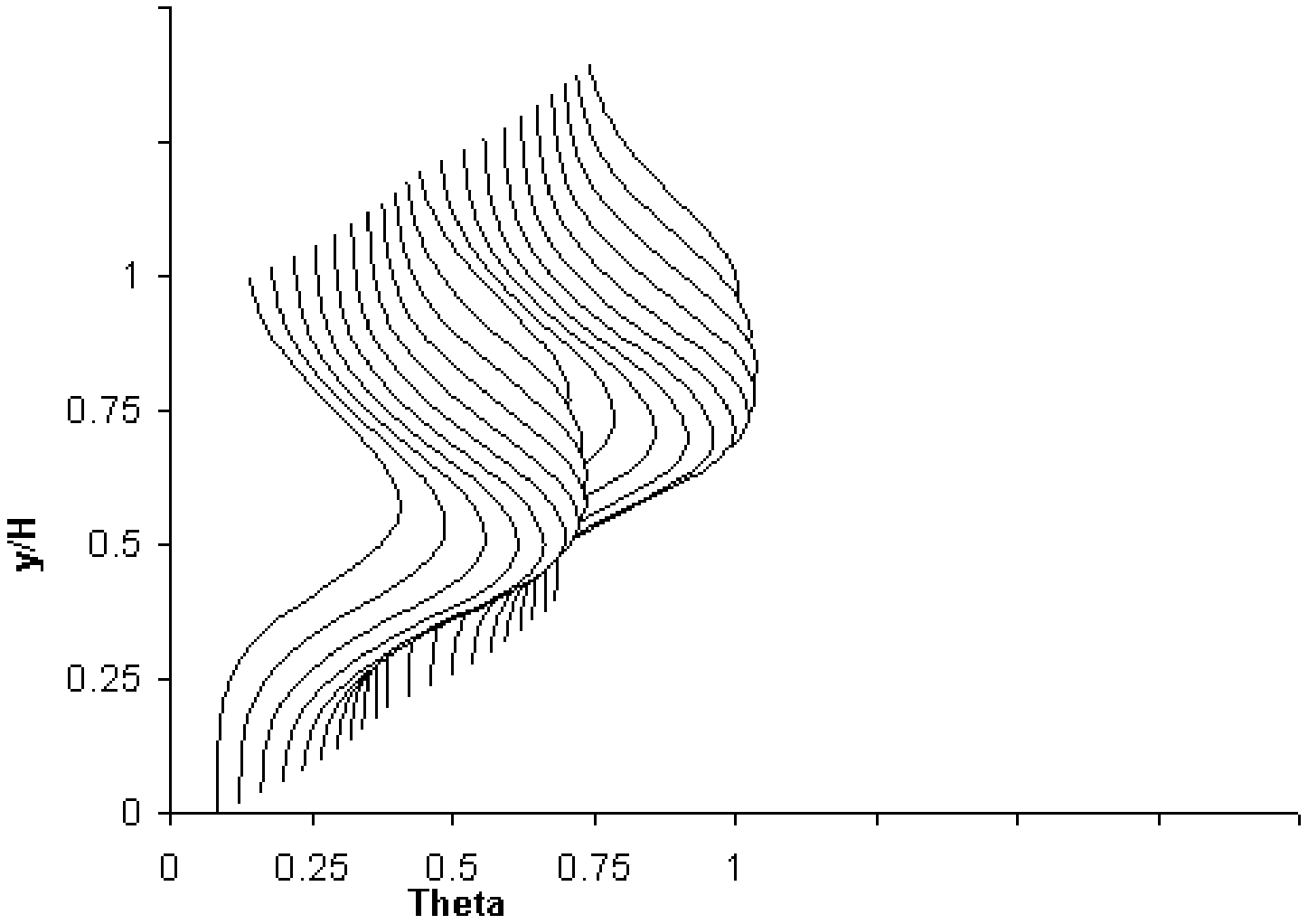


*x/H=0.5 (x/d=2.83)*

*J=26.4, S/H= 0.5, H/d=5.66, (S/d=2.83)*

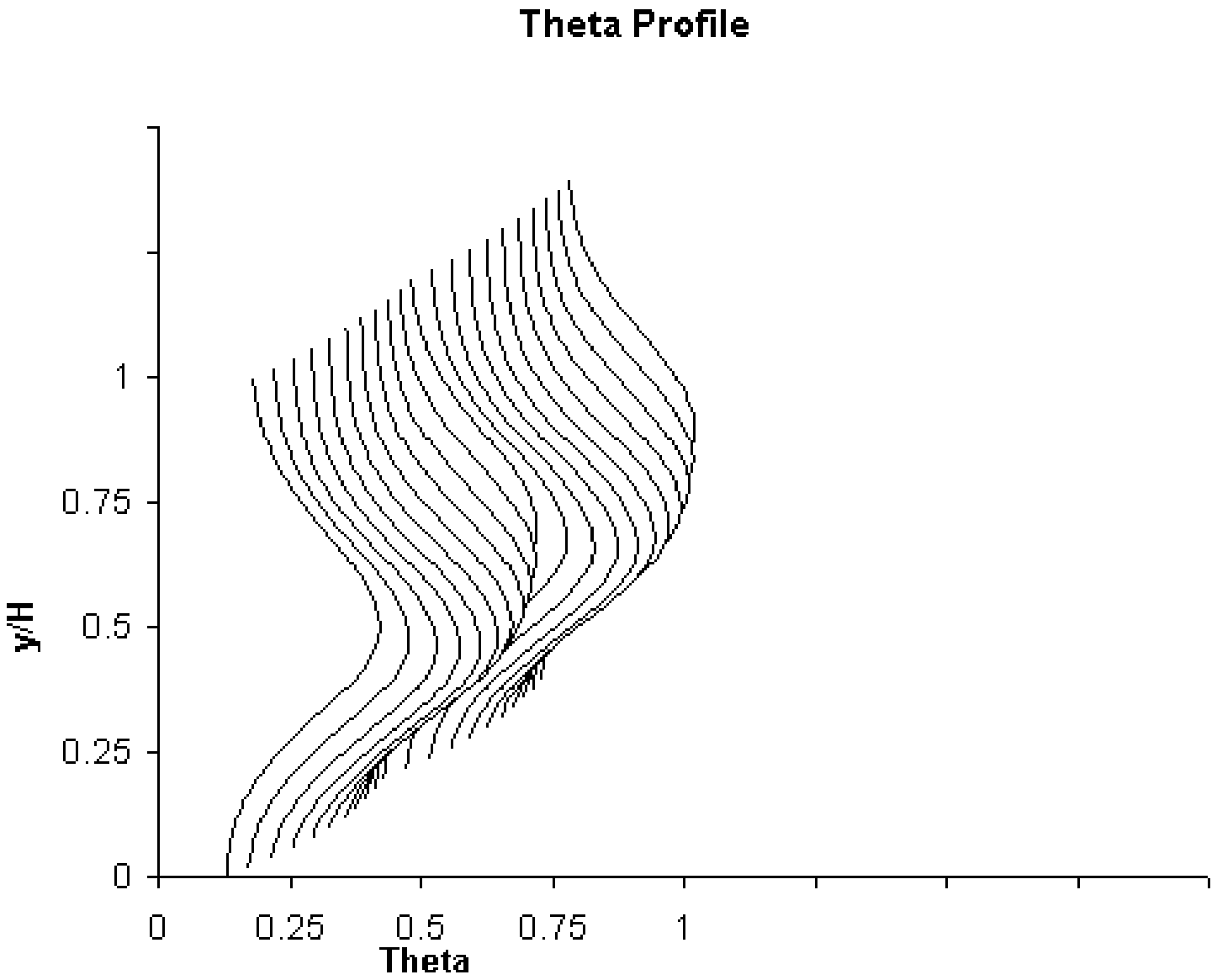


*x/H=0.75 (x/d=4.25)*

*J=26.4, S/H= 0.5, H/d=5.66, (S/d=2.83)*

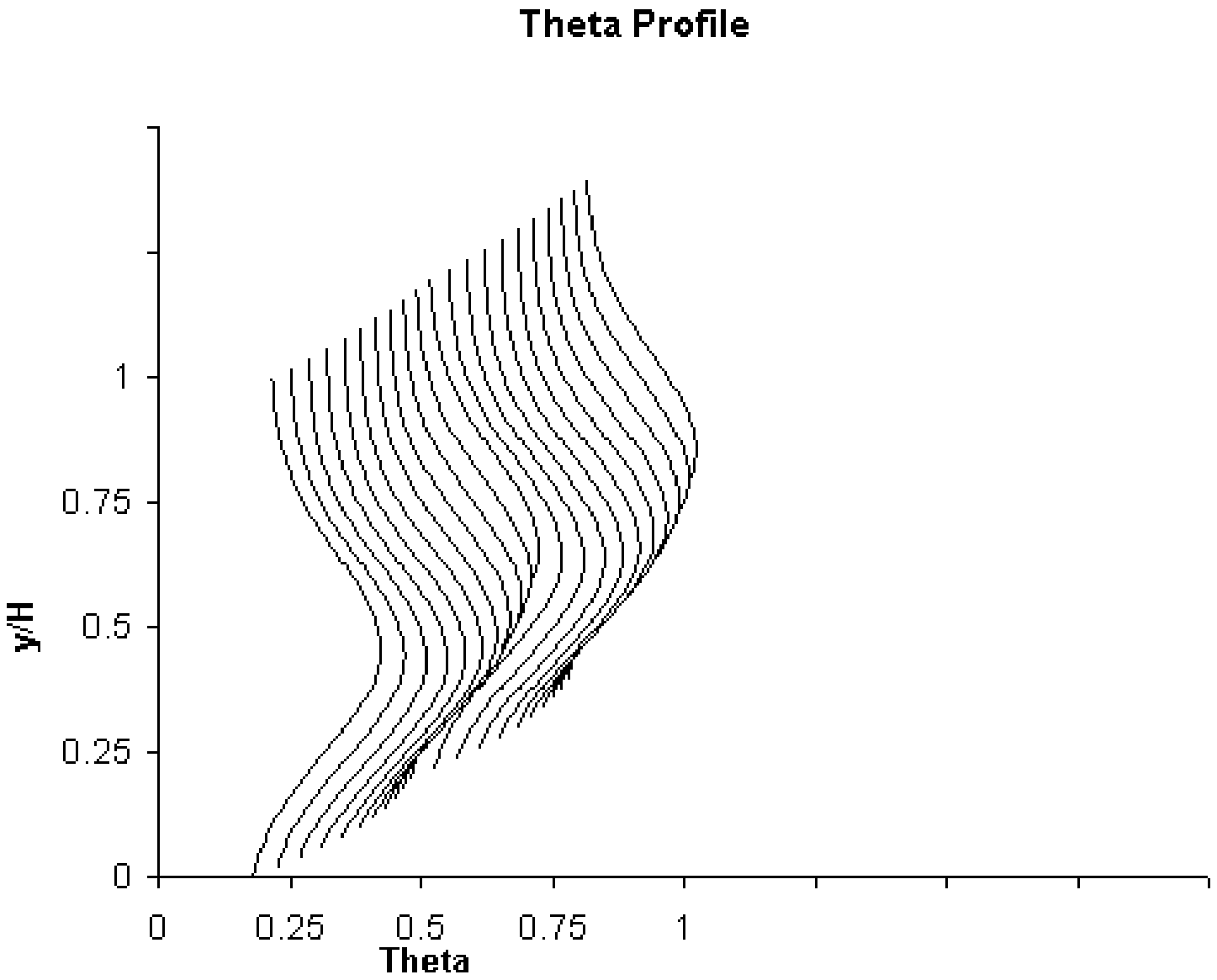


*x/H=1 (x/d=5.66)*

*J=26.4, S/H= 0.5, H/d=5.66, (S/d=2.83)*

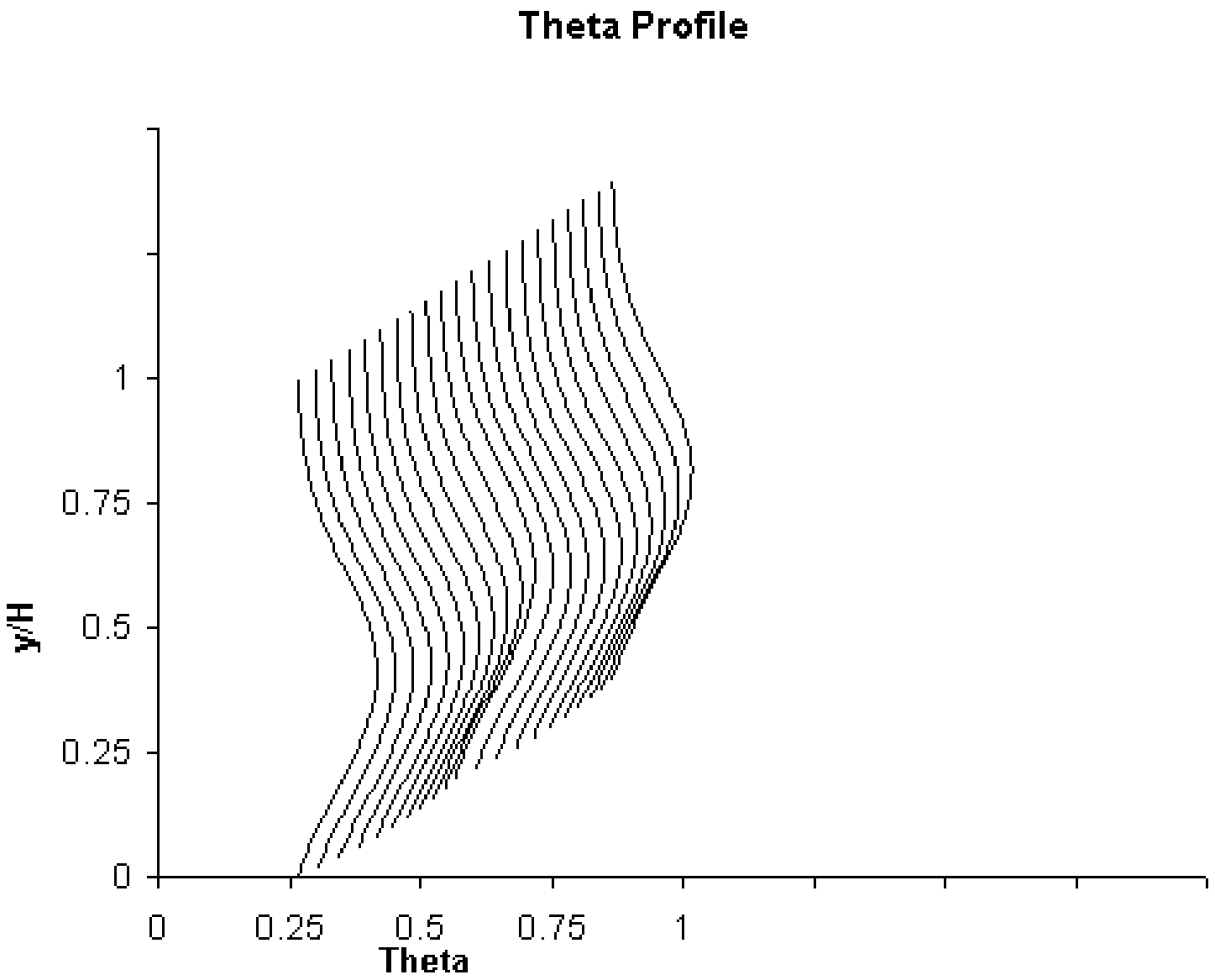


*x/H=1.5 (x/d=8.49)*

*J=26.4, S/H= 0.5, H/d=5.66, (S/d=2.83)*

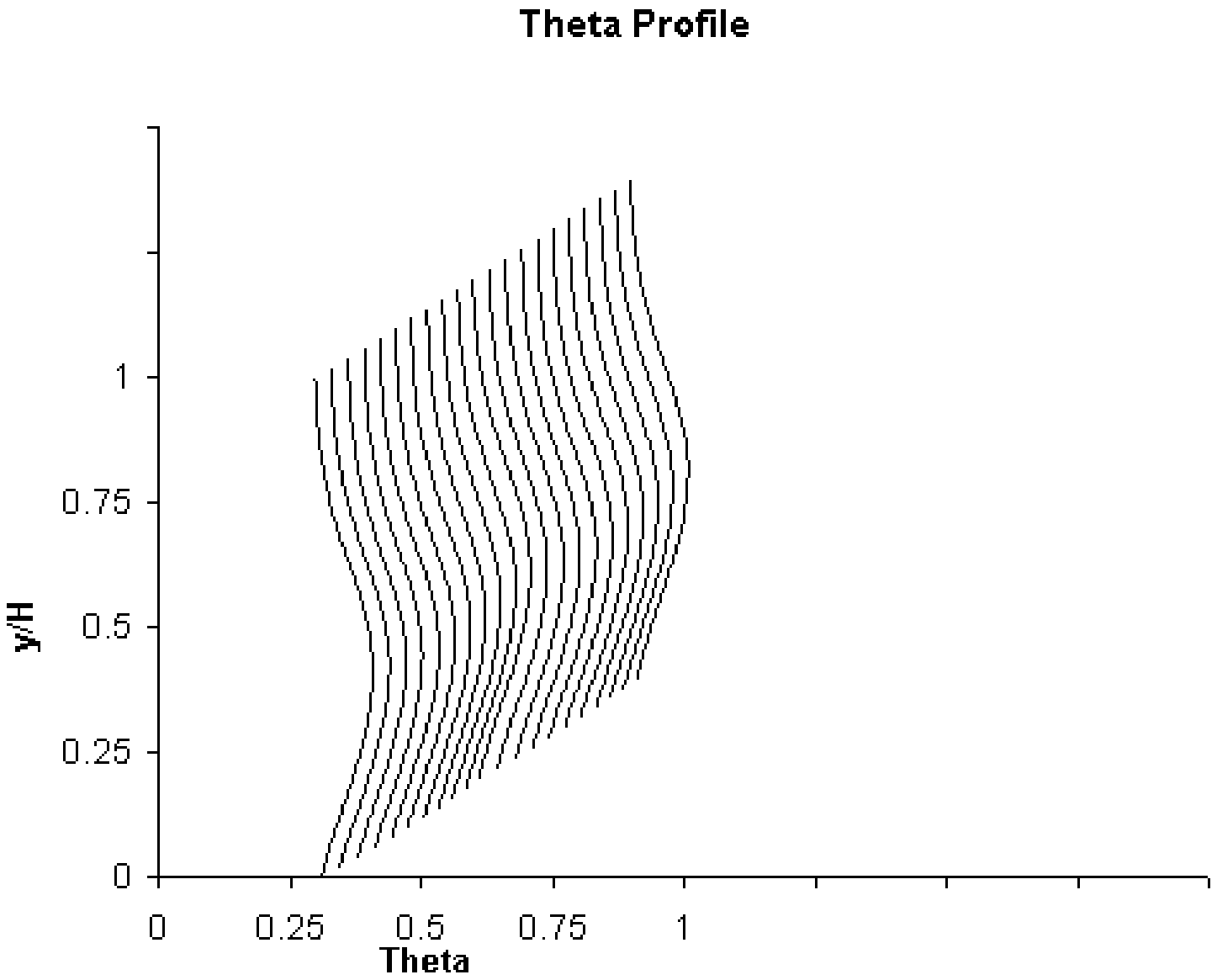


*x/H=2 (x/d=11.32)*

*J=26.4, S/H= 0.5, H/d=5.66, (S/d=2.83)*

Sequence 2

**Variations in scalar distributions with**
**Density ratio at constant velocity ratio**

*DR=0.45, 0.625, 1, 1.6, 2.2*

*x/H=0.5, R=7.66, S/H=0.5, H/d=4, $C_d$=0.64*

(cf. figure 7 in NASA TM–87294; see also
figure 10 in NASA/TM—2005-213137 and
figure 6 in NASA TM–83457)

## Theta Profile

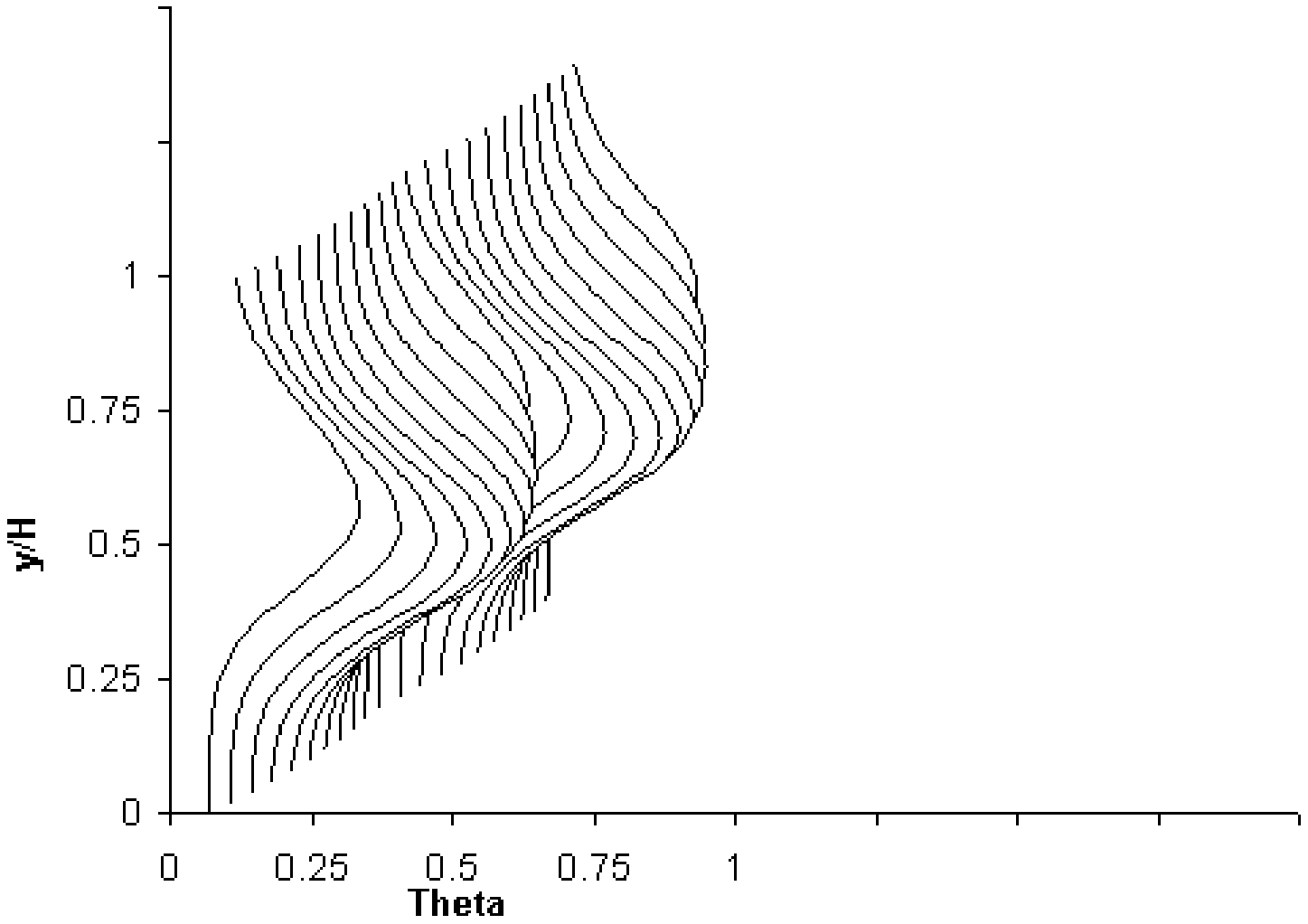


*x/H*=0.5, *S/H*=0.5, *H/d*=4, (*R=7.62)*

*DR=0.45* *J=26.4* *(M=3.46)*

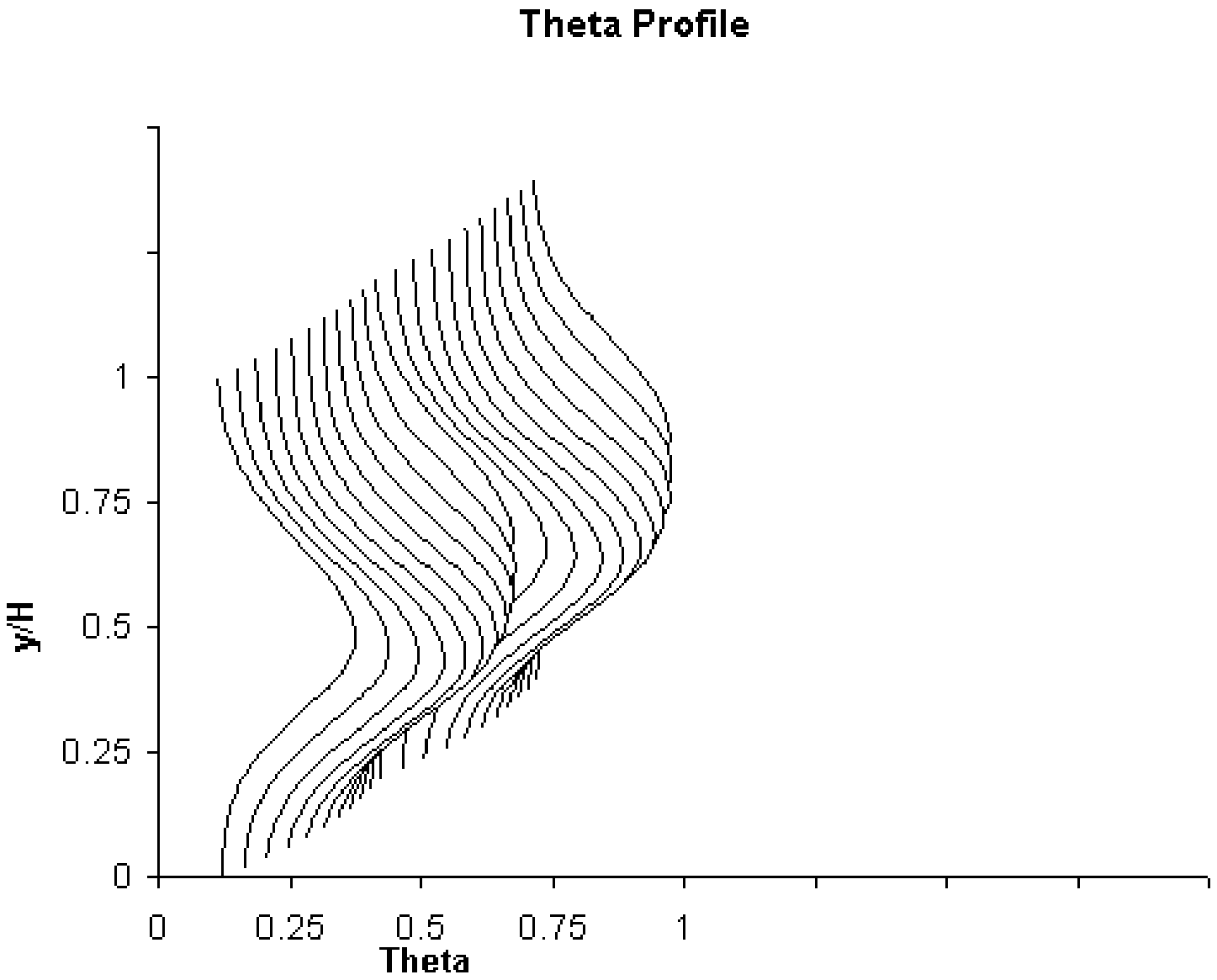


*x/H*=0.5, *S/H*=0.5, *H/d*=4, (*R=7.62)*

*DR=0.625* *J=36.67* *(M=4.76)*

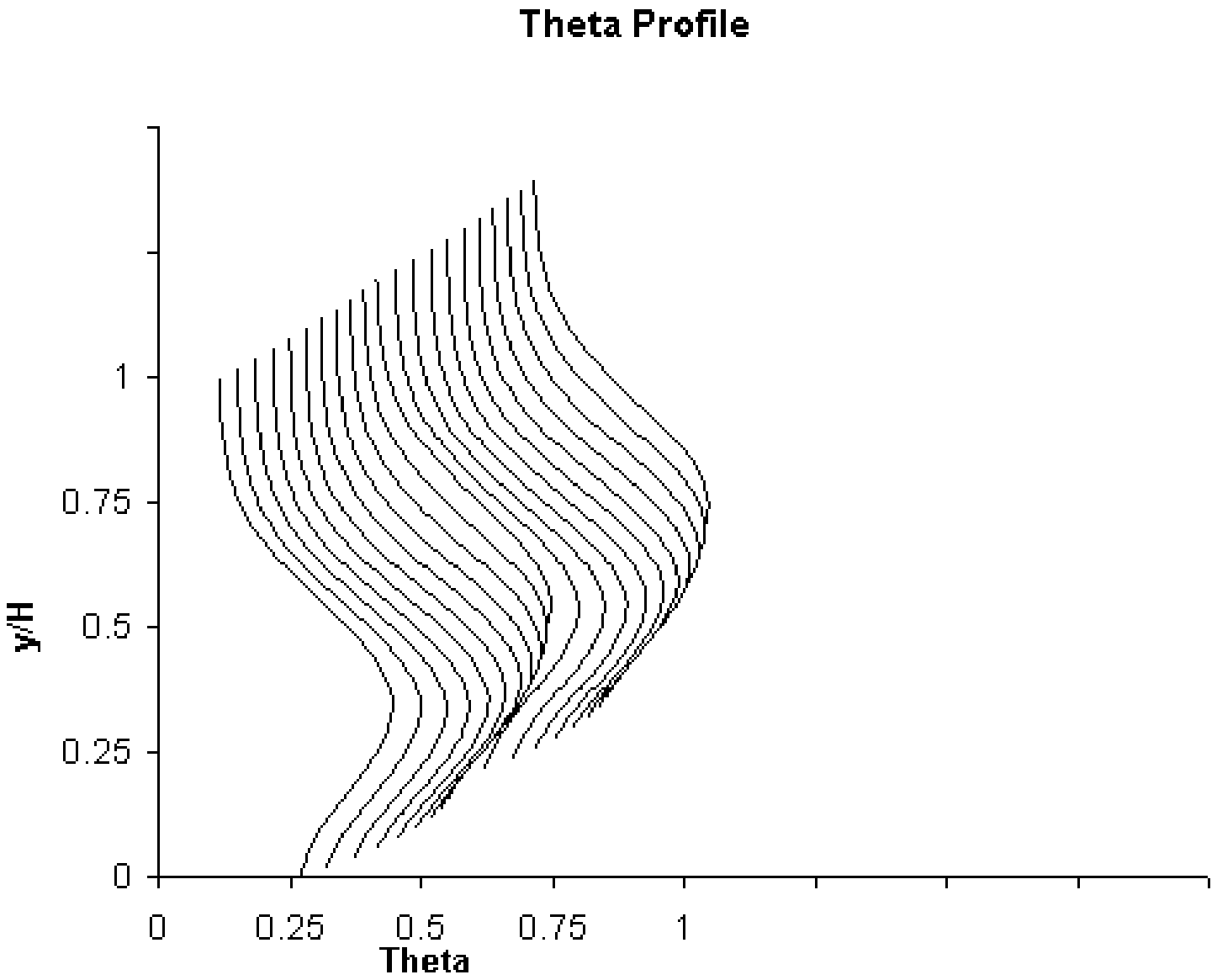


*x/H*=0.5, *S/H*=0.5, *H/d*=4, (*R=7.62)*

*DR=1* *J=58.68* *(M=7,62)*

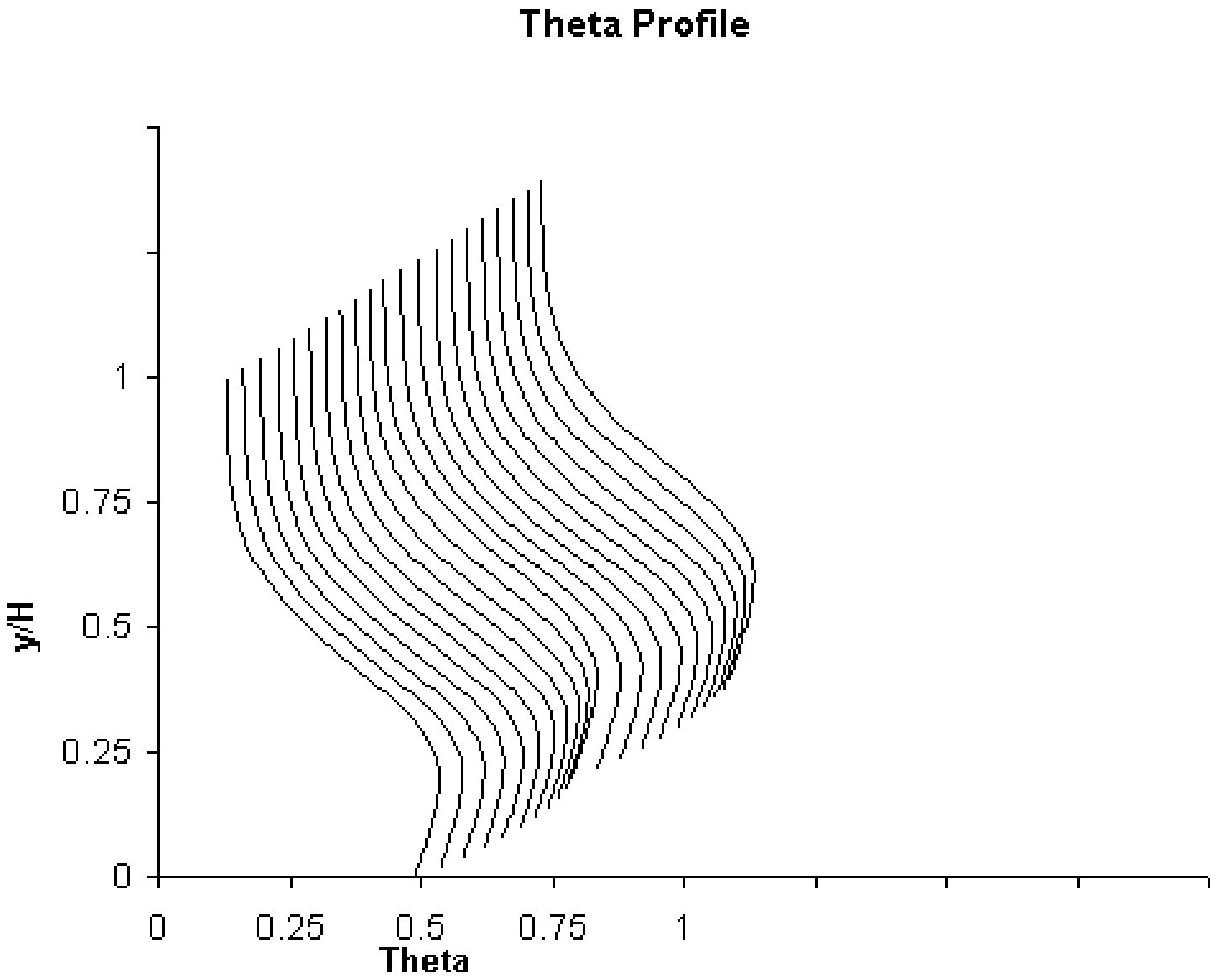


*x/H*=0.5, *S/H*=0.5, *H/d*=4, (*R=7.62)*

*DR=1.6* *J=93.88* *(M=12.1)*

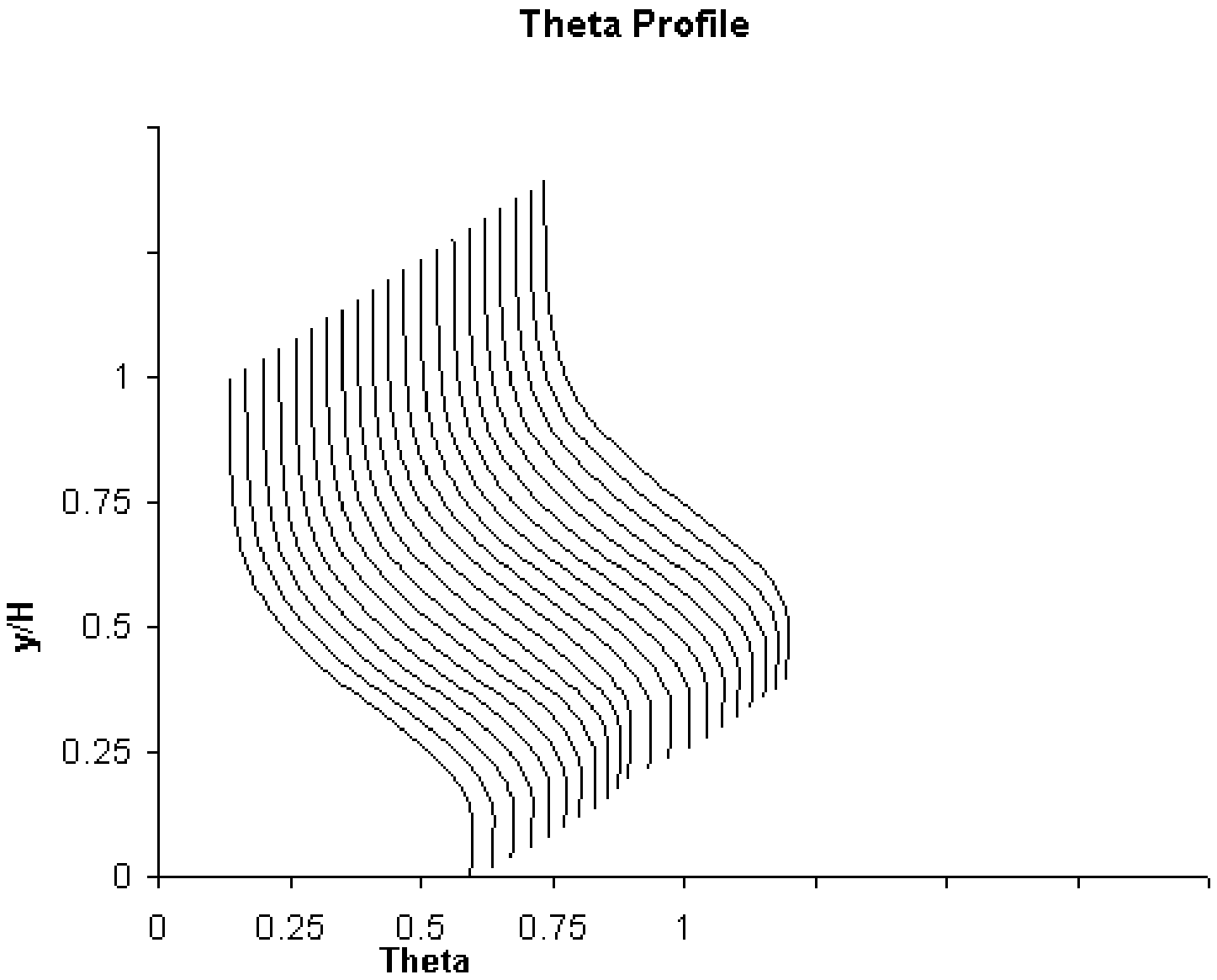


*x/H*=0.5, *S/H*=0.5, *H/d*=4, (*R=7.62)*

*DR=2.2* *J=129.09* *(M=16.76)*

Sequence 3

## Variations in scalar distributions with Density ratio at constant mass-flux ratio

*DR=0.45, 0.625, 1, 1.6, 2.2*

*x/H=0.5, M=3.45, S/H=0.5, H/d=4, $C_d$=0.64*

(cf. figure 7 in NASA TM–87294; see also figure 10 in NASA/TM—2005-213137 and figure 6 in NASA TM–83457)

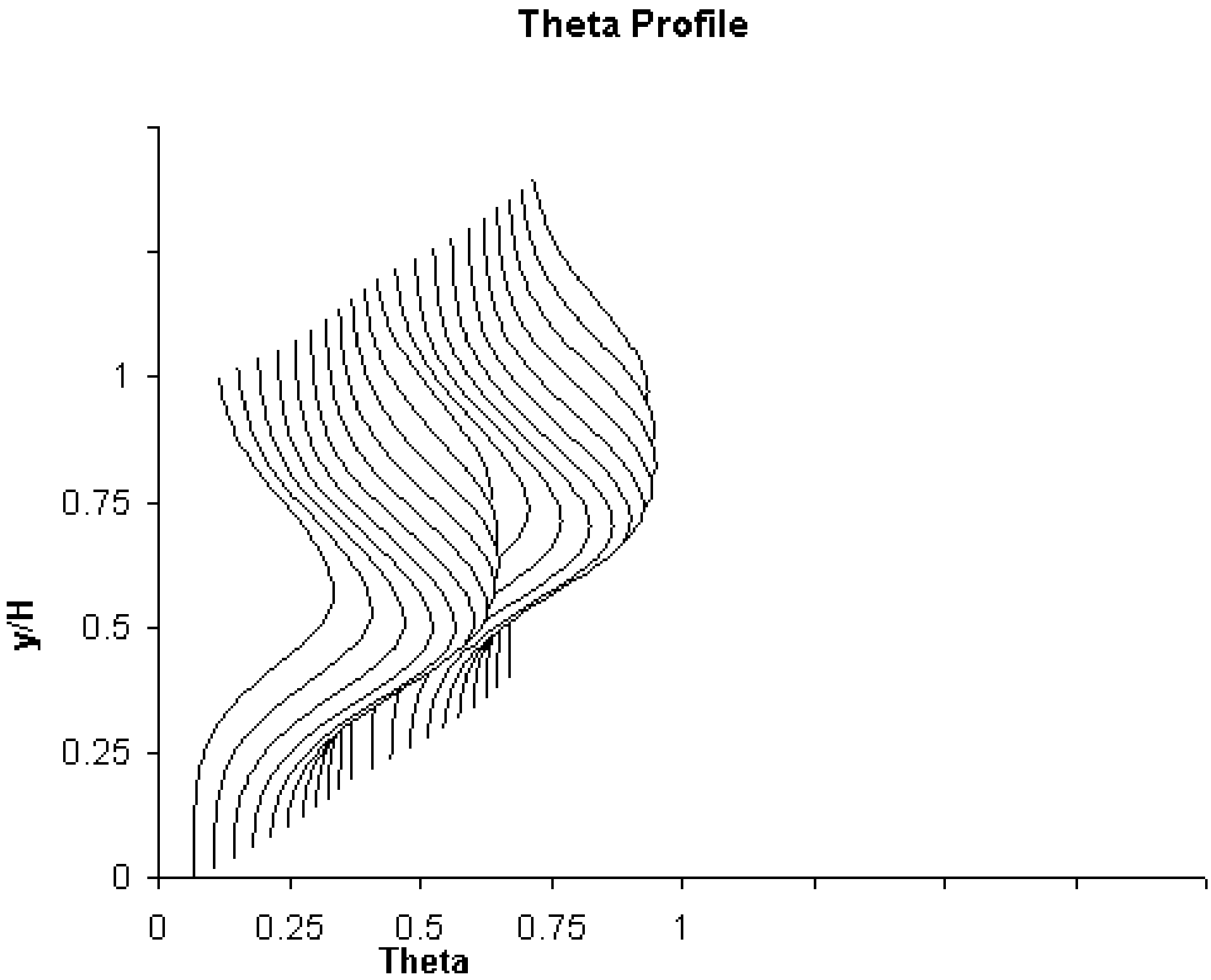


*x/H*=0.5, *S/H*=0.5, *H/d*=4, (*M=3.45)*

*DR=0.45* *J=26.45* *(R=7.55)*

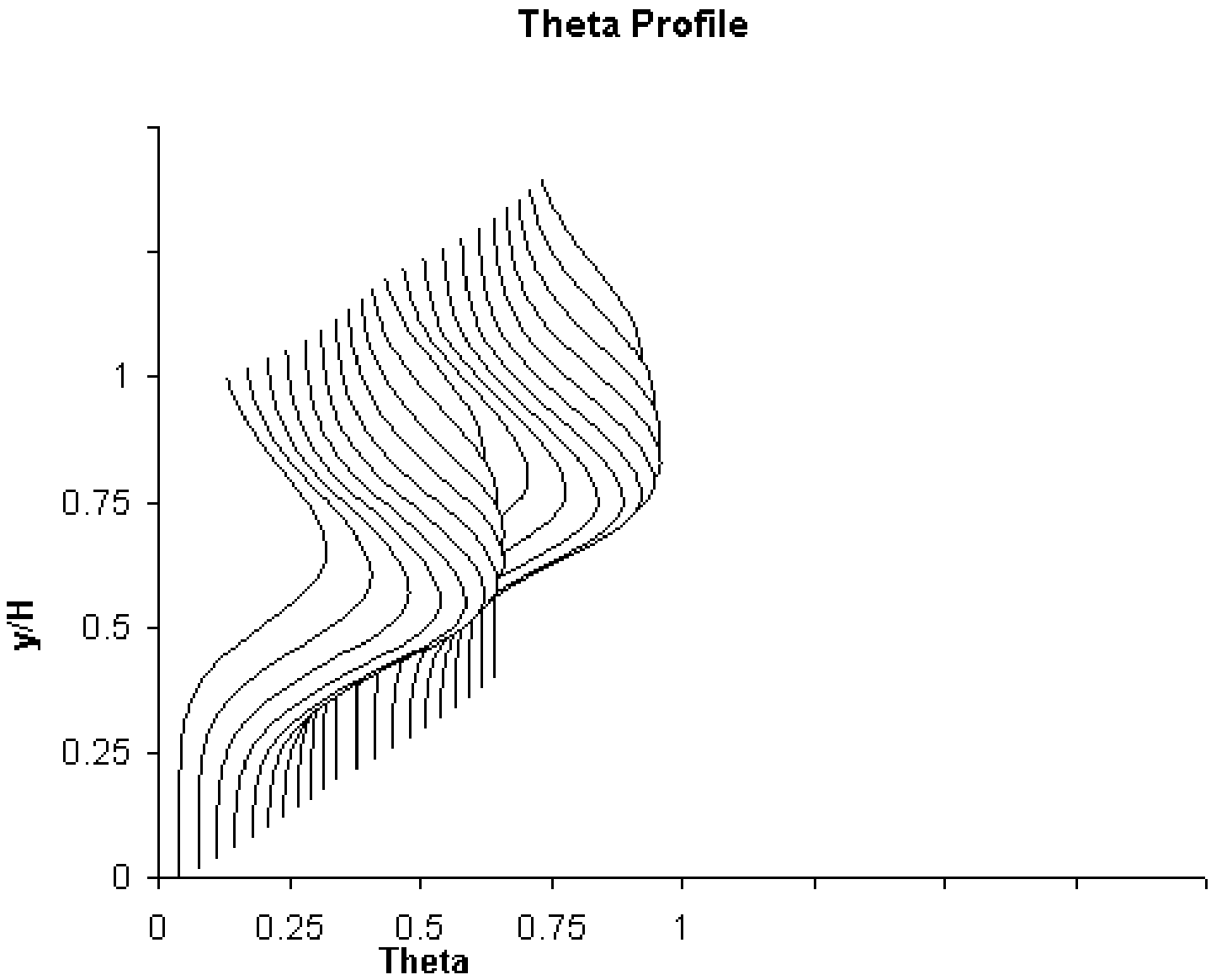


*x/H*=0.5, *S/H*=0.5, *H/d*=4, (*M=3.45)*

*DR=0.625* *J=19.04* *(R=5.52)*

## Theta Profile

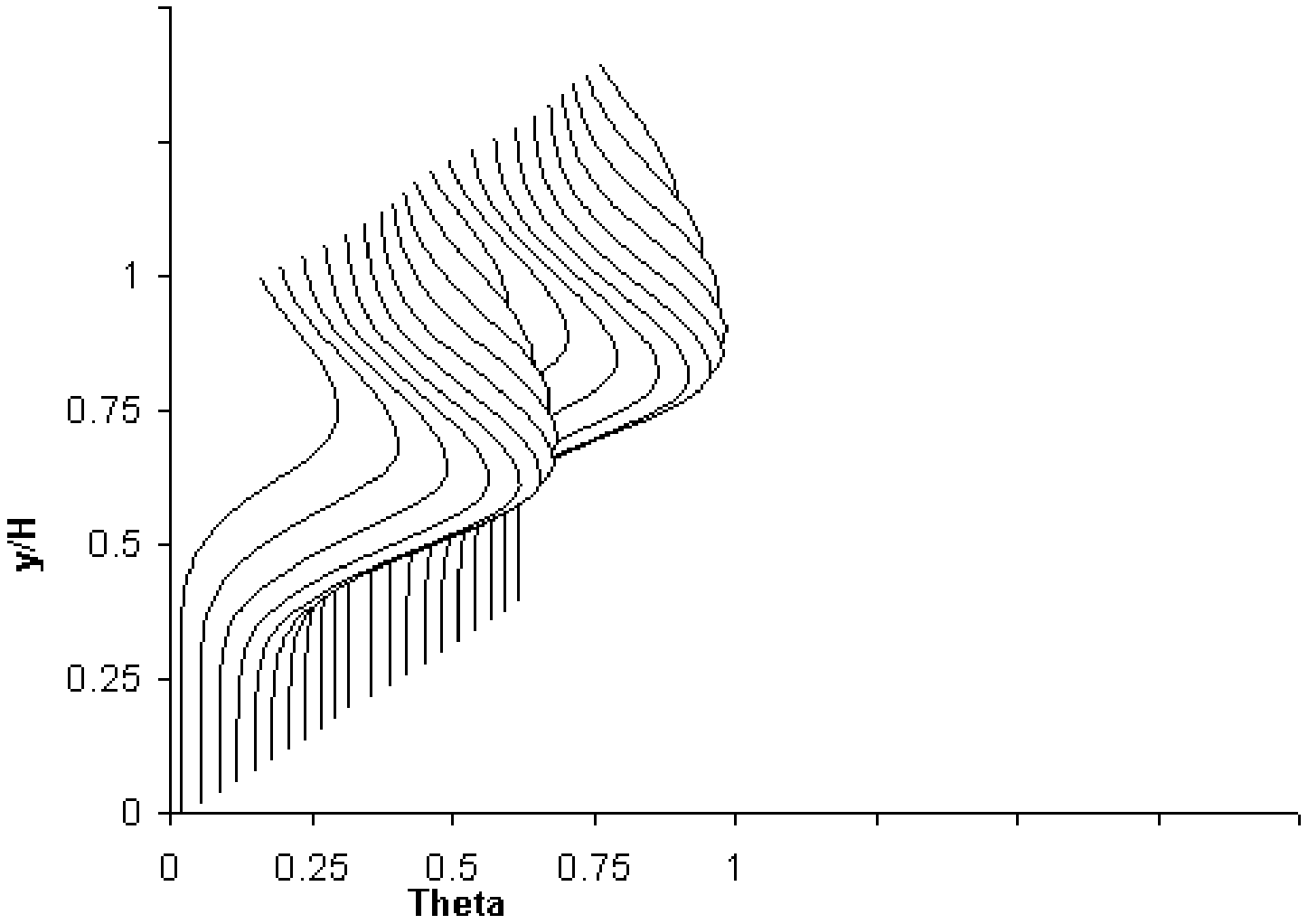


*x/H*=0.5, *S/H*=0.5, *H/d*=4, (*M=3.45)*

*DR=1* *J=11.9* *(R=3.45)*

## Theta Profile

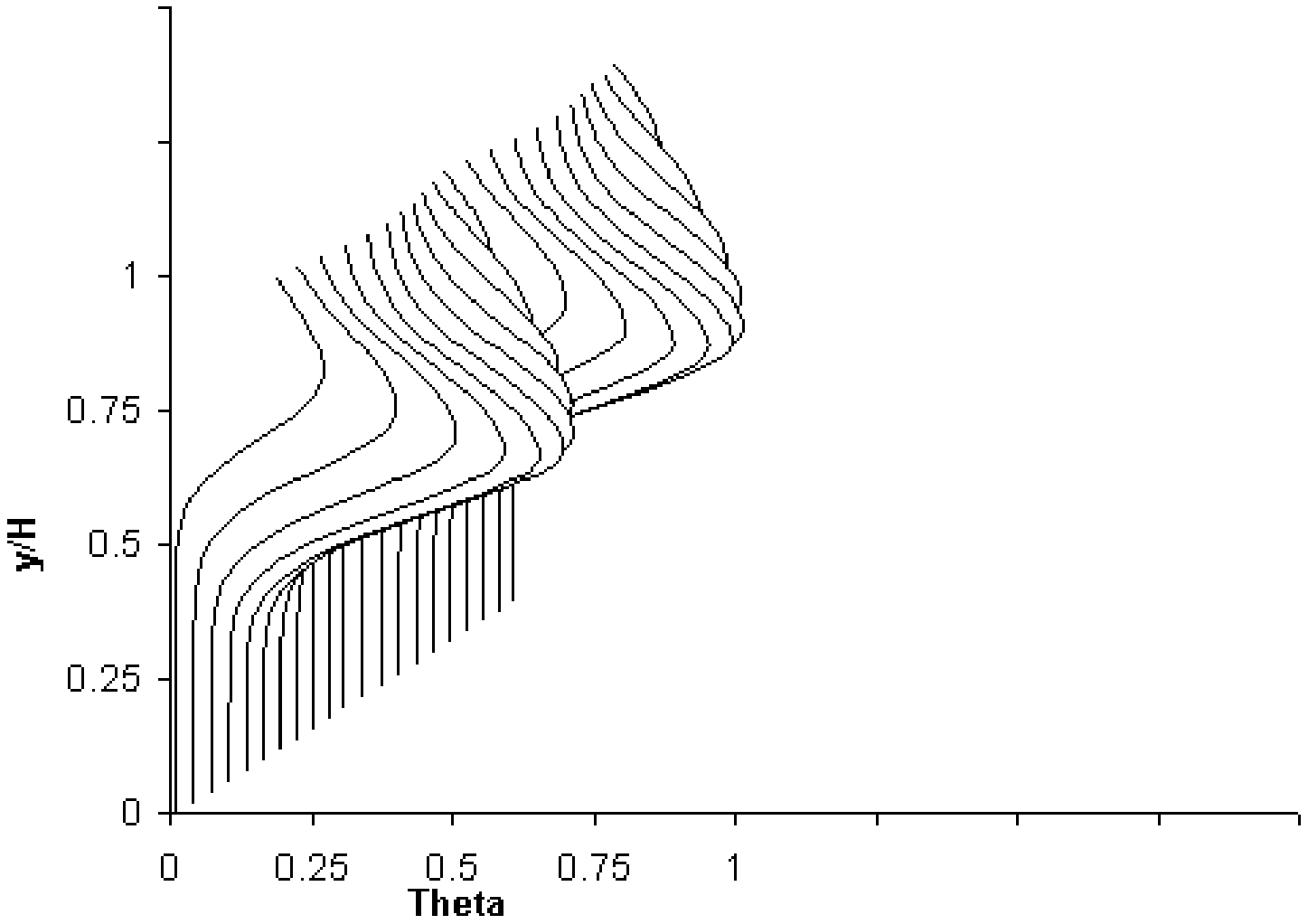


*x/H*=0.5, *S/H*=0.5, *H/d*=4, (*M=3.45)*

*DR=1.6* *J=7.44* *(R=2.16)*

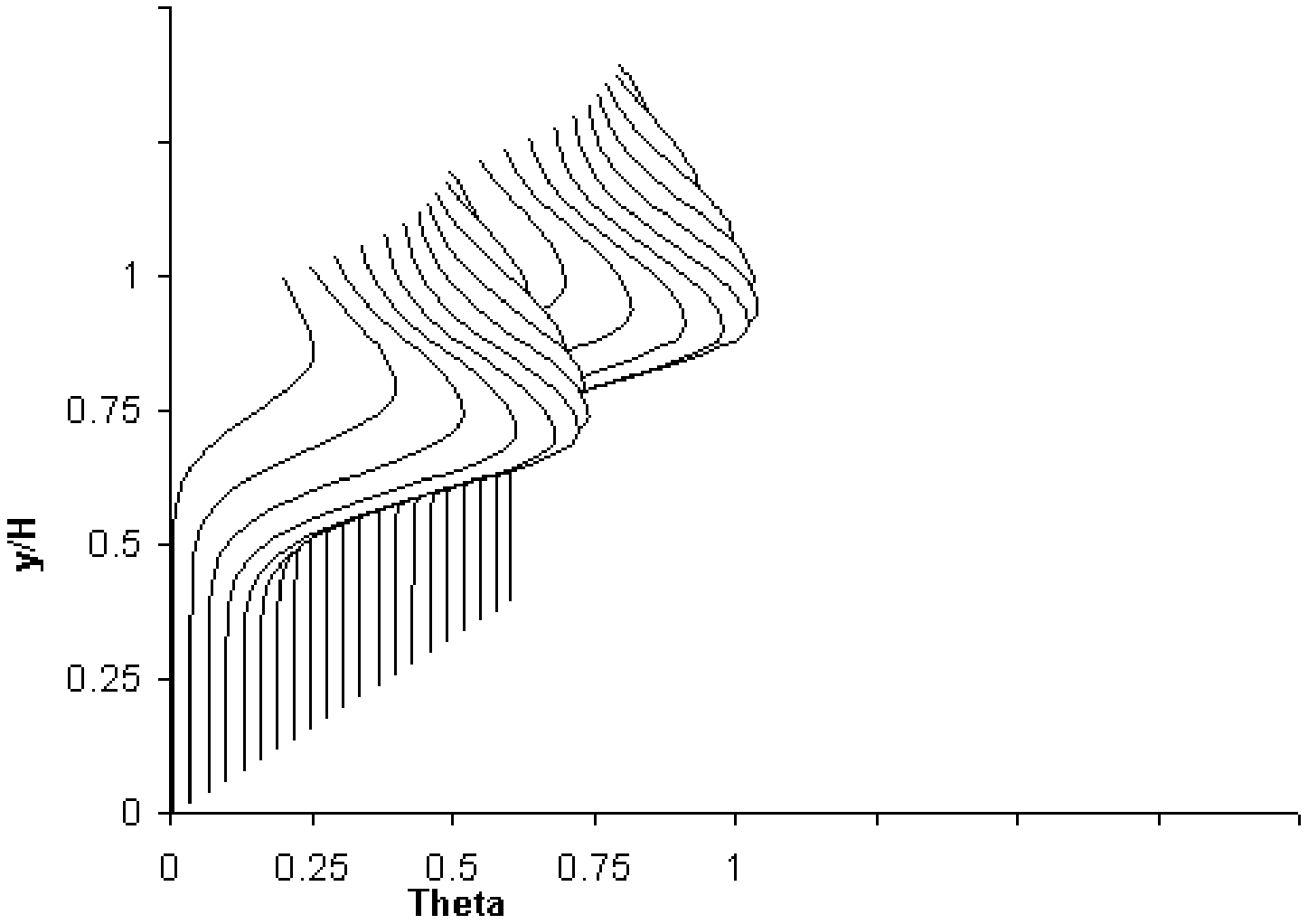


*x/H*=0.5, *S/H*=0.5, *H/d*=4, (*M=3.45)*

*DR=2.2* *J=5.41* *(R=1.56)*

Sequence 4

**Variations in scalar distributions with**
**Density ratio at constant momentum-flux ratio**

*DR=0.45, 0.625, 1, 1.6, 2.2*

*x/H=0.5, J=26.4, S/H=0.5, H/d=4, $C_d$=0.64*

(cf. figure 7 in NASA TM–87294; see also
figure 10 in NASA/TM—2005-213137 and
figure 6 in NASA TM–83457)

## Theta Profile

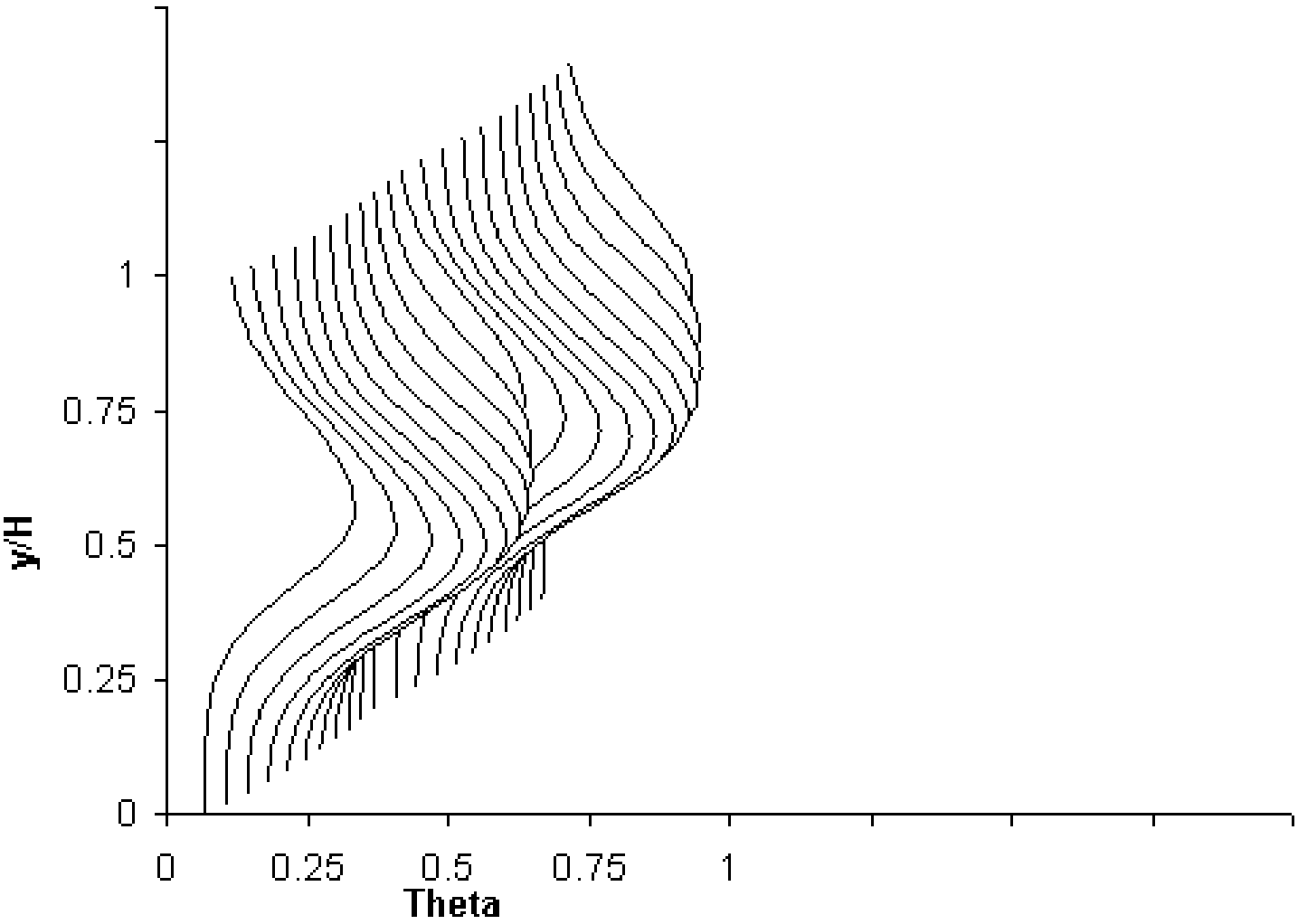


*x/H*=0.5, *S/H*=0.5, *H/d*=4, *J*=26.4

*DR=0.45* *(M=3.46* *R=7.62)*

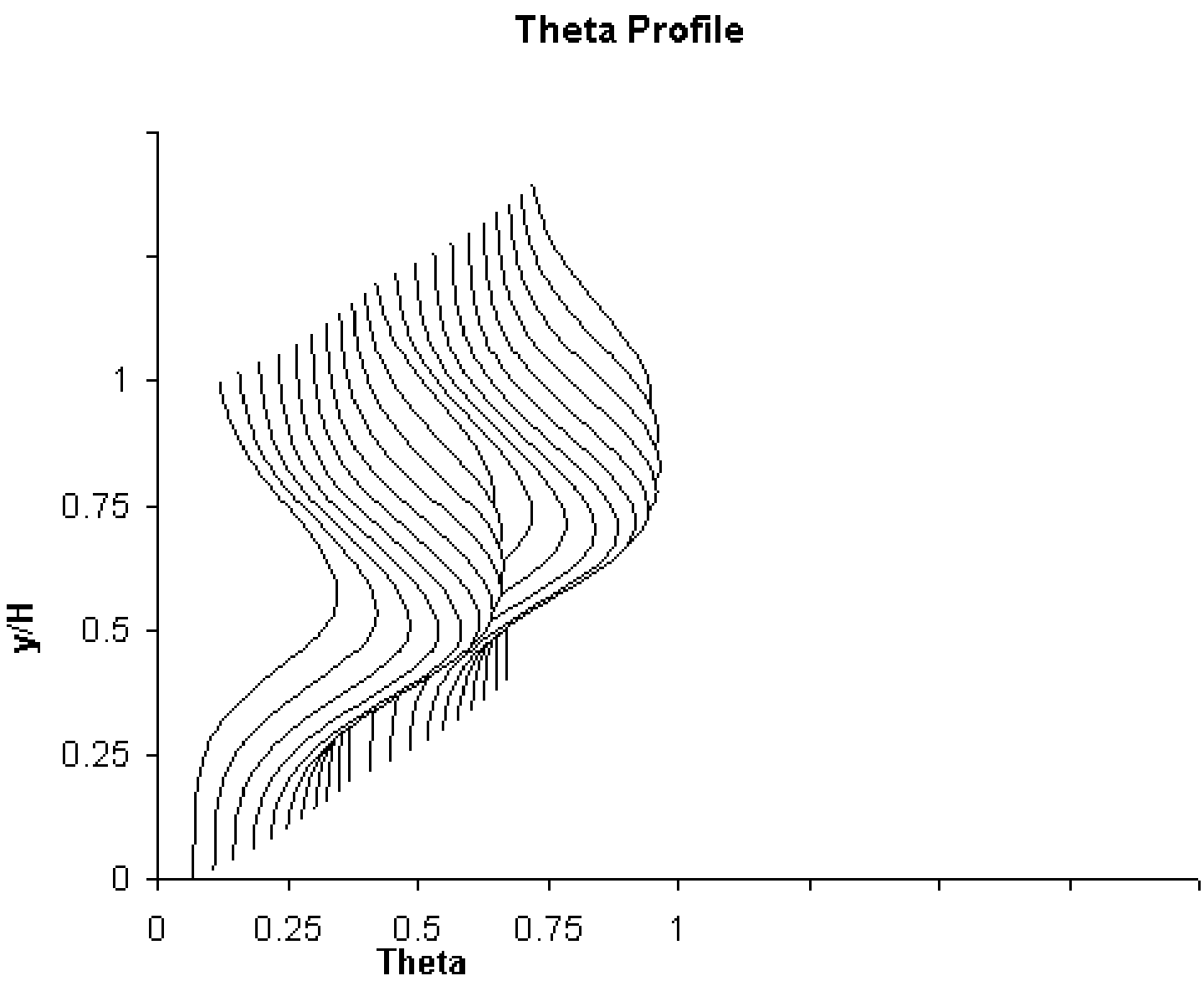


*x/H*=0.5, *S/H*=0.5, *H/d*=4, *J*=26.4

*DR=0.625* *(M=4,06* *R=6.5)*

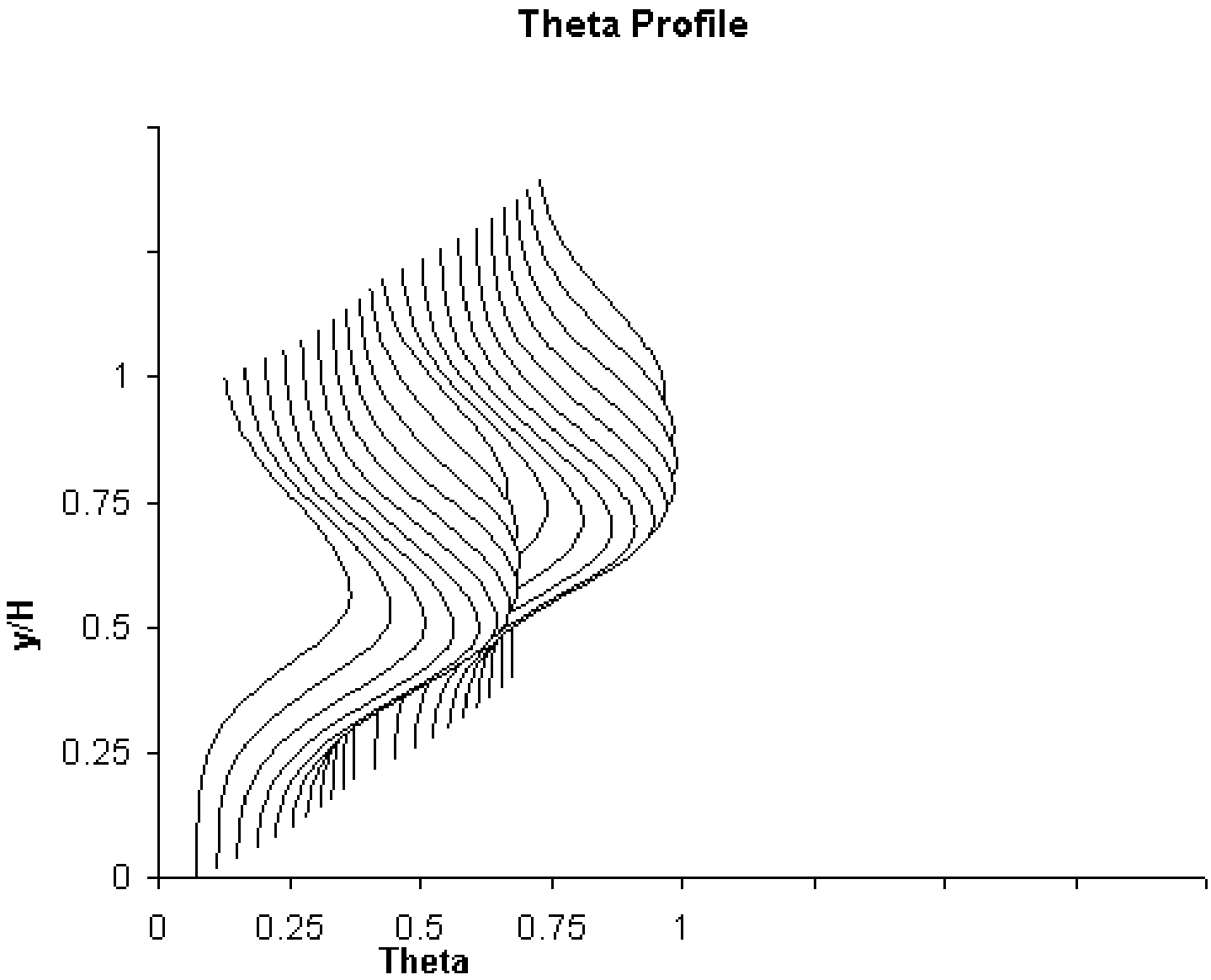


*x/H*=0.5, *S/H*=0.5, *H/d*=4, *J*=26.4

*DR=1* *(M=5.14* *R=5.14)*

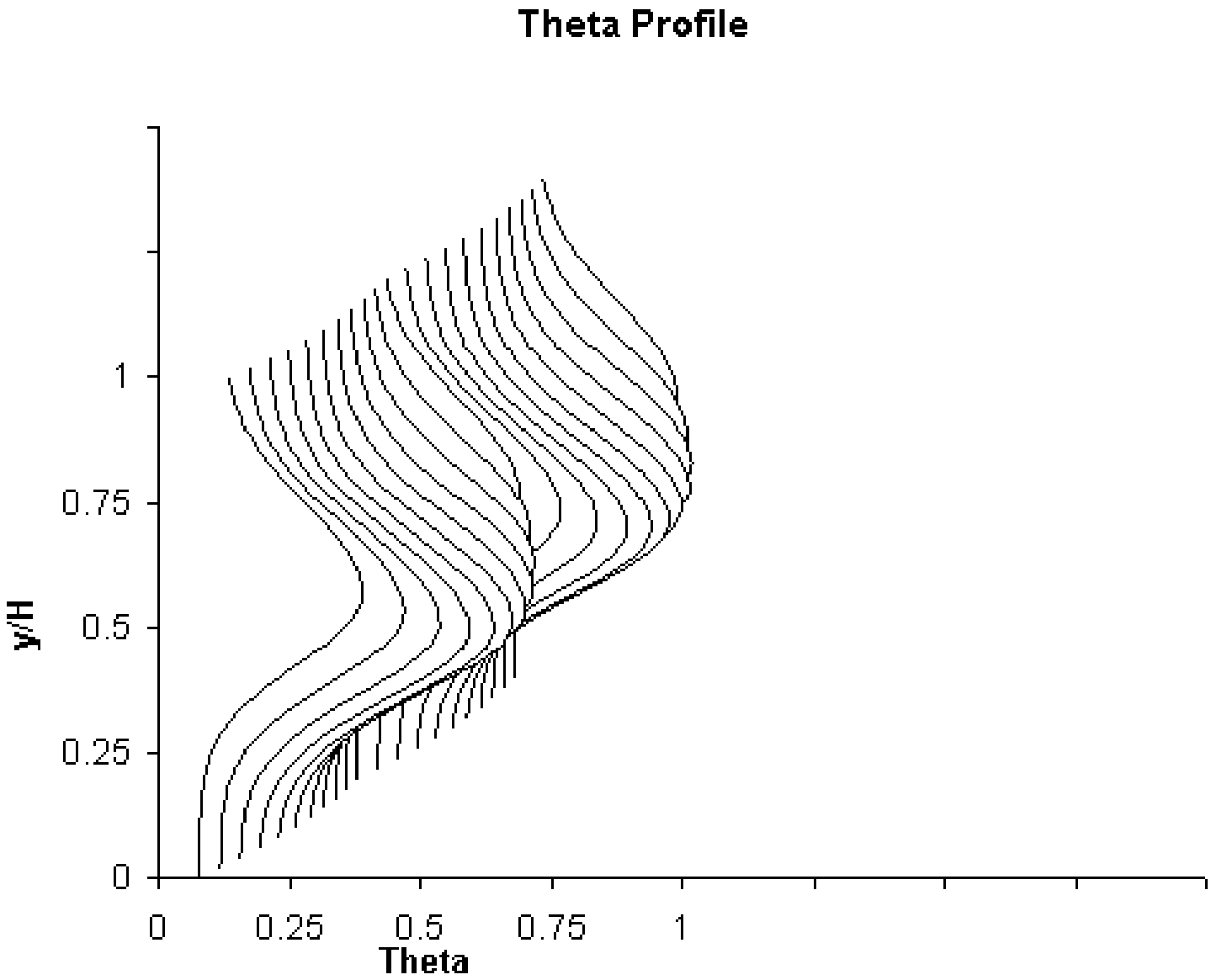


*x/H*=0.5, *S/H*=0.5, *H/d*=4, *J*=26.4

*DR=1.6* *(M=6.5* *R=4.06)*

## Theta Profile

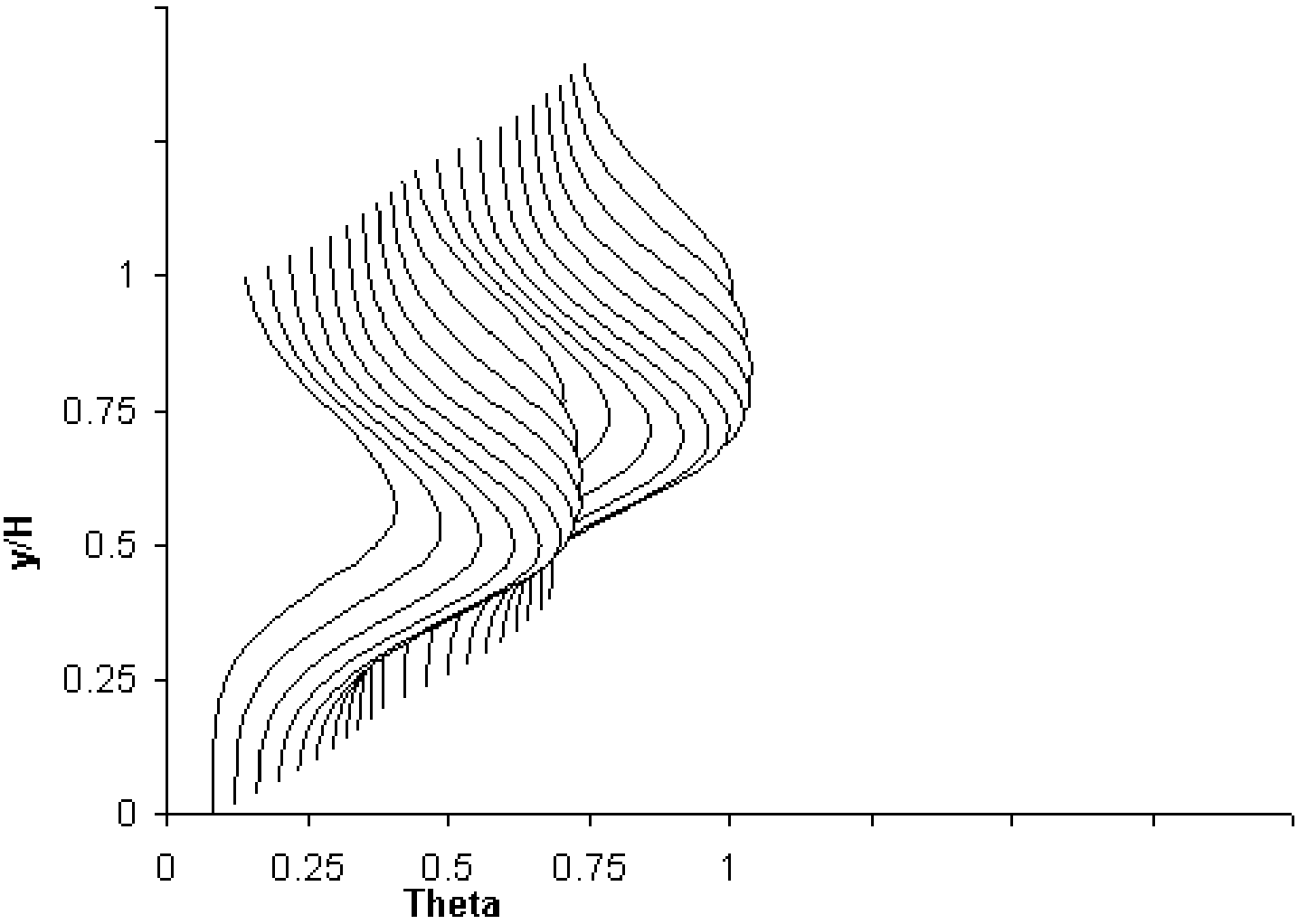


*x/H*=0.5, *S/H*=0.5, *H/d*=4, *J*=26.4

*DR=2 .2* *(M=7.62* *R=3.46)*

Sequence 5

## Variations in scalar distributions with Increasing momentum-flux ratio

*J=6.6, 8.8, 16, 26.4, 35.2, 64, 105.6*

*x/H=0.5, DR=2.2, S/H=0.5. H/d=5.66, $C_d$=0.64*

(cf. figure 9 in NASA/TM—2005-213137 and
figure 5 in NASA TM–83457; see also
figure 6 in NASA TM–87294)

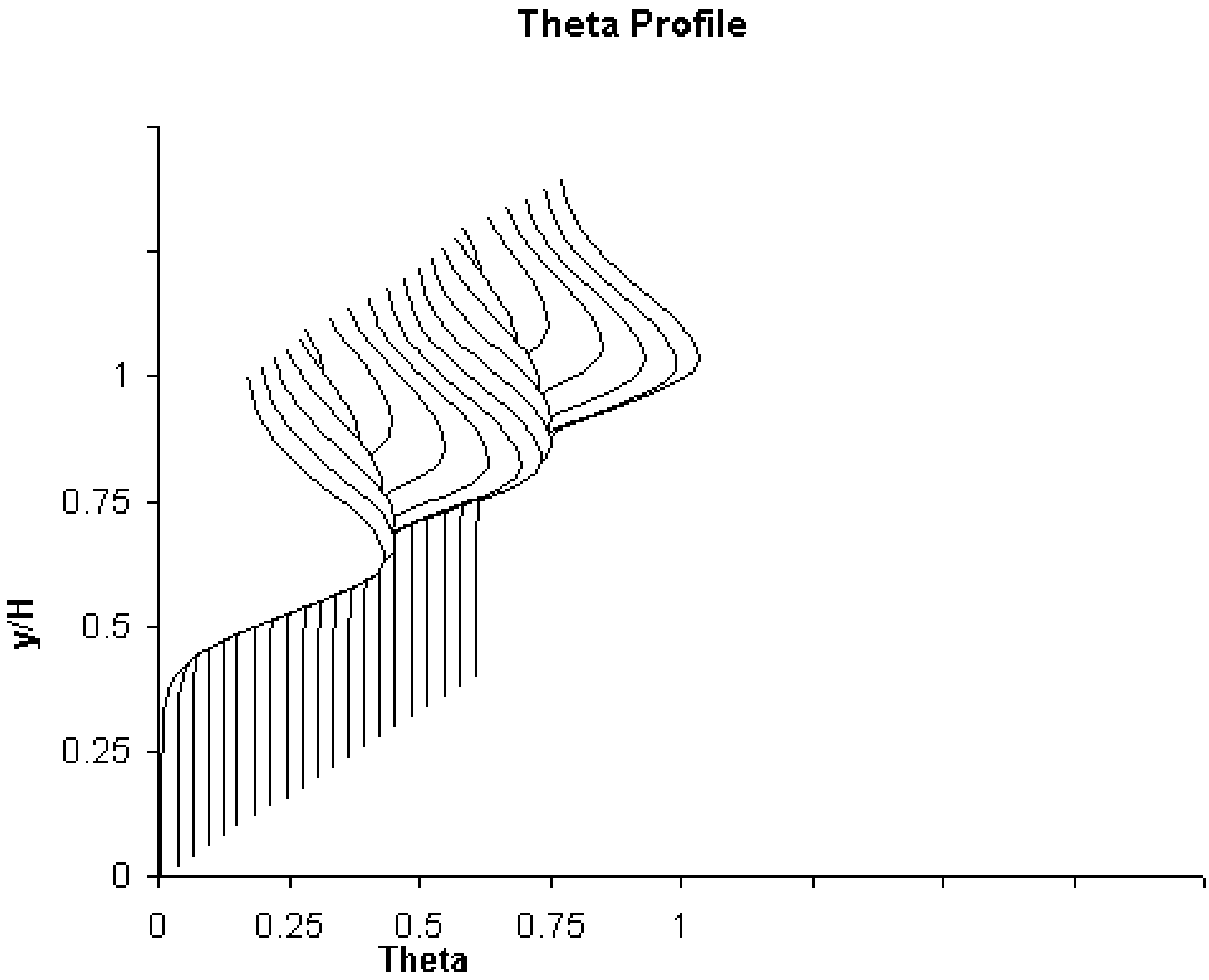


*x/H=0.5, S/H=0.5, H/d=5.66, (S/d=2.83. x/d=2.83)*

*J=6.6 (M=3.81 R=1.73)*

## Theta Profile

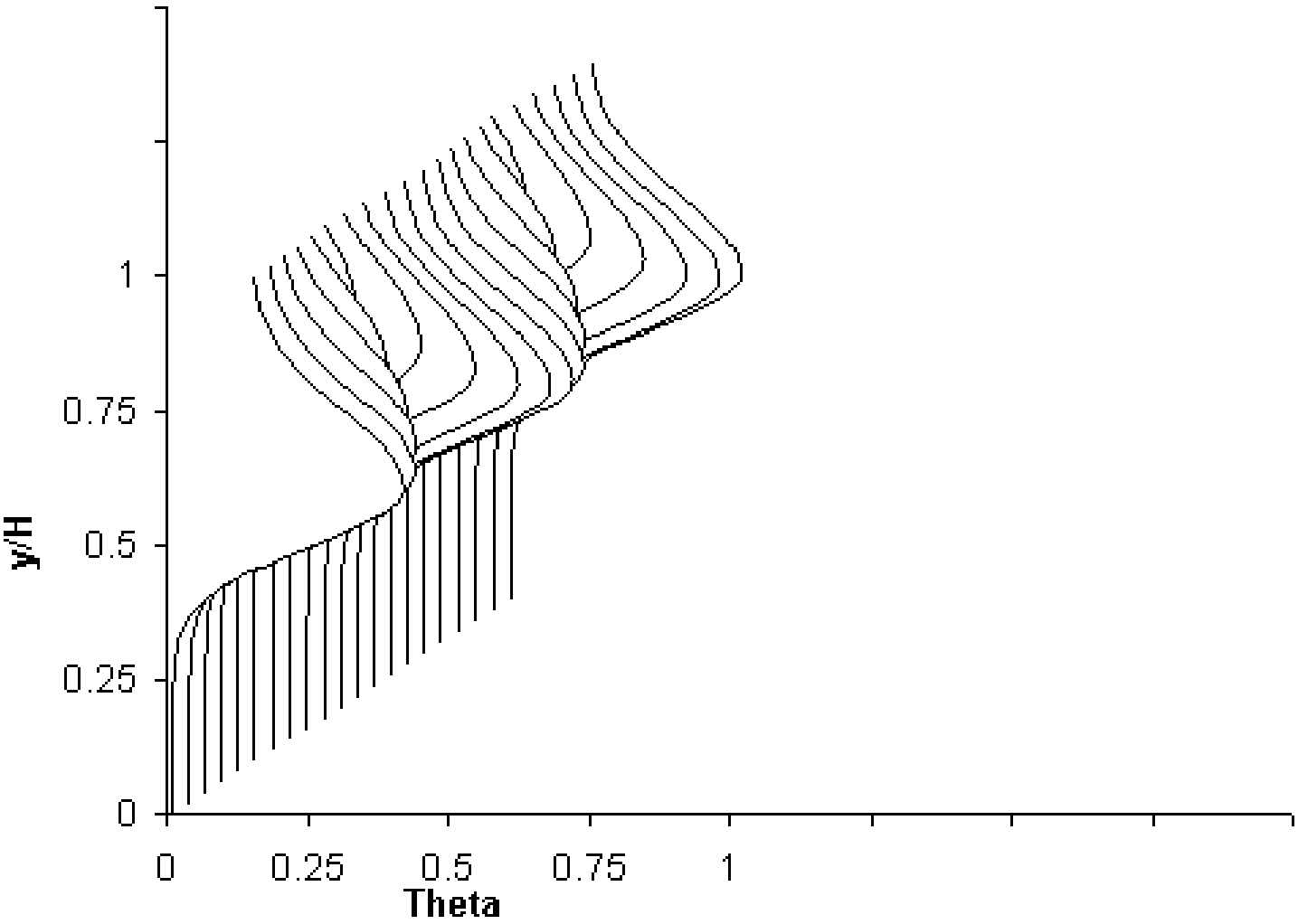


*x/H=0.5, S/H=0.5, H/d=5.66, (S/d=2.83, x/d=2.83)*

*J=8.8 (M=4.4 R=2)*

## Theta Profile

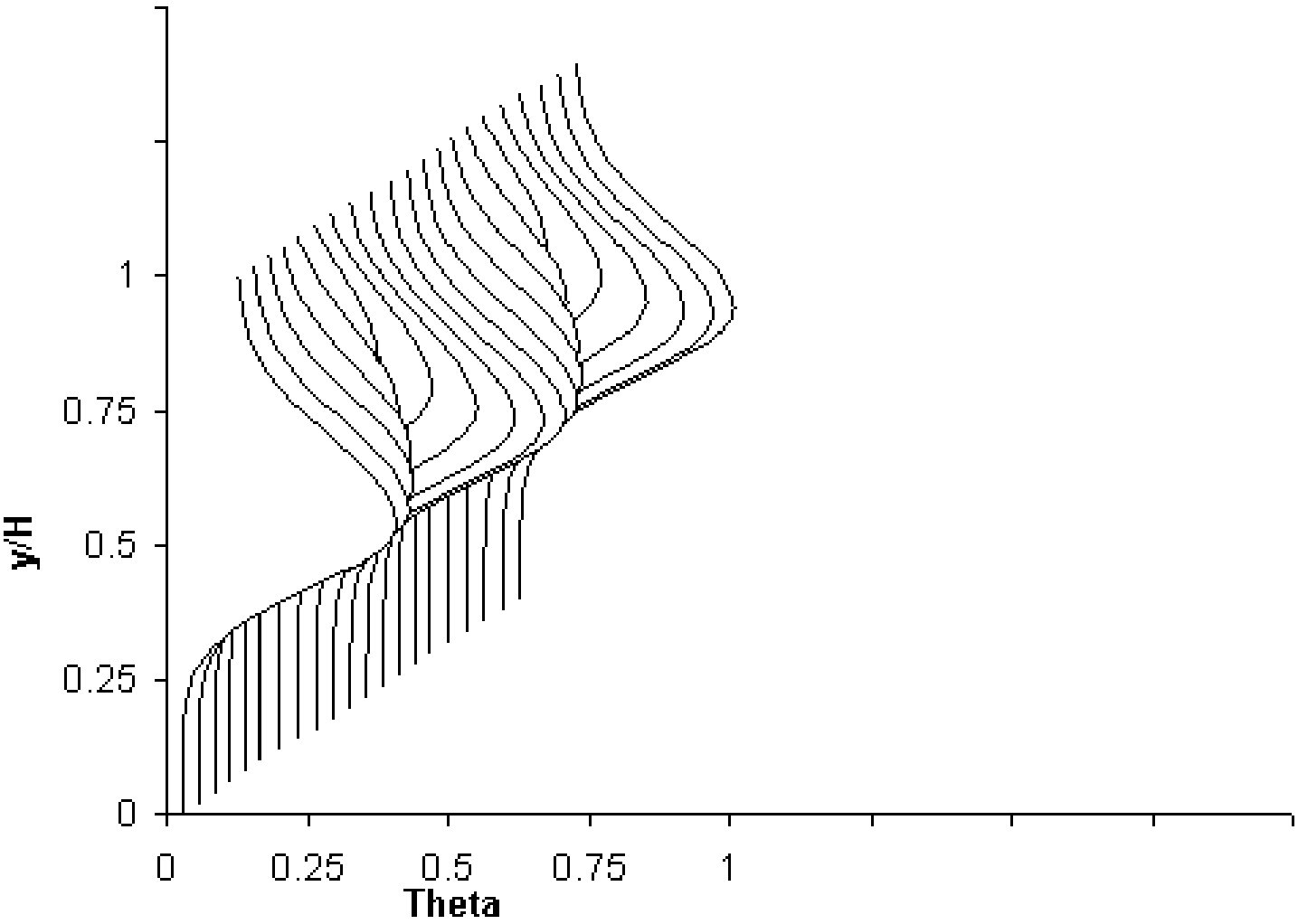


*x/H=0.5, S/H=0.5, H/d=5.66, (S/d=2.83, x/d=2.83)*
*J=16 (M=5.93 R=2.7)*

## Theta Profile

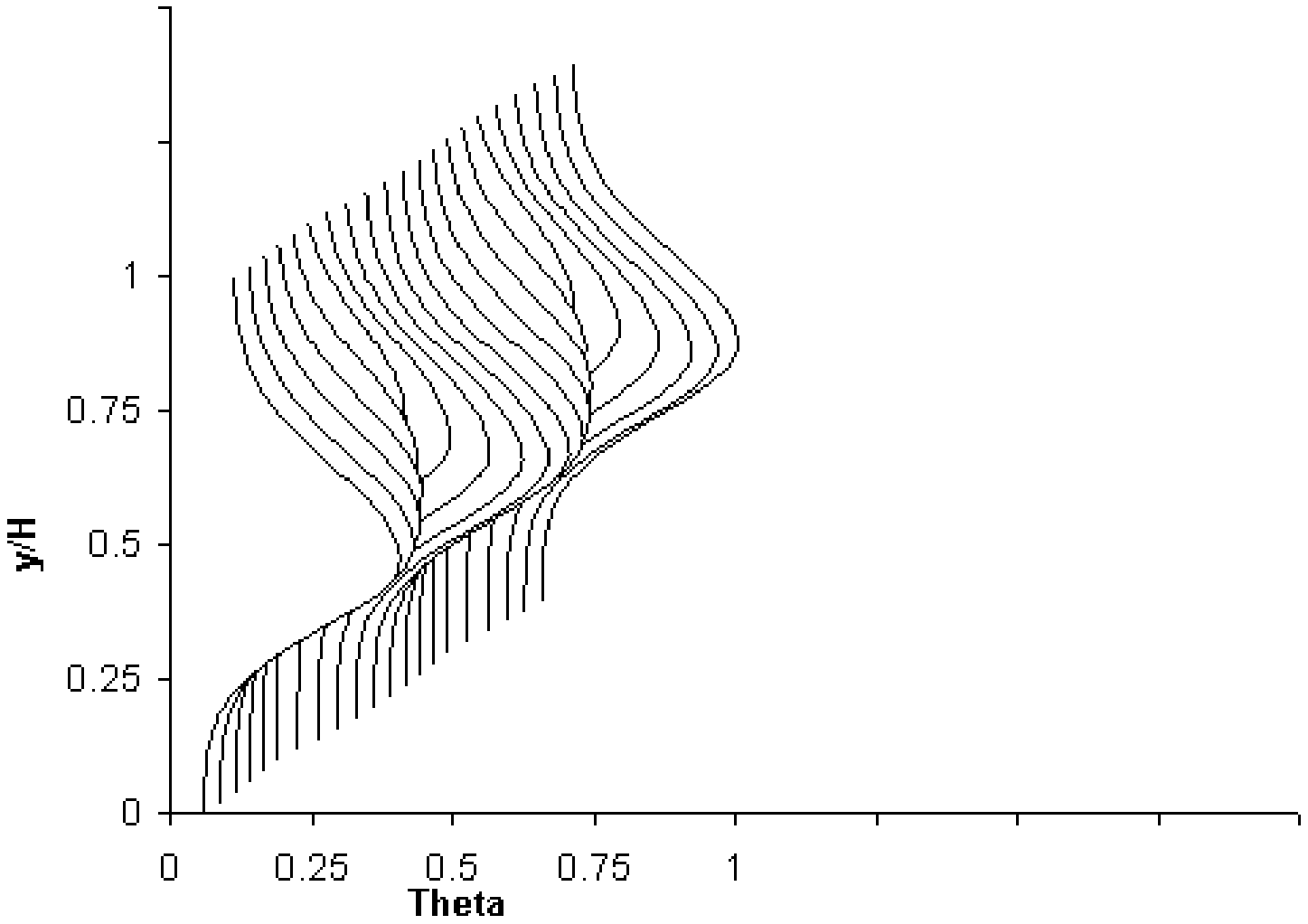


*x/H=0.5, S/H=0.5, H/d=5.66, (S/d=2.83, x/d=2.83)*

*J=26.4 (M=7.62 R=3.46)*

## Theta Profile

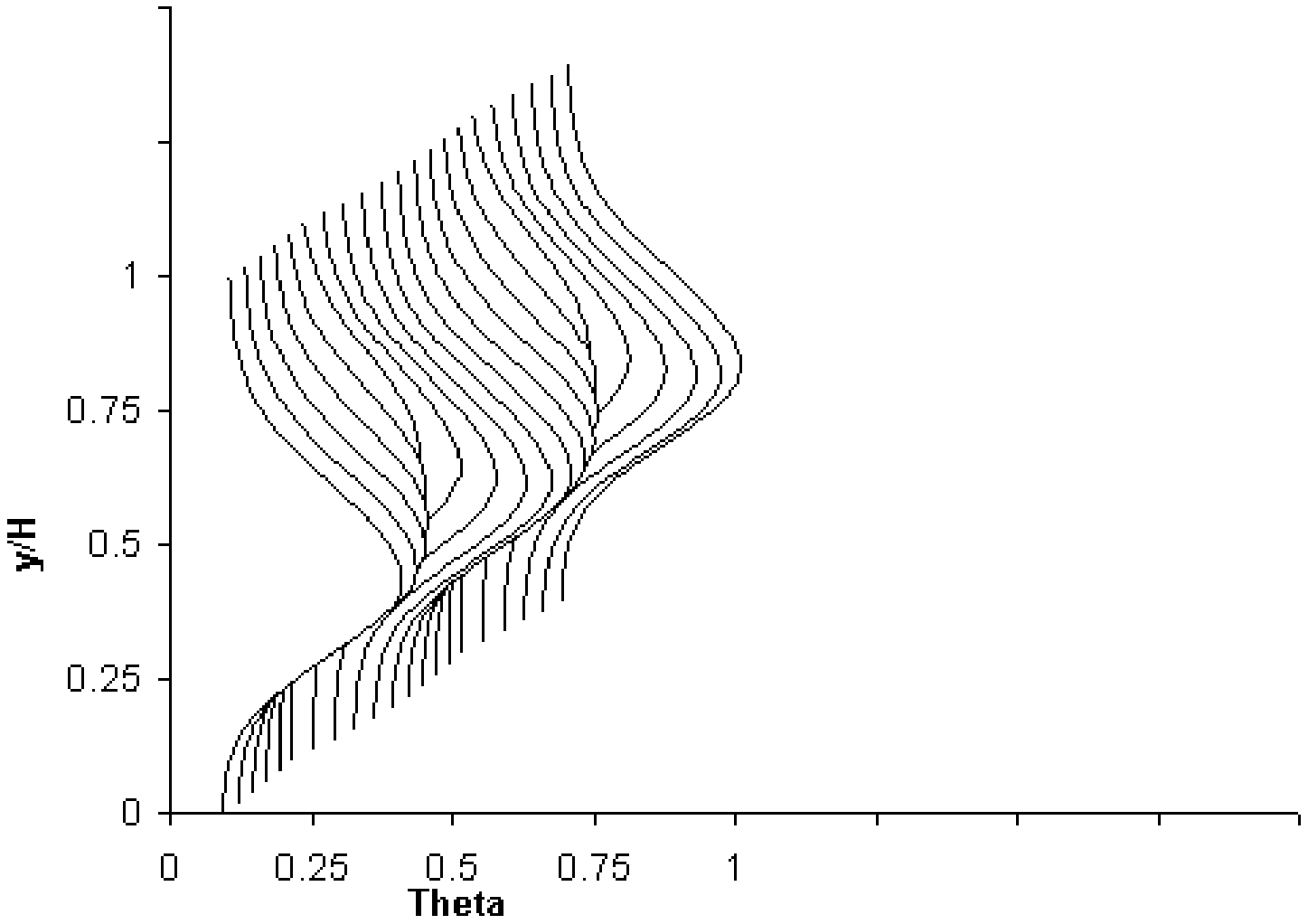


*x/H=0.5, S/H=0.5, H/d=5.66, (S/d=2.83, x/d=2.83)*

*J=35.2 (M=8.8 R=4)*

## Theta Profile

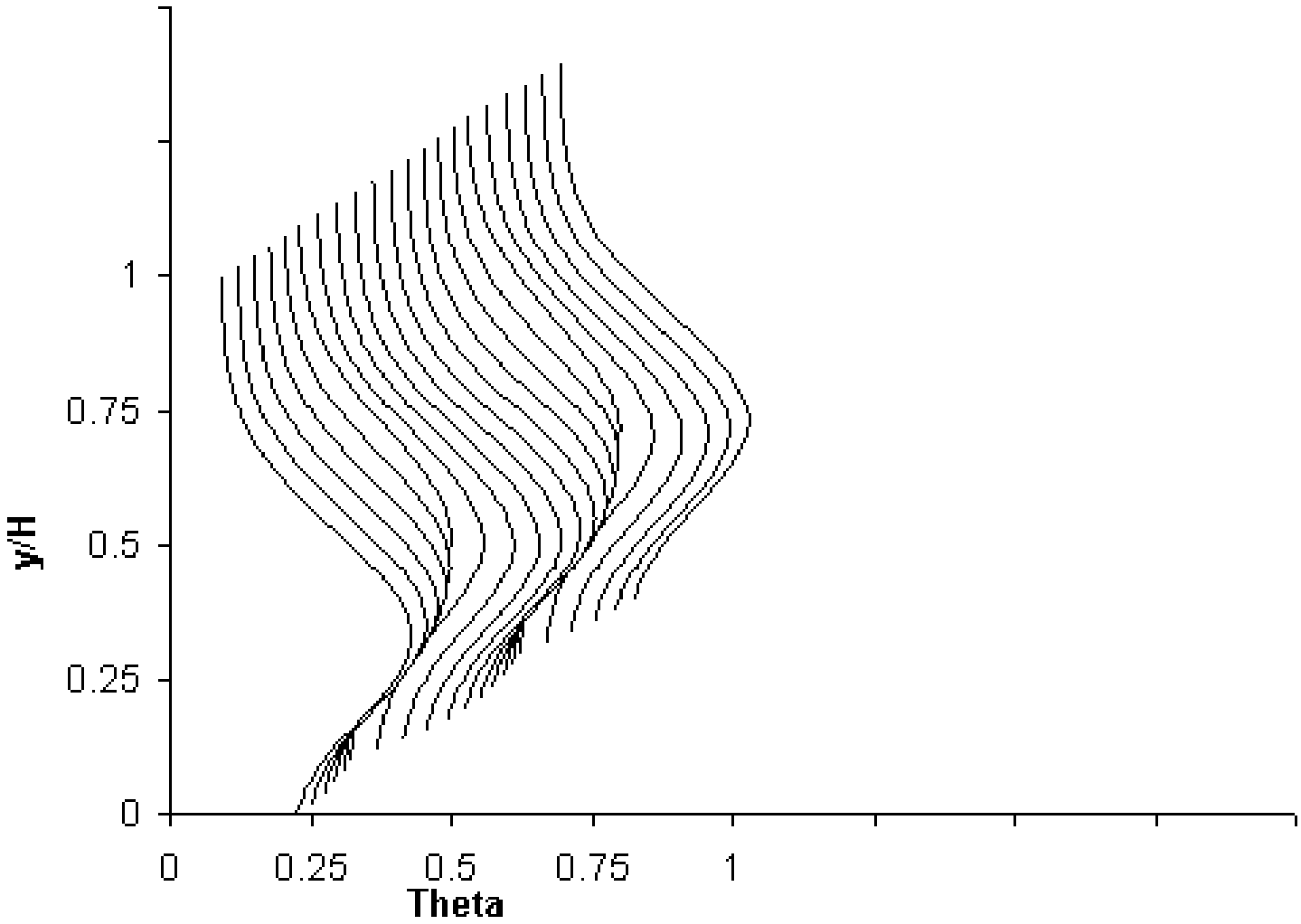


*x/H=0.5, S/H=0.5, H/d=5.66, (S/d=2.83, x/d=2.83)*

*J=64 (M=11.87 R=5.39)*

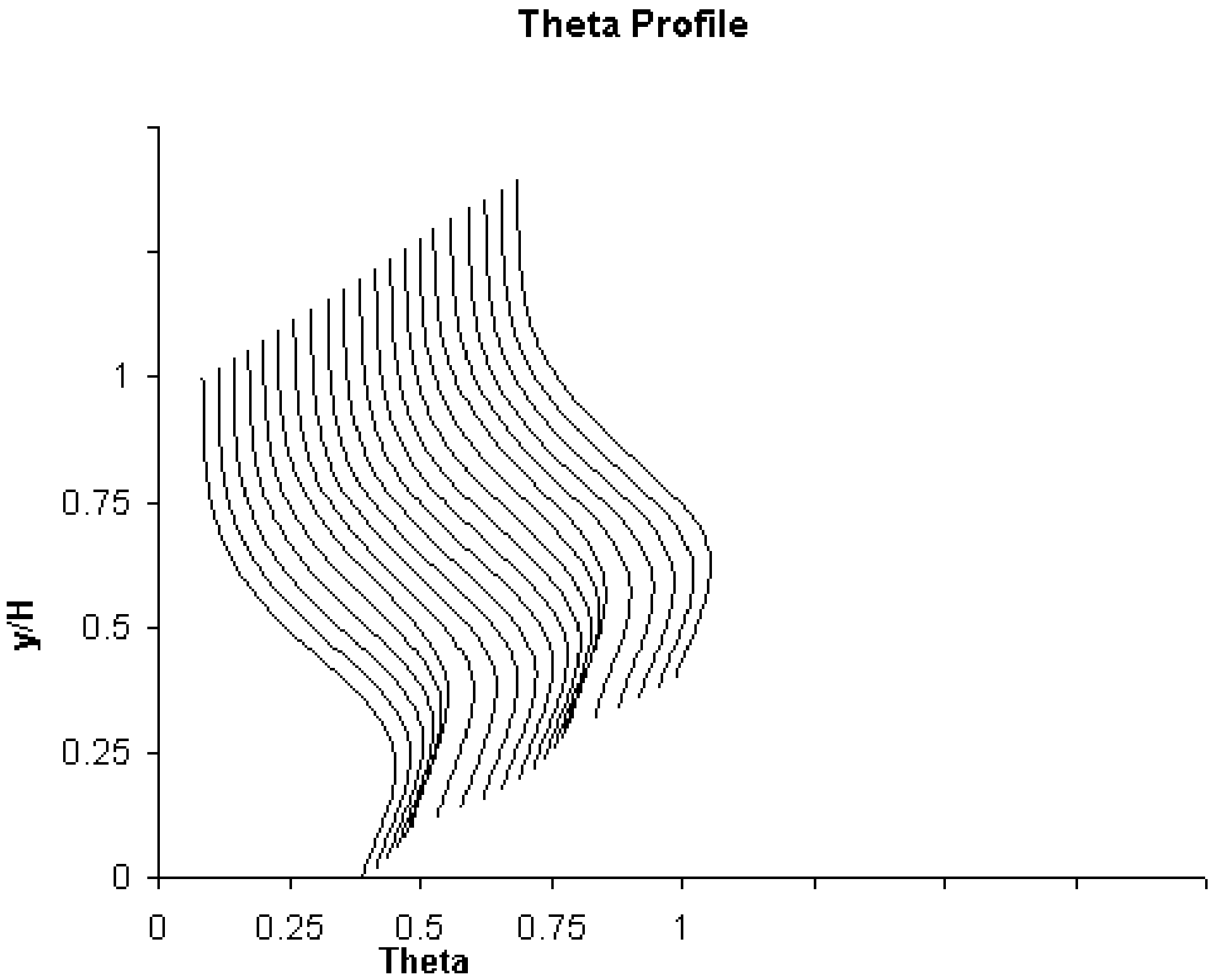


*x/H=0.5, S/H=0.5, H/d=5.66, (S/d=2.83, x/d=2.83)*

*J=105.6 (M=15.24 R=6.93)*

Sequence 6

## Variations in scalar distributions with Orifice spacing and diameter at constant orifice area

*S/H*=0.25; *H/d*=8
*S/H*=0.321; *H/d*=7.06
*S/H*=0.433; *H/d*=6.08
*S/H*=0.5; *H/d*=5.66
*S/H*=0.642; *H/d*=4.49
*S/H*=0.866; *H/d*=4.3
*S/H*=1; *H/d*=4

*x/H=0.5, DR=2.2, J=26.4, $C_d$=0.64*

(cf. figures 8(a) and 8(b) in (cf. figures 8(a) and 8(b) and, figures 3 and 4 in NASA TM–83457; see also figure 5 in NASA TM–87294)

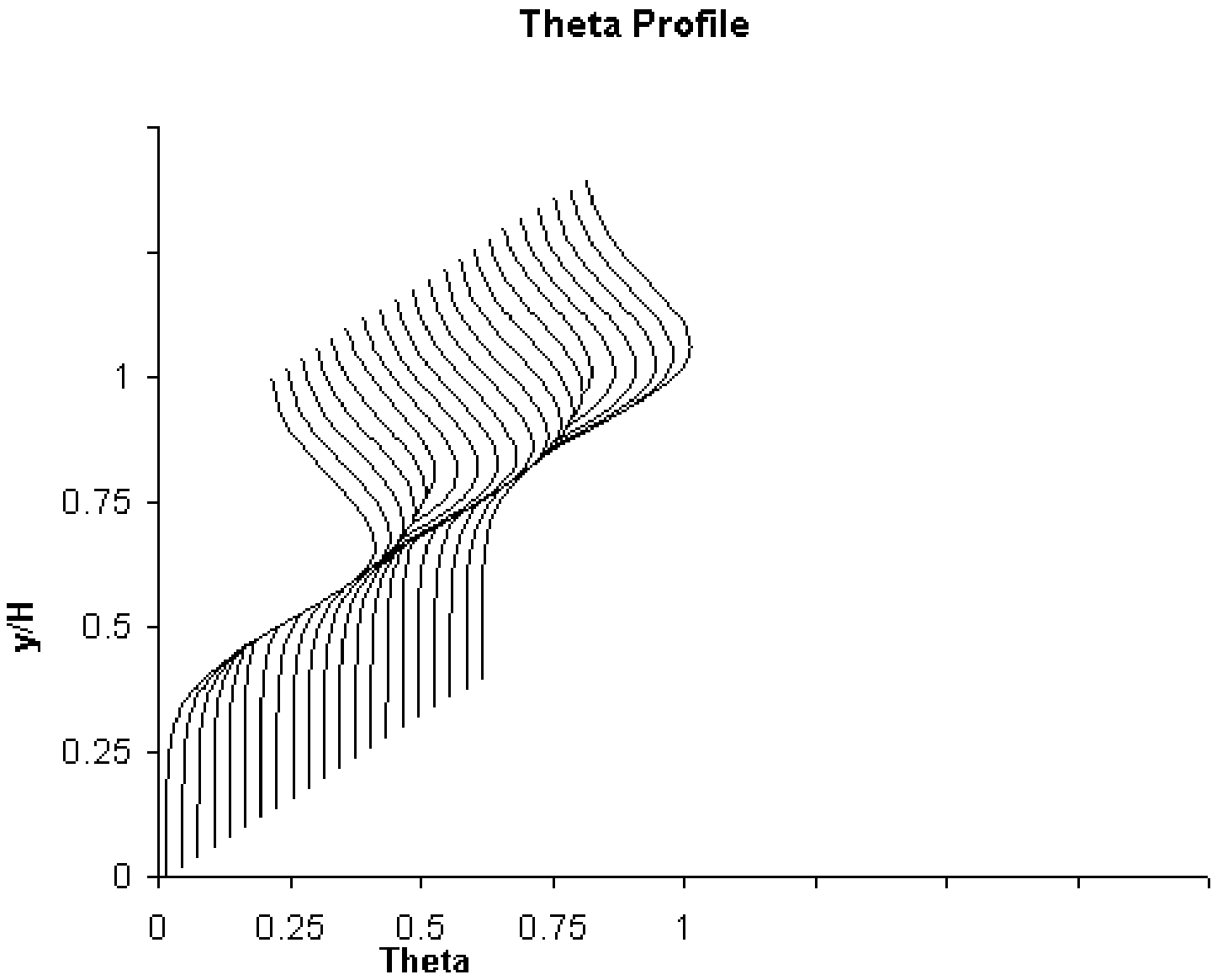


*x/H=0.5, J=26.4*

*S/H=0.25 H/d=8 (S/d=2 x/d=4)*

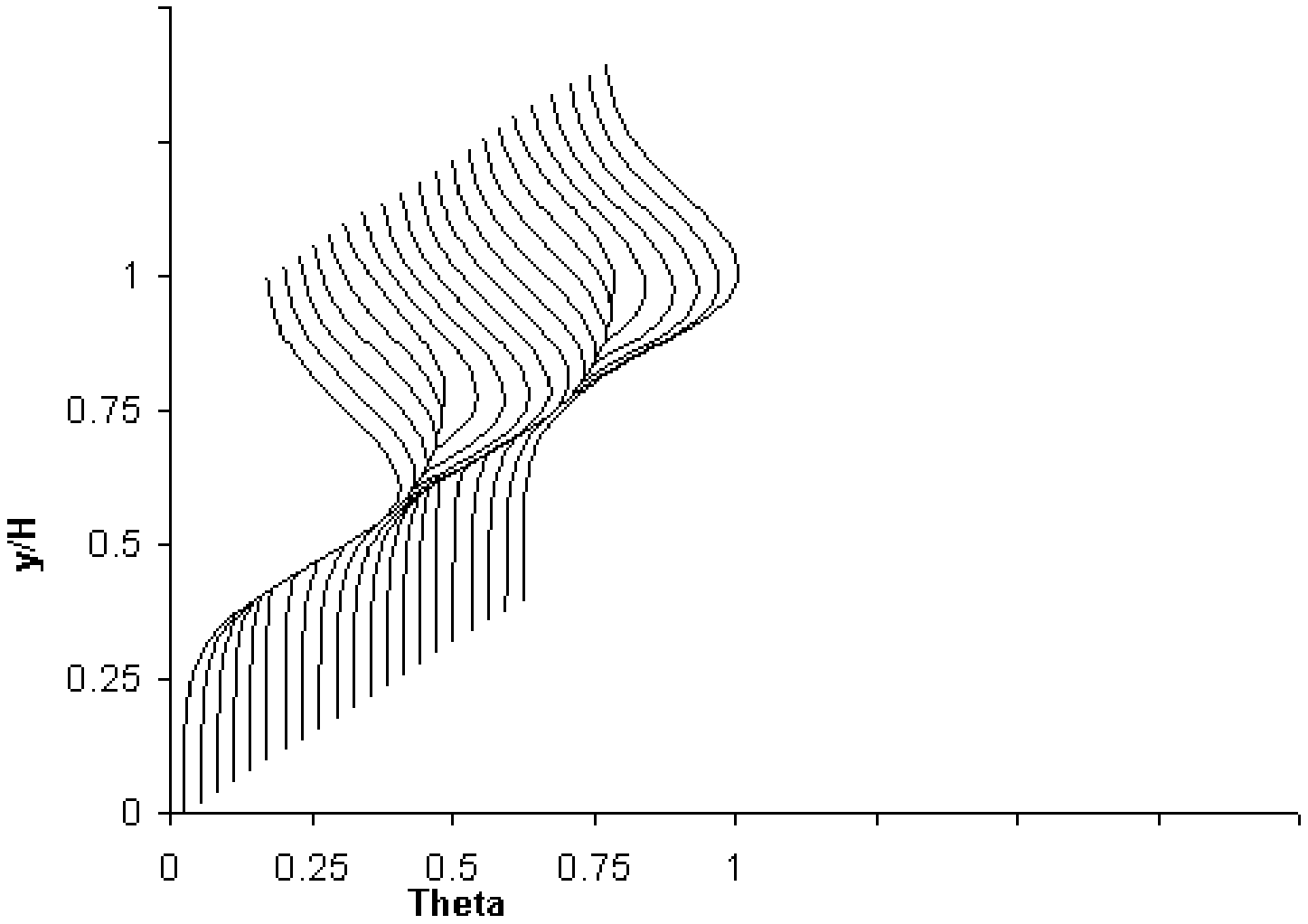


*x/H=0.5, J=26.4*

*S/H=0.321 H/d=7.06 (S/d=2.27 x/d=3.83)*

## Theta Profile

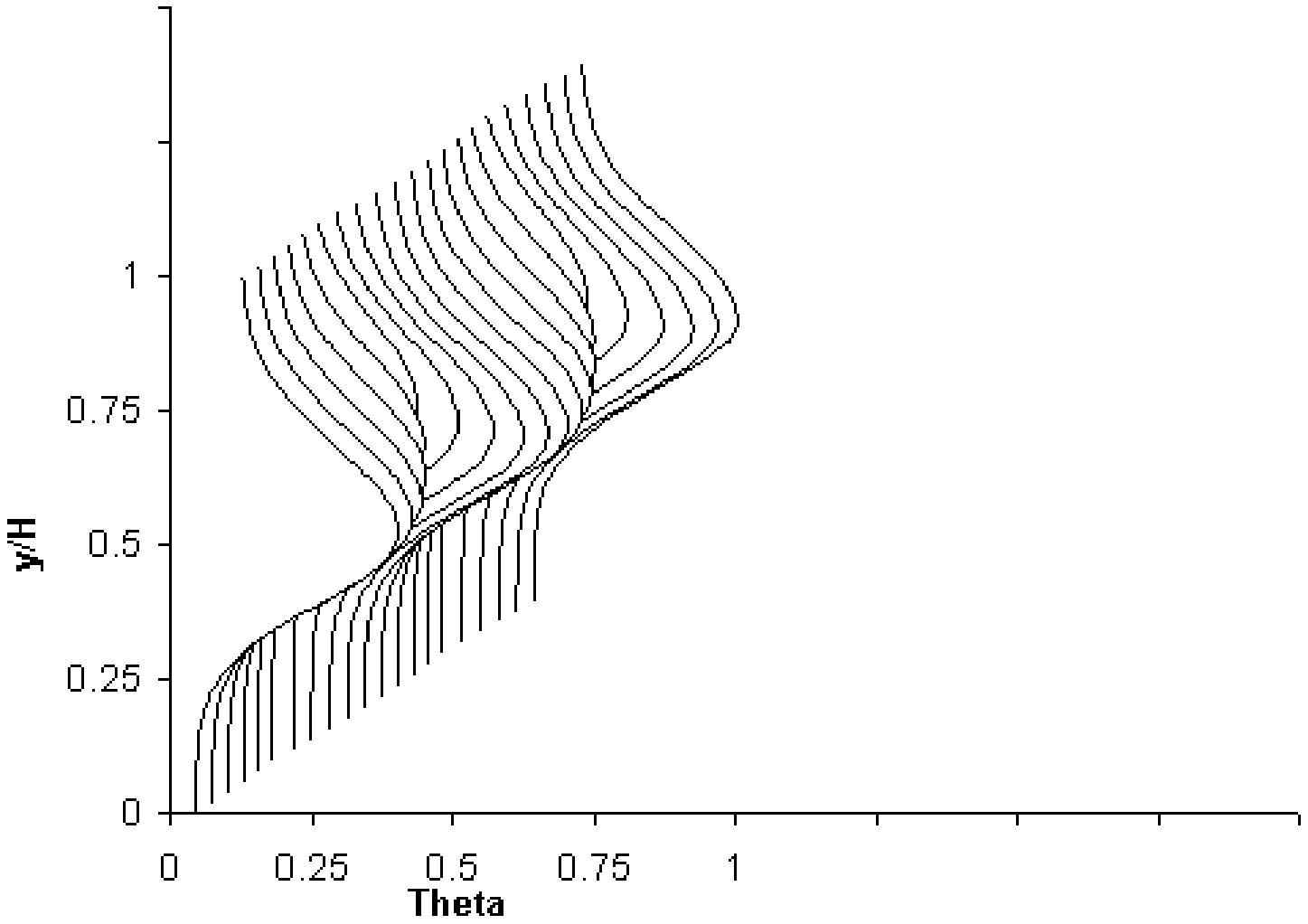


*x/H=0.5, J=26.4*

*S/H=0.433 H/d=6.08 (S/d=2.63 x/d=3.04)*

## Theta Profile

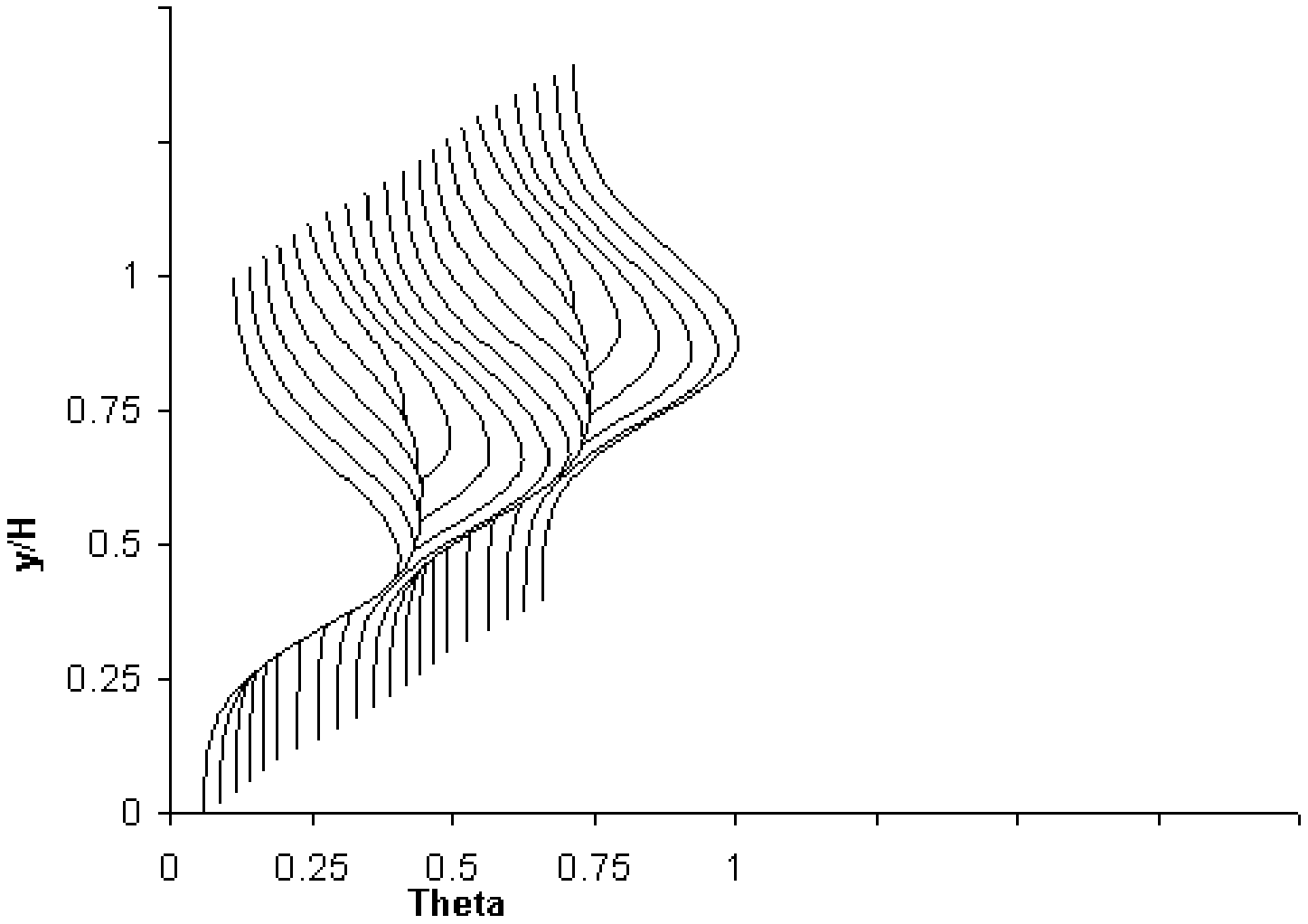


*x/H=0.5, J=26.4*

*S/H=0.5 H/d=5.66 (S/d=2.83 x/d=2.83)*

## Theta Profile

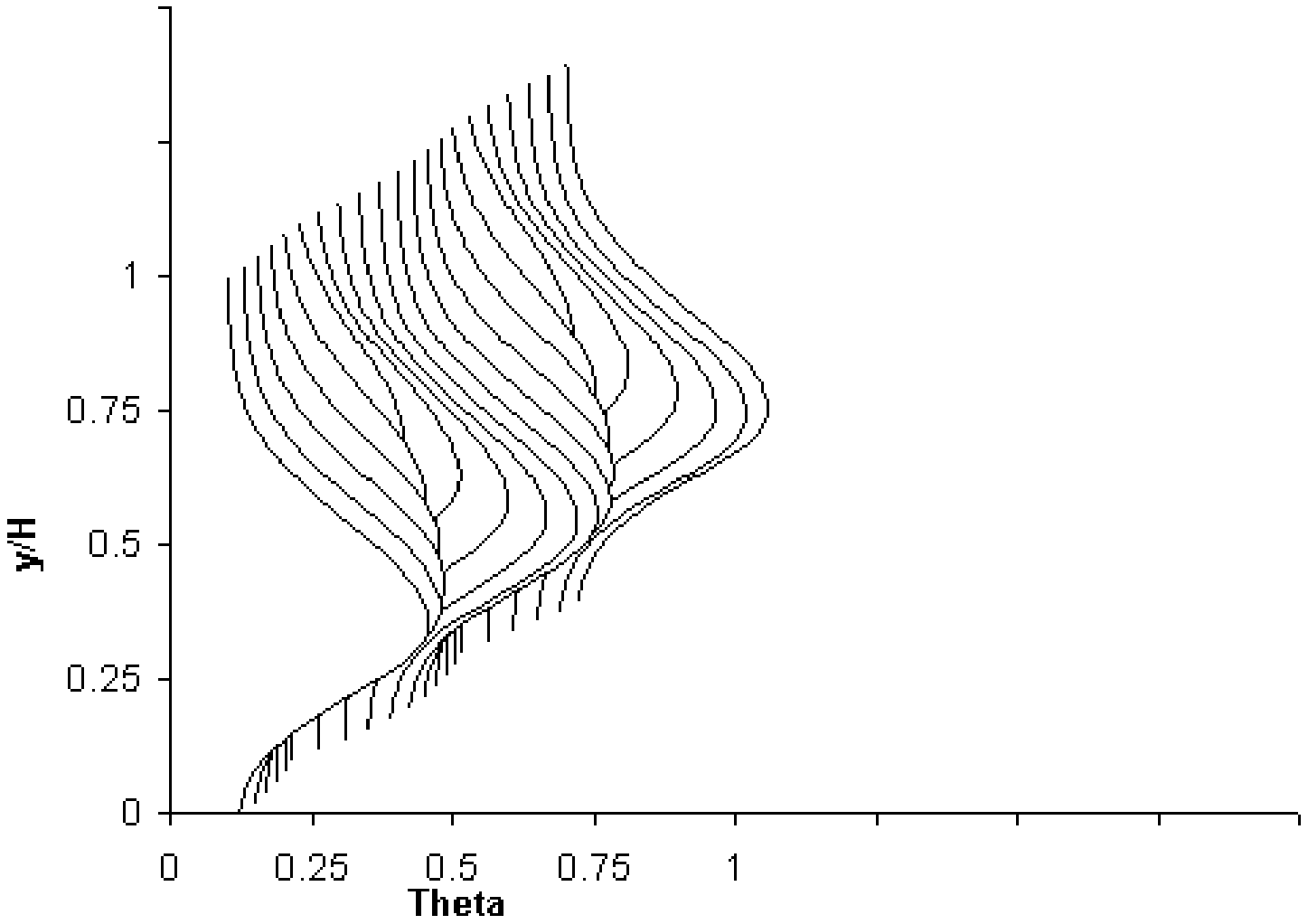


*x/H=0.5, J=26.4*

*S/H=0.642 H/d=4.49 (S/d=2.88 x/d=2.25)*

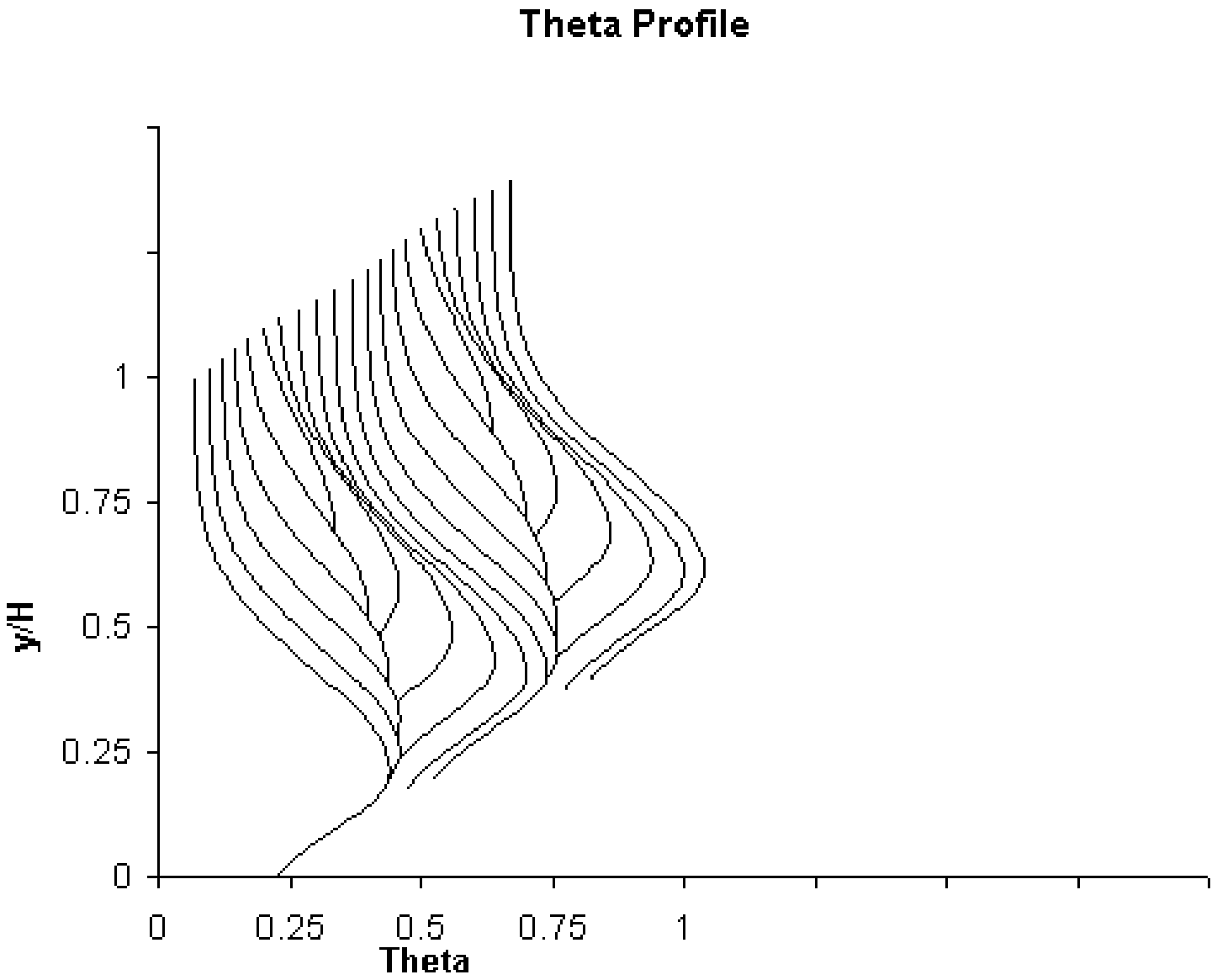


*x/H=0.5, J=26.4*

*S/H=0.866 H/d=4.3 (S/d=3.72 x/d=2.15)*

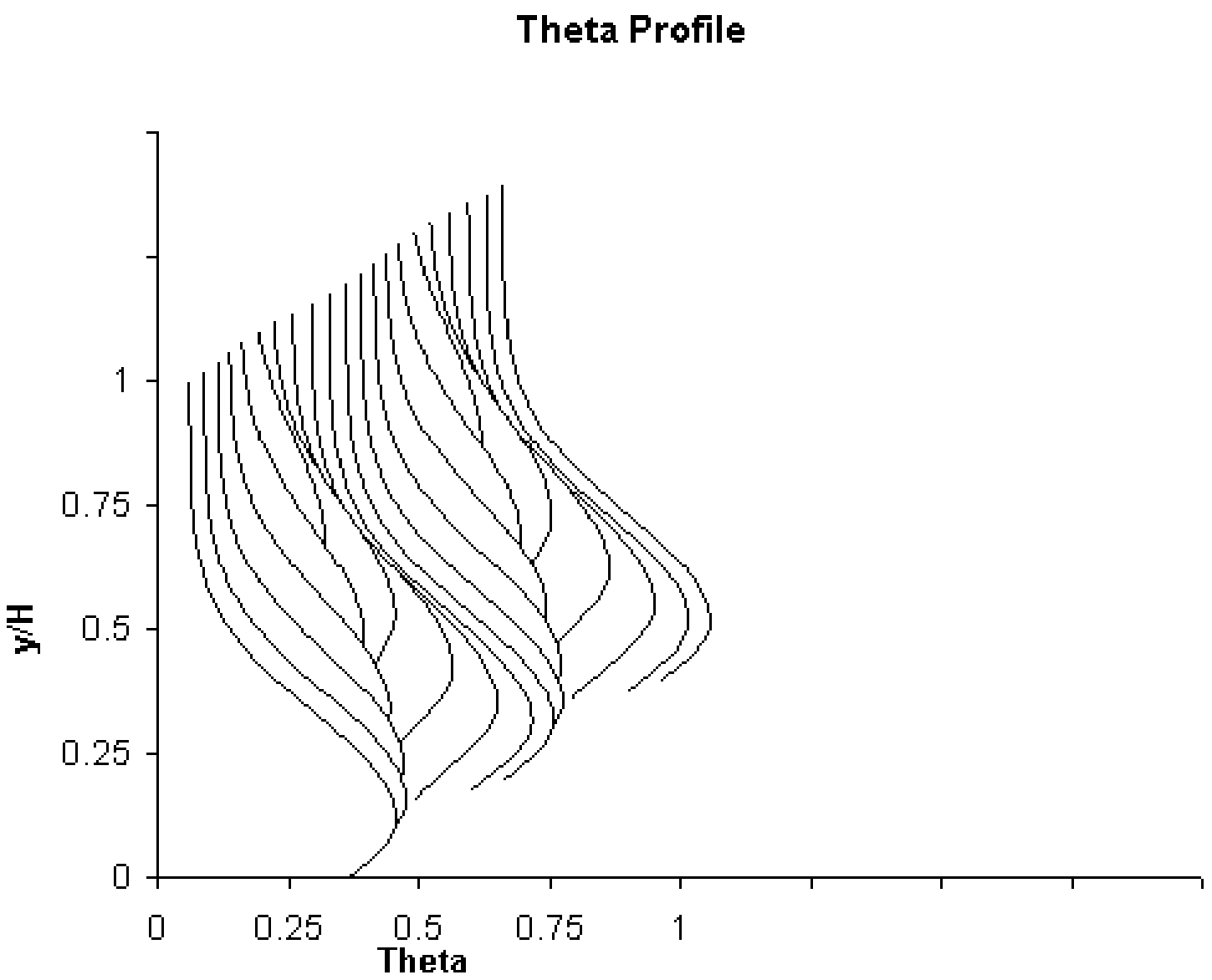


*x/H=0.5, J=26.4*

*S/H=1 H/d=4 (S/d=4 x/d=2)*

Sequence 7

## Variations in scalar distributions with Orifice diameter at constant spacing

*H/d=8, 7, 6, 5.5, 5, 4*

*x/H=0.5, DR=2.2, J=26.4, S/H=0.5, $C_d$=0.64*

(cf. figure 13(a) in NASA/TM—2005-213137 and figure 9(a) in NASA TM–83457; see also figure 10(a) in NASA TM–87294)

## Theta Profile

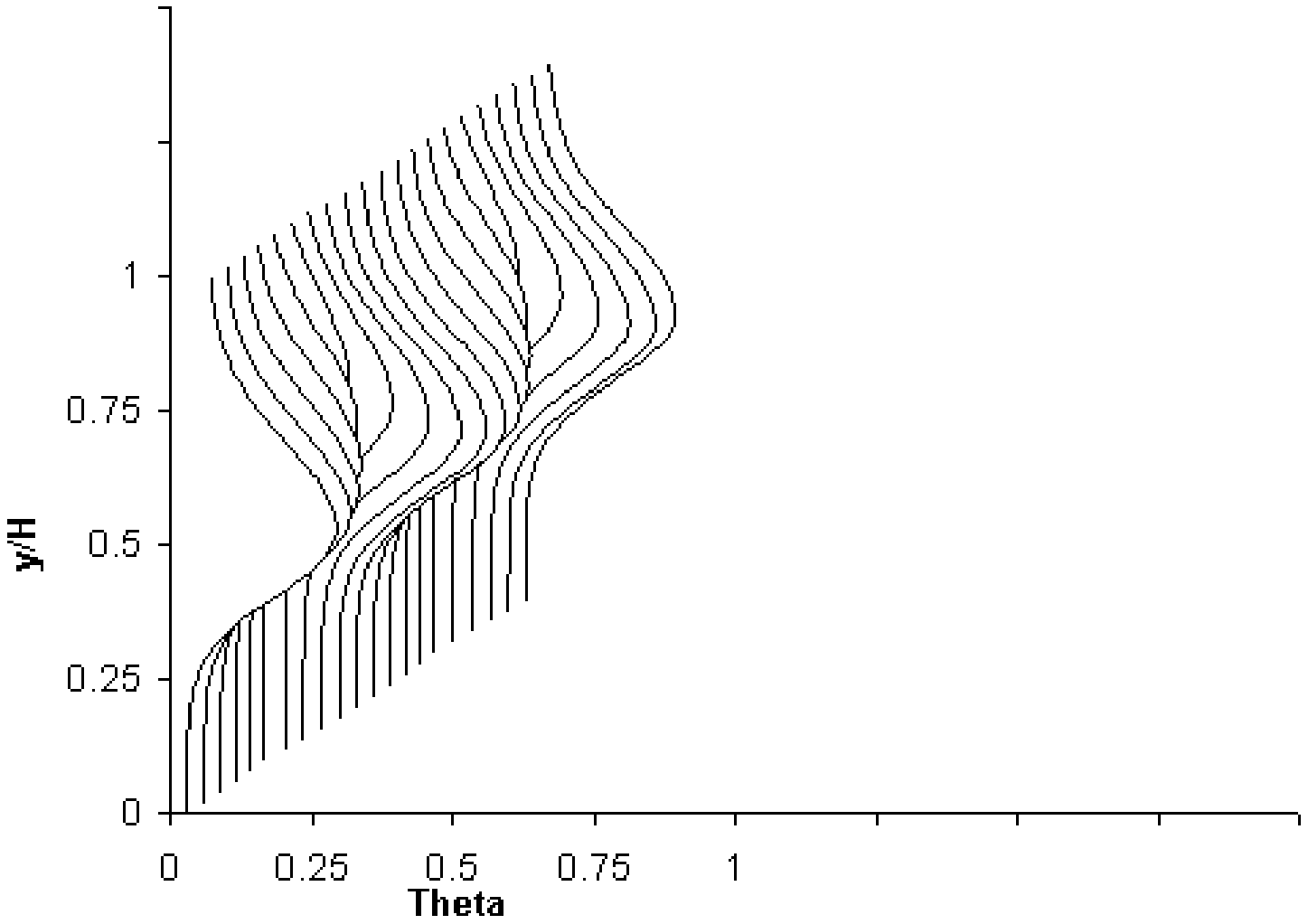


*x/H*=0.5, *S/H*=0.5, *J*=26.4

*H/d*=8 (S/d=4 x/d=4)

## Theta Profile

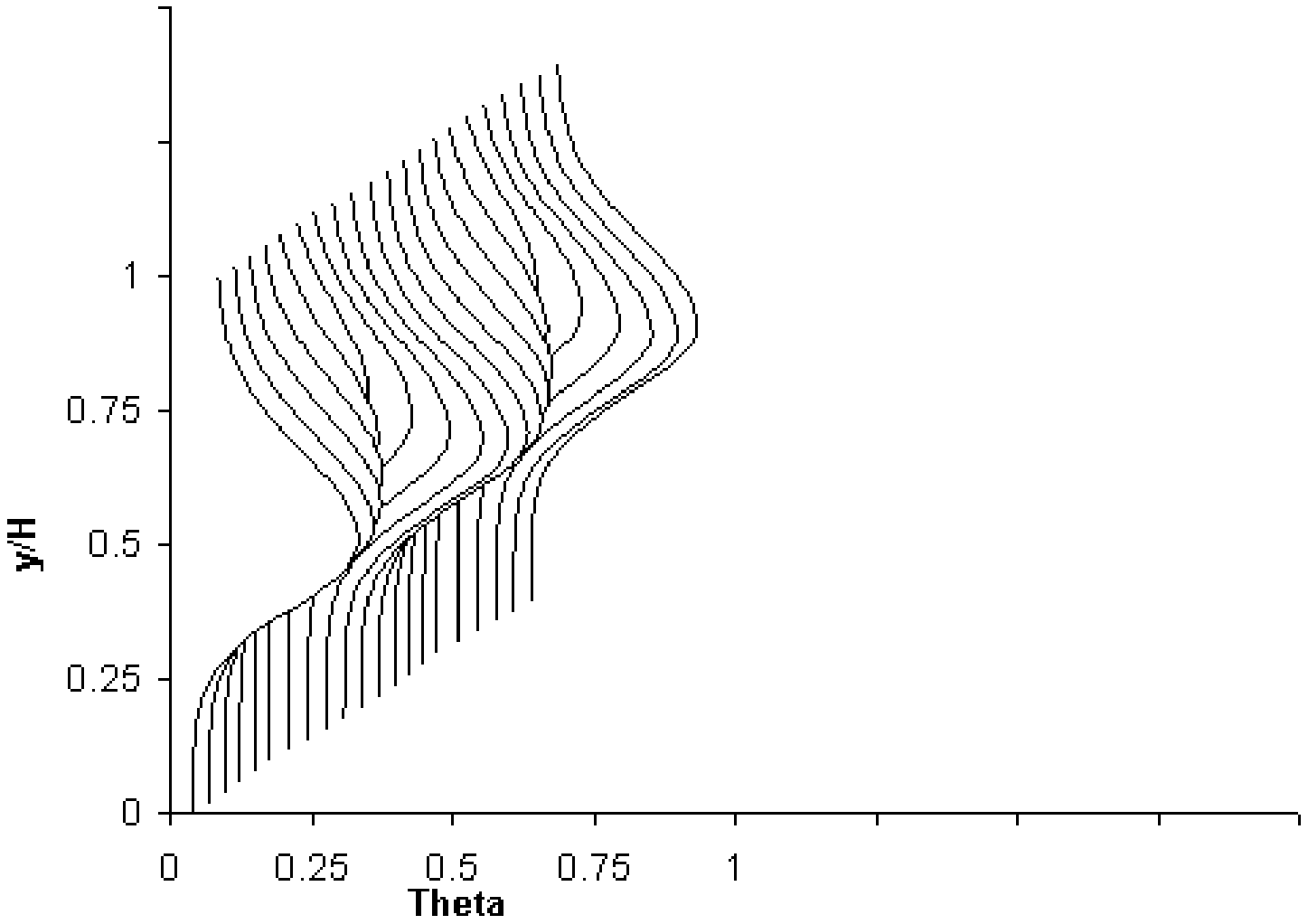


*x/H*=0.5, *S/H*=0.5, *J*=26.4

*H/d*=7 (S/d=3.5 x/d=3.5)

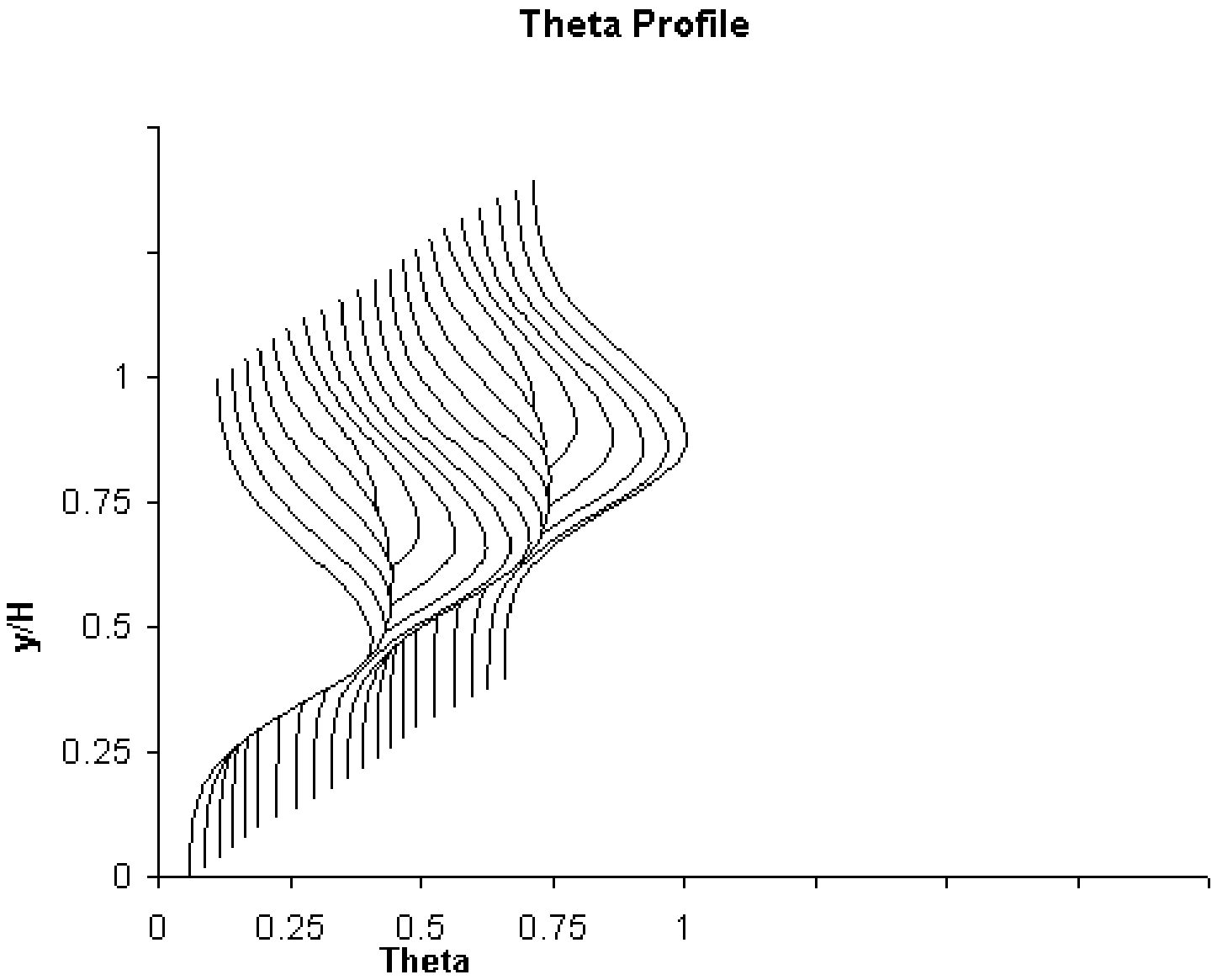


*x/H*=0.5, *S/H*=0.5, *J*=26.4

*H/d*=5.66 (S/d=2.83 x/d=2,83)

## Theta Profile

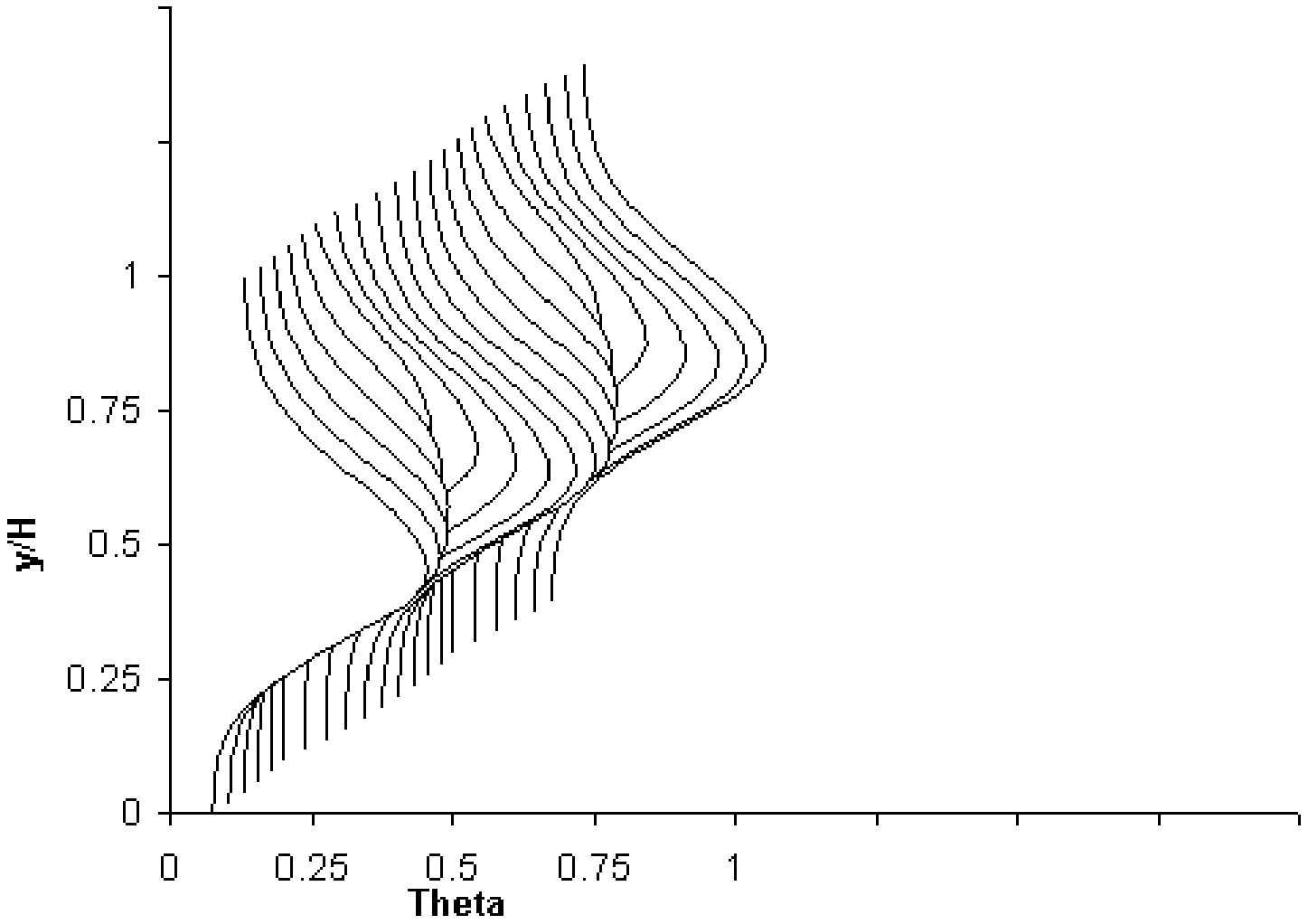


*x/H*=0.5, *S/H*=0.5, *J*=26.4

*H/d*=5 (S/d=2.5 x/d=2.5)

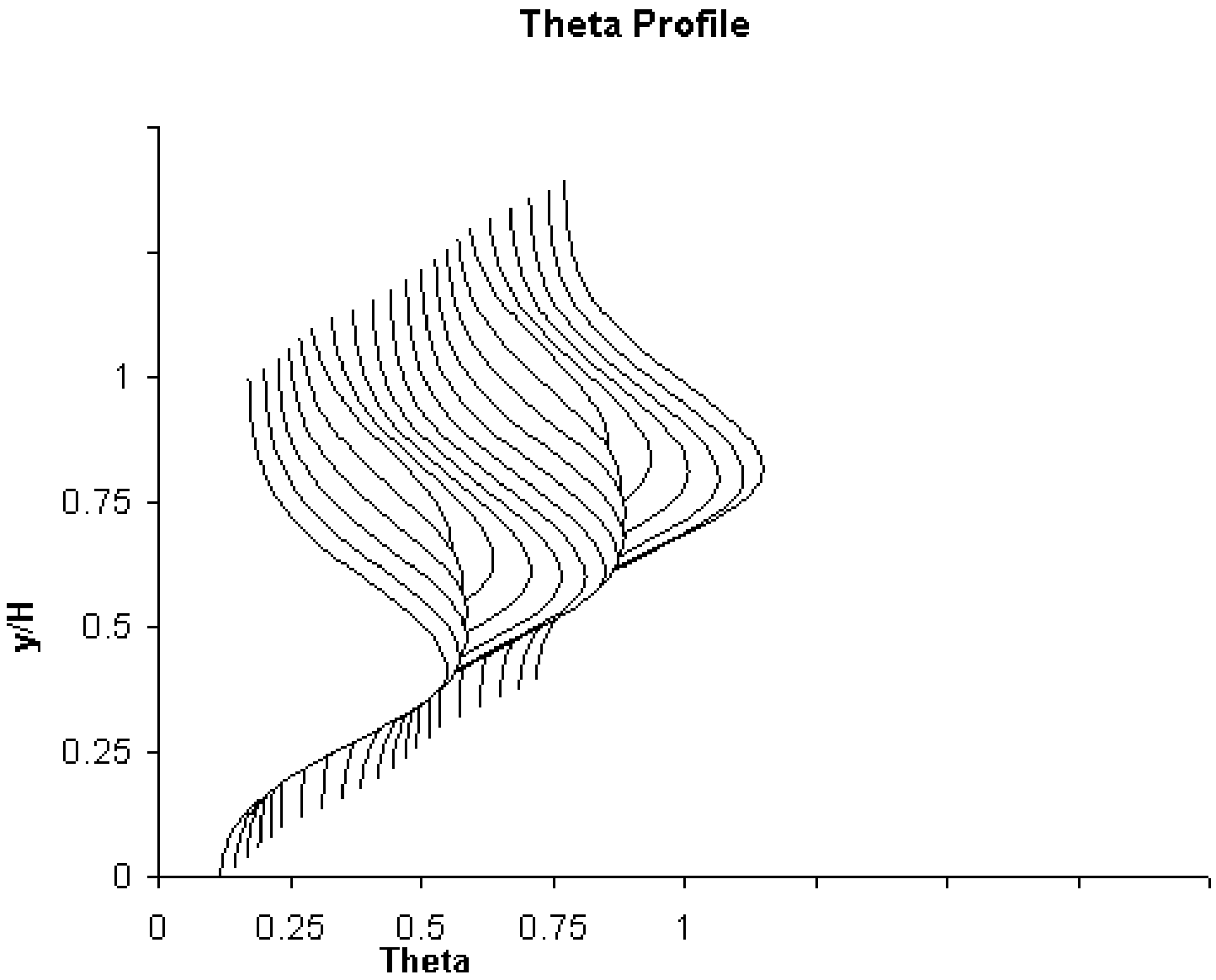


*x/H*=0.5, *S/H*=0.5, *J*=26.4

*H/d*=4 (S/d=2 x/d=2)

Sequence 8

## Variations in scalar distributions with Orifice diameter at constant spacing

*H/d=8, 7, 6, 5.5, 5, 4*

*x/H=2, DR=2.2, J=26.4, S/H=0.5, $C_d$=0.64*

(cf. figure 13(b) in NASA/TM–2005-213137 and figure 9(b) in NASA TM–83457; see also figure 10(b) in NASA TM–87294)

## Theta Profile

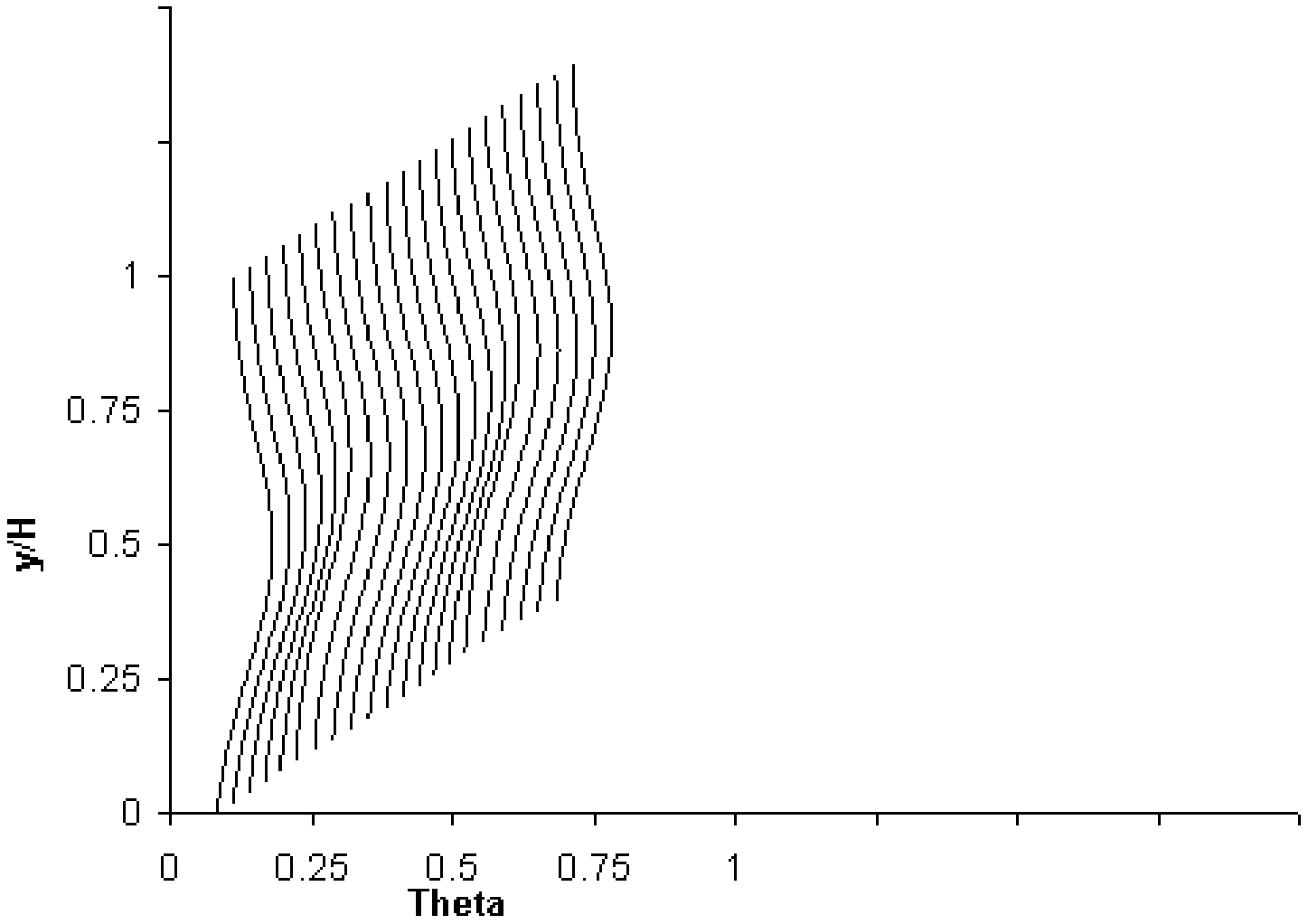


*x/H*=2, *S/H*=0.5, *J*=26.4

*H/d*=8 (S/d=4 x/d=16)

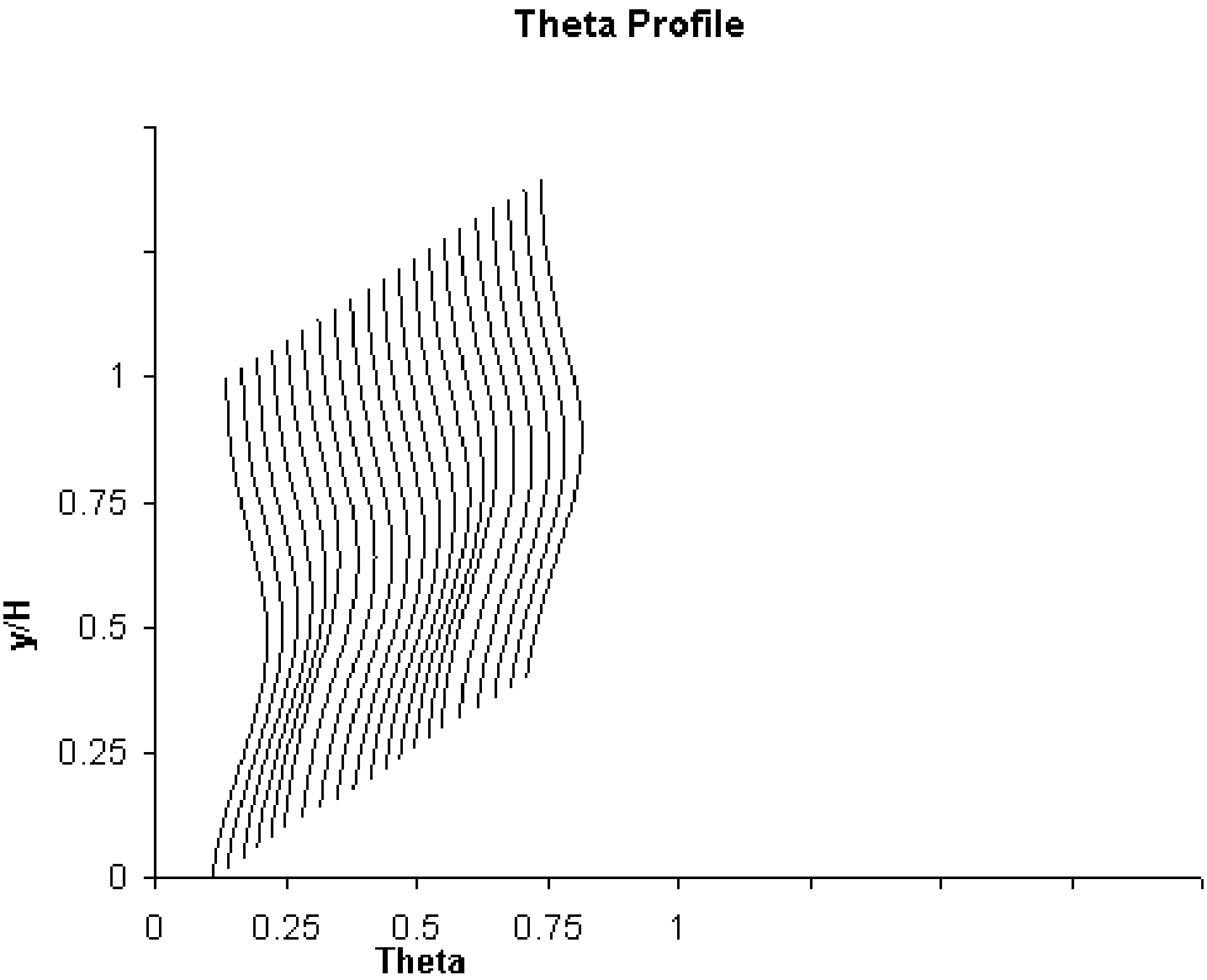


*x/H*=2, *S/H*=0.5, *J*=26.4

*H/d*=7 (S/d=3.5 x/d=14)

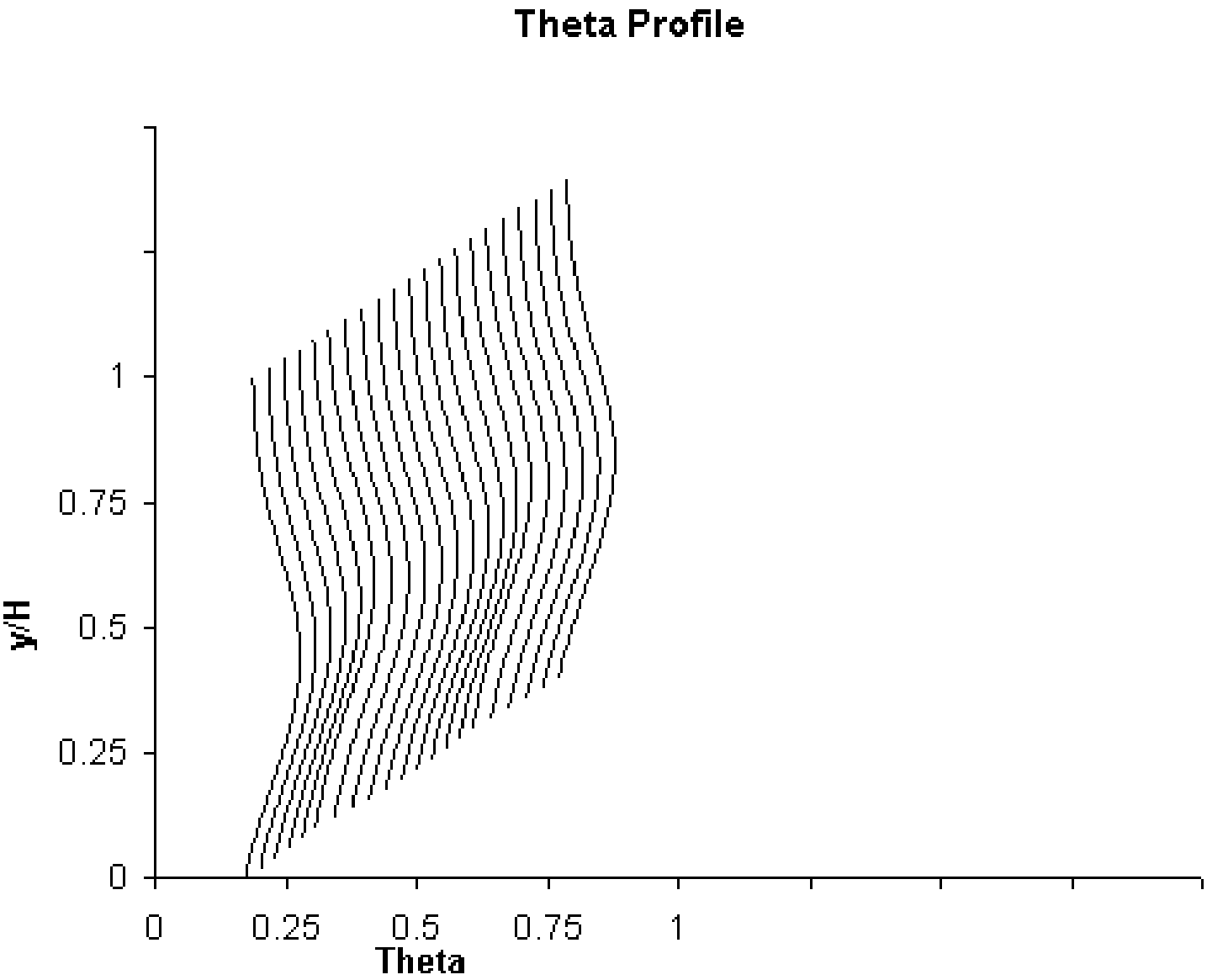


*x/H*=2, *S/H*=0.5, *J*=26.4

*H/d*=5.66 (S/d=2,83 x/d=11.32)

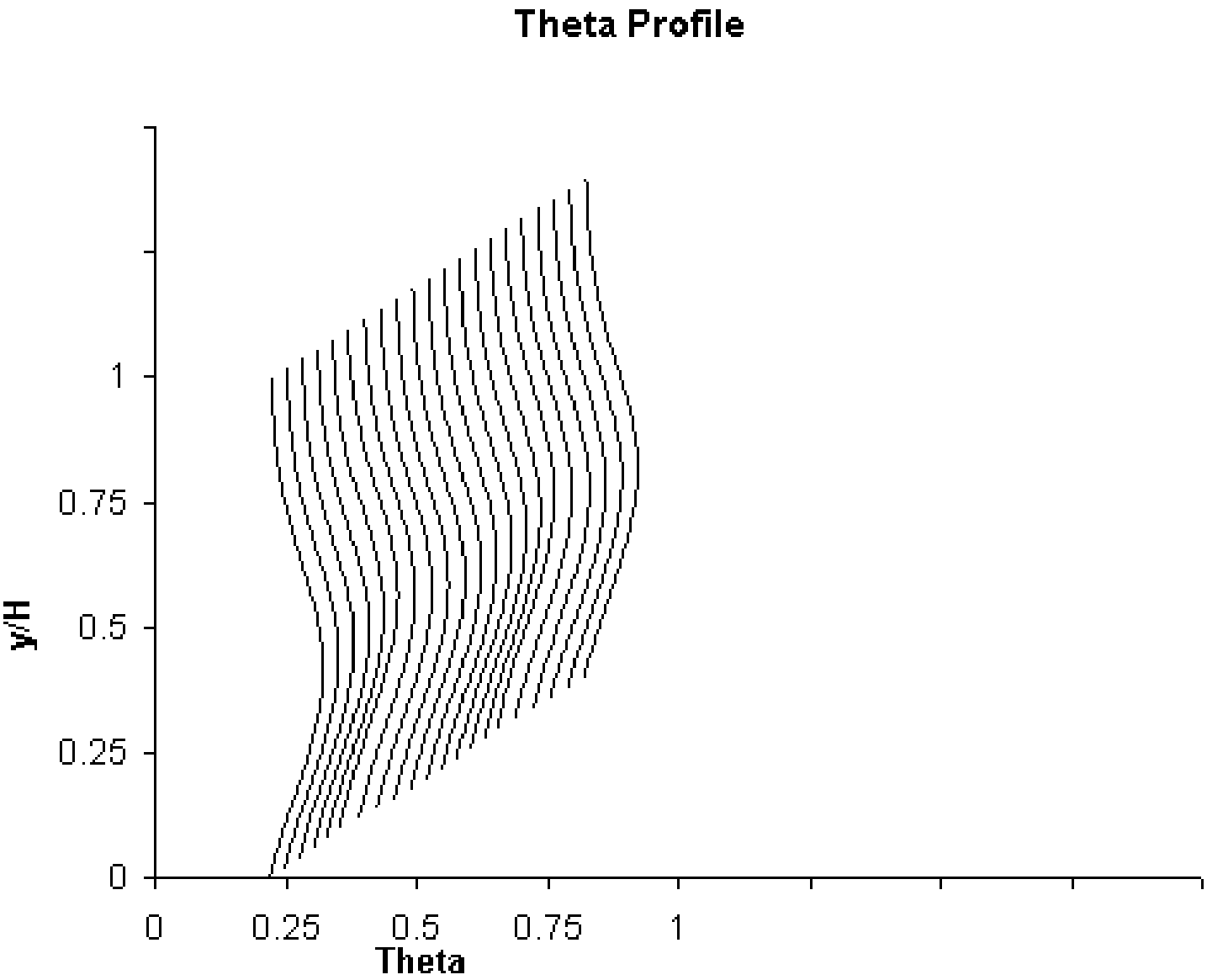


*x/H*=2, *S/H*=0.5, *J*=26.4

*H/d*=5 (S/d=2,5 x/d=10)

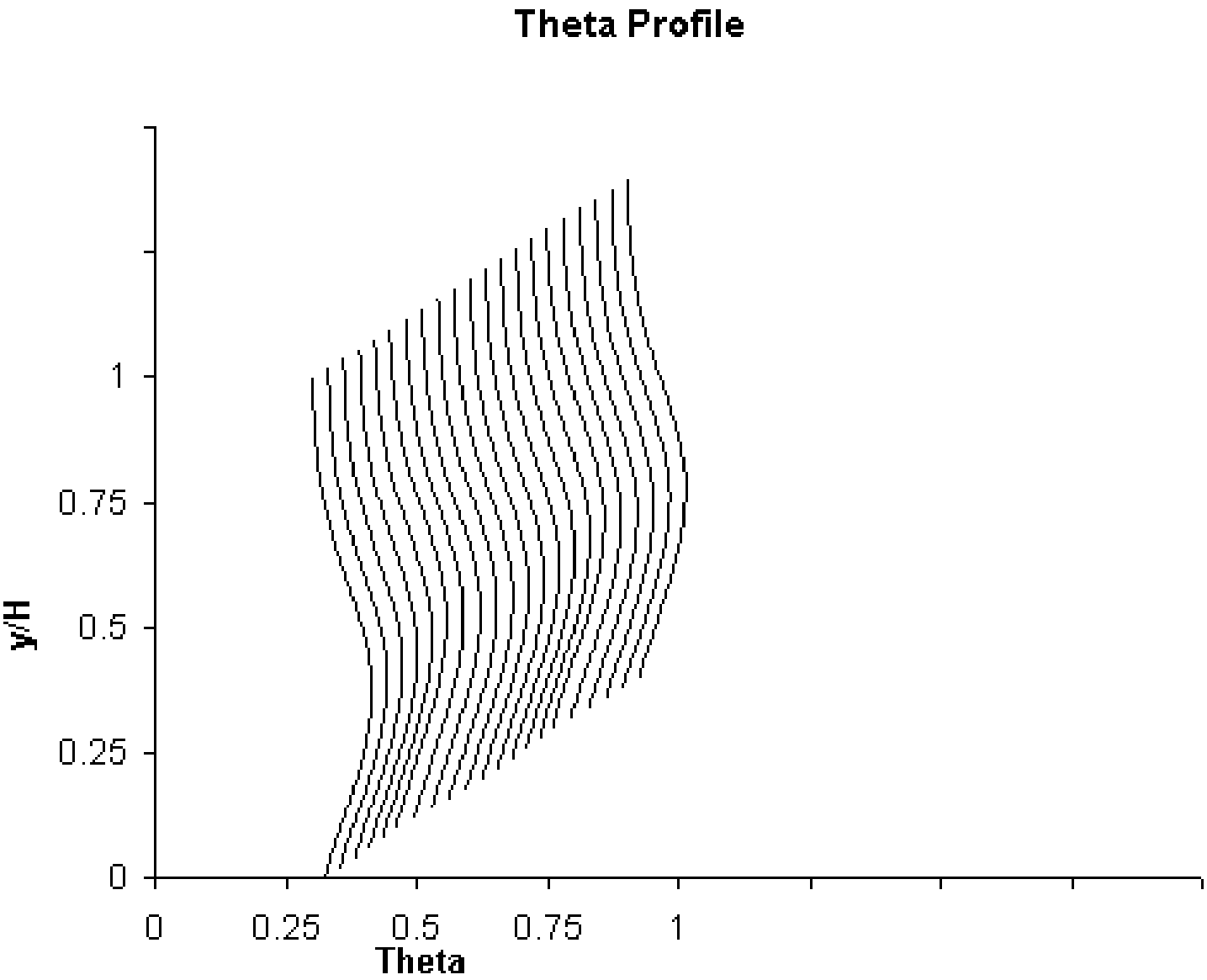


*x/H*=2, *S/H*=0.5, *J*=26.4

*H/d*=4 (S/d=2 x/d=8)

Sequence 9

## Variations in scalar distributions with Coupled orifice spacing and momentum-flux ratio

*S/H=0.25; H/d=11.32, J=105.8*
*S/H=0.321; H/d=8.81, J=64*
*S/H=0.433; H/d=6.54*, J=35.2
*S/H=0.5; H/d=5.66, J=26.4*
*S/H=0.642; H/d=4.41, J=16*
*S/H=0.866; H/d=3.27, J=9.8*
*S/H=1; H/d=2.83, J=6.6*

*x/H=0.5, DR=2.2, $C_d$=0.64*

(cf. figure 14(a) in NASA/TM—2005-213137 and figure10(a) in NASA TM–83457; see also figure 9(a) in NASA TM–87296)

## Theta Profile

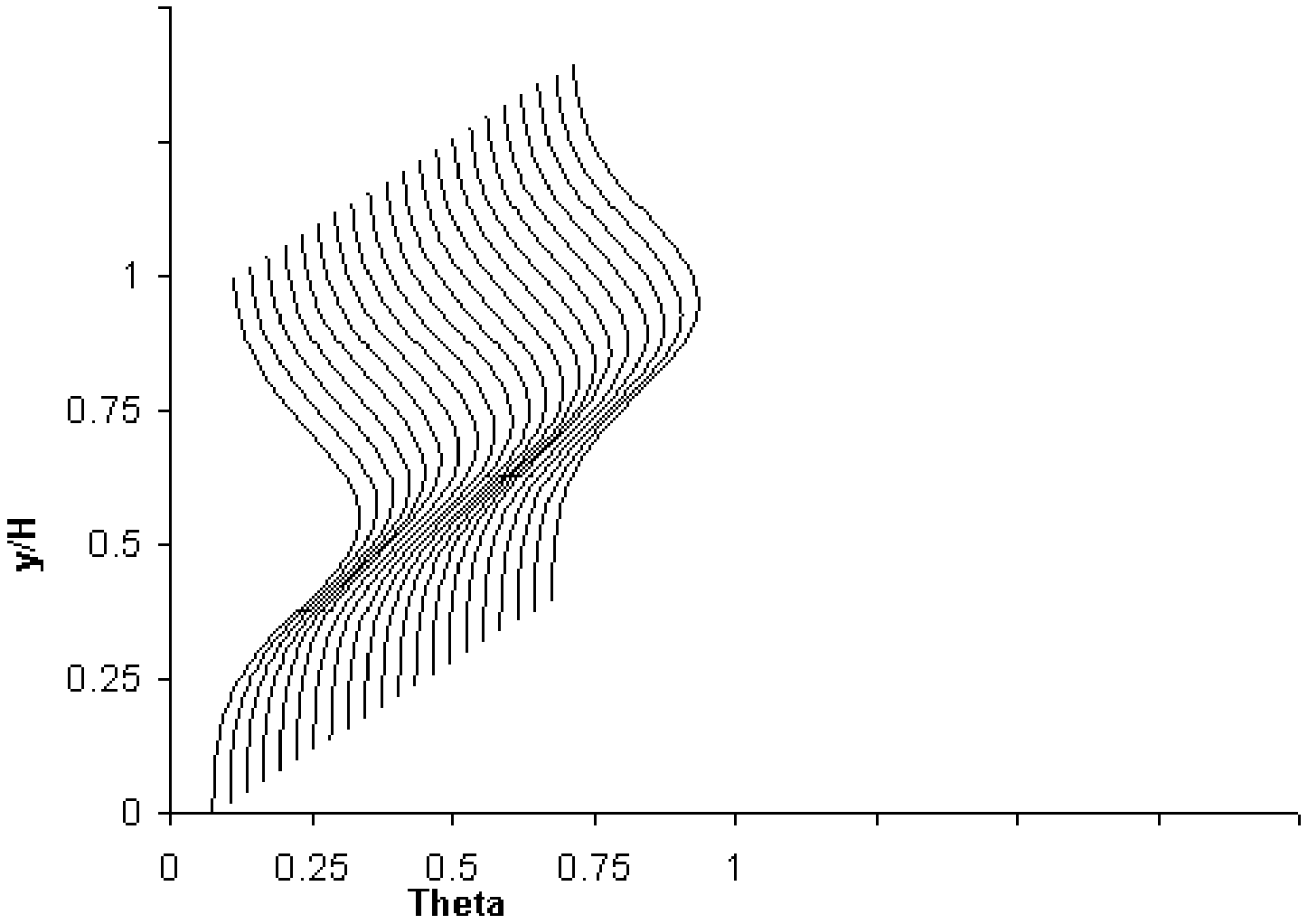


*x/H=0.5, (S/d=2.83)*

*J=105.6* *S/H=0.25* *H/d=11.32* *(x/d=5.66)*

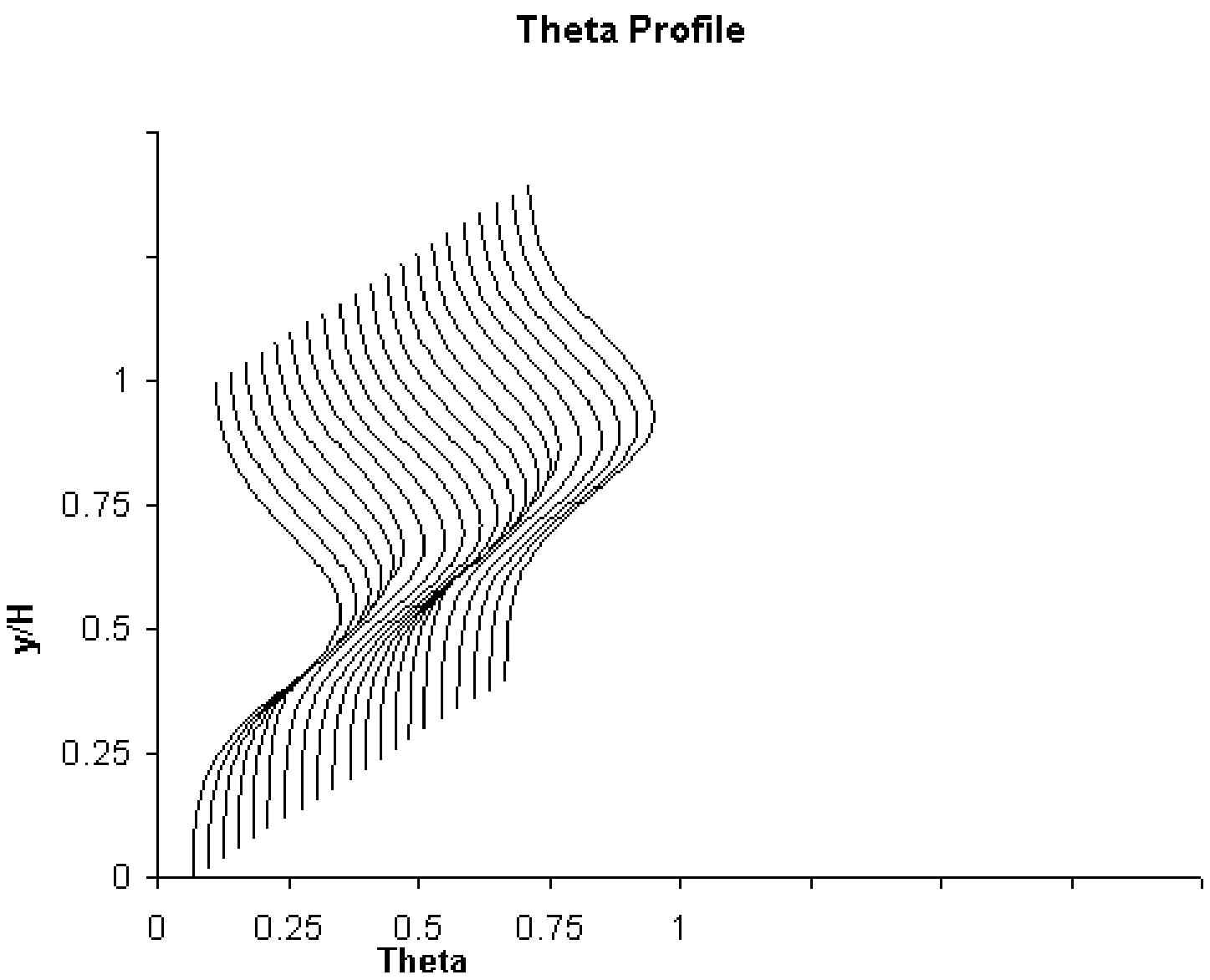


*x.H=0.6, (S/d=2.83)*

*J=64 S/H=0.321 H/d=8.81 )x/d=4.41)*

## Theta Profile

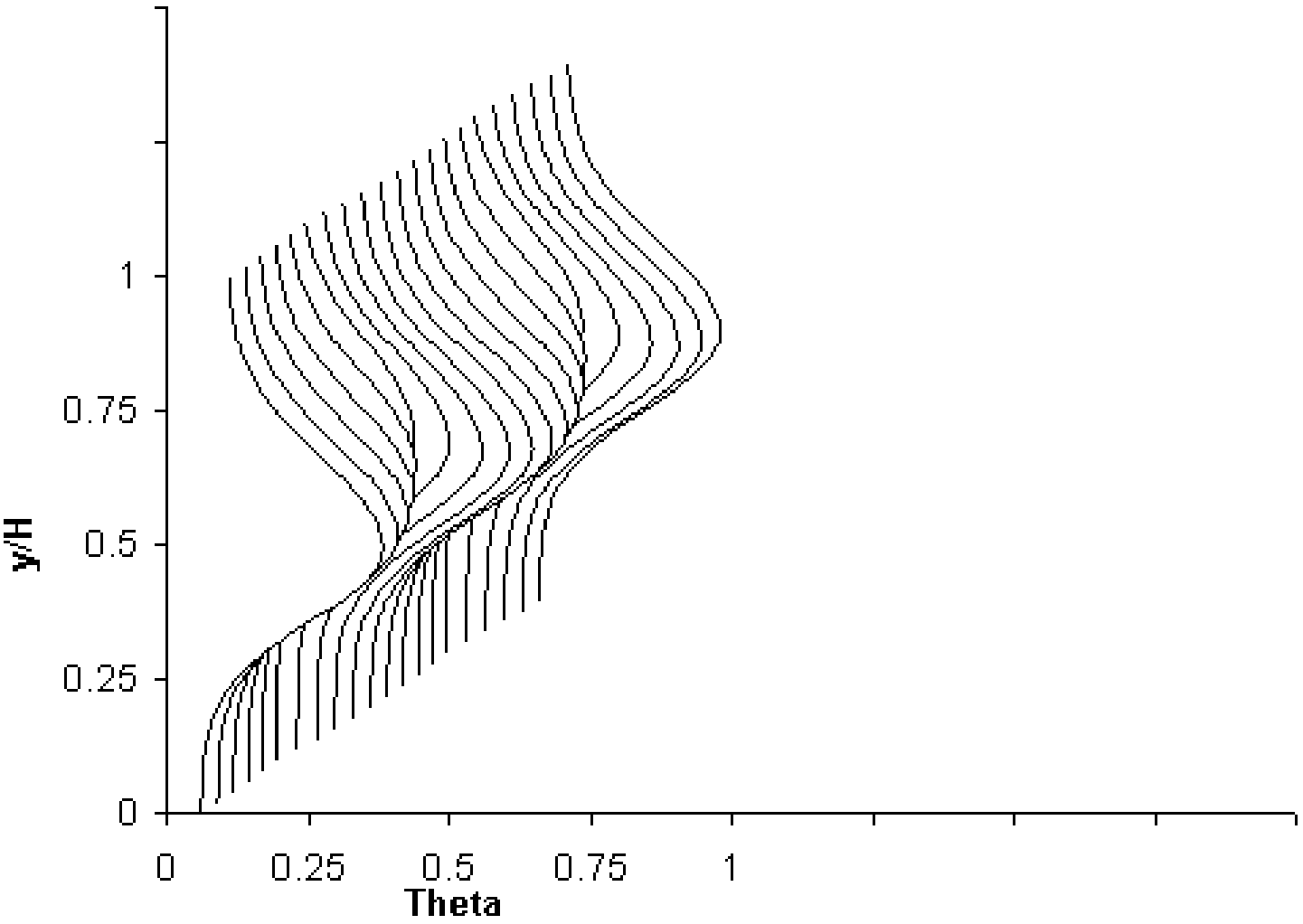


*x/H=0.5, (S/d=2.83)*

*J=35.2* *S/H=0.433* *H/d=6.54* *(x/d=3.27)*

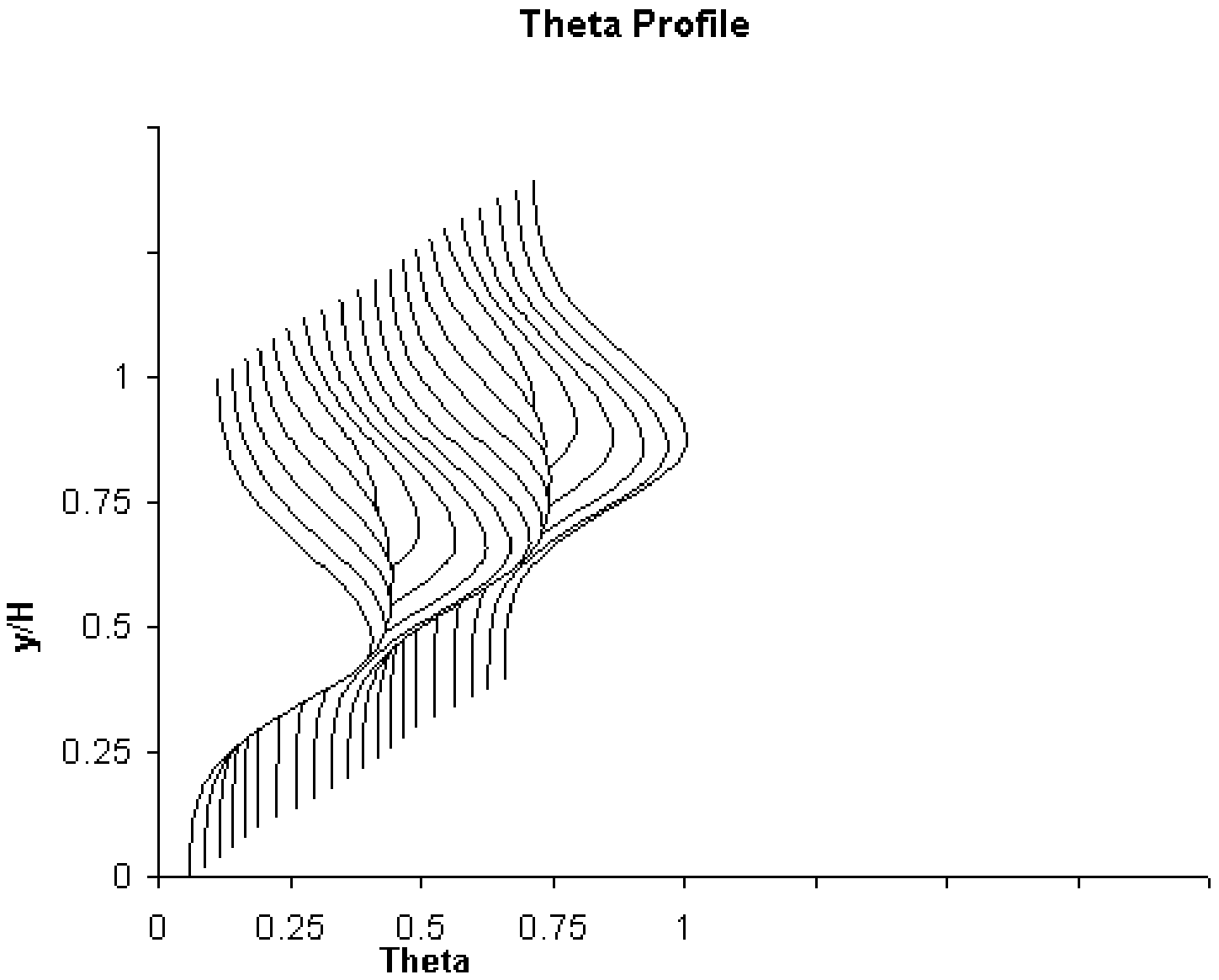


*x/H=0.6, (S/d=2.83)*

*J=26.4* *S/H=0.5* *H/d=5.66* *(x/d=2.83)*

## Theta Profile



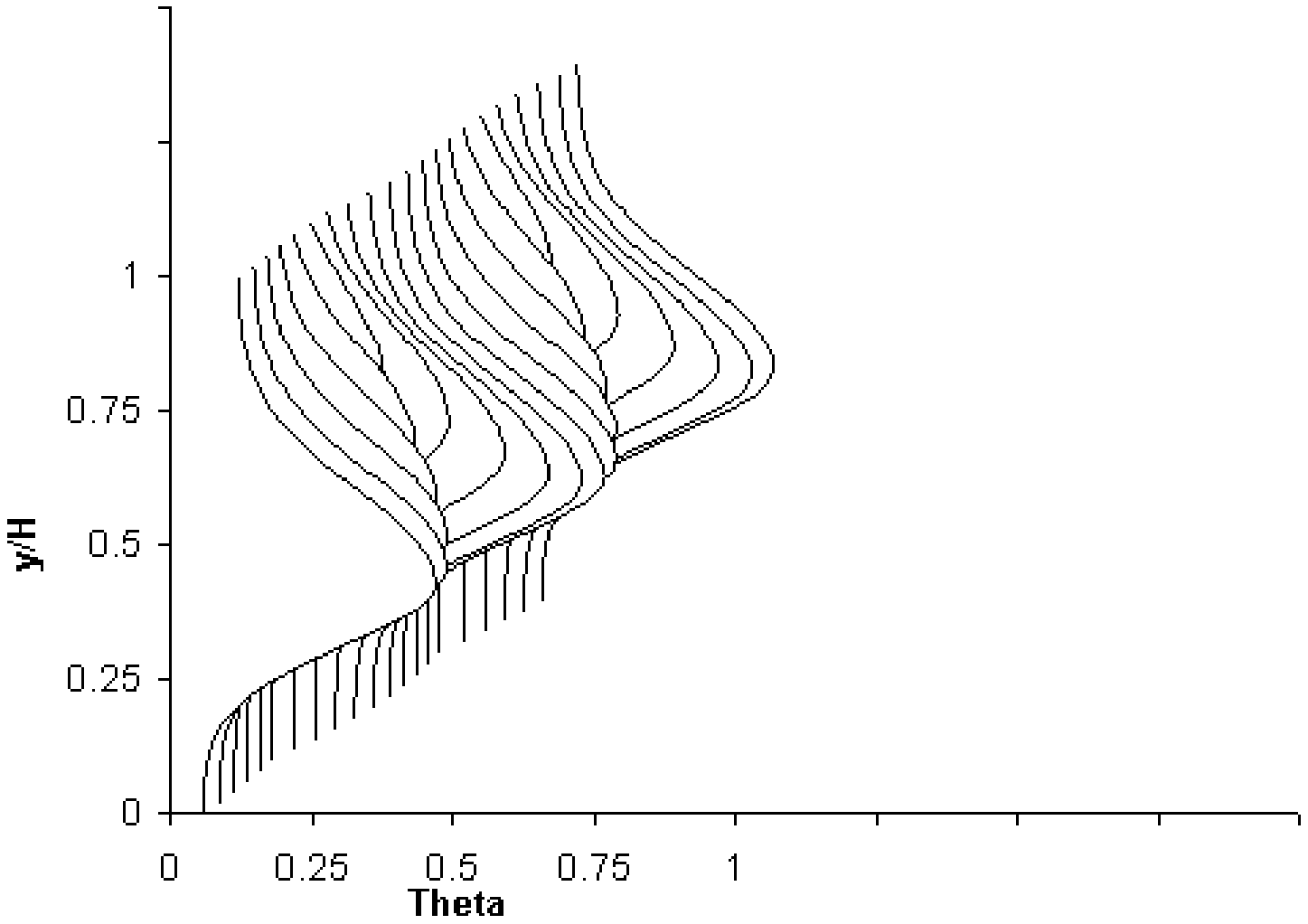


*x/H=0.5, (S/d=2.83)*

*J=16* *S/H=0.642* *H/d=4.41* *(x/d=2.21)*

## Theta Profile



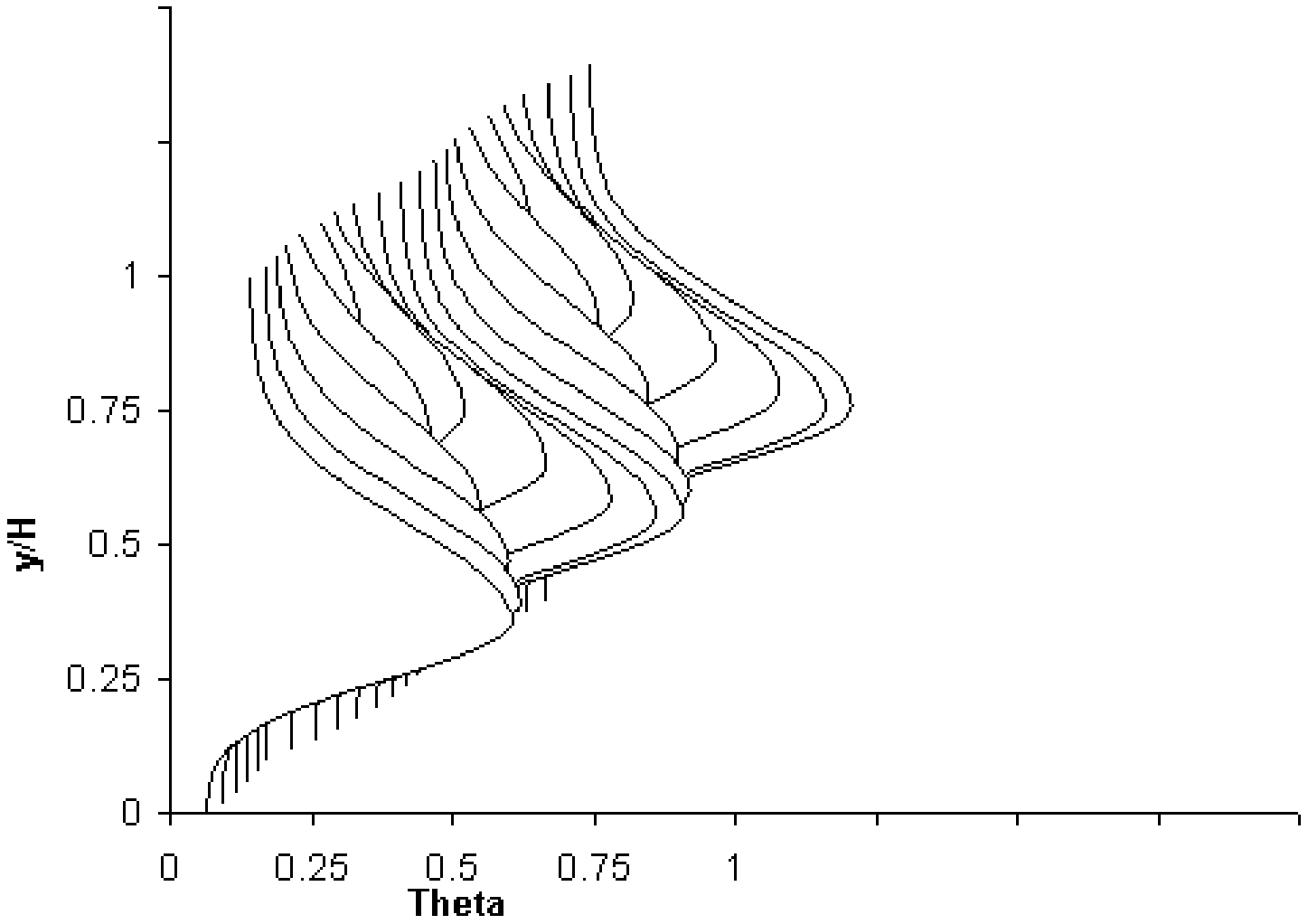


*x/H=0.5, (S/d=2.83)*

*J=8.8* *S/H=0.866* *H/d=3.27* *(x/d=1.64)*

## Theta Profile

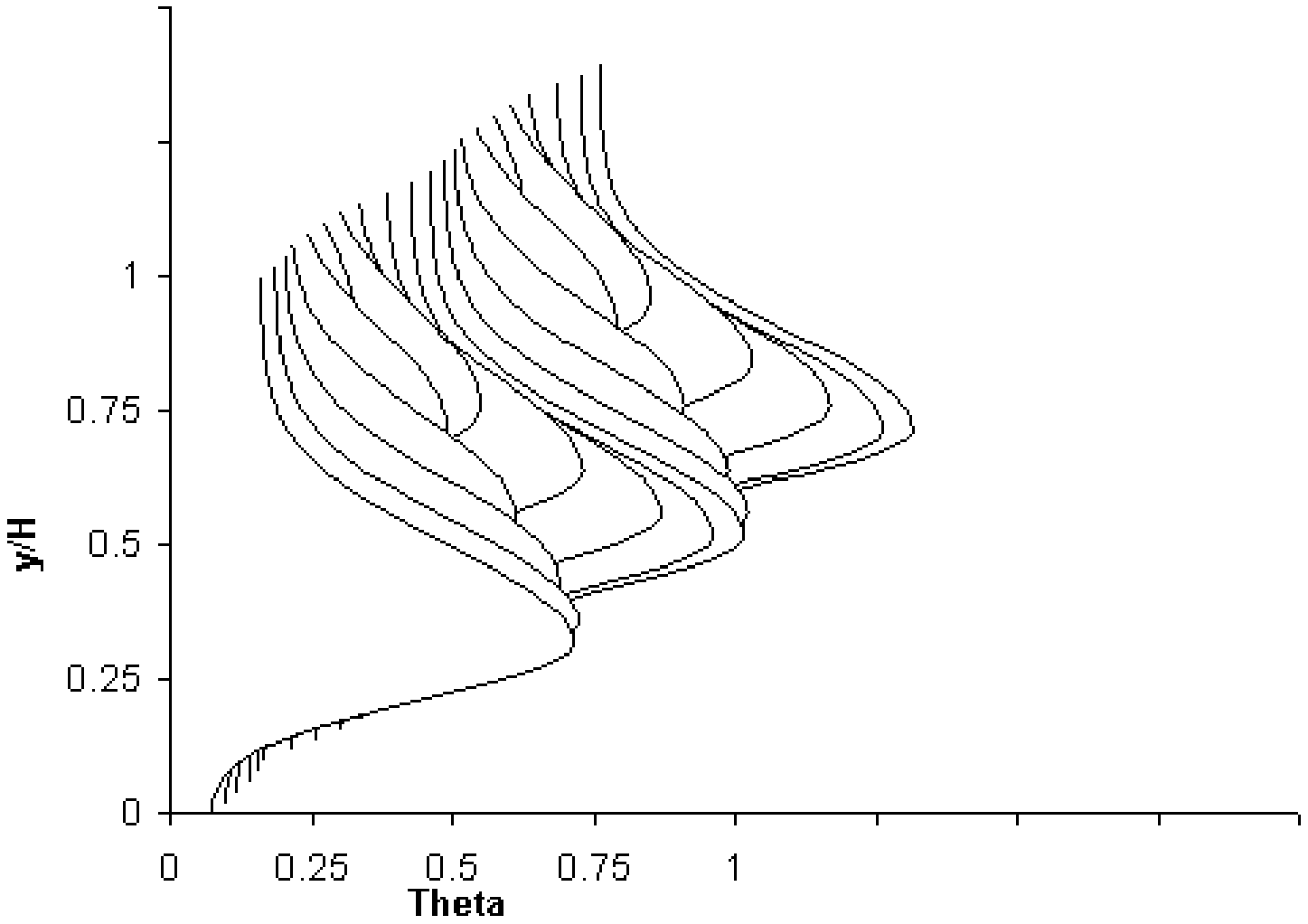


*x/H=0.5, (S/d=2.83)*

*J=6.6* *S/H=1* *H/d=2.83* *(x/d=1.42)*

Sequence 10

## Variations in scalar distributions with Coupled momentum-flux ratio and orifice spacing

*S/H*=0.25; *H/d*=11.32, J=105.6
*S/H*=0.321; *H/d*=8.81, J=64
*S/H*=0.433; *H/d*=6.54, J=35.2
*S/H*=0.5; *H/d*=5.66, J=26.4
*S/H*=0.642; *H/d*=4.41, J=16
*S/H*=0.866; *H/d*=3.27, J=8.8
*S/H*=1; *H/d*=2.83, J=6.6

*x/H=2, DR=2.2, $C_d$=0.64*

(cf. figure 14(b) in NASA/TM—2005-213137 and
figure 10(b) in NASA TM–83457; see also
figure 9(b) in NASA TM–87294)

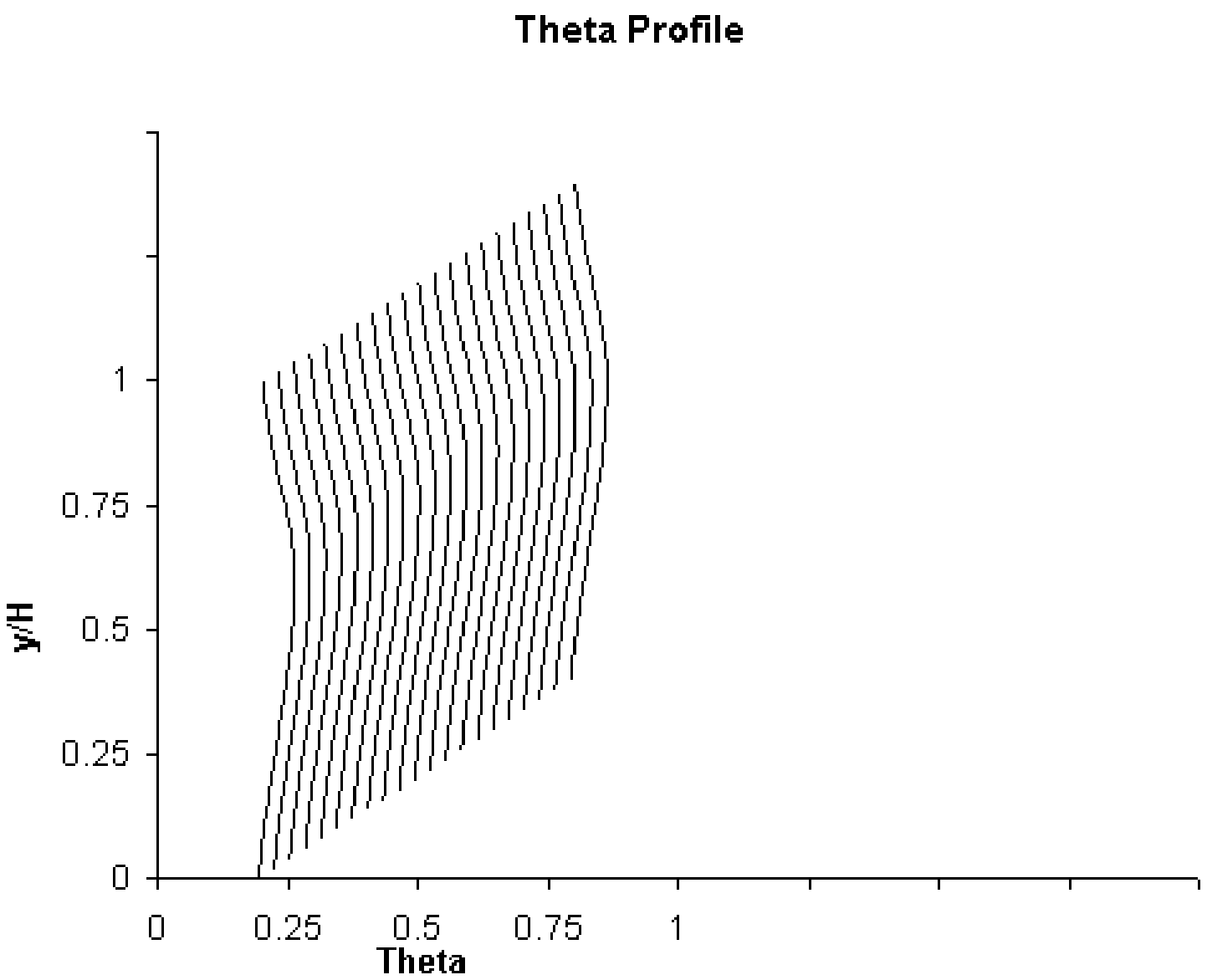


*x/H=2, (S/d=2.83)*

*J=105.6* *S/H=0.25* *H/d=11.32* *(x/d=22.64)*

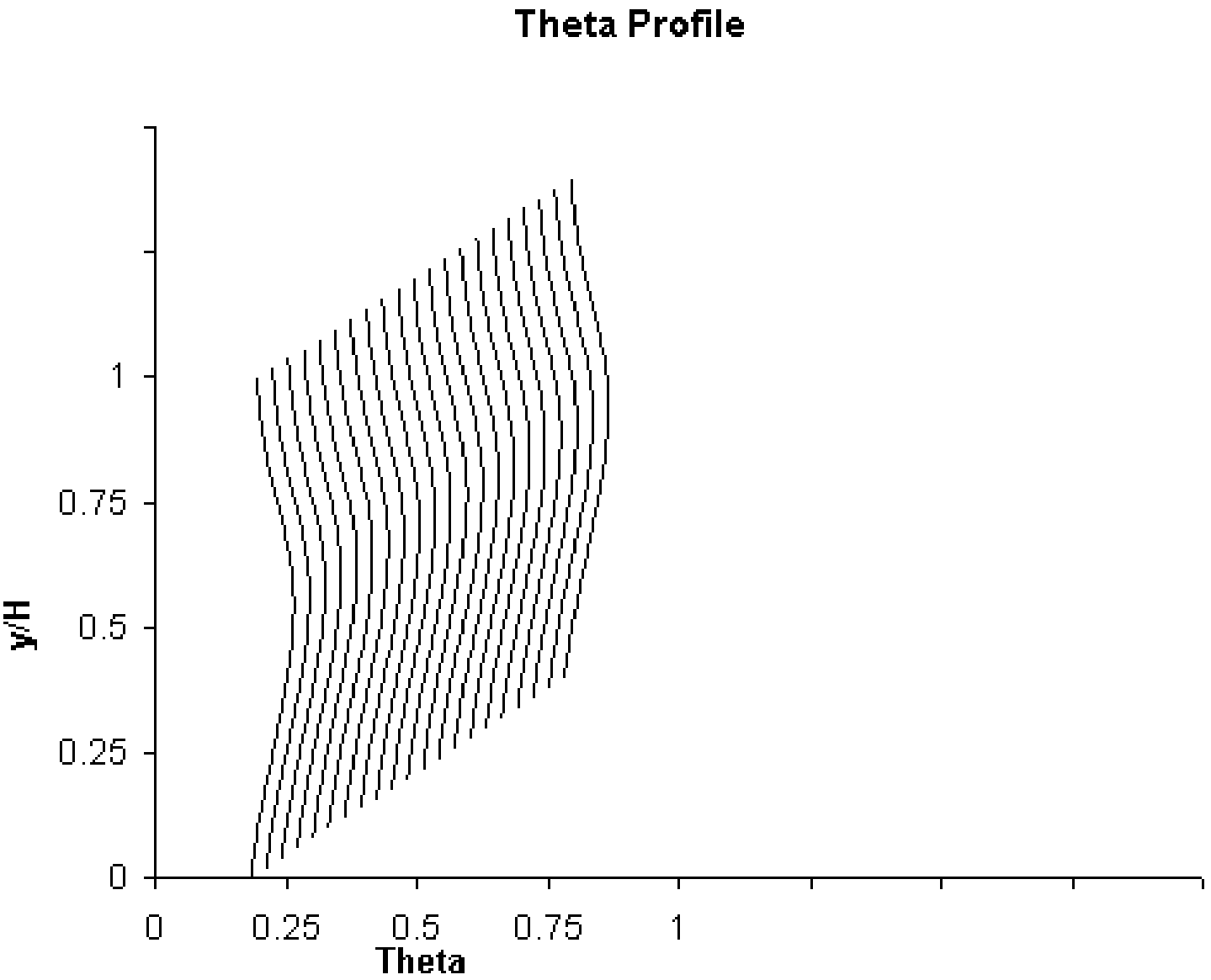


*x/H=2, (S/d=2.83)*

*J=64* *S/H=0.321* *H/d=8.81* *(x/d=17.62)*

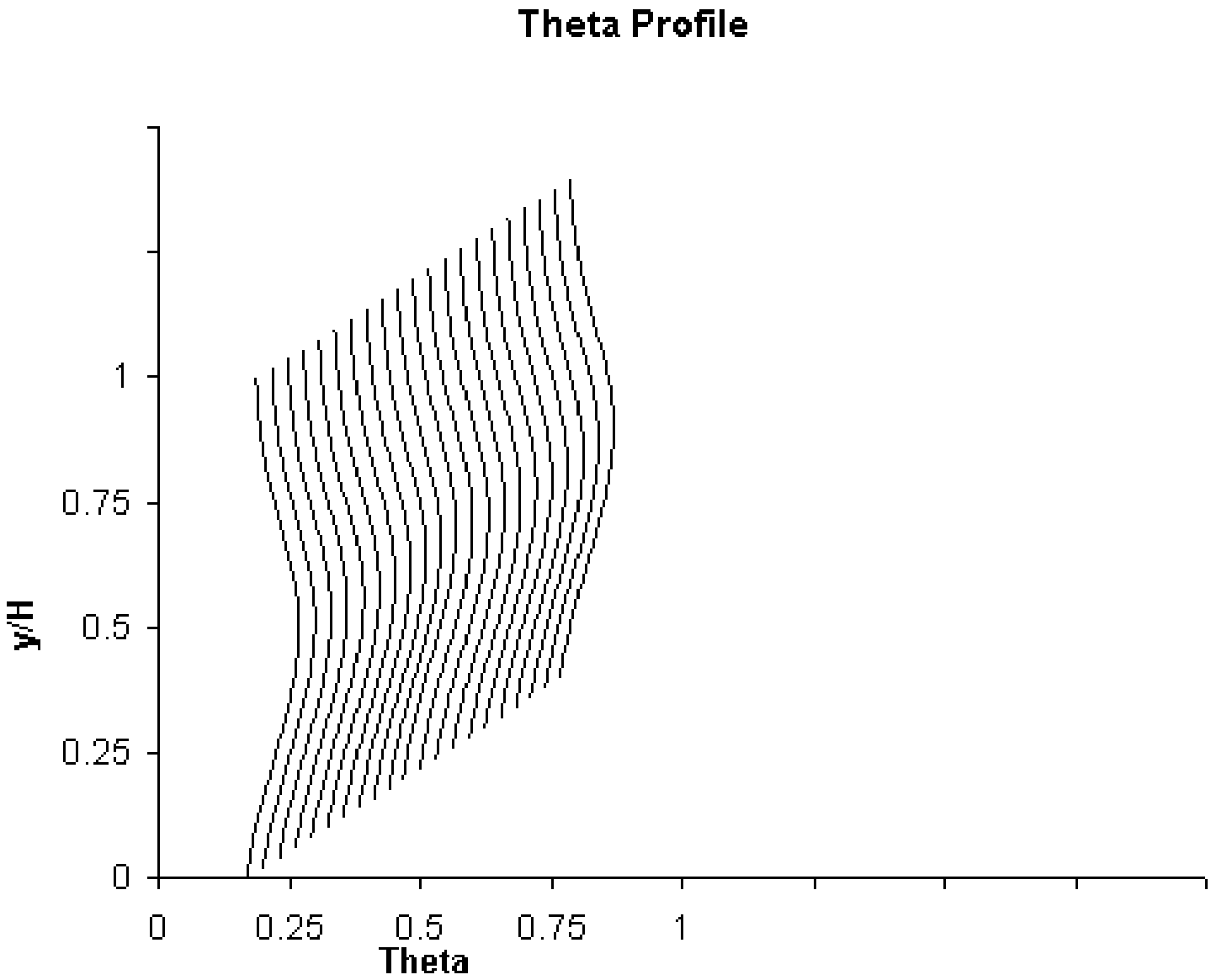


*x/H=2, (S/d=2.83)*

*J=35.2* *S/H=0.433* *H/d=6.54* *(x/d=13.08)*

## Theta Profile



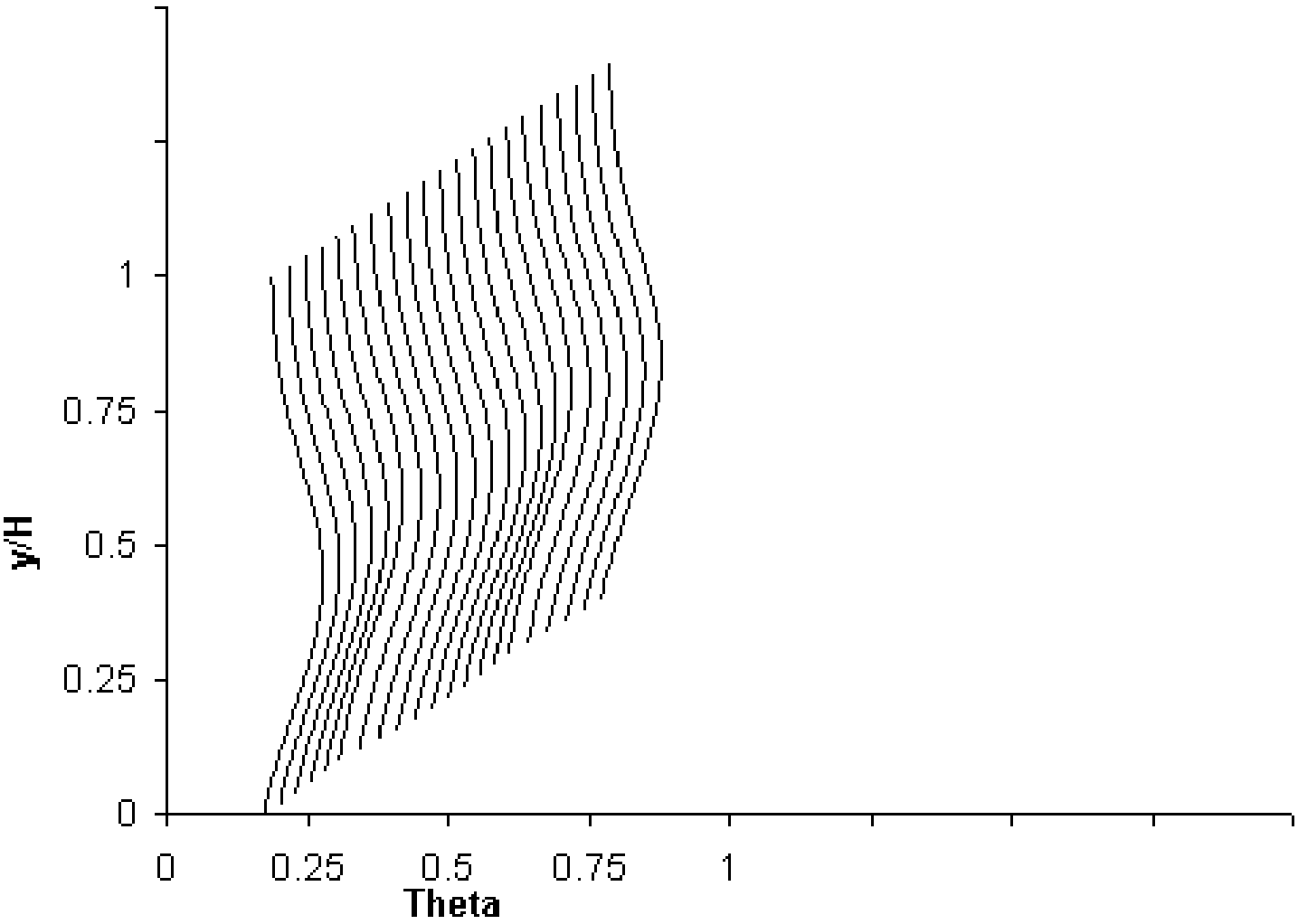


*x/H=2, (S/d=2.83)*

*J=26.4* *S/H=0.5* *H/d=5.66* *(x/d=11.32)*

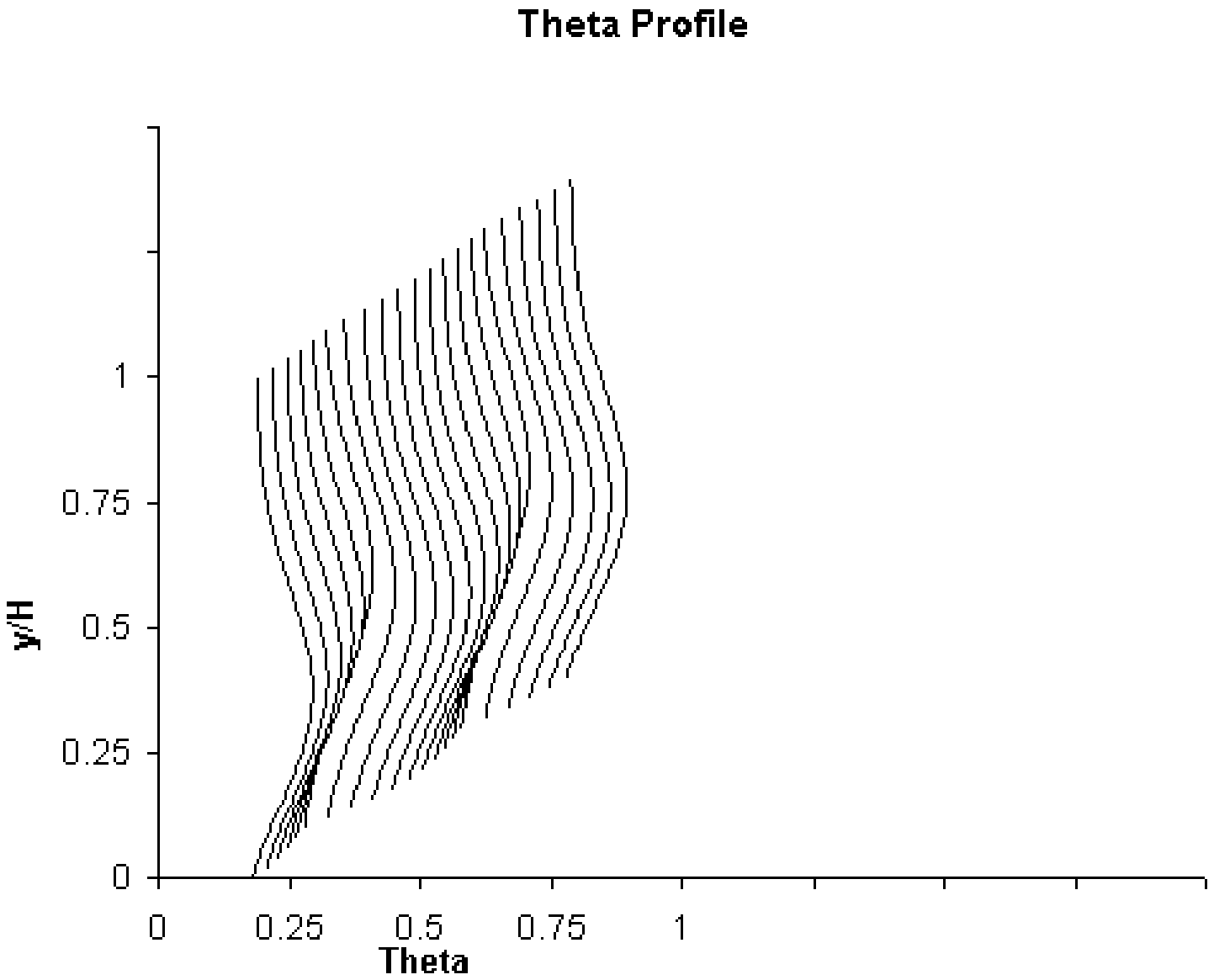


*x/H=2, (S/d=2.83)*

*J=16* *S/H=0.642* *H/d=4.41* *(x/d=8.81)*

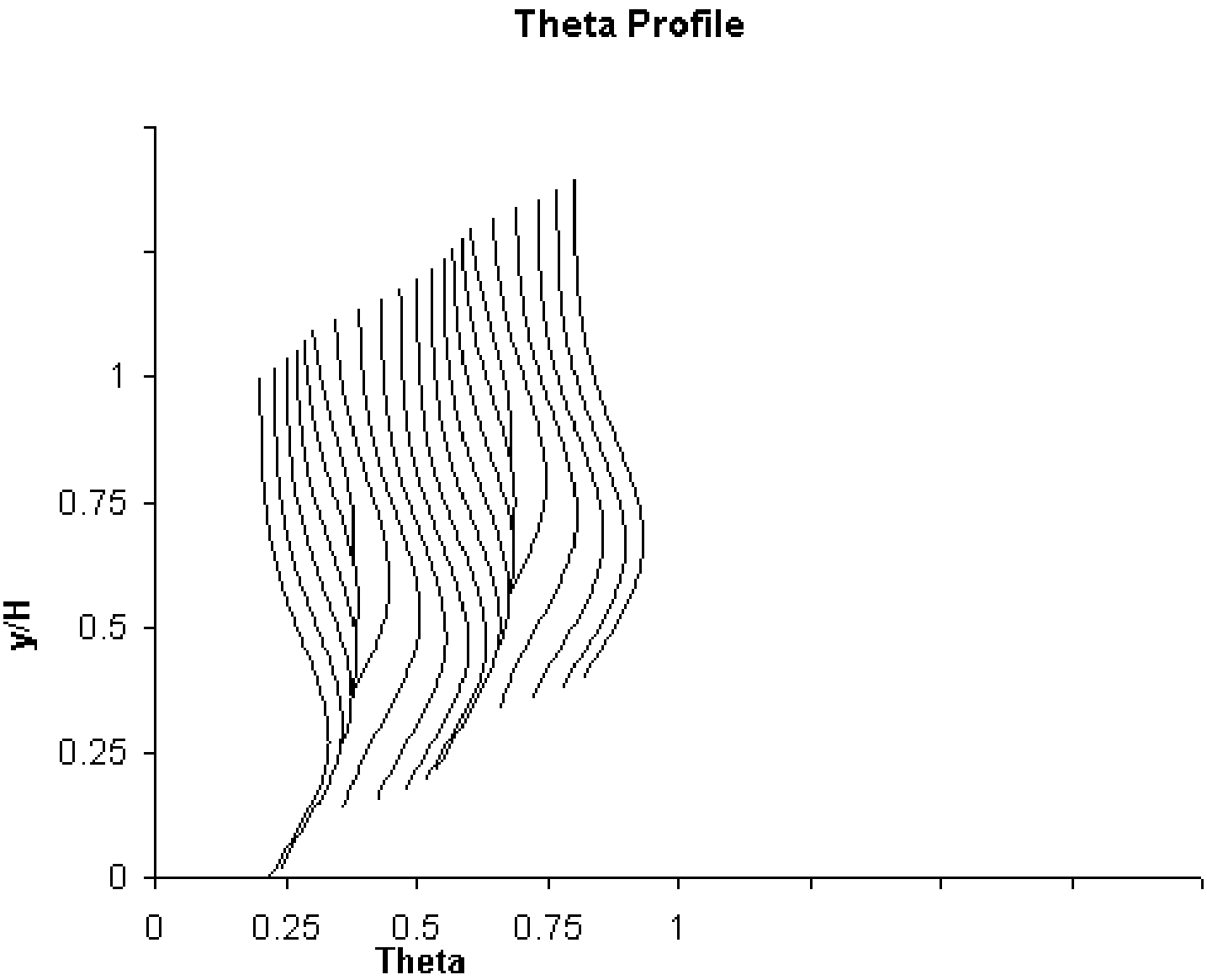


*x/H=2, (S/d=2,83)*

*J=8,8* *S/H=0.866* *H/d=3.27* *(x/d=6.54)*

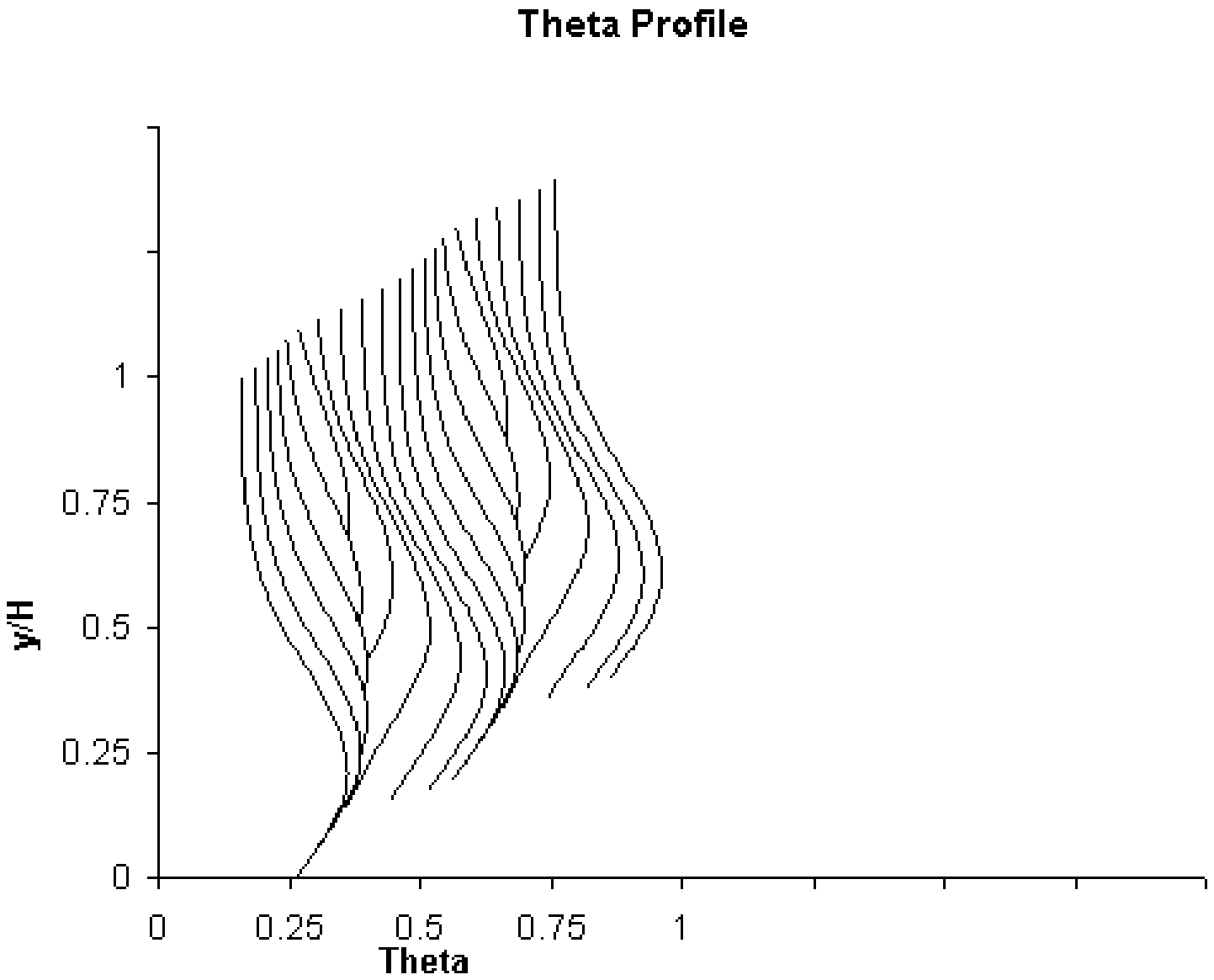


*x/H=2, (S/d=2.83)*

*J=6.6* *S/H=1* *H/d=2.83* *(x/d=5.66)*

Sequence 11

## Variations in scalar distributions with downstream distance for variable mainstream scalar distribution

*x/H= 0.25. 0.375, 0.5, 0.76, 1, 1.5, 2*

*DR=2.2, J=26.4, S/H=0.25, H/d=8, $C_d$=0.64*

Mainstream $\theta$=0.5 at bottom wall.
and does not change with distance

(cf. figure 15(a) in NASA/TM—2005-213137; see also figure 11(a) in NASA TM–87294)

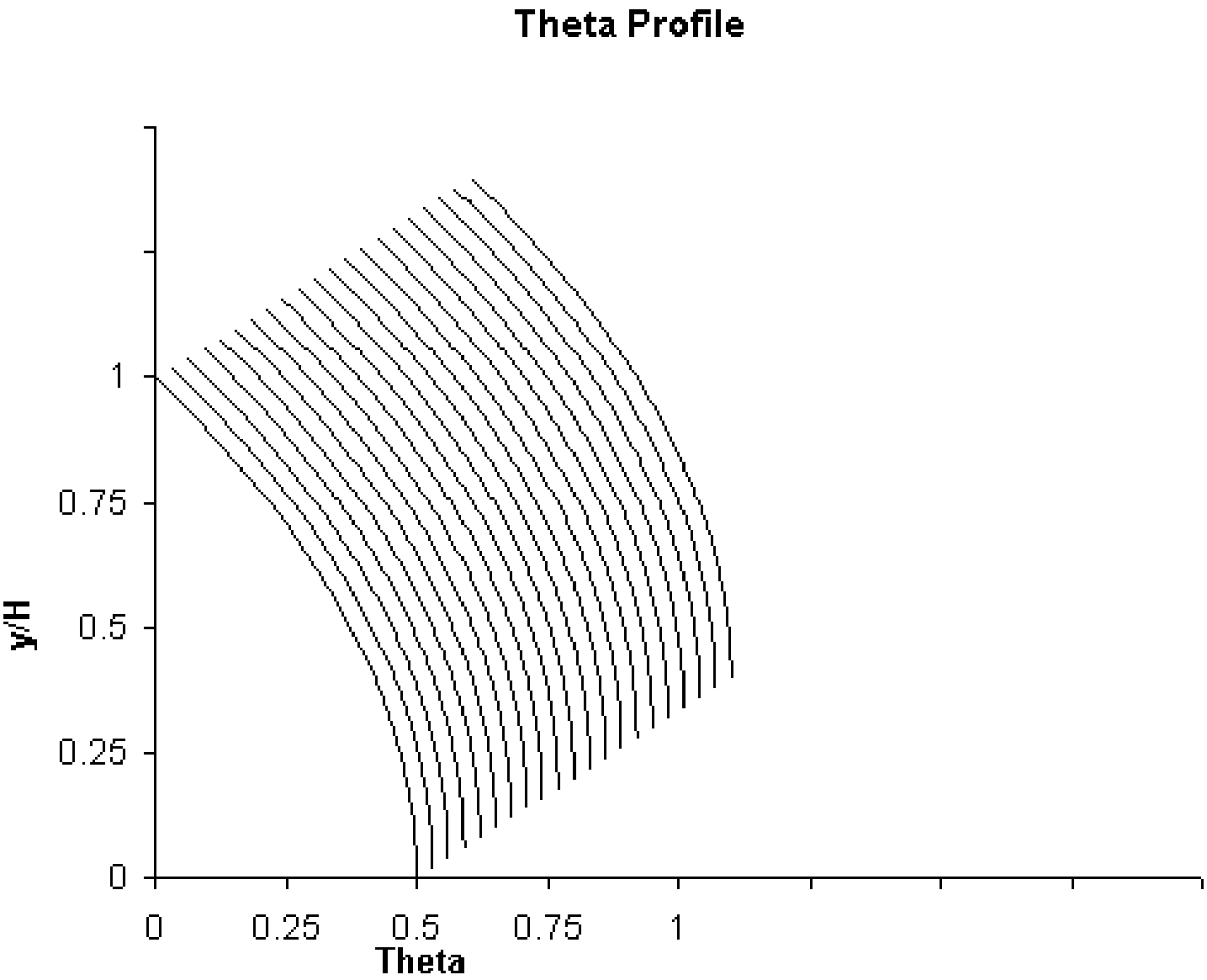


Mainstream profile

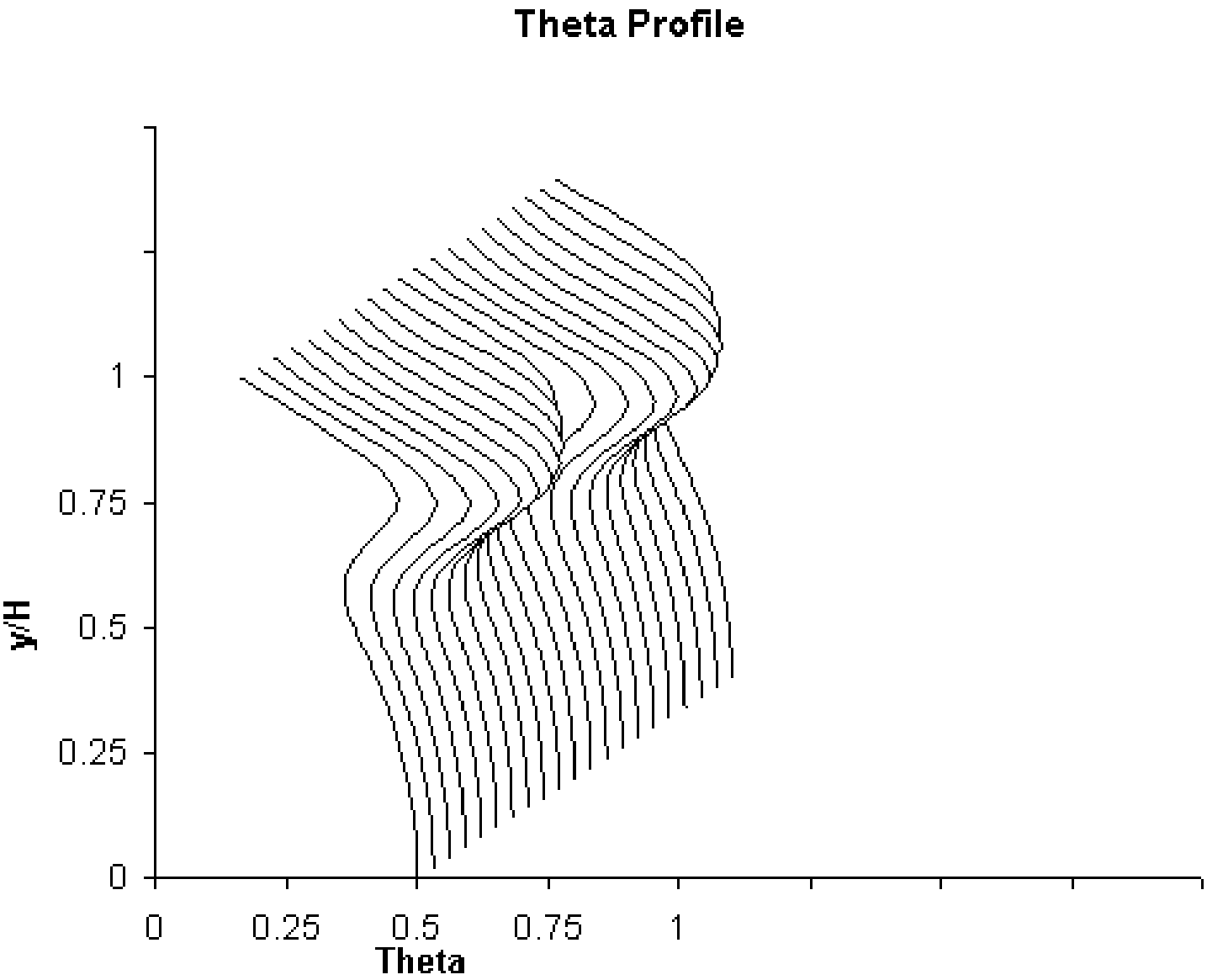


*x/H= 0.25 (x/d=2)*

*J=26.4, S/H=0.25; H/d=8, (S/d=2)*

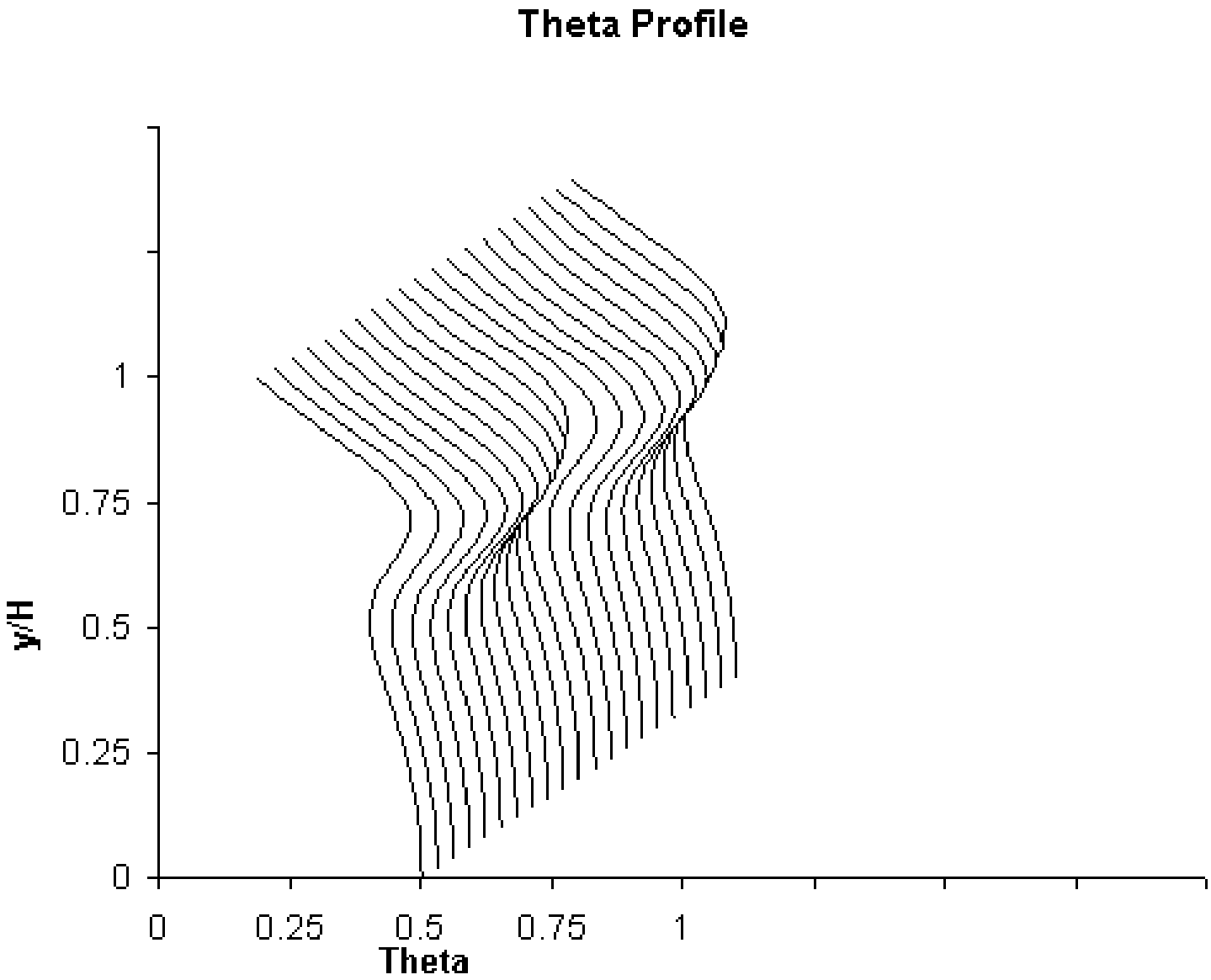


*x/H= 0.375 (x/d=3)*

*J=26.4, S/H=0.25; H/d=8, (S/d=2)*

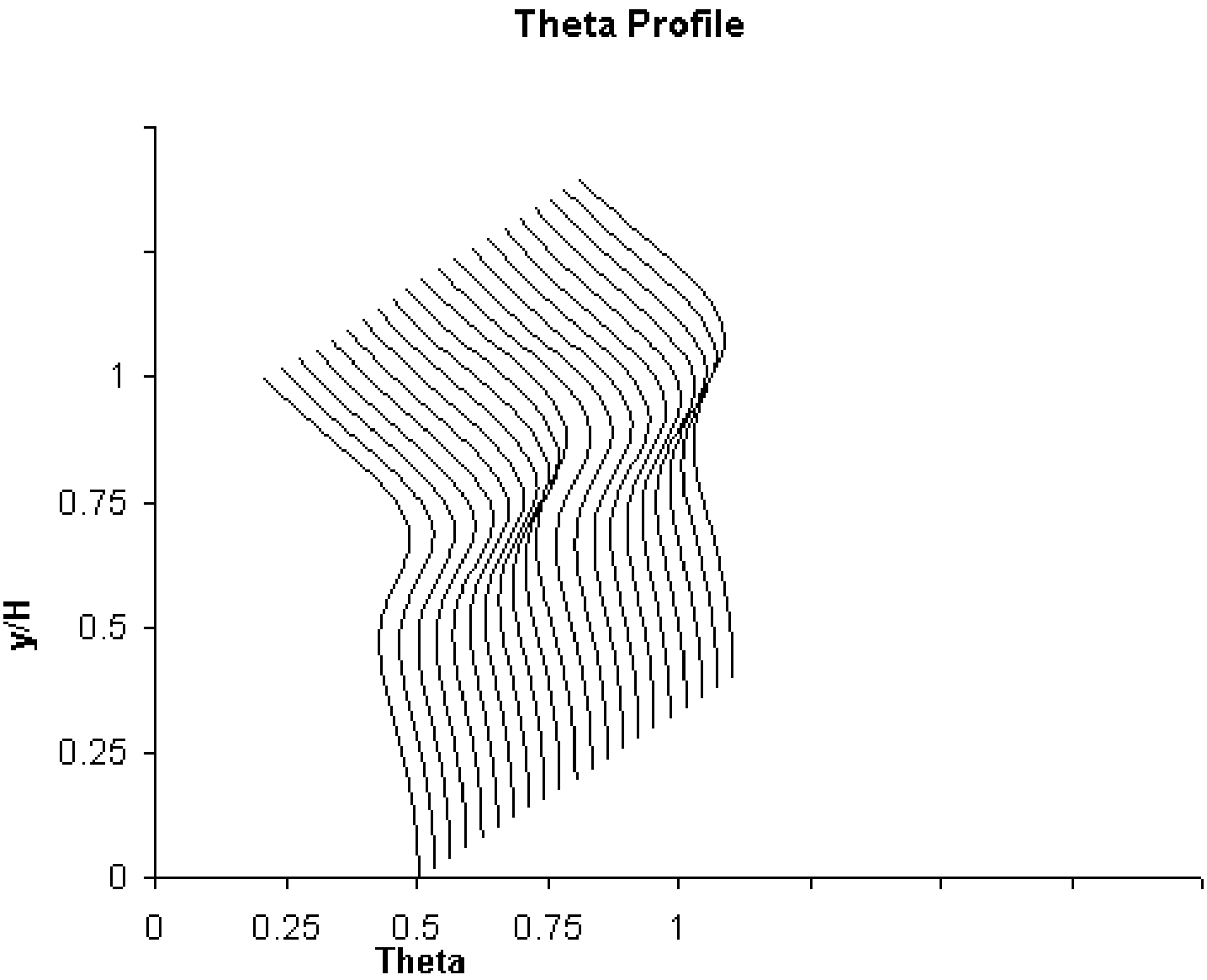


*x/H= 0.5 (x/d=4)*

*J=26.4, S/H=0.25; H/d=8, (S/d=2)*

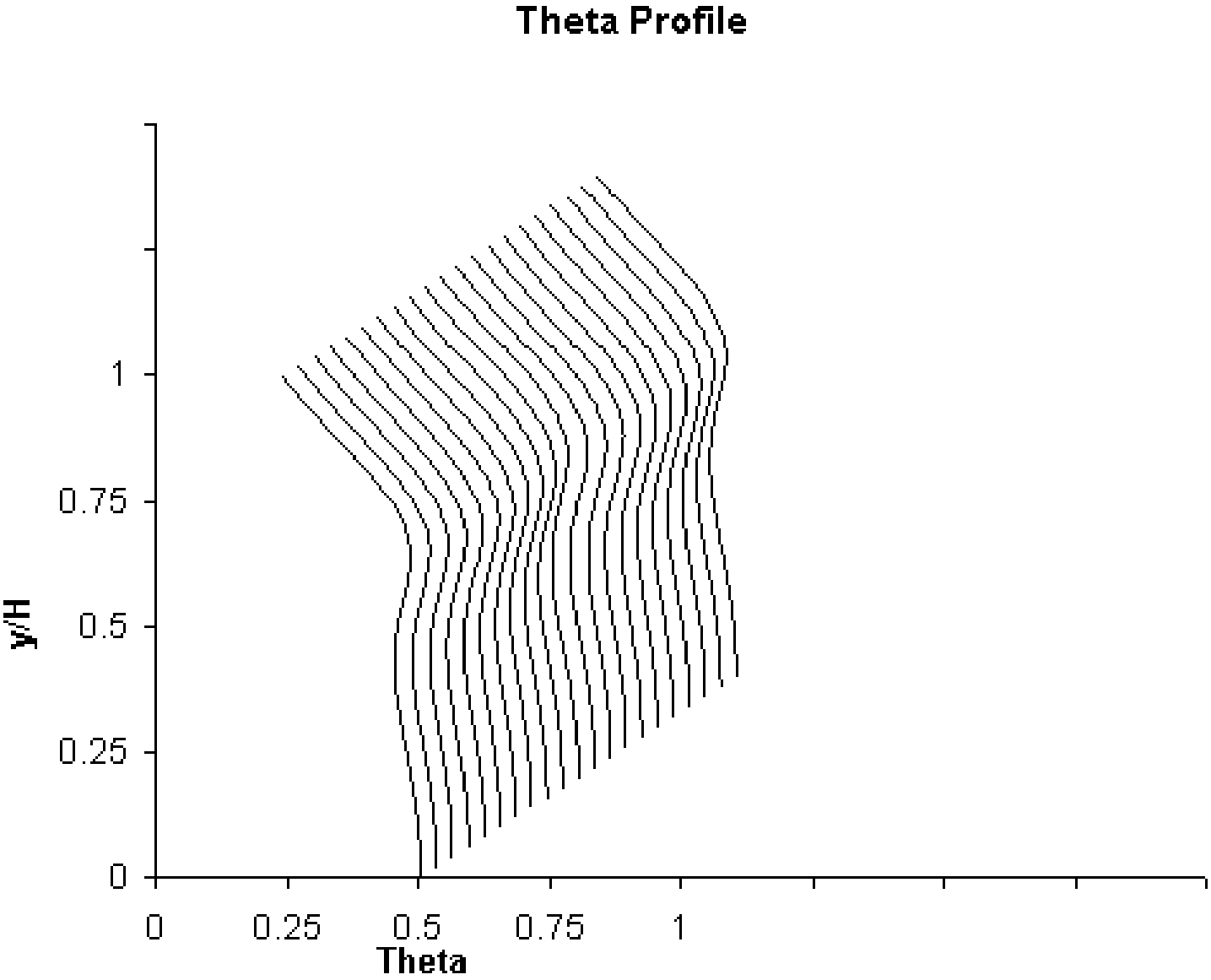


*x/H= 0.75 (x/d=6)*

*J=26.4, S/H=0.25; H/d=8, (S/d=2)*

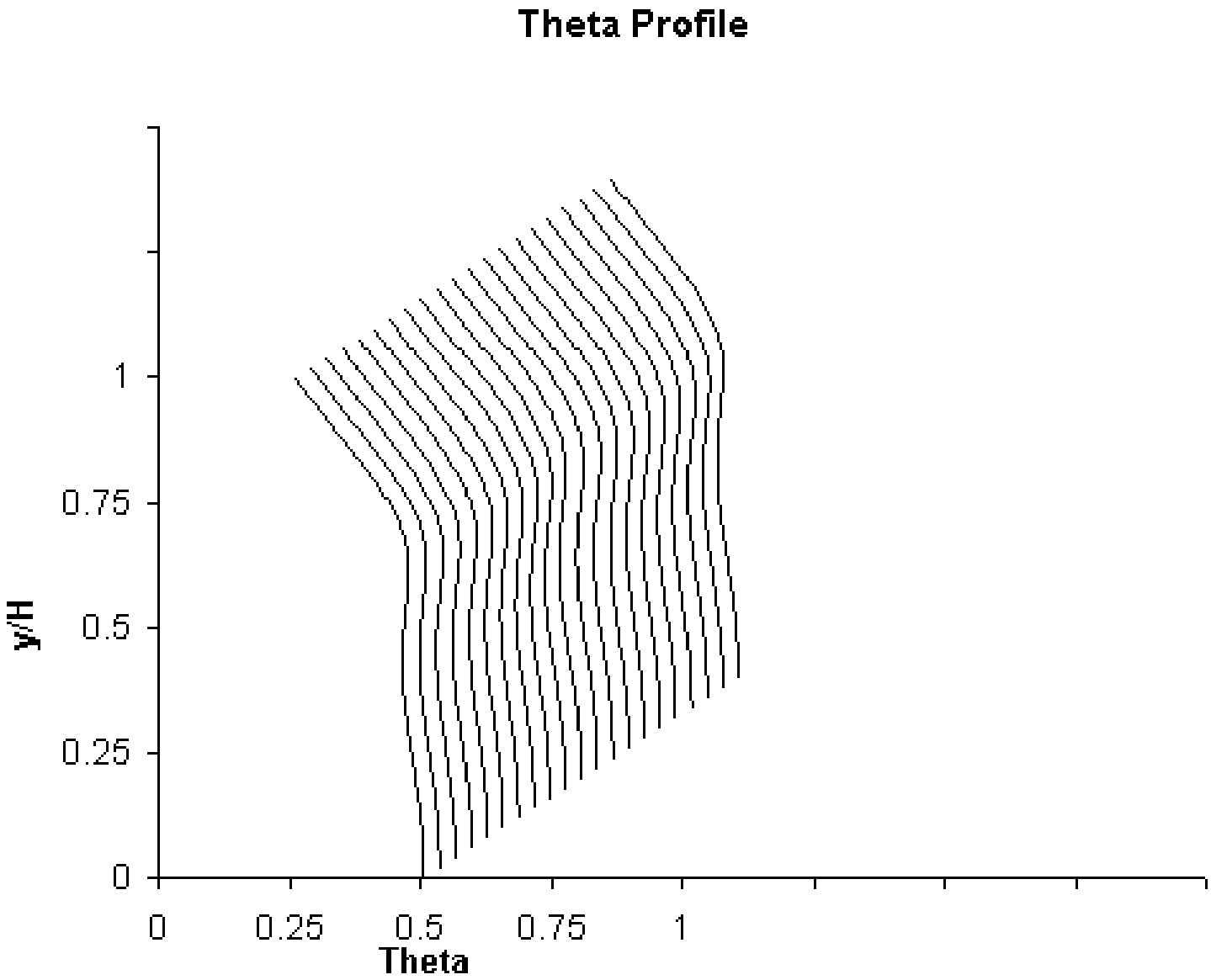


*x/H= 1 (x/d=8)*

*J=26.4, S/H=0.25; H/d=8, (S/d=2)*

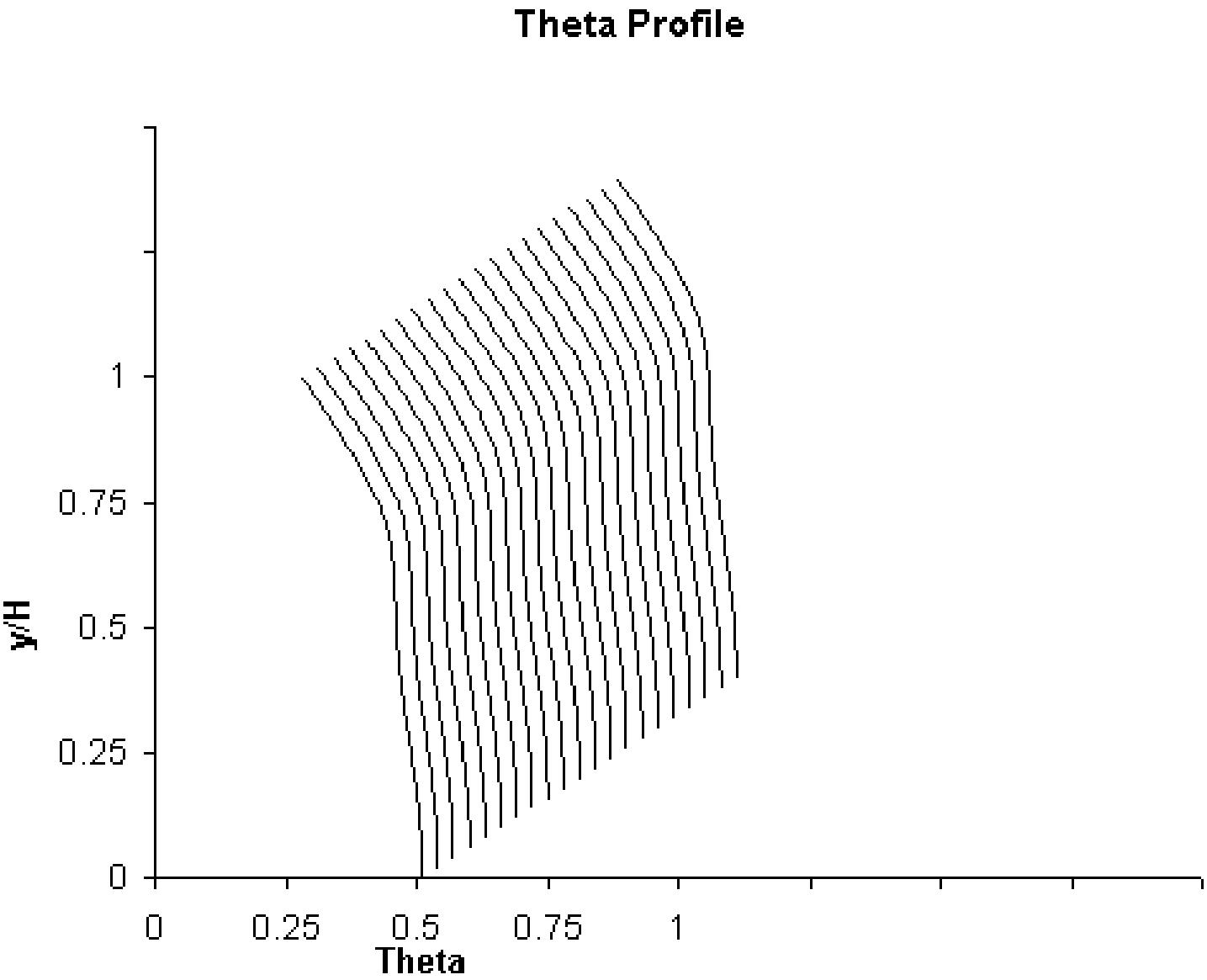


*x/H= 1.5 (x/d=12)*

*J=26.4, S/H=0.25; H/d=8, (S/d=2)*

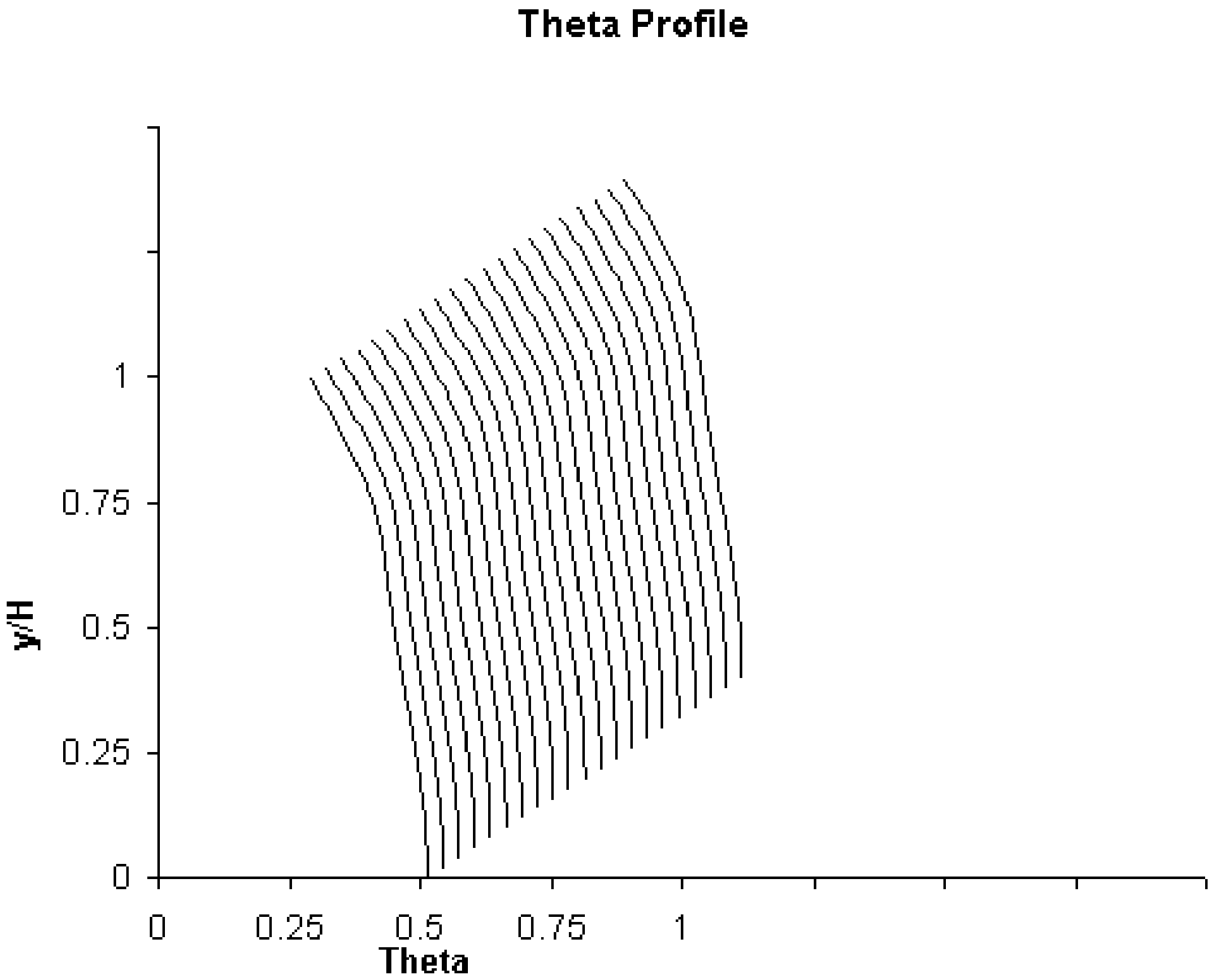


*x/H= 2 (x/d=16)*

*J=26.4, S/H=0.25; H/d=8, (S/d=2)*

Sequence 12

## Variations in scalar distributions with Increasing flow area convergence

*dH/dx*=0, 0.1, 0.2, 0.3, 0.4, 0.5

*x/H=1, DR=2.2, J=26.4, S/H=0.5, H/d=4,* $C_d$*=0.64*

(cf. figures 16(a) and 16(b) in NASA/TM—2005-213137 and figure 12 in NASA TM–87204)

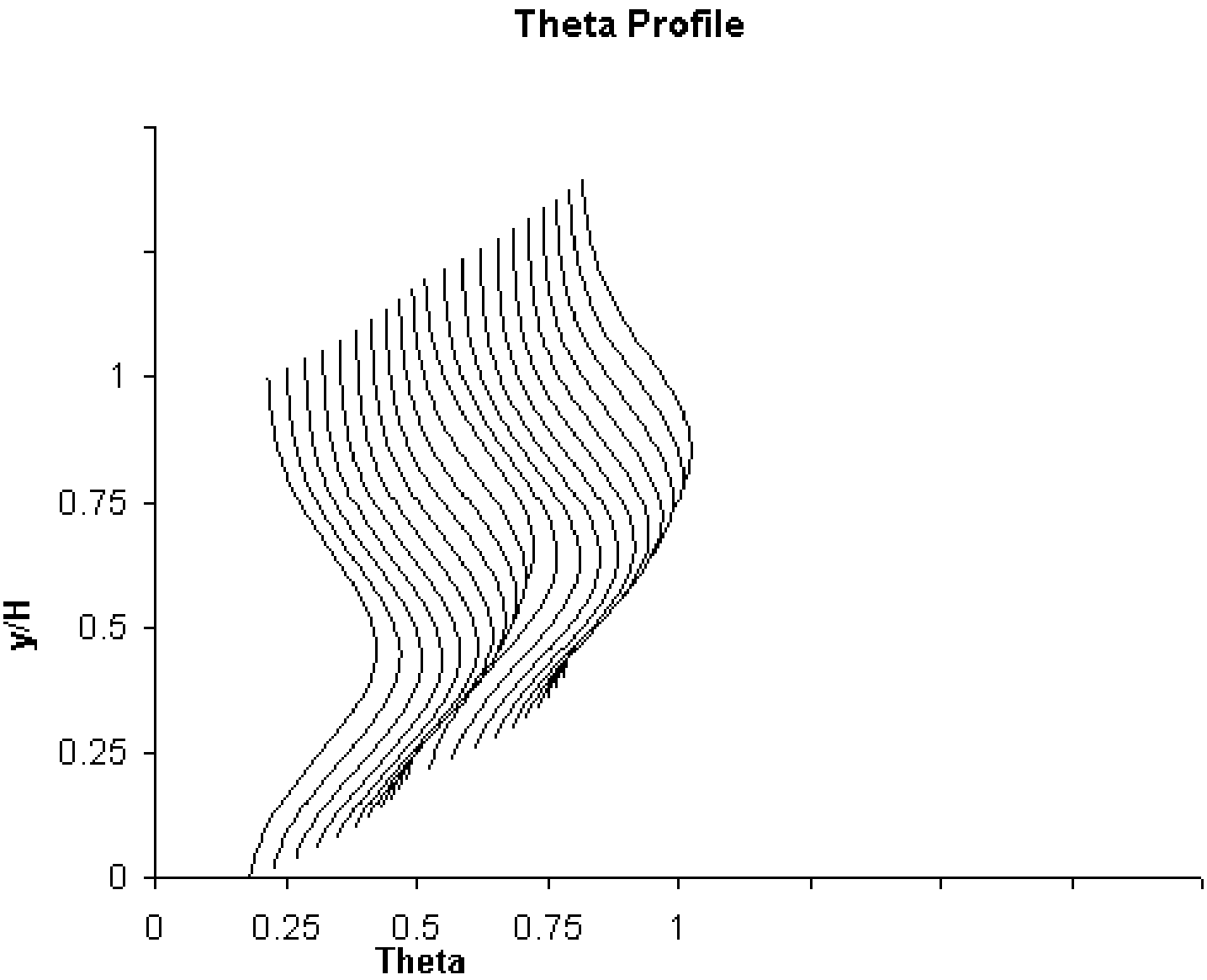


*x/H=1, J=26.4, S/H=0.5, H/d=4, (S/d=2, x/d=4)*
*dH/dx=0*

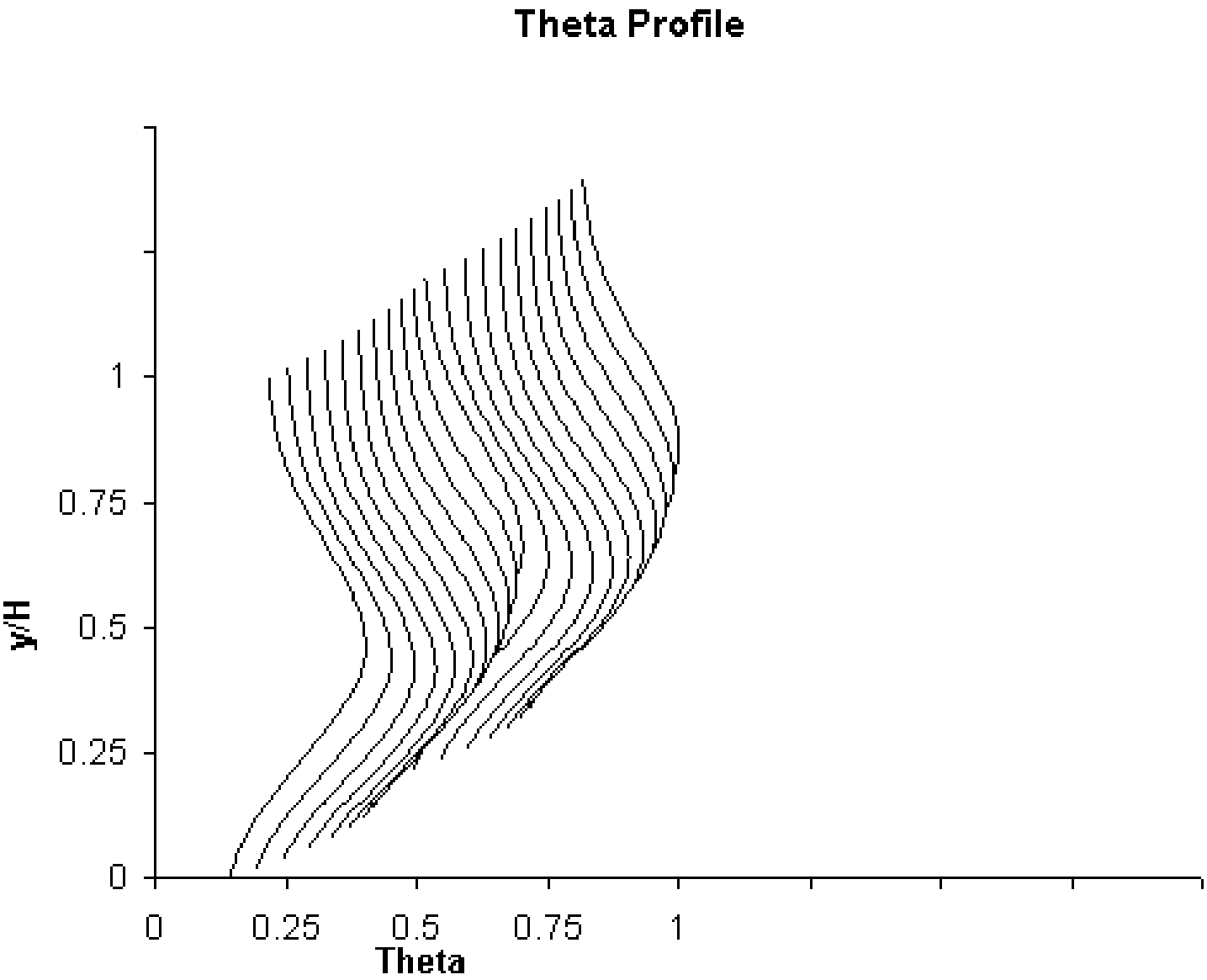


*x/H=1, J=26.4, S/H=0.5, H/d=4, (S/d=2, x/d=4)*
*dH/dx=0.1*

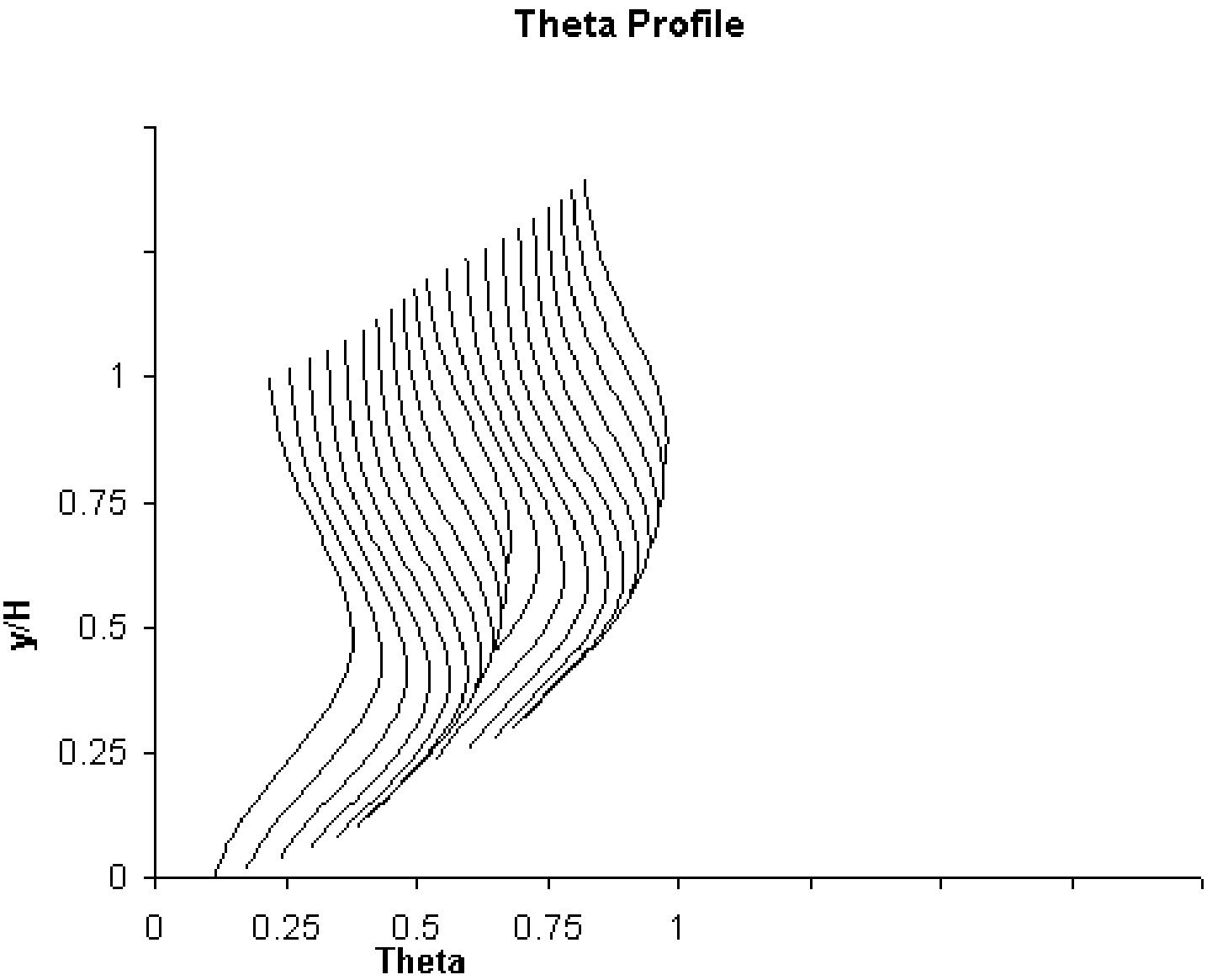


*x/H=1, J=26.4, S/H=0.5, H/d=4, (S/d=2, x/d=4)*
*dH/dx=0.2*

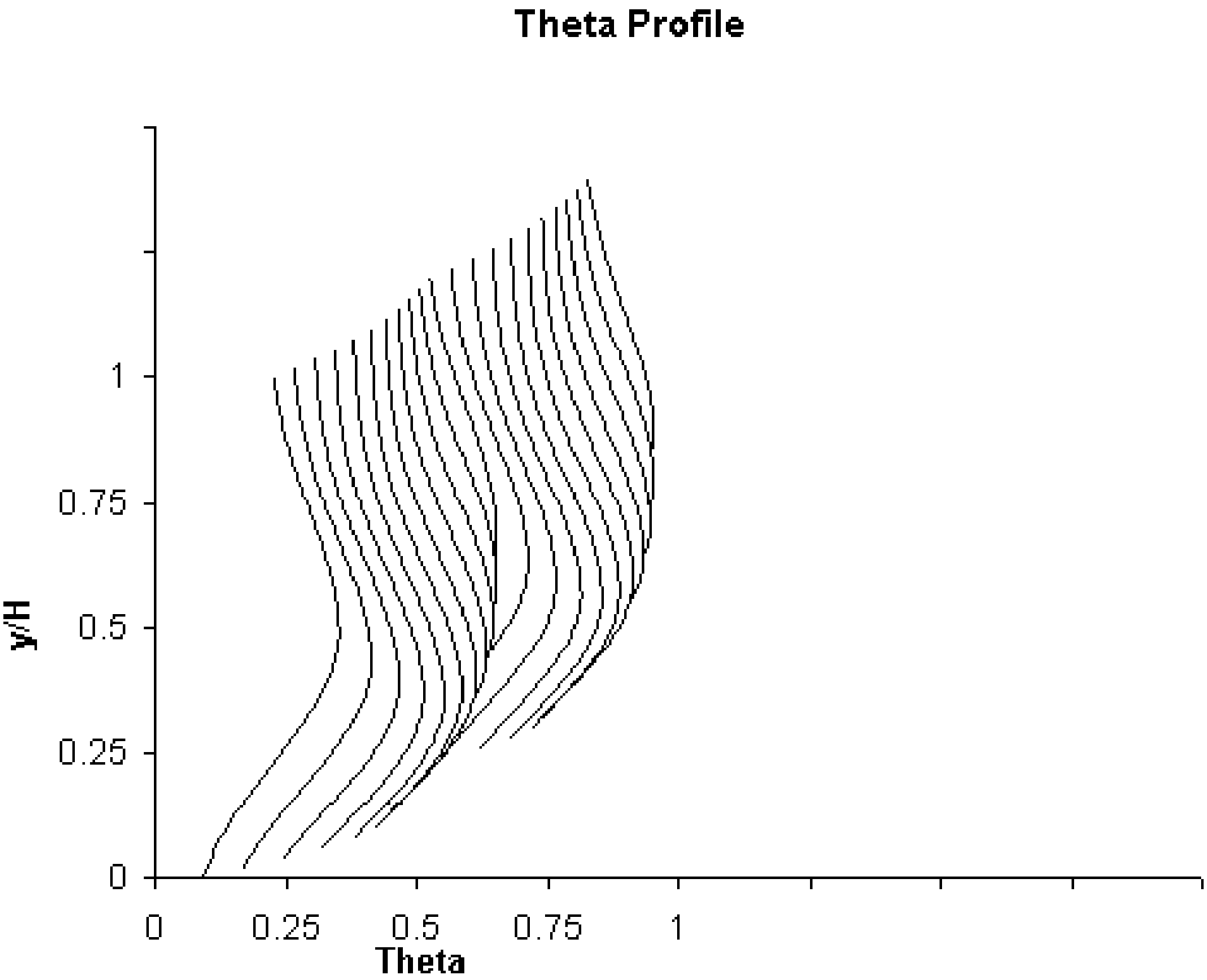


*x/H=1, J=26.4. S/H=0.5, H/d=4, (S.d=2, x/d=4)*
*dH/dx=0.3*

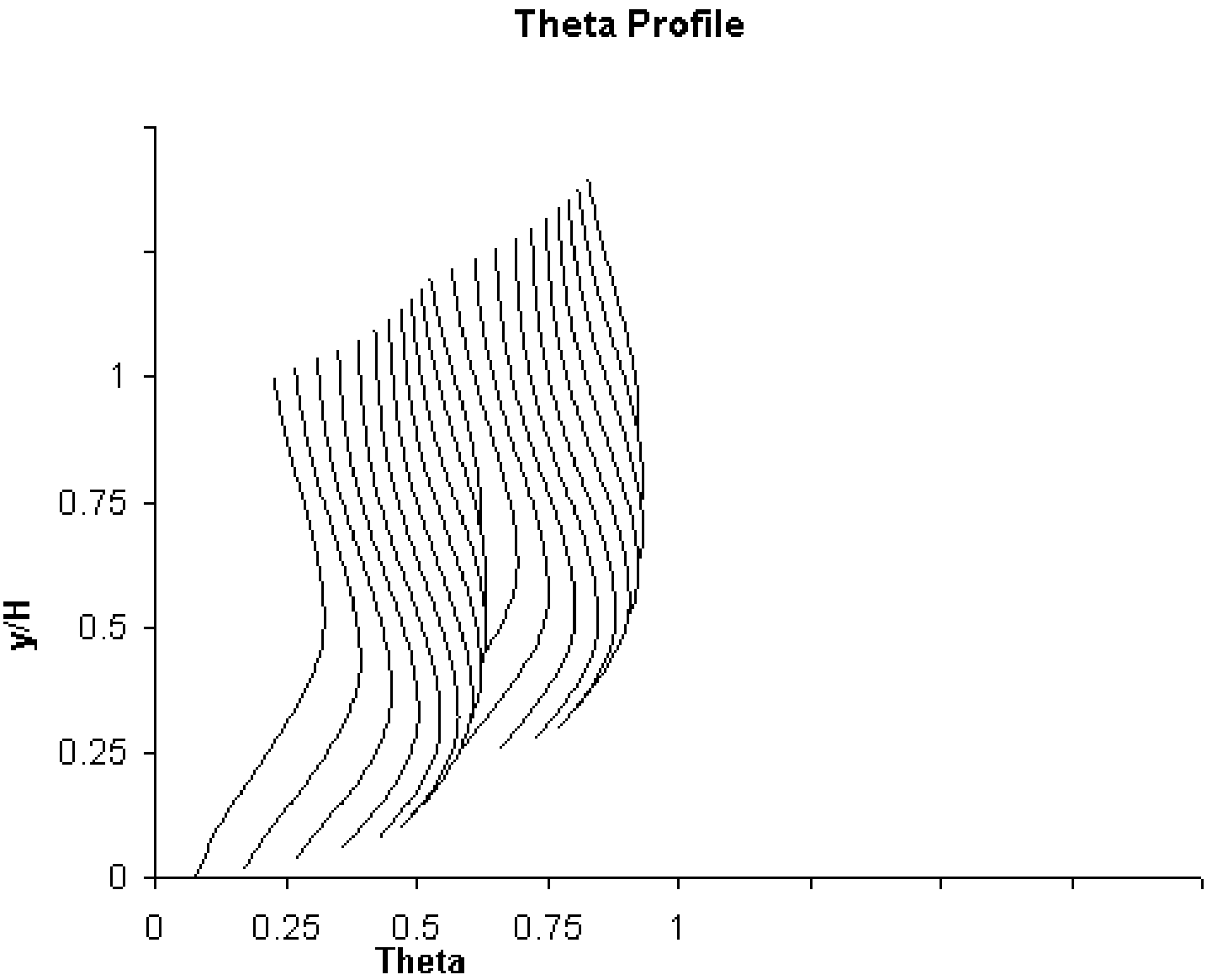


*x/H=1, J=26.4, S/H=0.5, H/d=4, (S/d=2, x/d=4)*
*dH/dx=0.4*

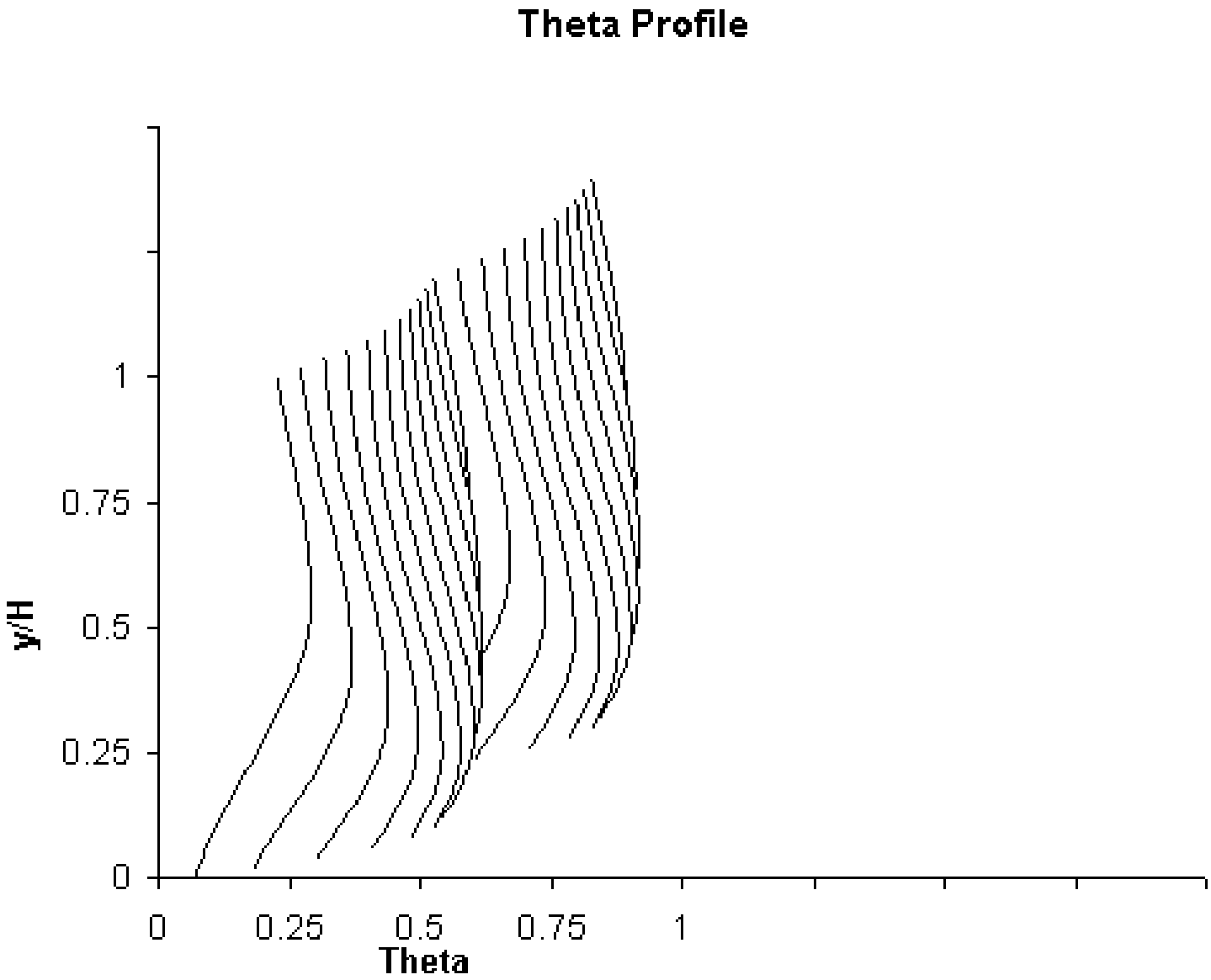


*x/H=1, J=26.4, S/H=0.5, H/d=4, (S/d=2, x/d=4)*
*dH/dx=0.5*

Sequence 13

## Variations in scalar distributions for bluff and streamlined slots

*Bluff slot; L/W=2.85*
*Bluff slot; L/W=2*
*Bluff slot; L/W=1.33*
*Round hole; L/W=1*
*Streamlined slot; L/W=1.33*
*Streamlined slot; L/W=2*
*Streamlined slot; L/W=2.85*

*x/H=0.5, DR=2.2, J=26.4, S/H=0.5, H/d=4, $C_d$=0.64*

(cf. figure 13 in NASA TM–87294; see also
figures 17(a) and 17(b) in NASA/TM—2005-213137)

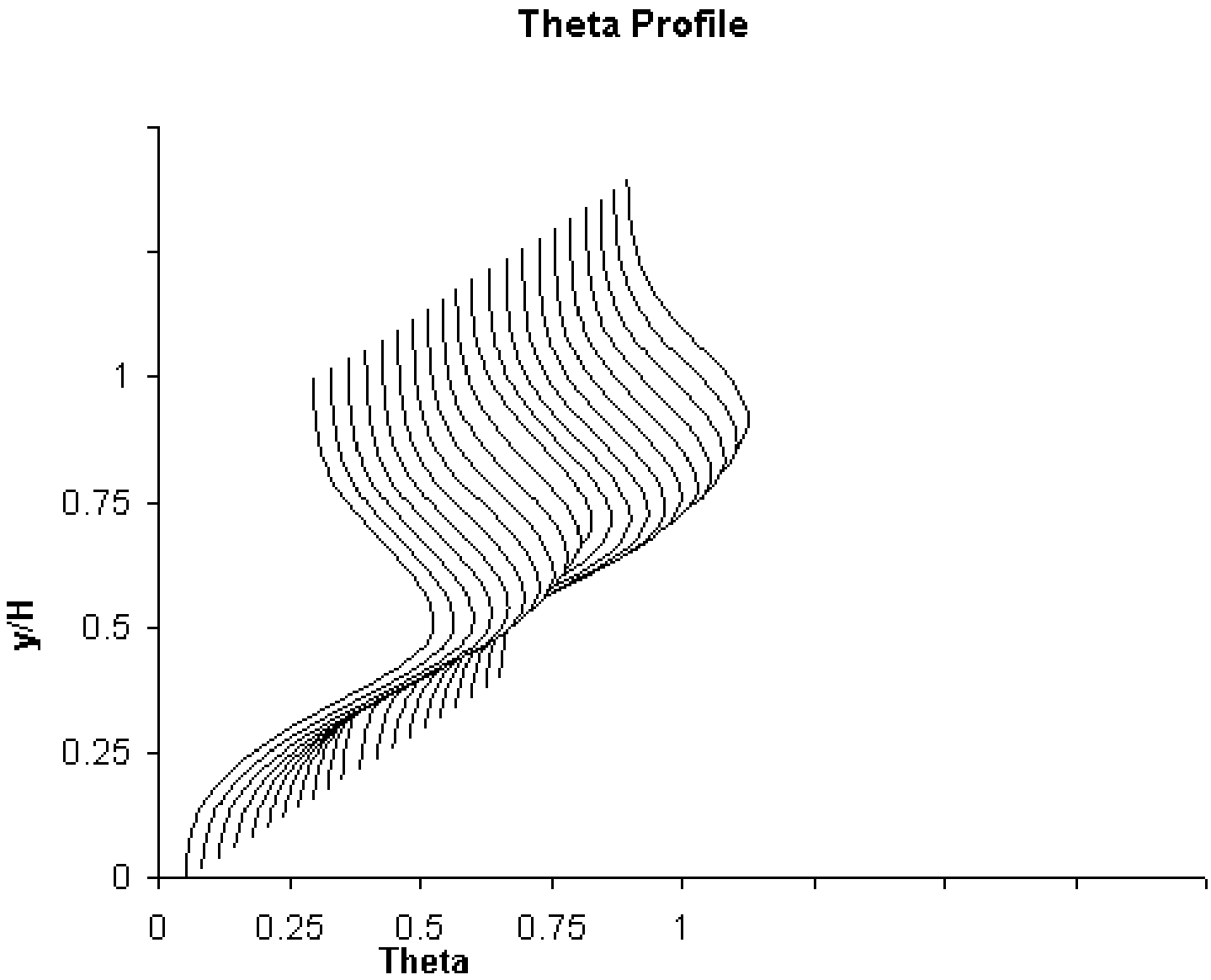


*Bluff slot* *L/W=2.85*

*x/H=0.5; J=26.4; S/H=0.5; H/d=4, (S/d=2, x/d=2)*

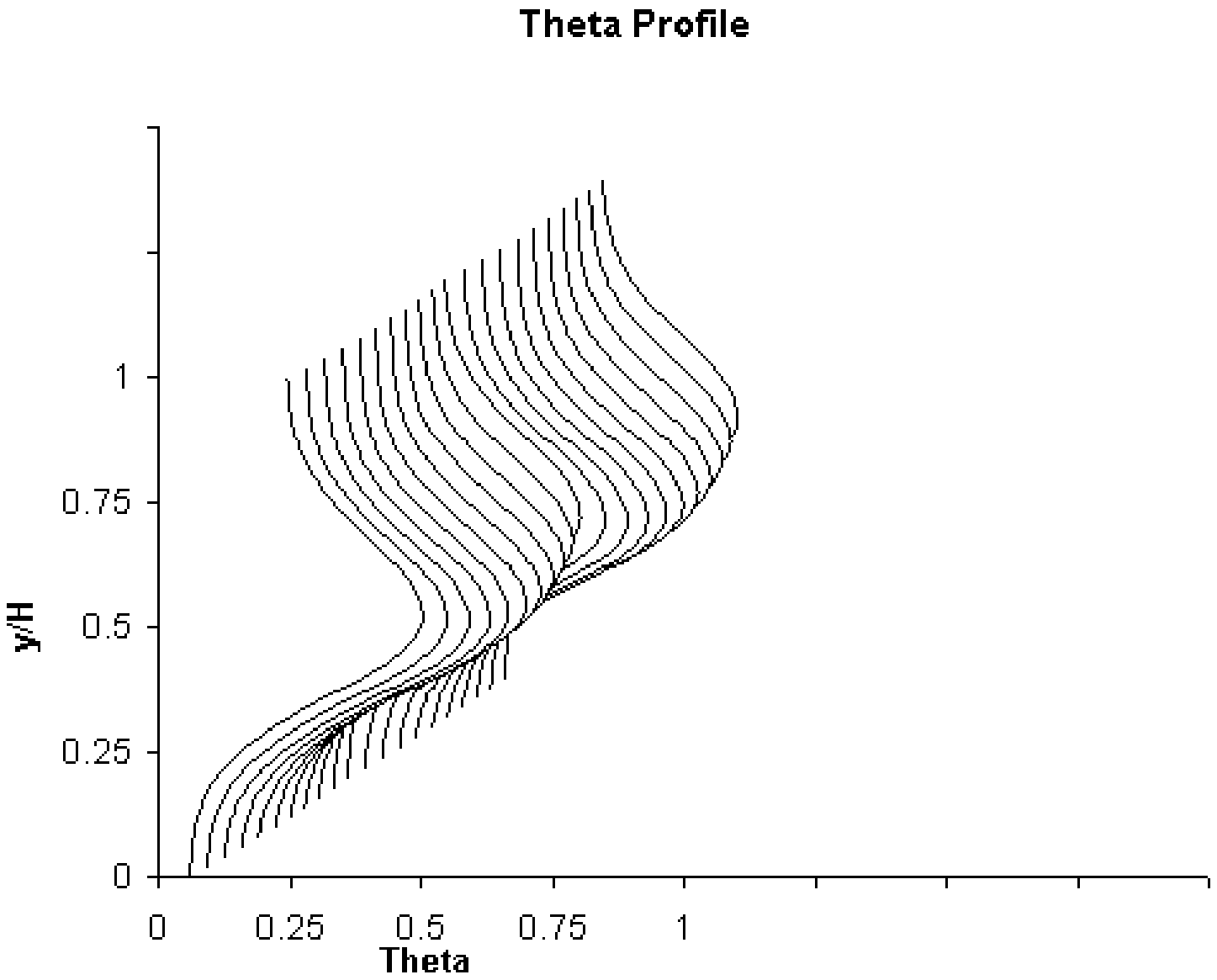


*Bluff slot* *L/W=2*

*x/H=0.5; J=26.4; S/H=0.5; H/d=4, (S/d=2, x/d=2)*

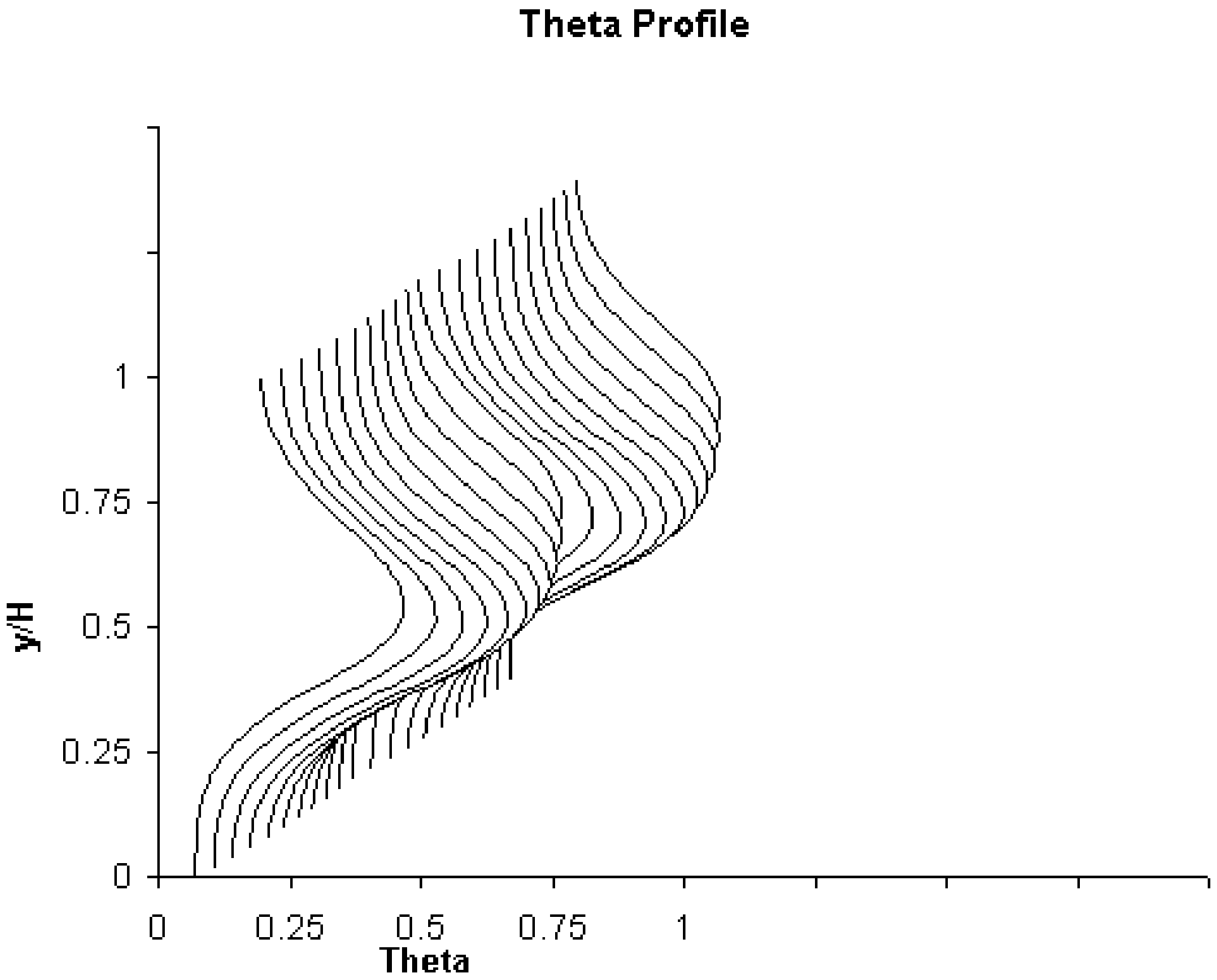


*Bluff slot* *L/W=1.33*

*x/H=0.5; J=26.4; S/H=0.5; H/d=4, (S/d=2, x/d=2)*

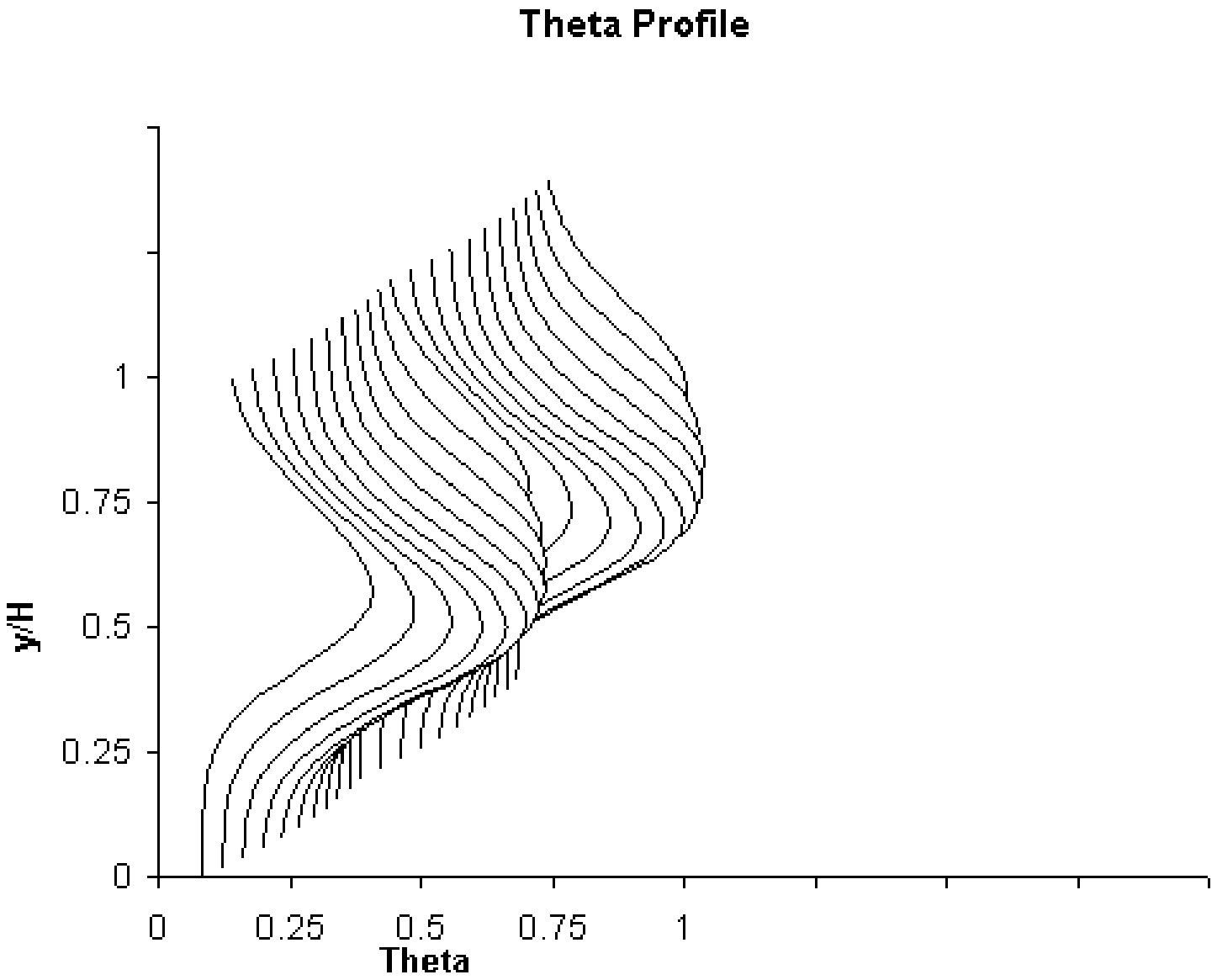


*Round hole L/W=1*

*x/H=0.5; J=26.4; S/H=0.5; H/d=4, (S/d=2, x/d=2)*

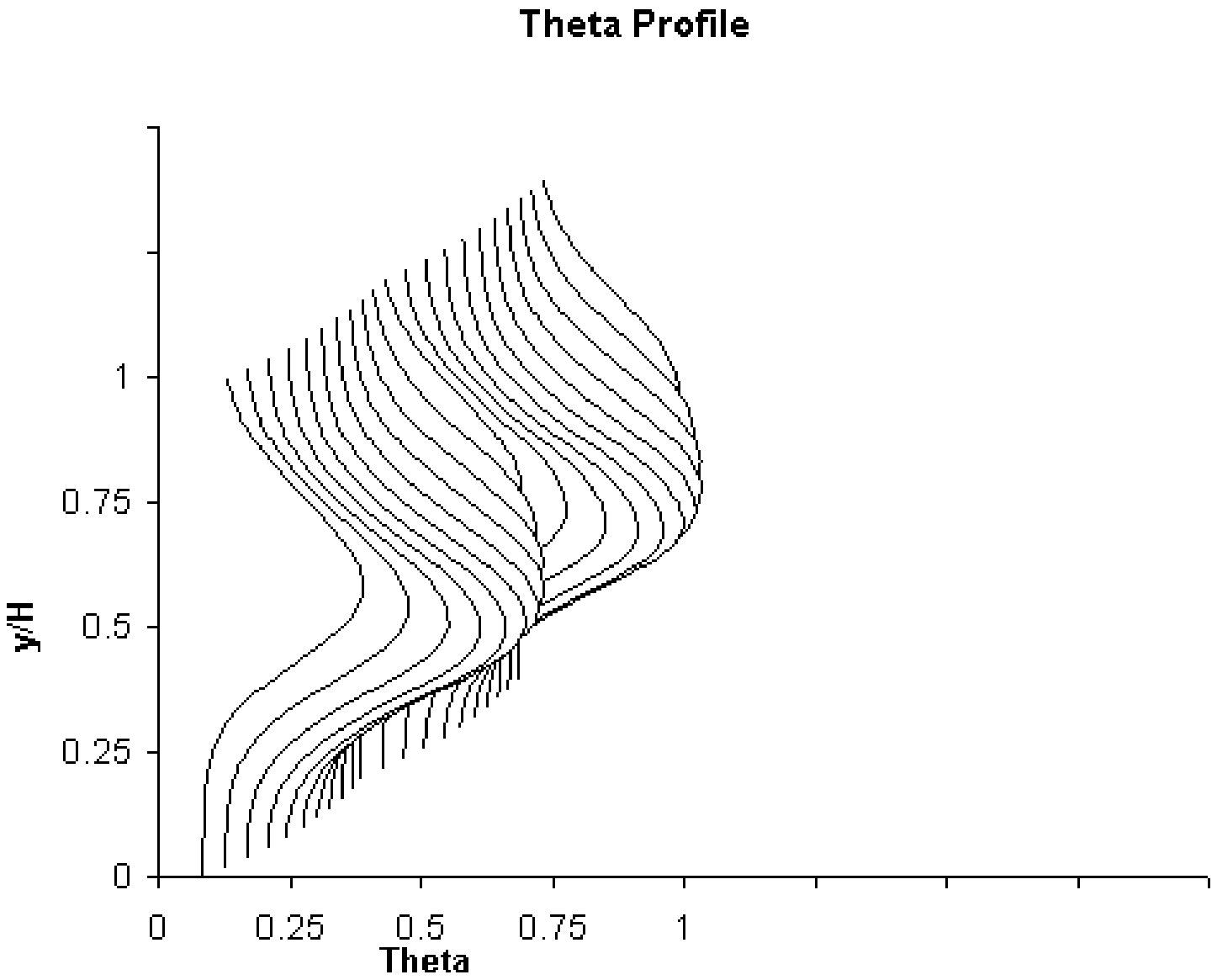


*Streamlined slot L/W=1.33*

*x/H=0.5; J=26.4; S/H=0.5; H/d=4, (S/d=2, x/d=2)*

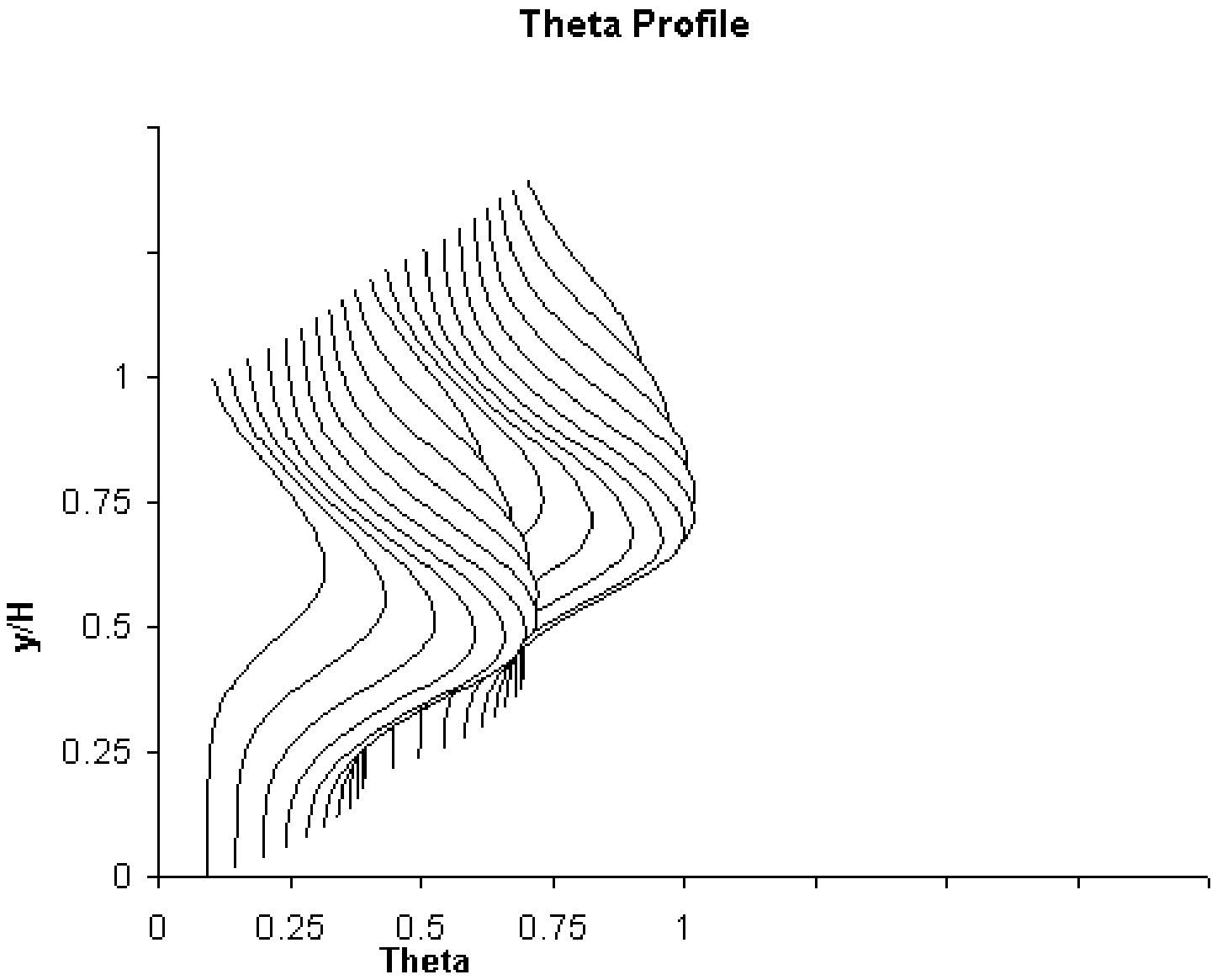


*Streamlined slot L/W=2*

*x/H=0.5; J=26.4; S/H=0.5; H/d=4, (S/d=2, x/d=2)*

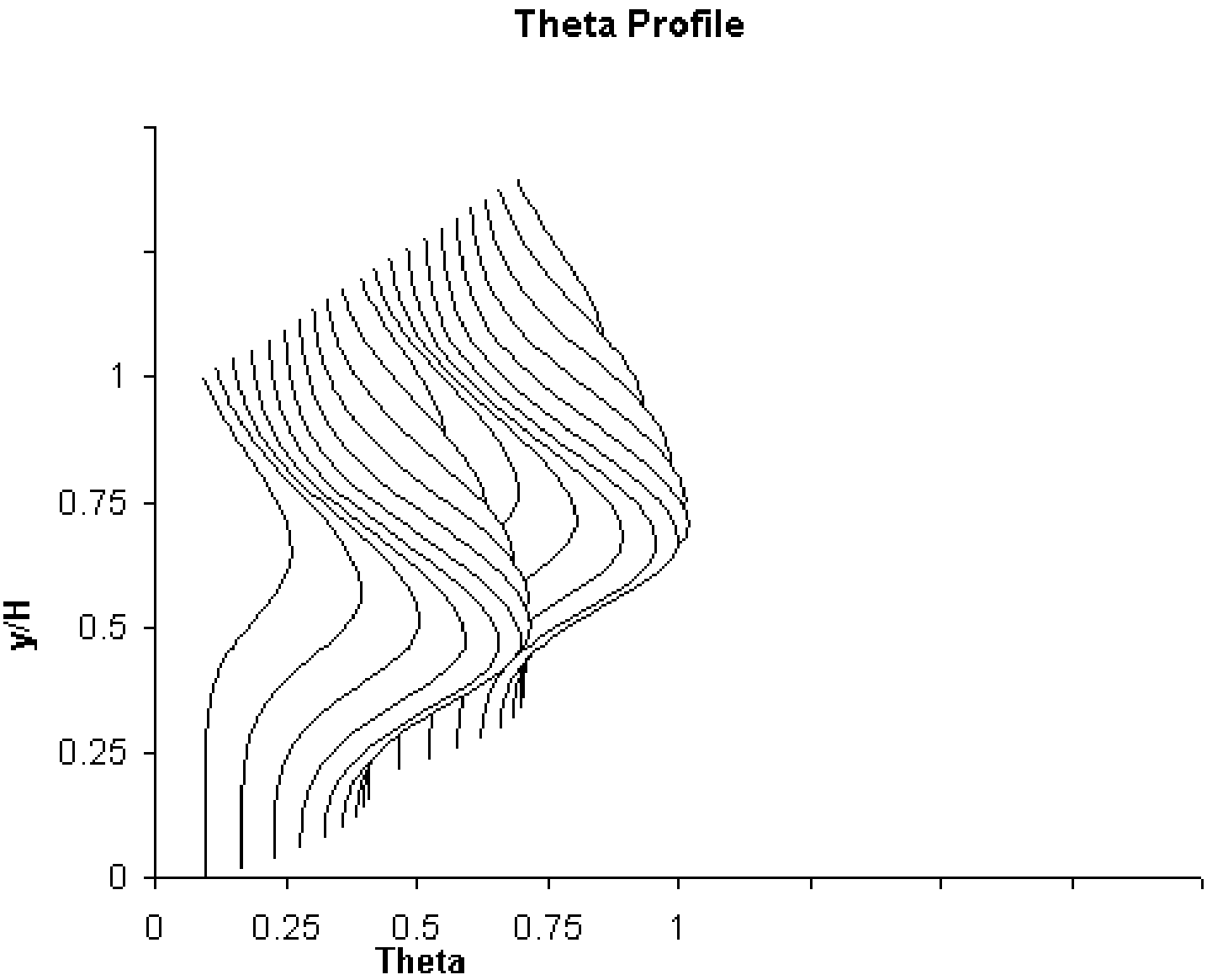


*Streamlined slot L/W=2.85*

*x/H=0.5; J=26.4; S/H=0.5; H/d=4, (S/d=2, x/d=2)*

Sequence 14

## Variations in scalar distributions with downstream distance for slanted slots

*x/H= 0.125, 0.25, 0.375, 0.5, 0.75, 1, 1.5, 2*

*L/W=2.8, DR=2.2, J=26.4, S/H=0.5, H/d=4. $C_d$=0.64*

(cf. figure 18 in NASA/TM—2007-213137)

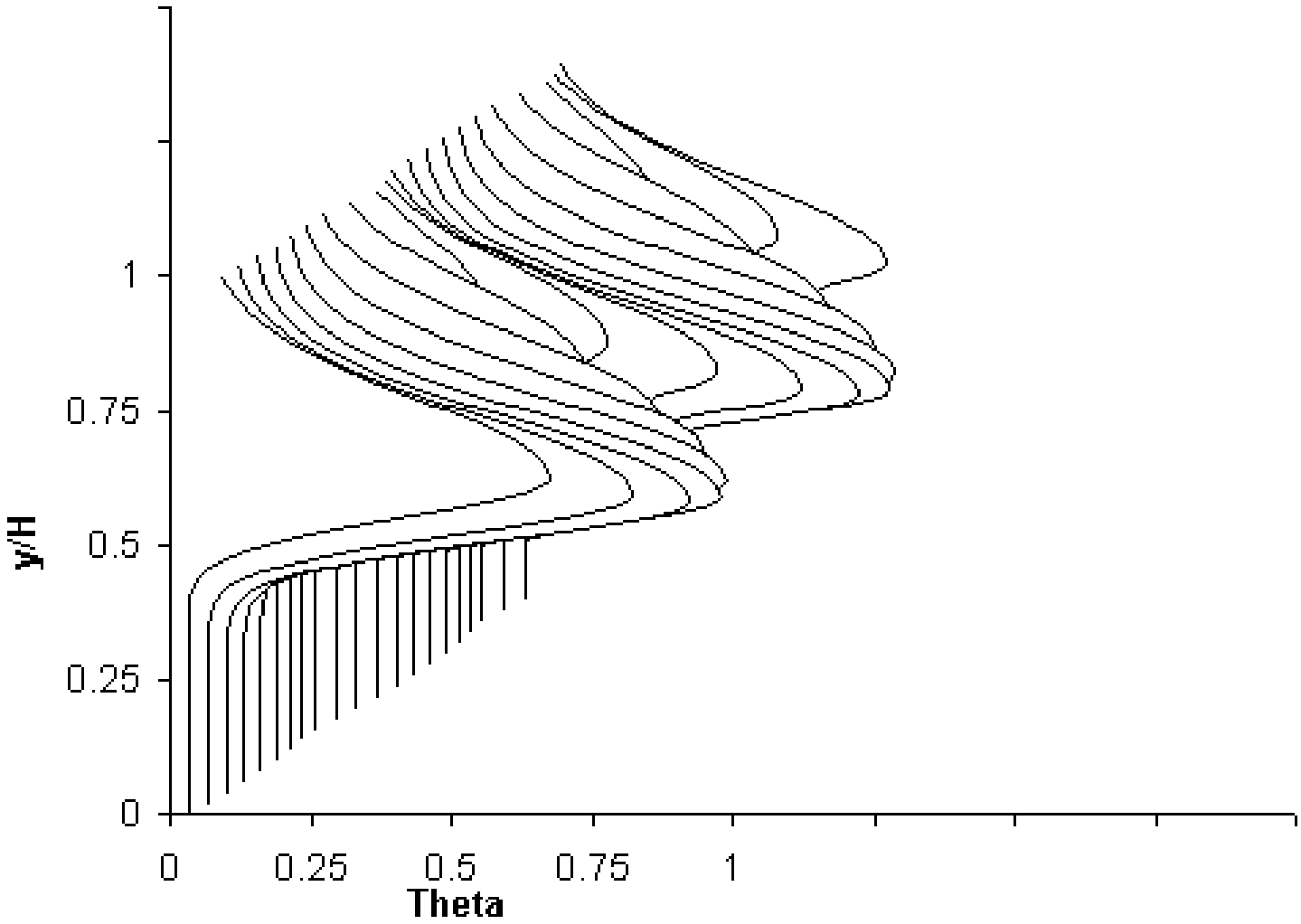


*x/H=0.125 (x/d=0.5)*

*J=26.4; S/H= 0.5; H/d=4, (S/d=2)*

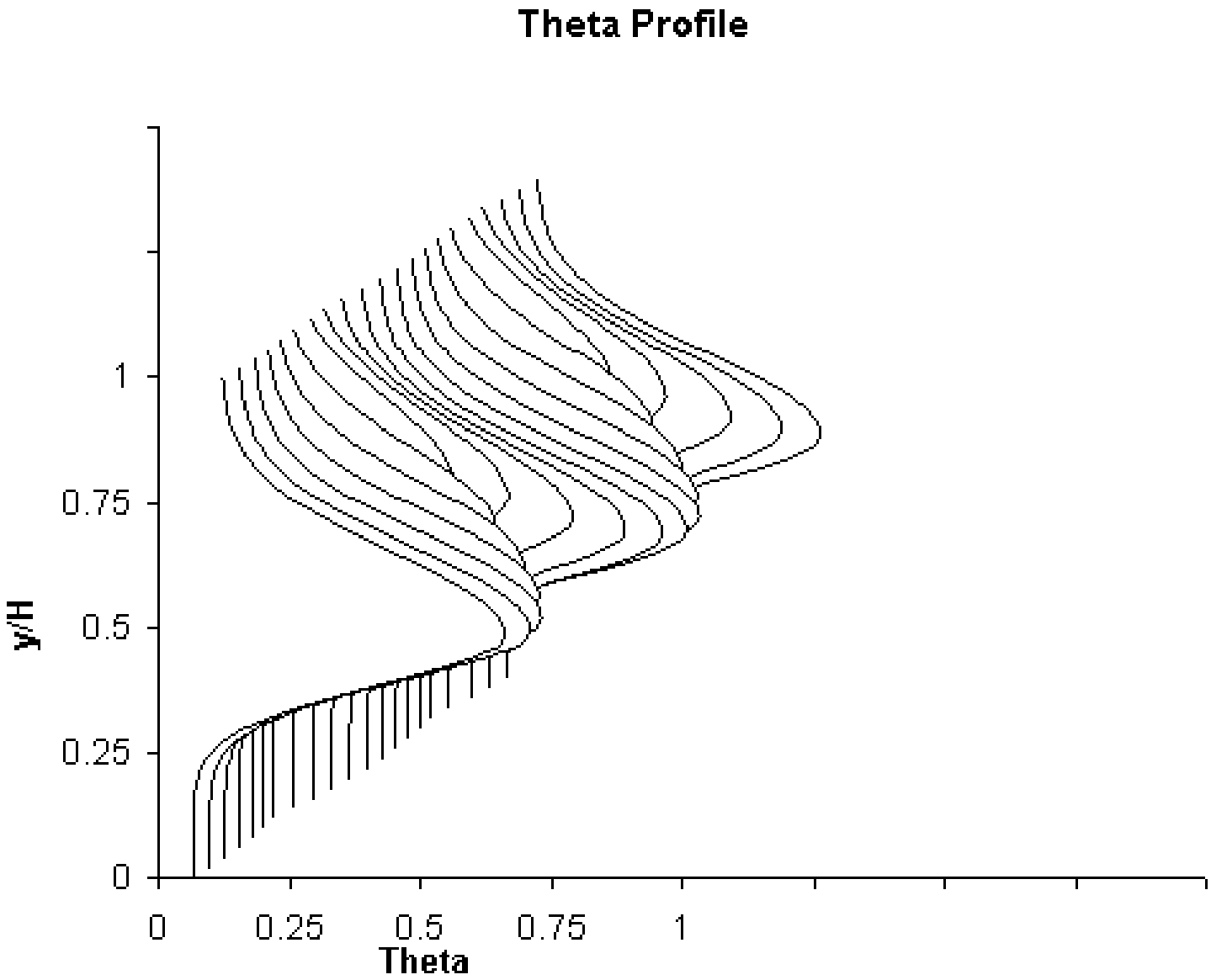


*x/H=0.25 (x/d=1)*

*J=26.4; S/H= 0.5; H/d=4, (S/d=2)*

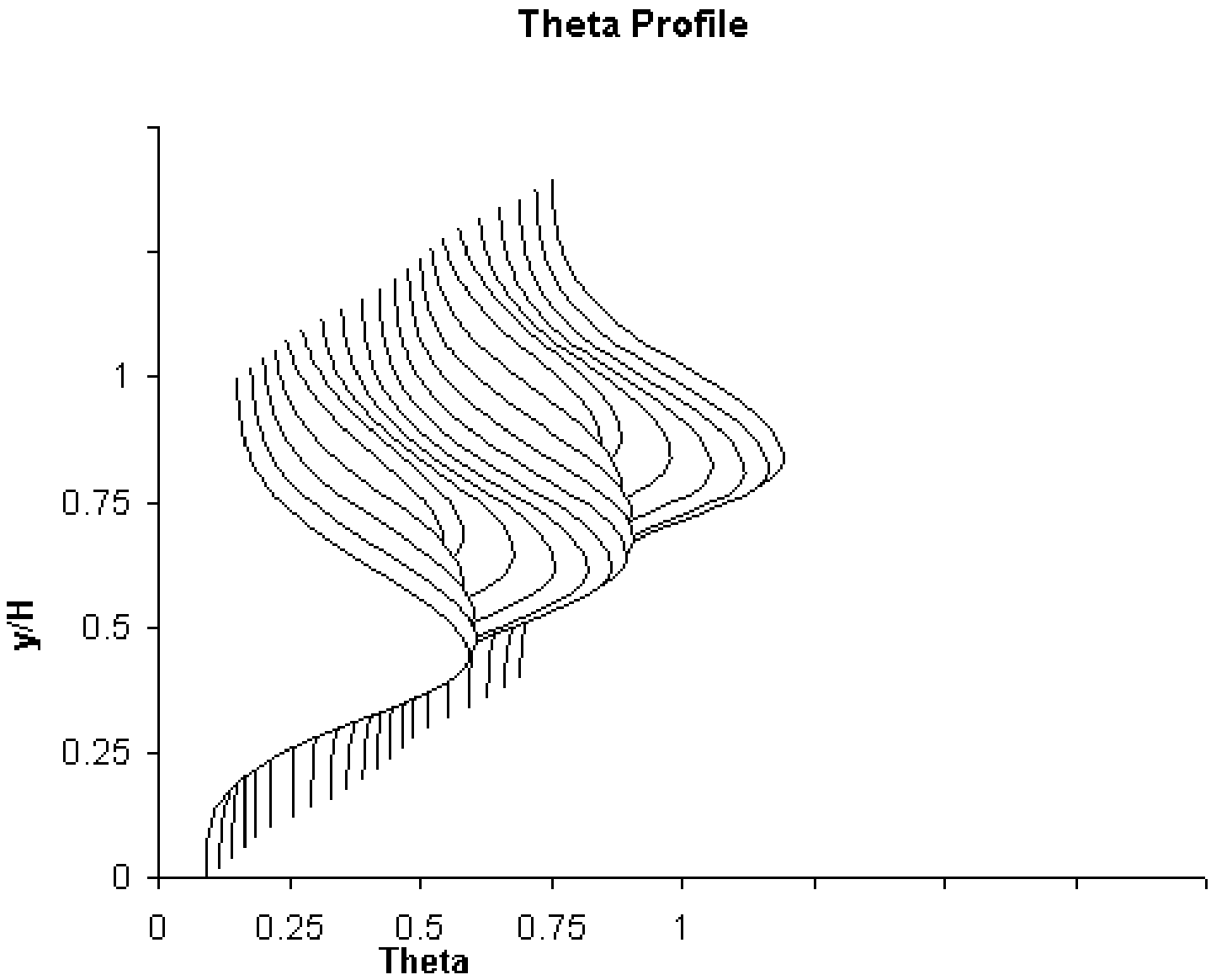


*x/H=0.375* *(x/d=1.5)*

*J*=26.4; *S/H*= 0.5; *H/d*=4, (S/d=2)

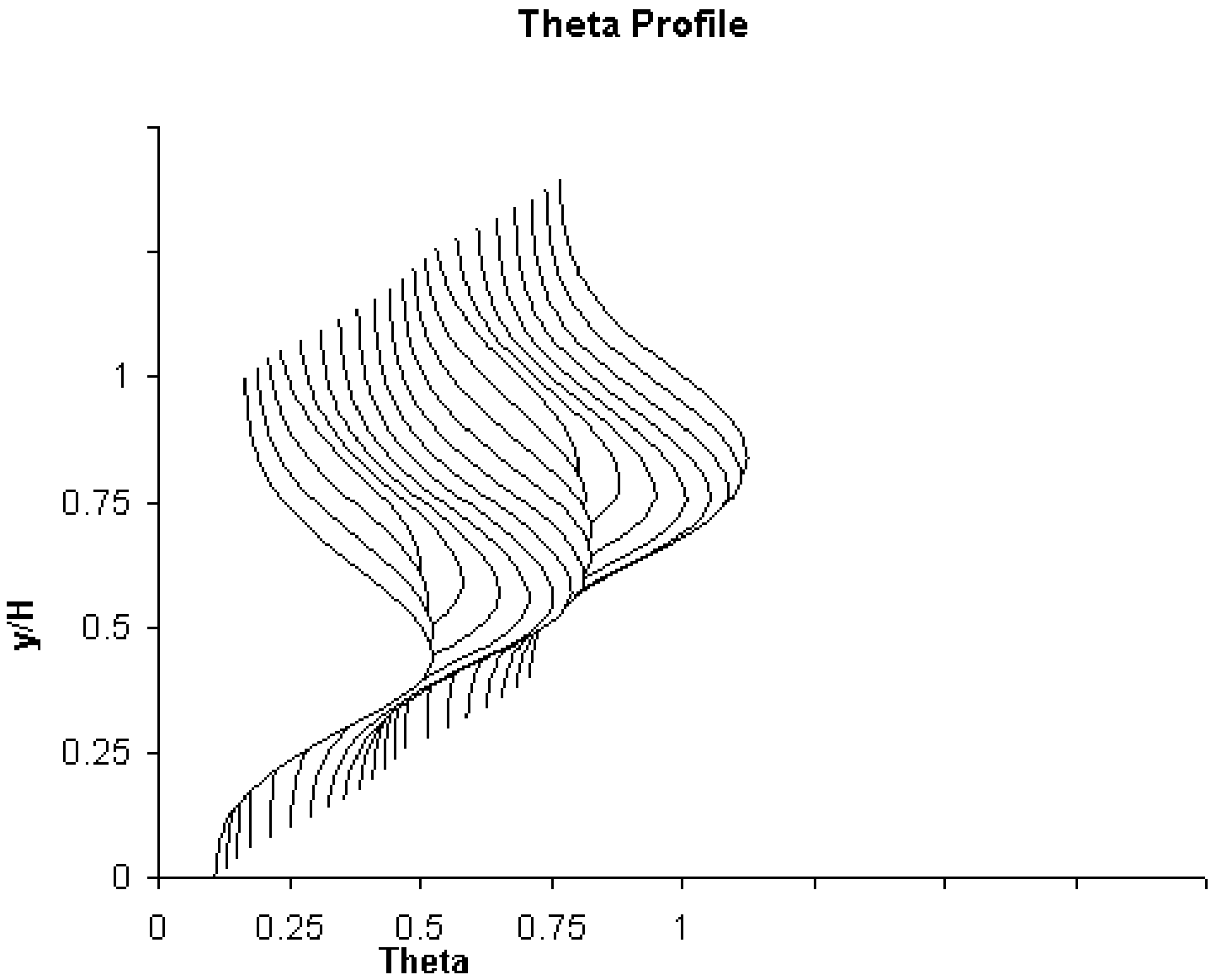


*x/H=0.5 (x/d=2)*

*J=26.4; S/H= 0.5; H/d=4, (S/d=2)*

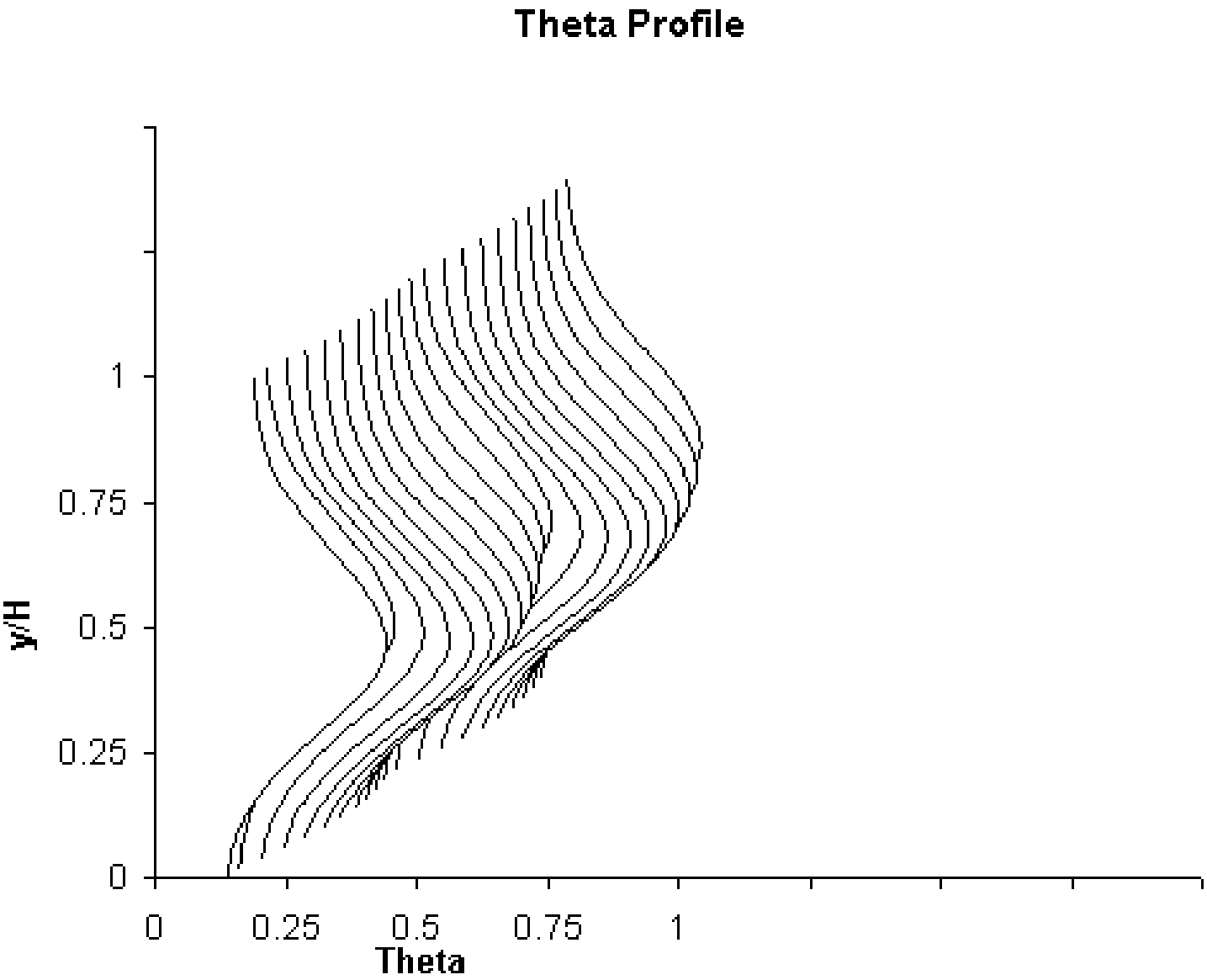


*x/H=0.75 (x/d=3)*

*J=26.4; S/H= 0.5; H/d=4, (S/d=2)*

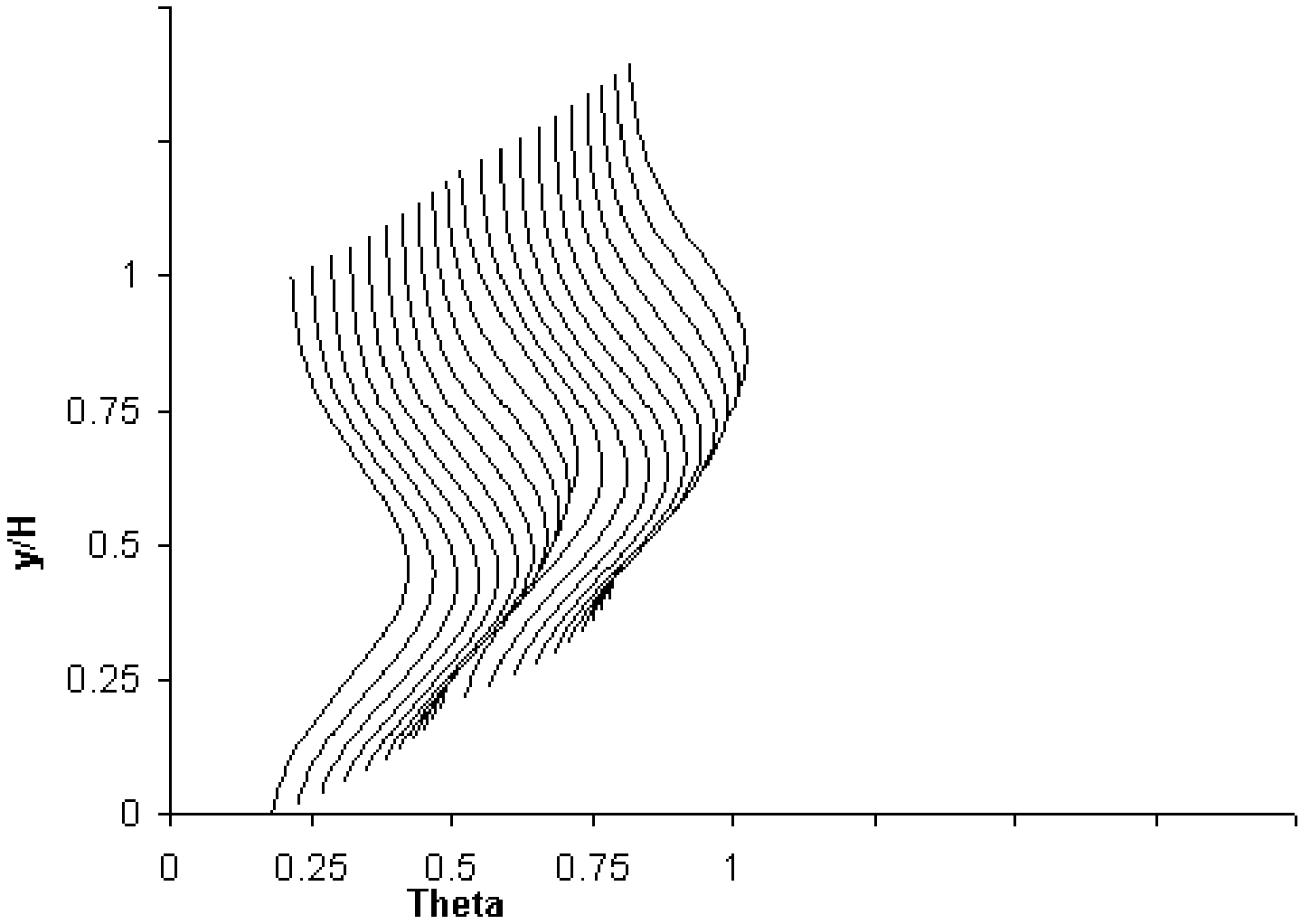


*x/H=1 (x/d=4)*

*J=26.4; S/H= 0.5; H/d=4, (S/d=2)*

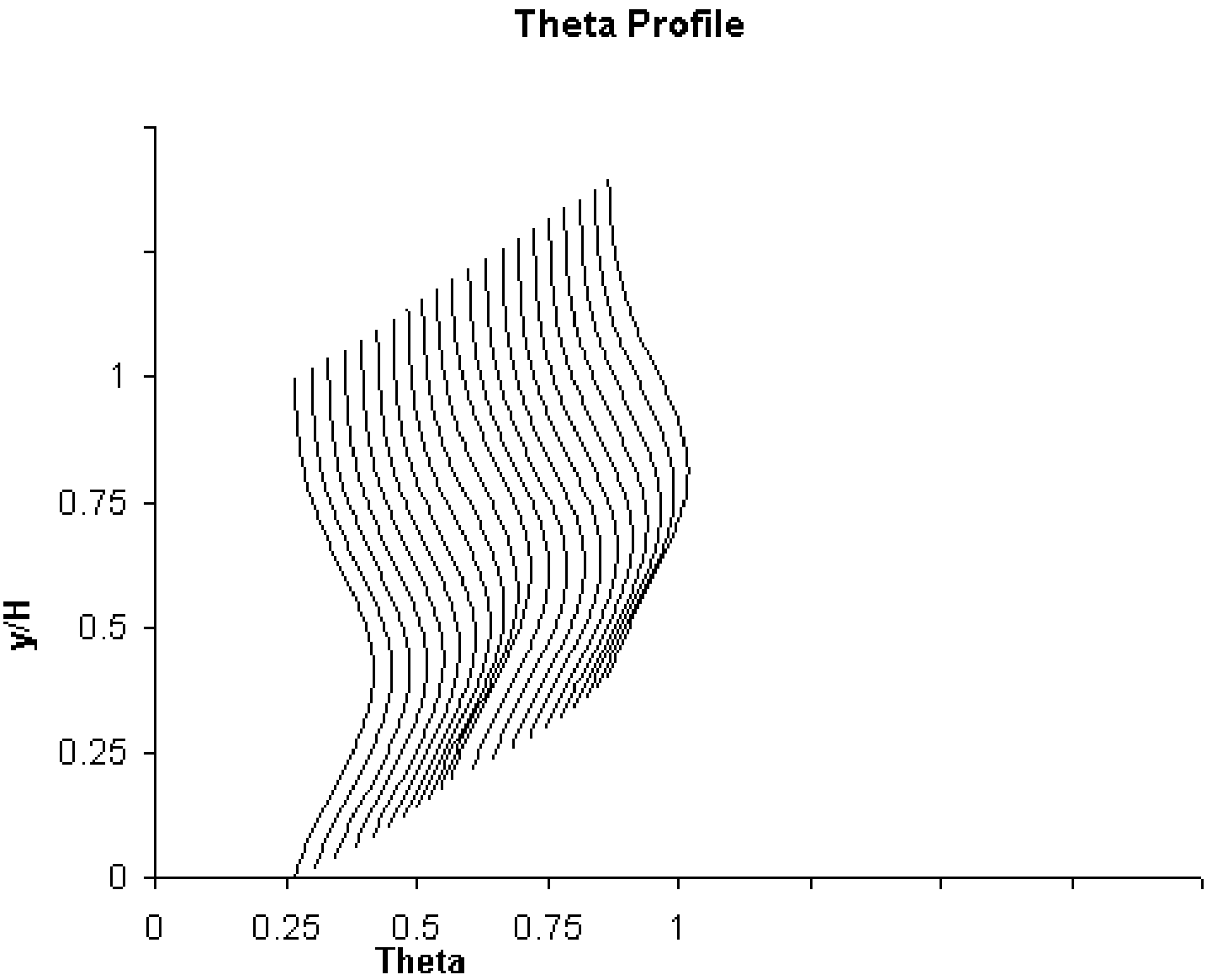


*x/H=1.5 (x/d=6)*

*J=26.4; S/H= 0.5; H/d=4, (S/d=2)*

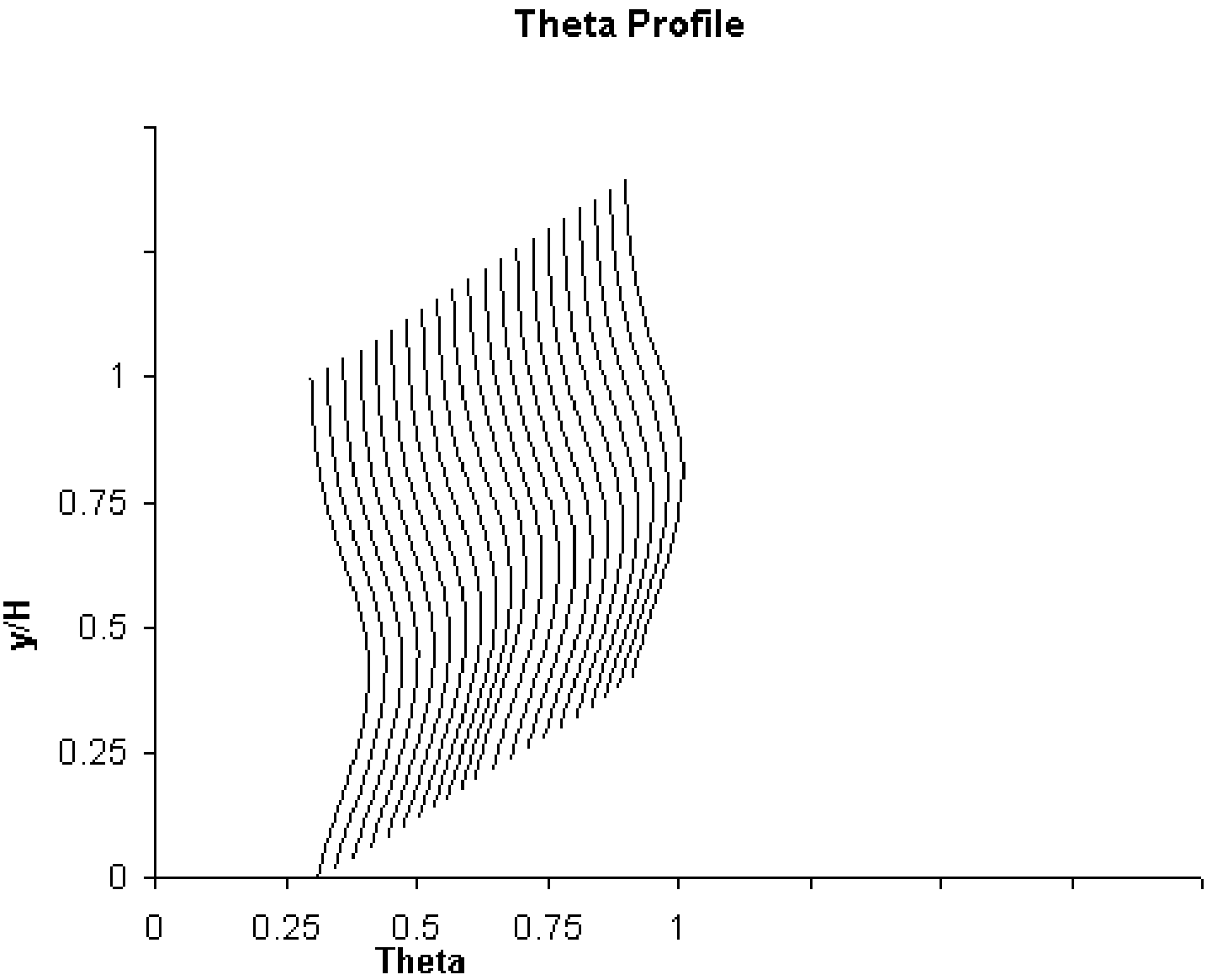


*x/H=2 (x/d=8)*

*J=26.4; S/H= 0.5; H/d=4, (S/d=2)*

Sequence 15

**Variations in scalar distributions with downstream distance for opposed rows of jets with centerlines inline: equal orifice configurations and momentum-flux ratios on opposite sides**

*x/H=0.25, 0.375 , 0.5, 0.75, 1, 1.5, 2*

*DR=2.2, J=26.4, S/H=0.25, H/d=8, $C_d$=0.64*

(cf. figure 16(b) in NASA/TM—2006-214226)

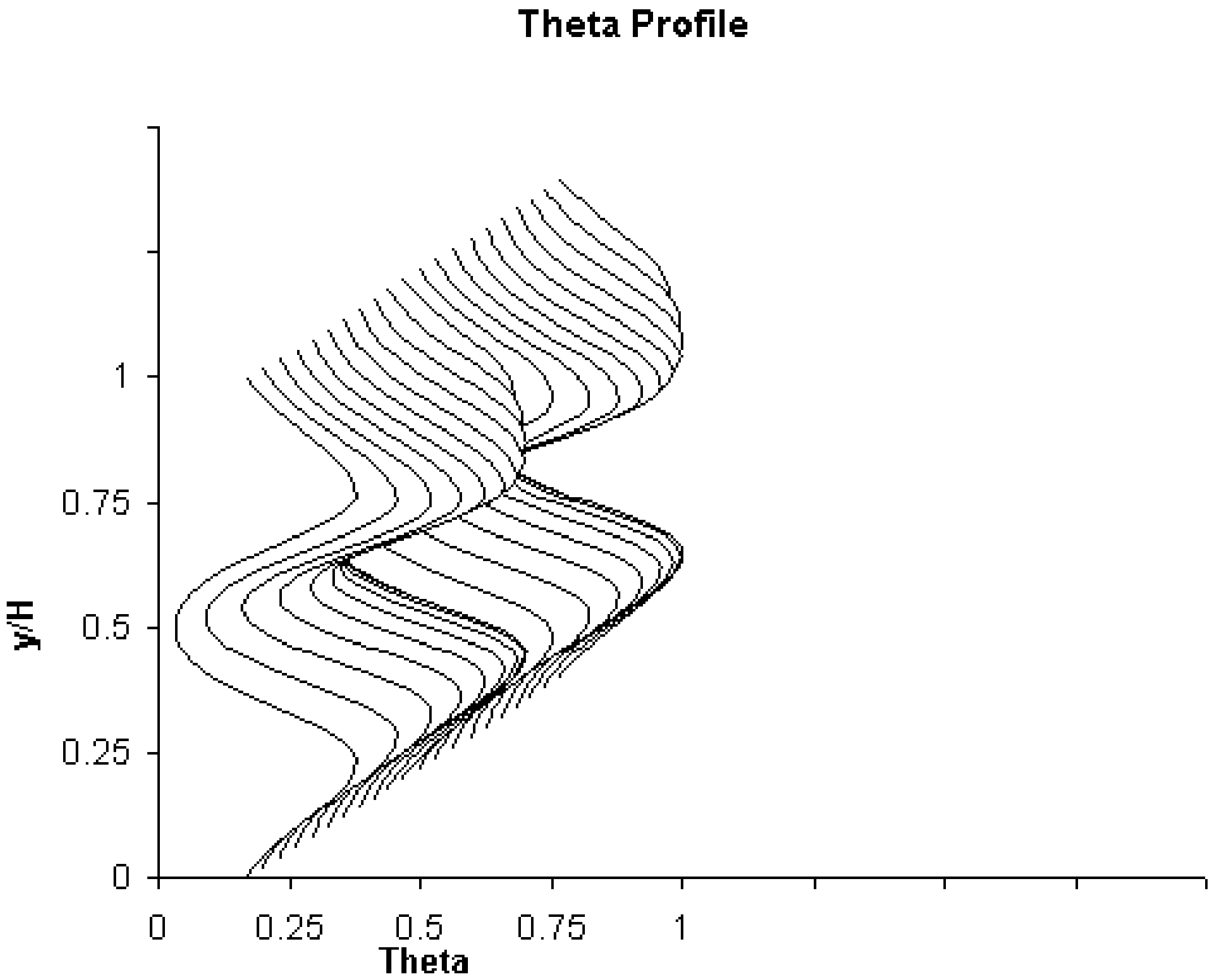


*x/H=0.25 (x/d=2)*

*J=26.4, S/H=0.25, H/d=8, (S/d=2)*

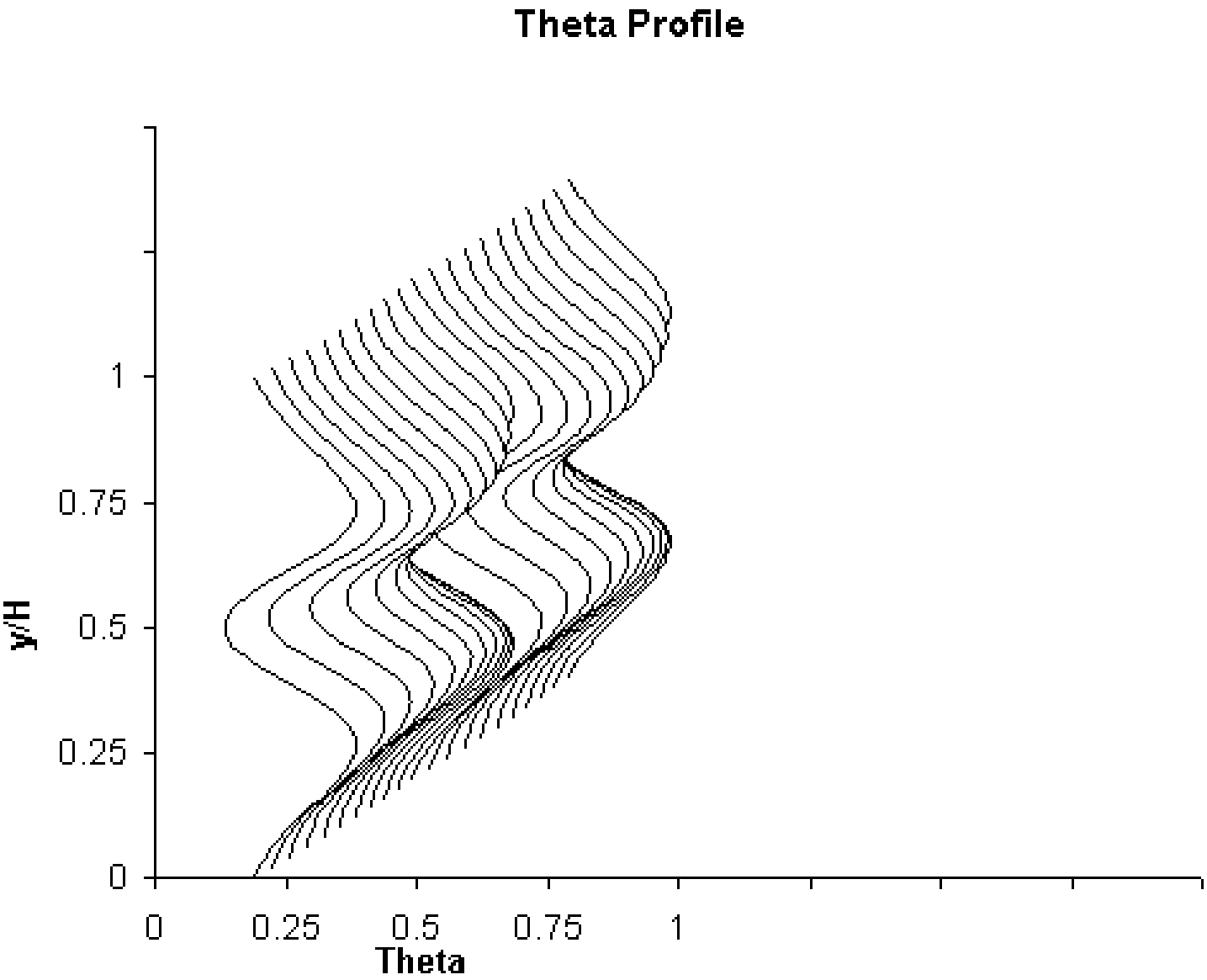


*x/H=0.375 (x/d=3)*

*J=26.4, S/H=0.25, H/d=8, (S.d=2)*

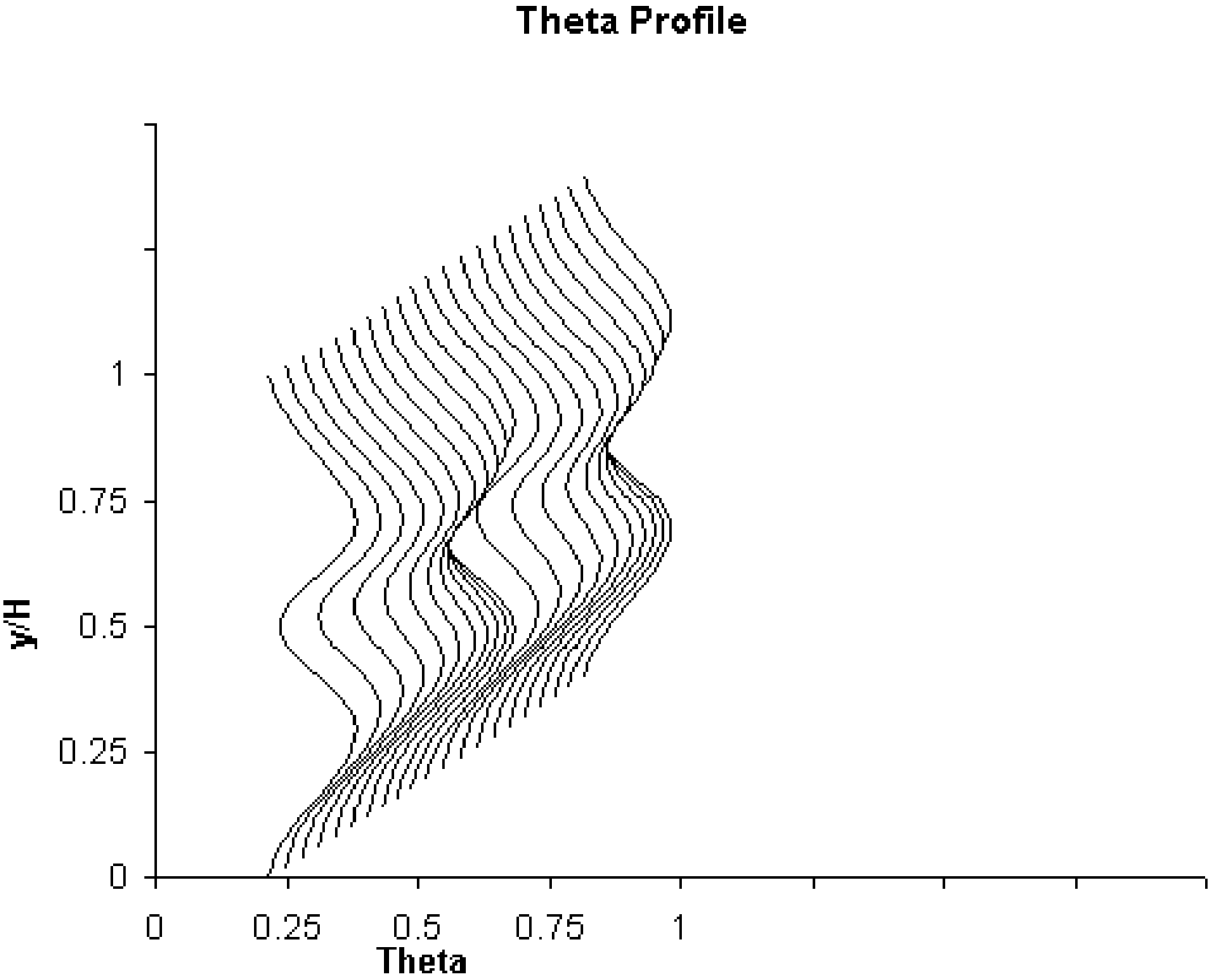


*x/H=0.5 (x/d=4)*

*J=26.4, S/H=0.25, H/d=8, (S/d=2)*

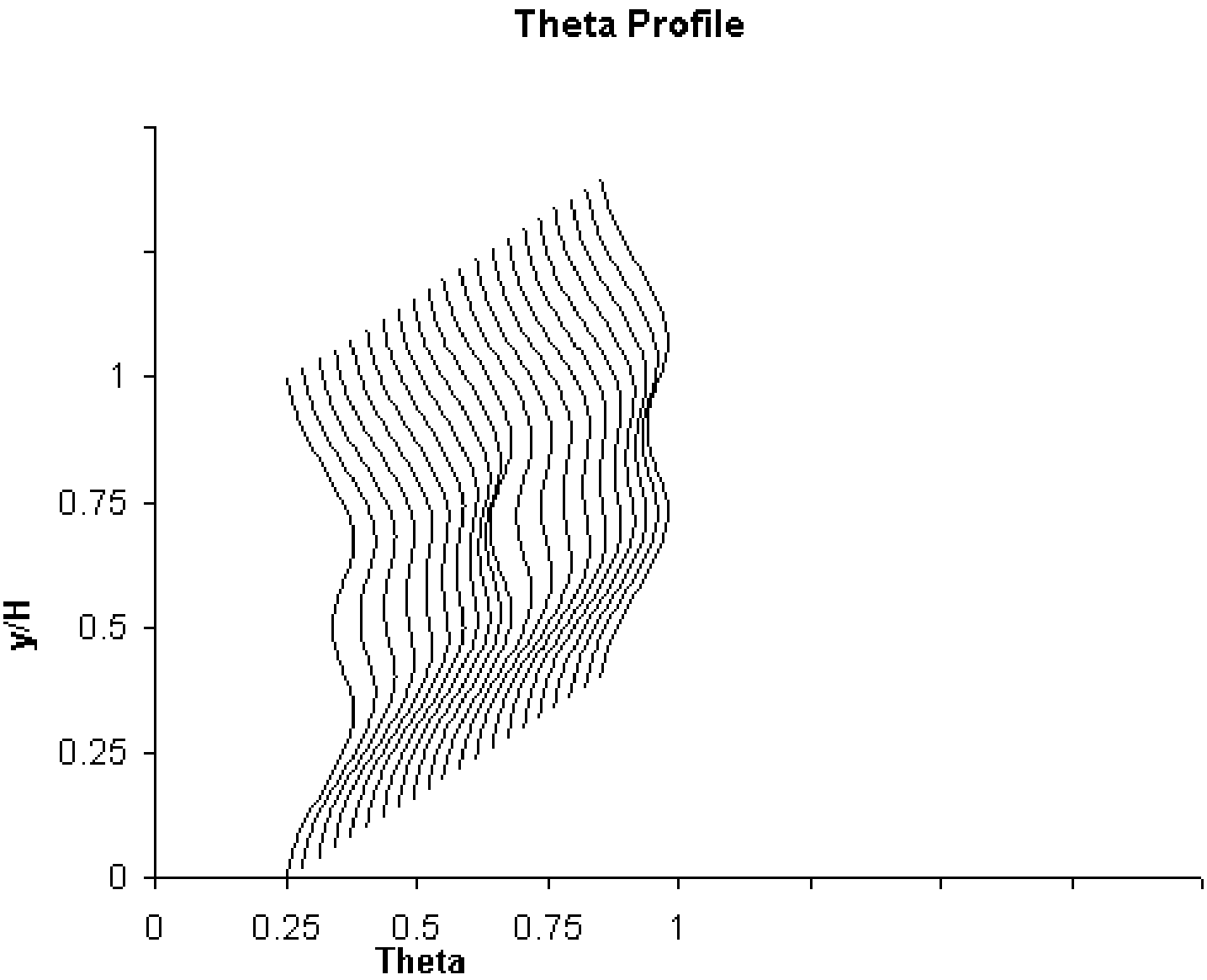


*x/H=0.75 (x/d=6)*

*J=26.4, S/H=0,25, H/d=8, (S/d=2)*

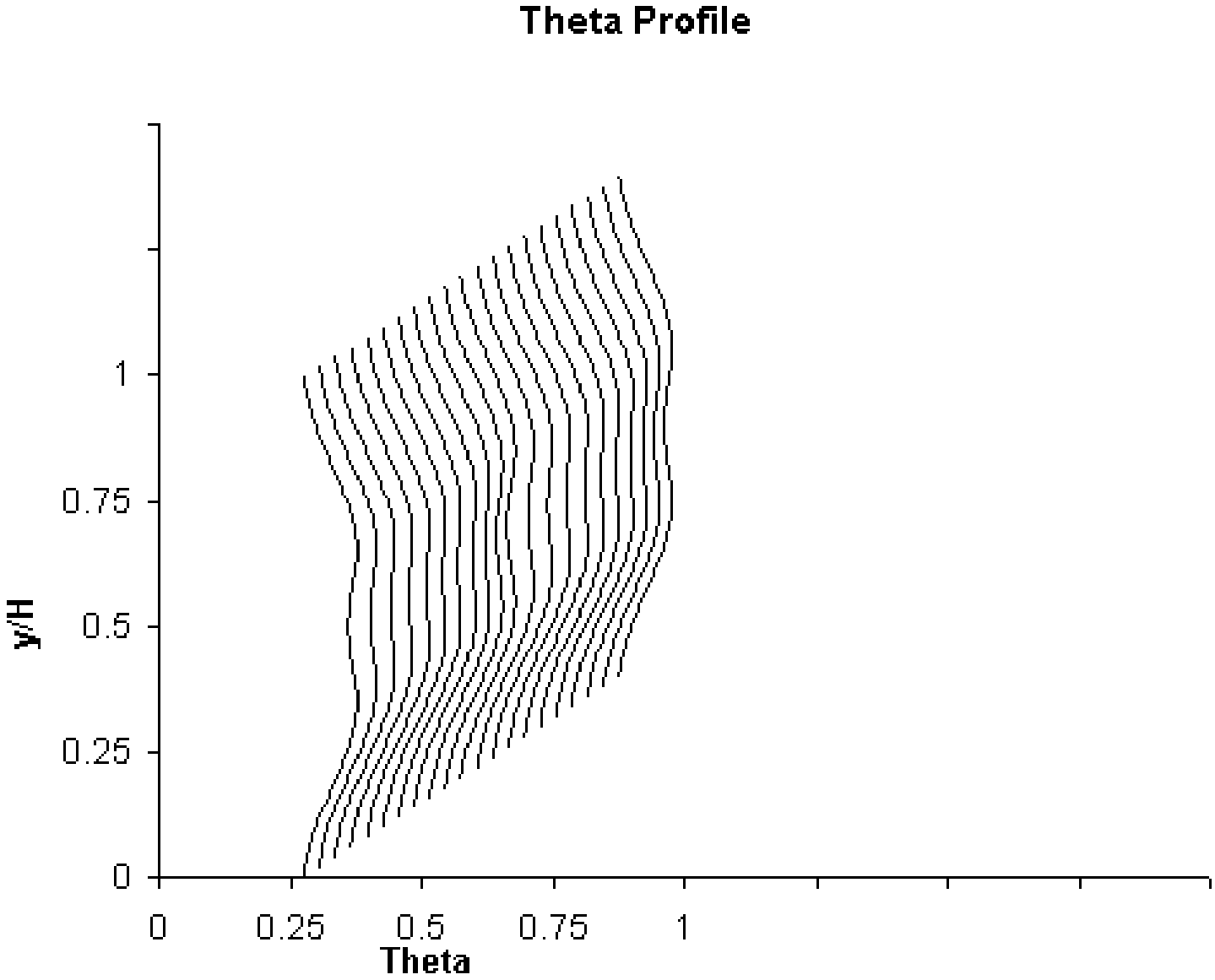


*x/H=1 (x/d=8)*

*J=26.4, S/H=0.25, H/d=8, (S/d=2)*

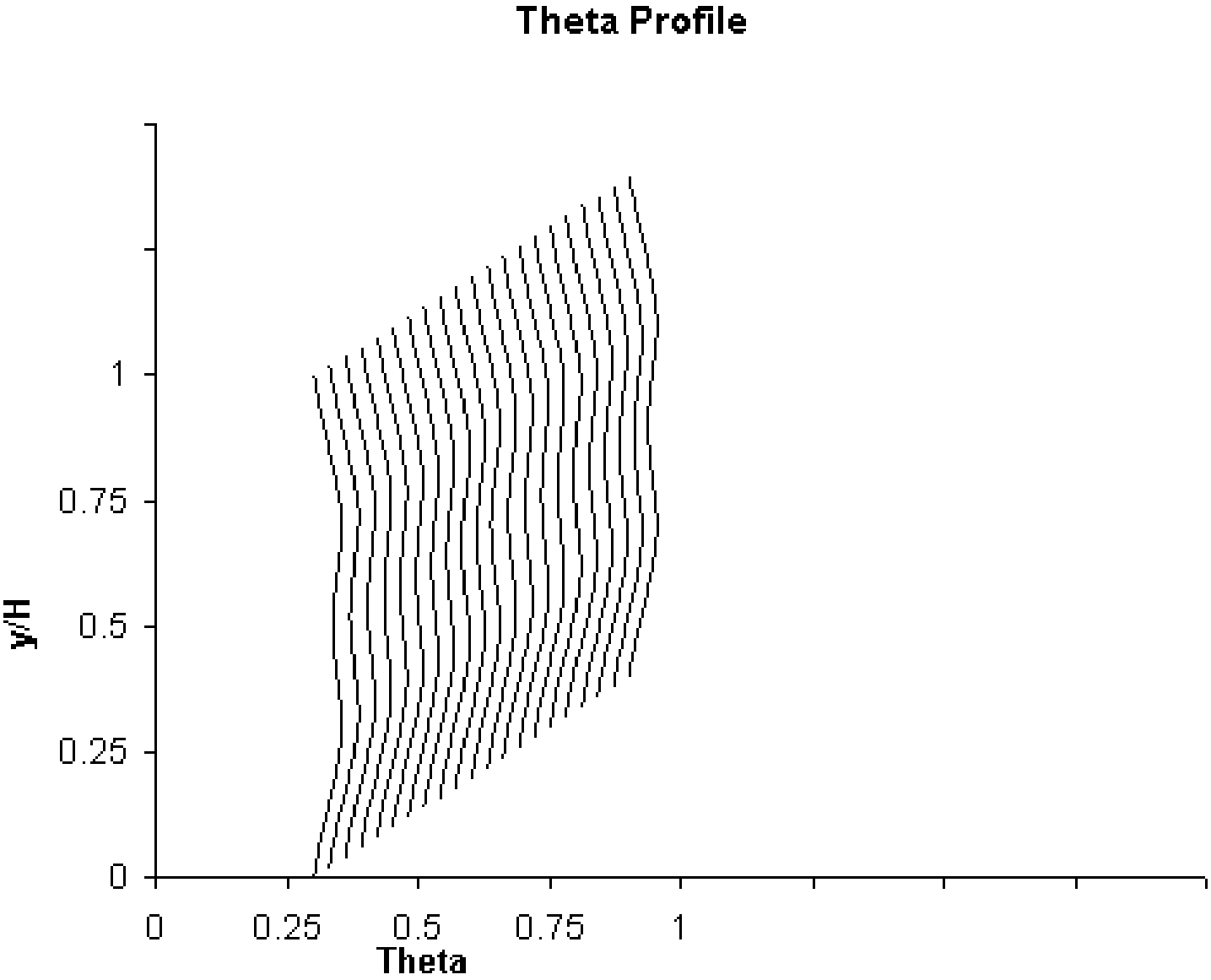


*x/H=1.5 (x/d=12)*

*J=26.4, S/H=0.25, H/d=8, (S/d=2)*

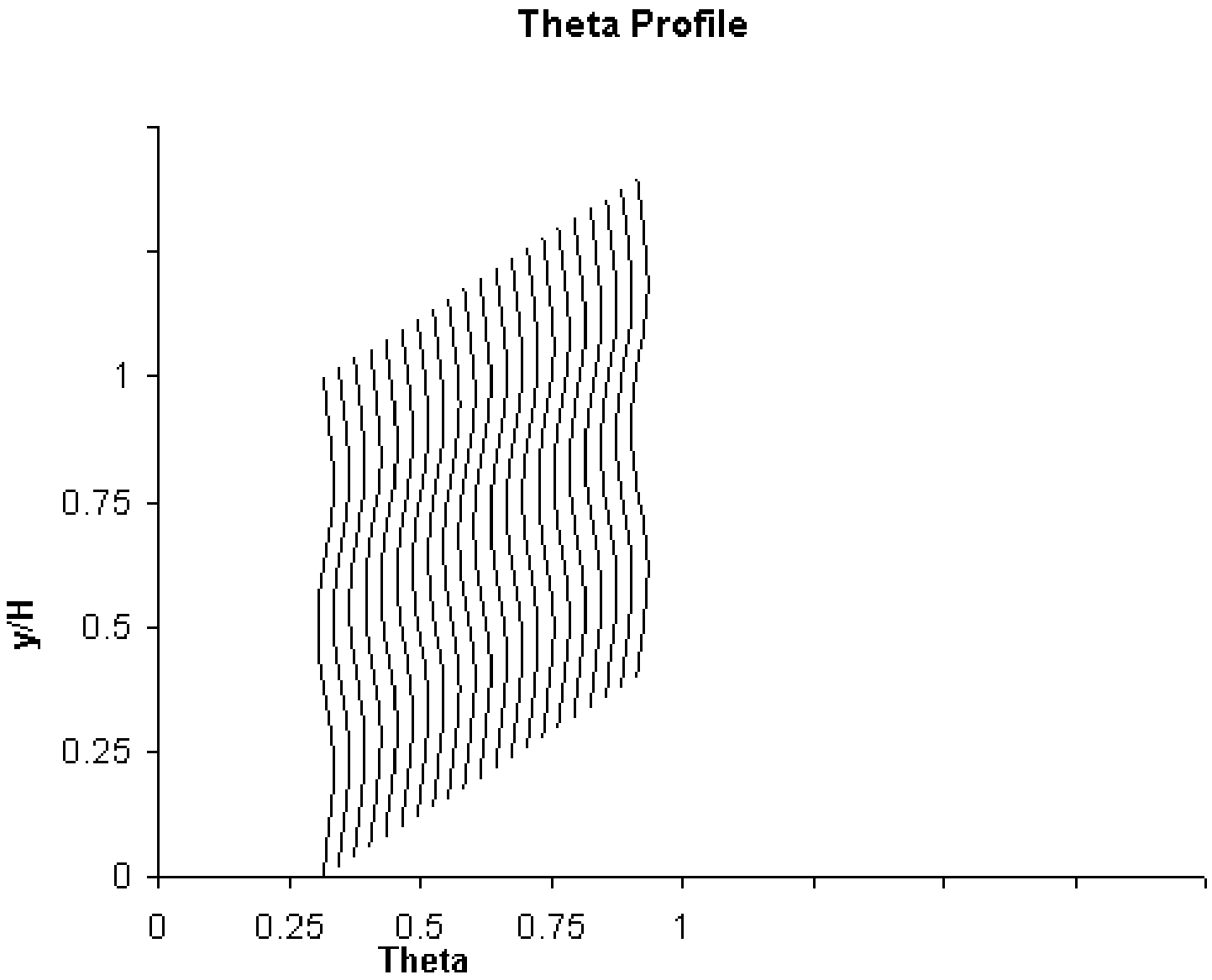


*x/H=2 (x/d=16)*

*J=26.4, S/H=9.25, H/d=8, (S/d=2)*

Sequence 16

**Variations in scalar distributions for opposed rows of jets with centerline in-line but with different hole sizes on opposite sides**

$H/d|_{top}=11.32;\ H/d|_{bottom}=11.32$
$H/d|_{top}=13;\ H/d|_{bottom}=10.17$
$H/d|_{top}=16;\ H/d|_{bottom}=9.25$
$H/d|_{top}=22.5;\ H/d|_{bottom}=8.57$
$H/d|_{top}=none;\ H/d|_{bottom}=8$

$x/H=0.5,\ DR=2.2.\ J|_{top}=J|_{bottom}=26.4,$
$S/H=0.25,\ C_d=0.64$

(cf. figure 21 in NASA/TM—2006-214226)

## Theta Profile

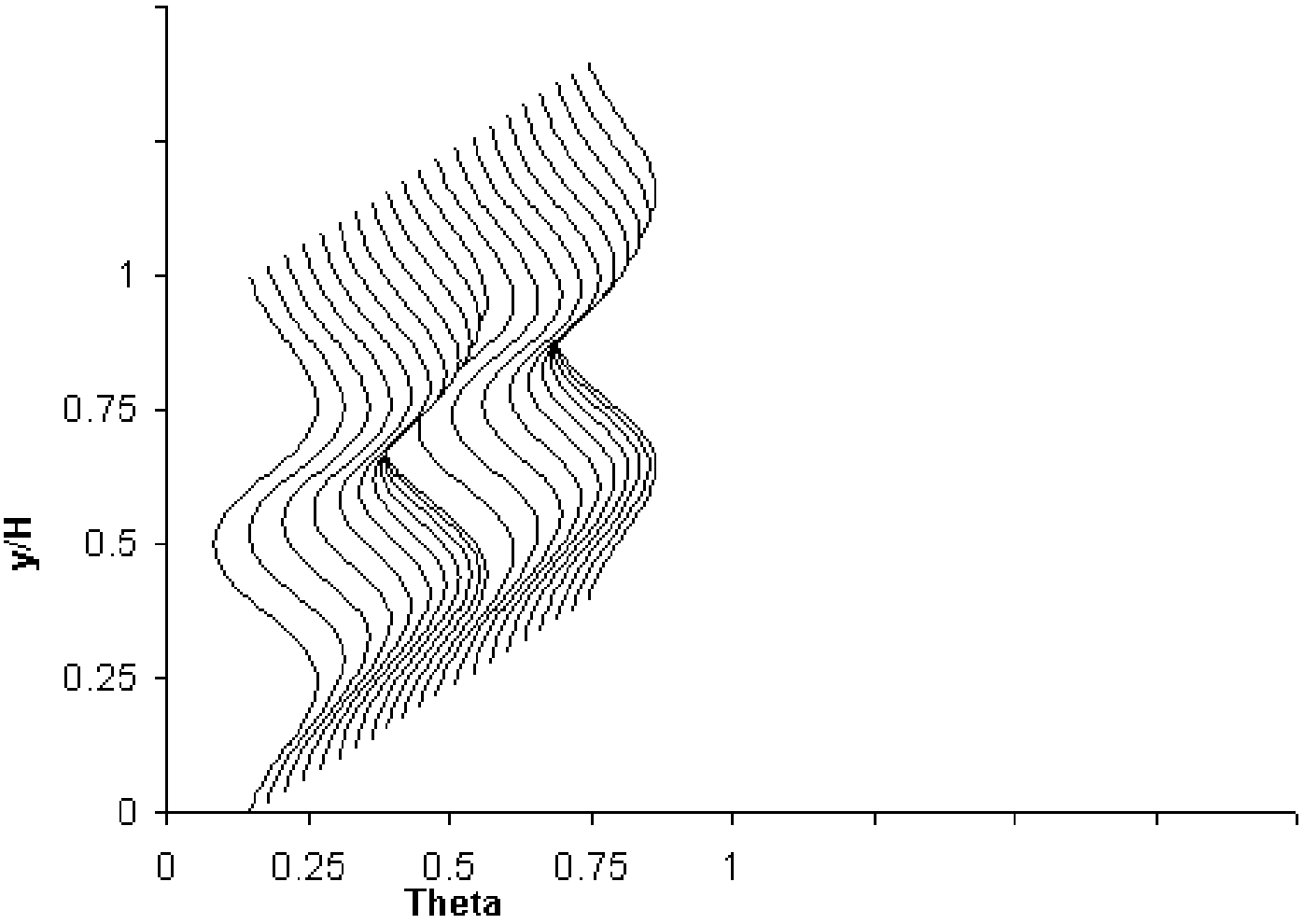


$H/d|_{top}=11.32$ $H/d|_{bottom}=11.32$

$x/H=0.5$, $J|_{top}=J|_{bottom}=26.4$, $S/H=0.25$

## Theta Profile



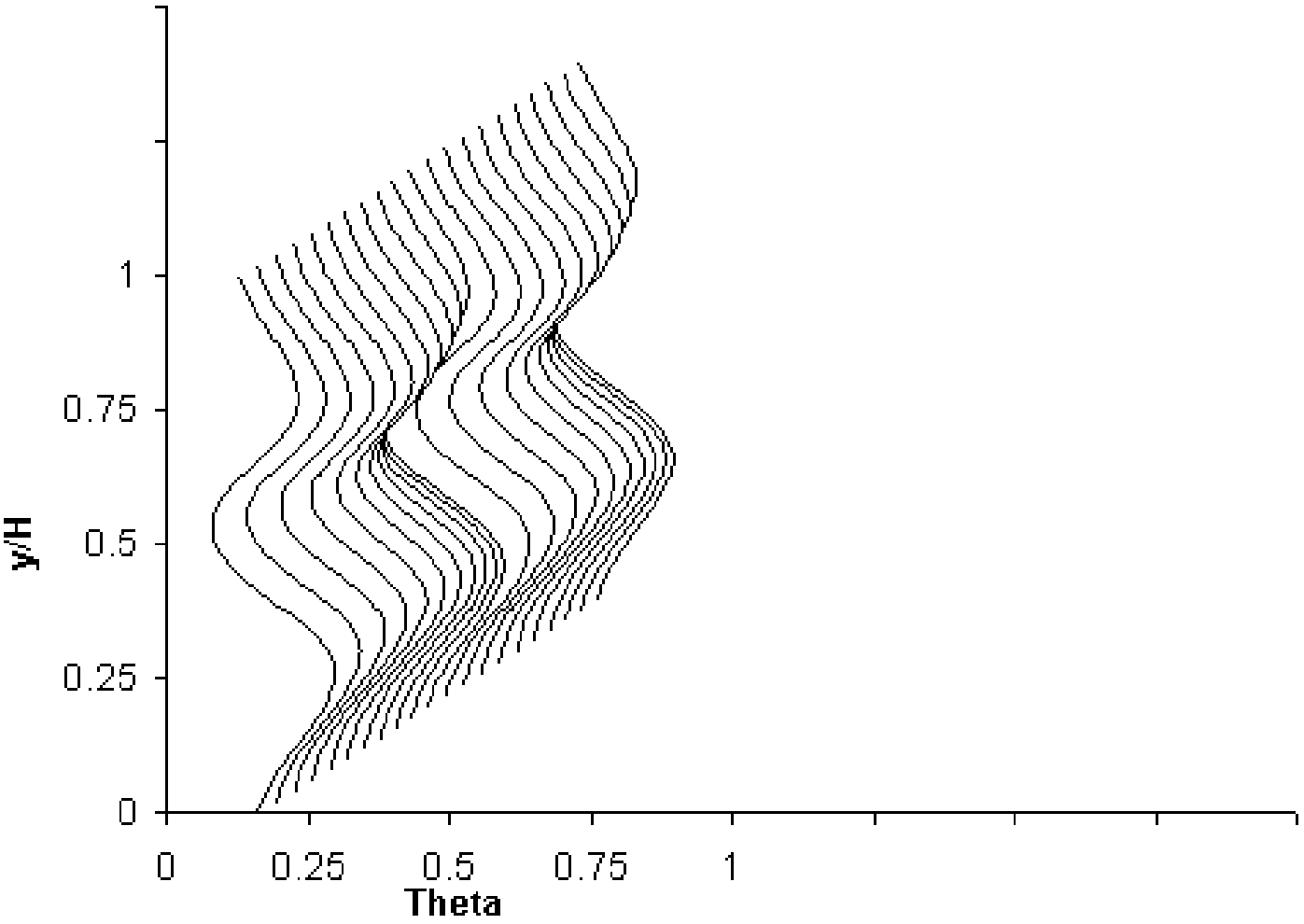


$H/d|_{top}=13$ $H/d|_{bottom}=10.17$

$x/H=0.5$, $J|_{top}=J|_{bottom}=26.4$, $S/H=0.25$

## Theta Profile



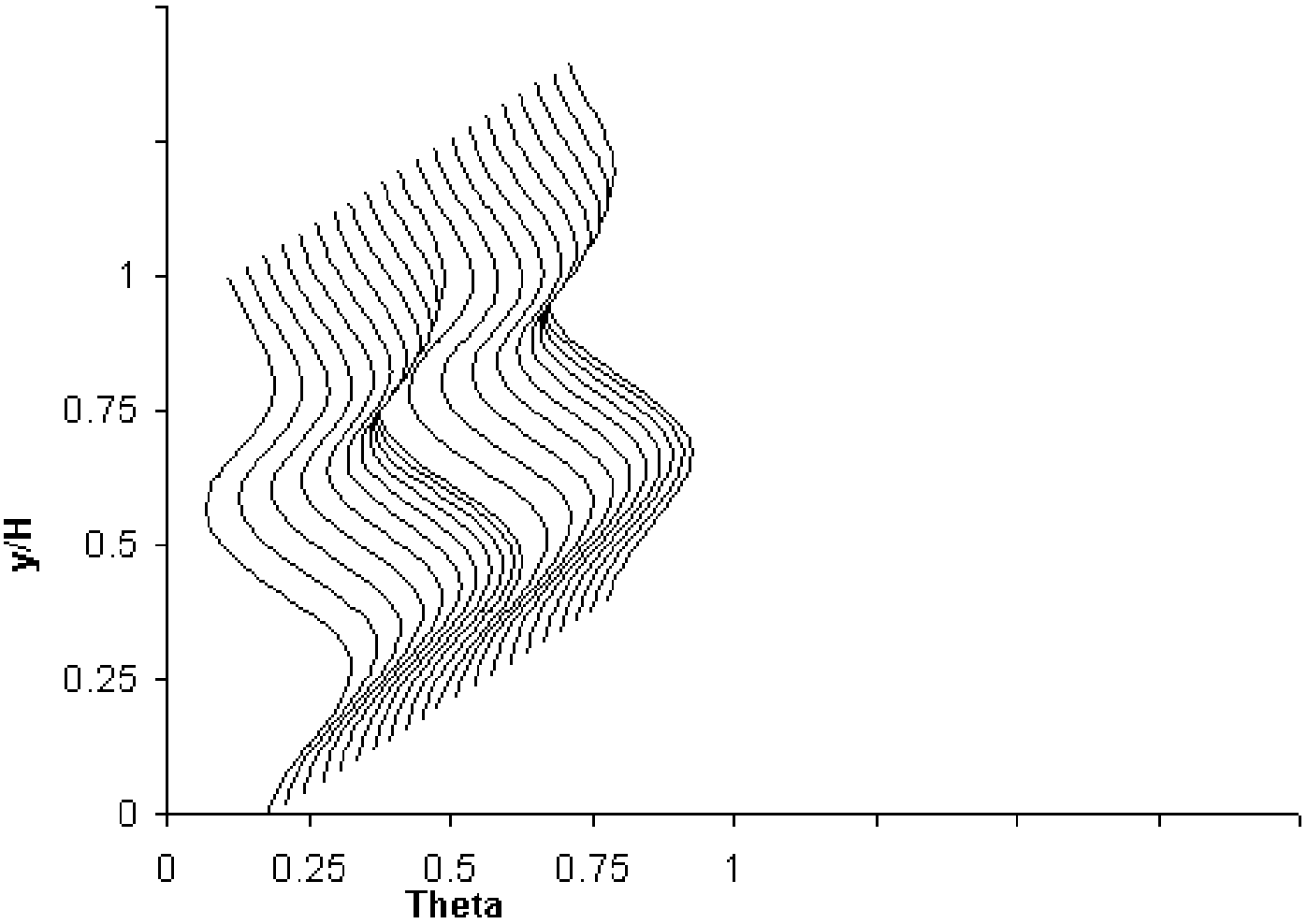


$H/d|_{top}=16$ $H/d|_{bottom}=9.25$

$x/H=0.5$, $J|_{top}=J|_{bottom}=26.4$, $S/H=0.25$

## Theta Profile



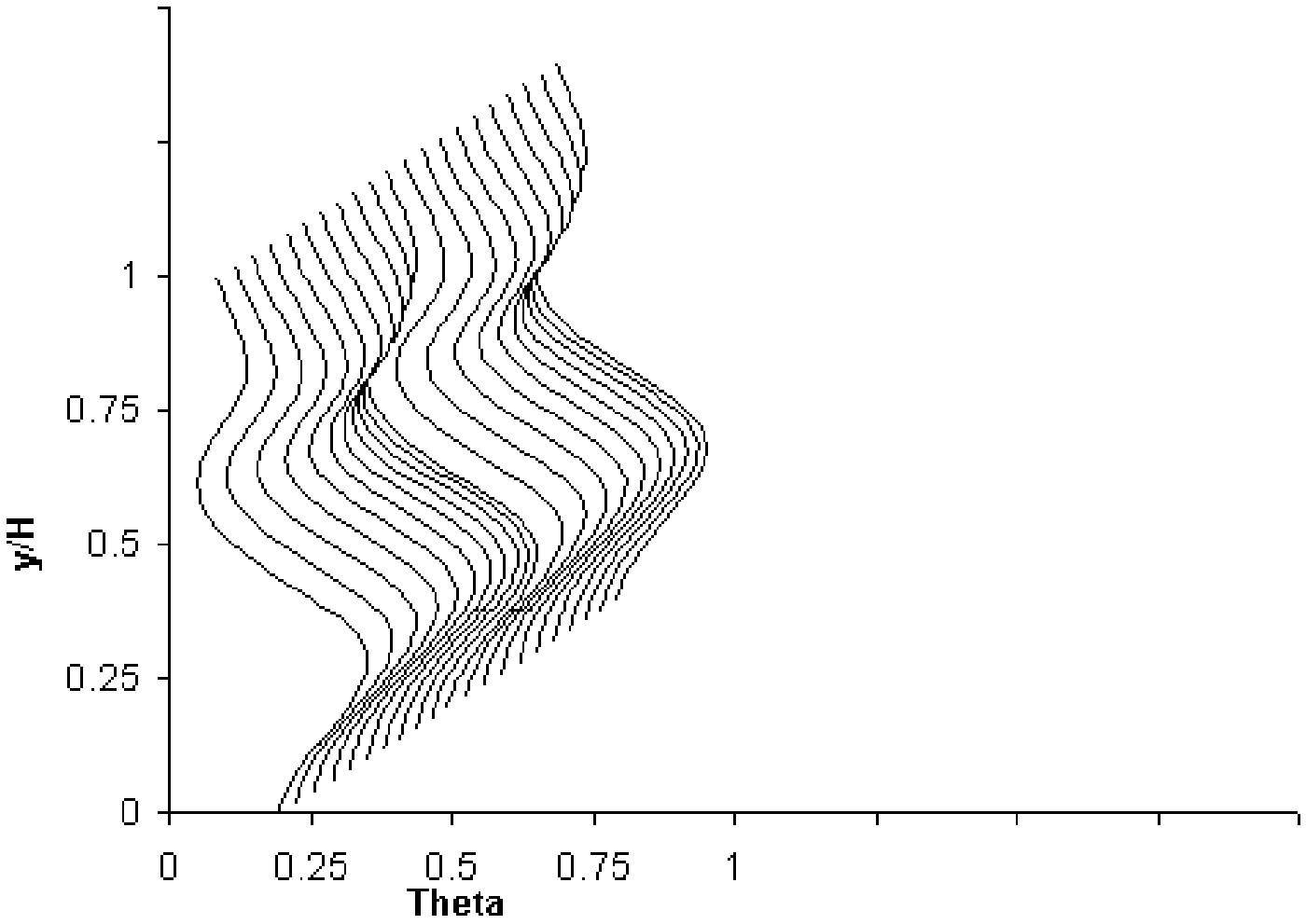


$H/d|_{top}=22.5$ $H/d|_{bottom}=8.57$

$x/H=0.5$, $J|_{top}=J|_{bottom}=26.4$, $S/H=0.25$

## Theta Profile

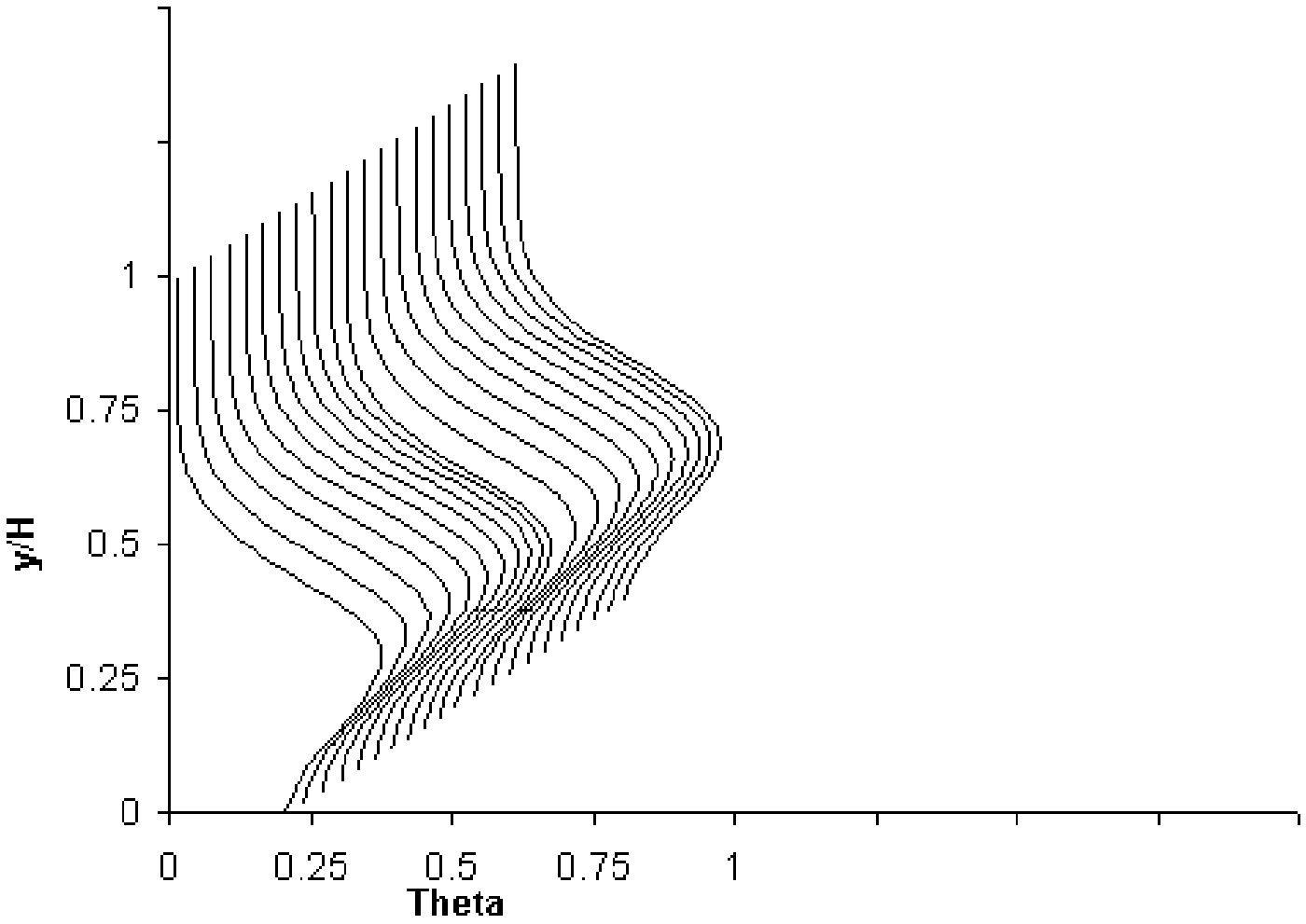


$H/d|_{top}$=none $H/d|_{bottom}$=8

$x/H$=0.5, $J|_{top}=J|_{bottom}$=26.4, $S/H$=0.25

Sequence 17

**Variations in scalar distributions for opposed rows of jets with centerline in-line but with different momentum-flux ratios on opposite sides**

$J|_{top}=24.6;\ J|_{bottom}=24.6$
$J|_{top}=38.8\ J|_{bottom}=16.9$
$J|_{top}=51.7;\ J|_{bottom}=9.5$
$J|_{top}=67.6;\ J|_{bottom}=4.2$
$J|_{top}=105.6\ ;\ J|_{bottom}=0$

$x/H=0.5,\ DR=2.2.\ S/H=0.25,\ H/d|_{top}=H/d|_{bottom}=8,\ C_d=0.64$

(cf. figure 24b in NASA/TM—2006-214226)

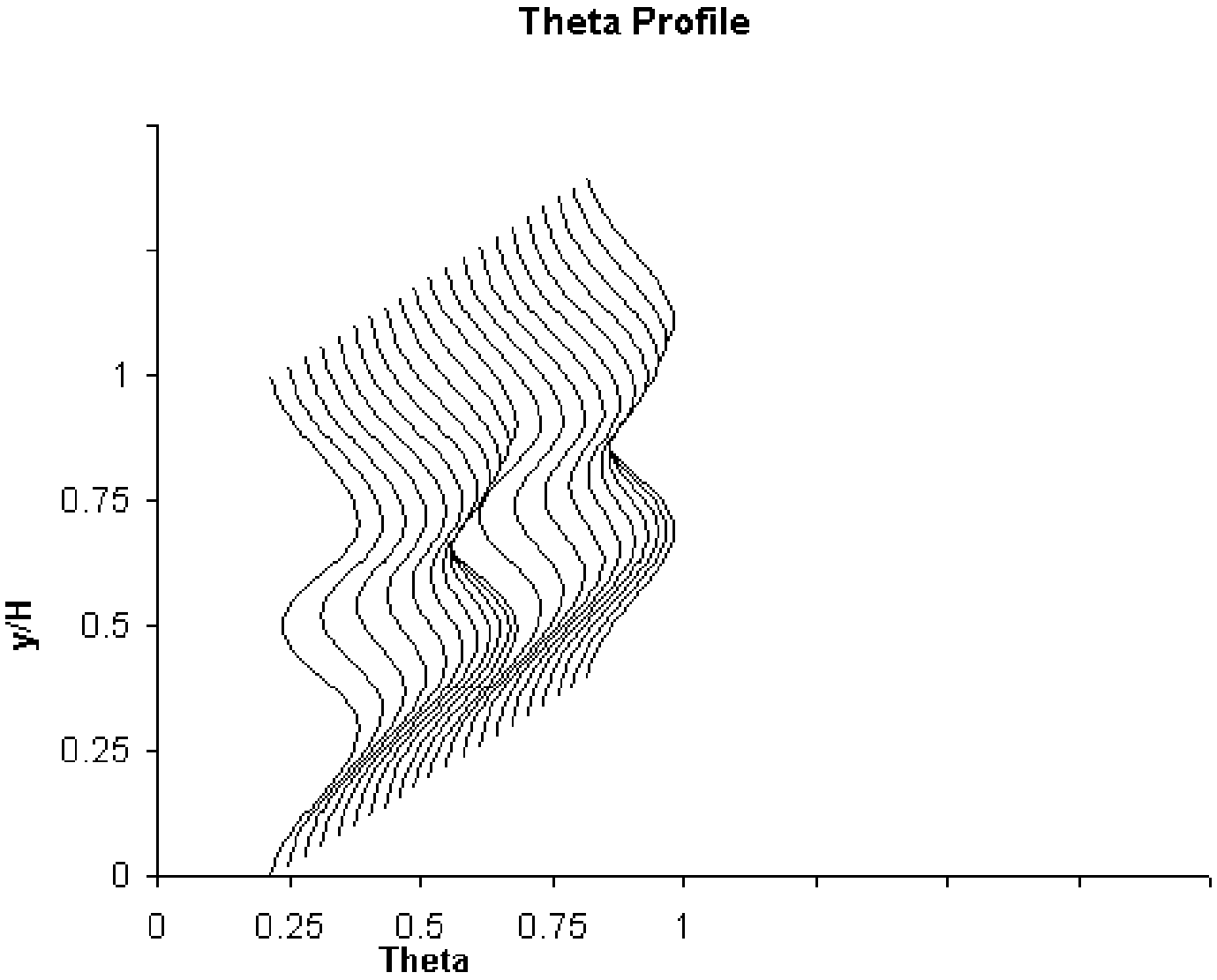


$J|_{top}=26.4$ $J|_{bottom}=26.4$

$x/H=0.5$, DR=2;2. $S/H=0.25$, $H/d|_{top}=H/d|_{bottom}=8$, $C_d=0.64$

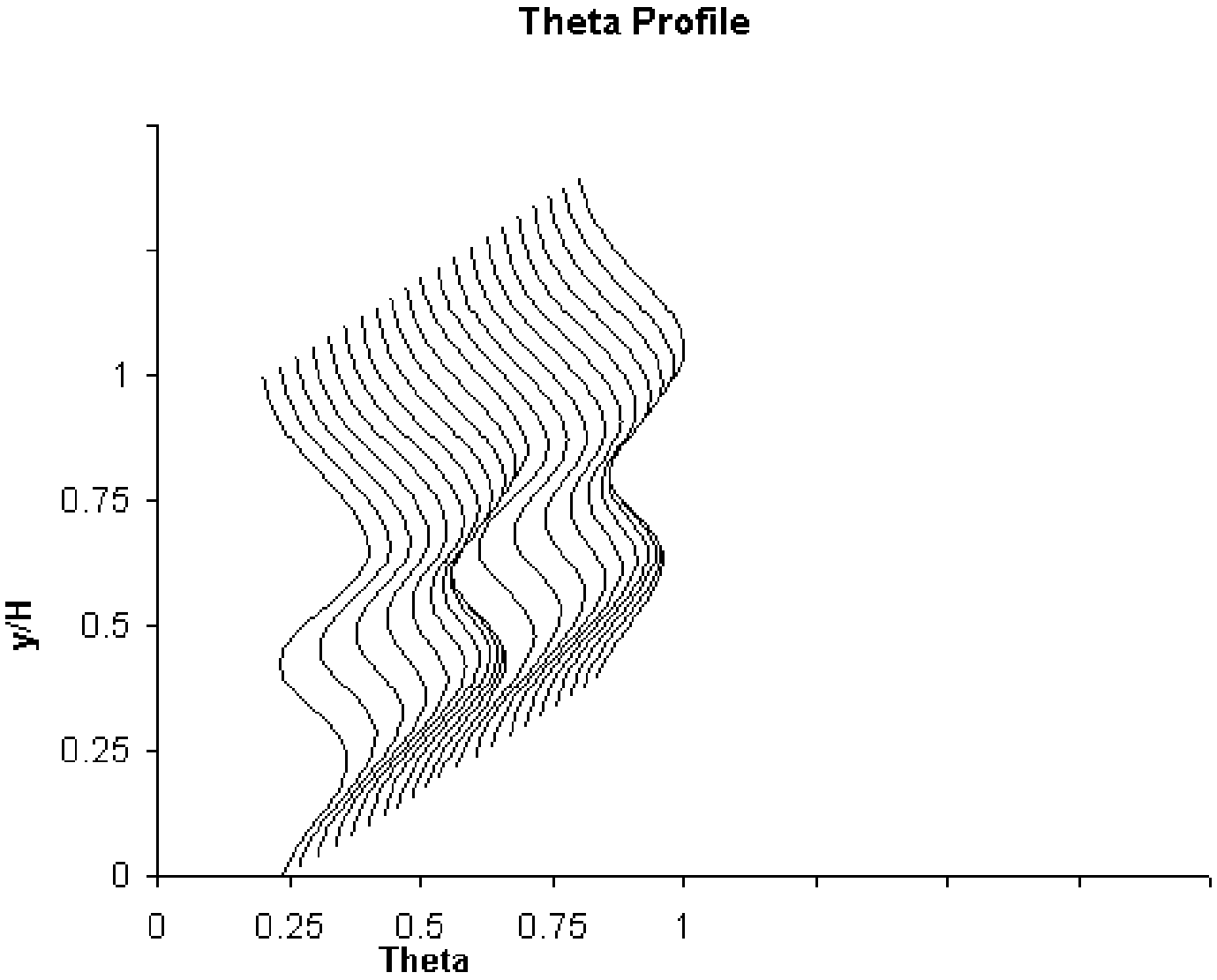


$J|_{top}=38.8$ $J|_{bottom}=16.9$

$x/H=0.5$, DR=2;2. $S/H=0.25$, $H/d|_{top}=H/d|_{bottom}=8$, $C_d=0.64$

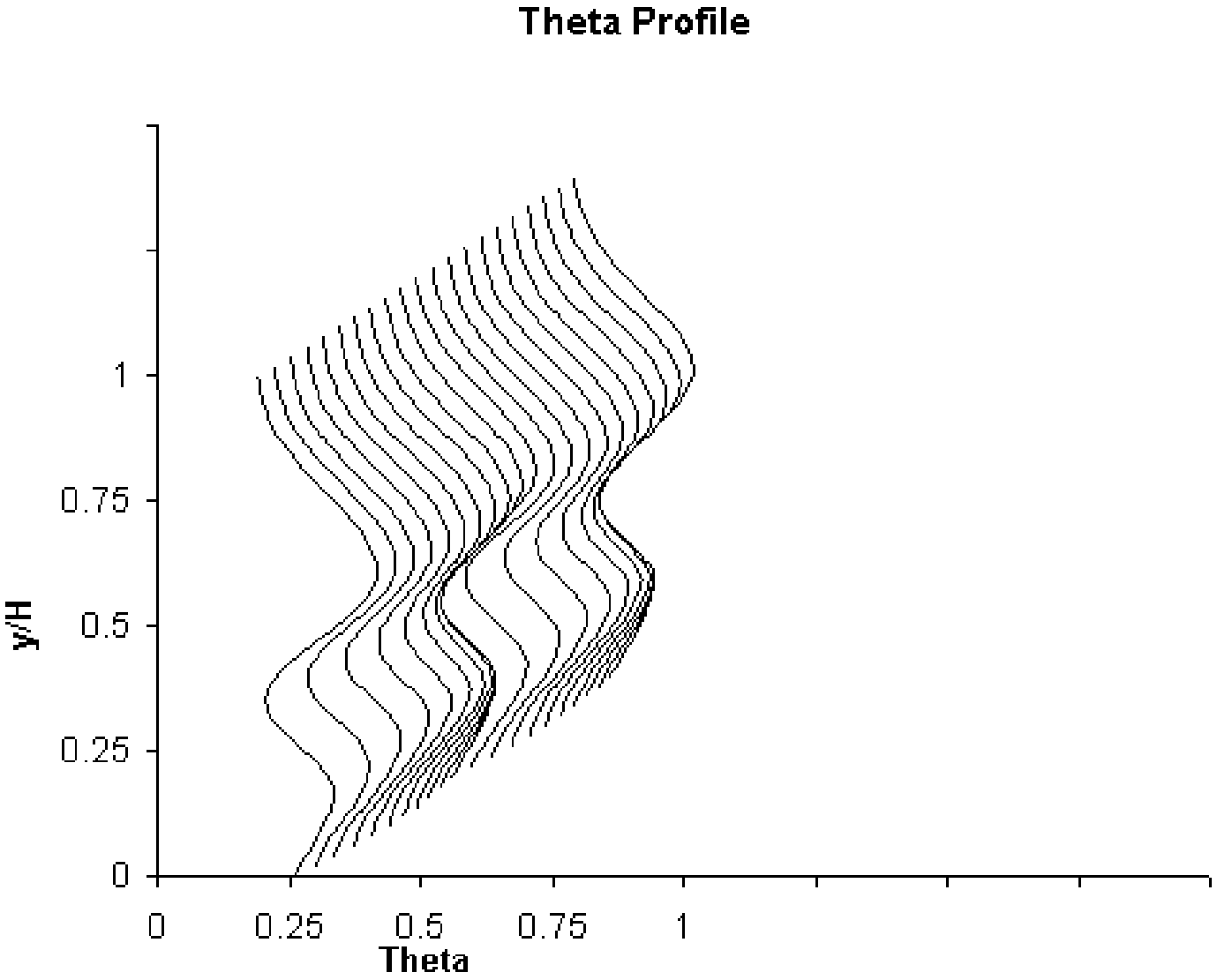


$J|_{top}=51.7$ $J|_{bottom}=9.5$

$x/H=0.5$, DR=2;2. $S/H=0.25$, $H/d|_{top}=H/d|_{bottom}=8$, $C_d=0.64$

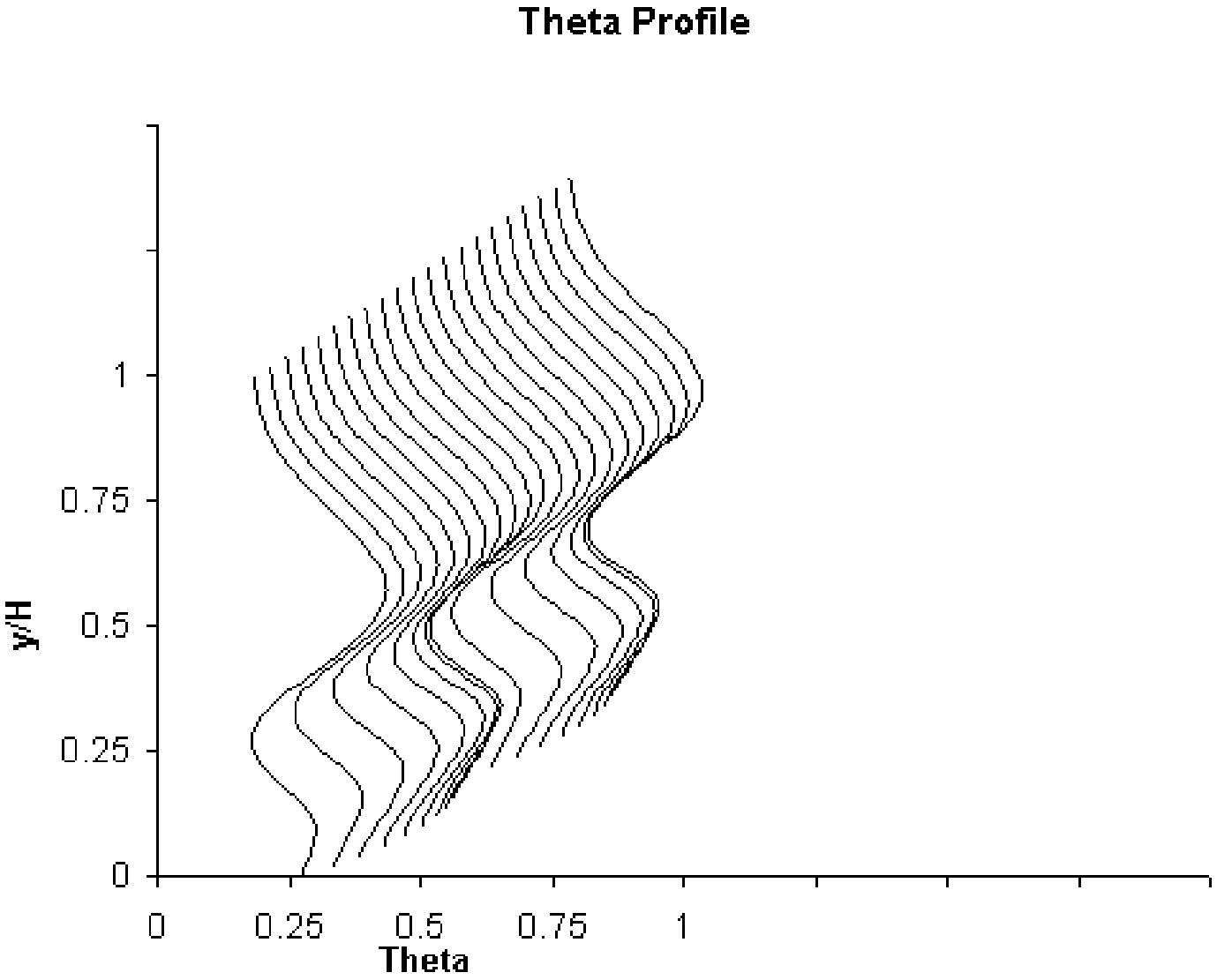


$J|_{top}=67.6$ $J|_{bottom}=4.2$

$x/H=0.5$, DR=2;2. $S/H=0.25$, $H/d|_{top}=H/d|_{bottom}=8$, $C_d=0.64$

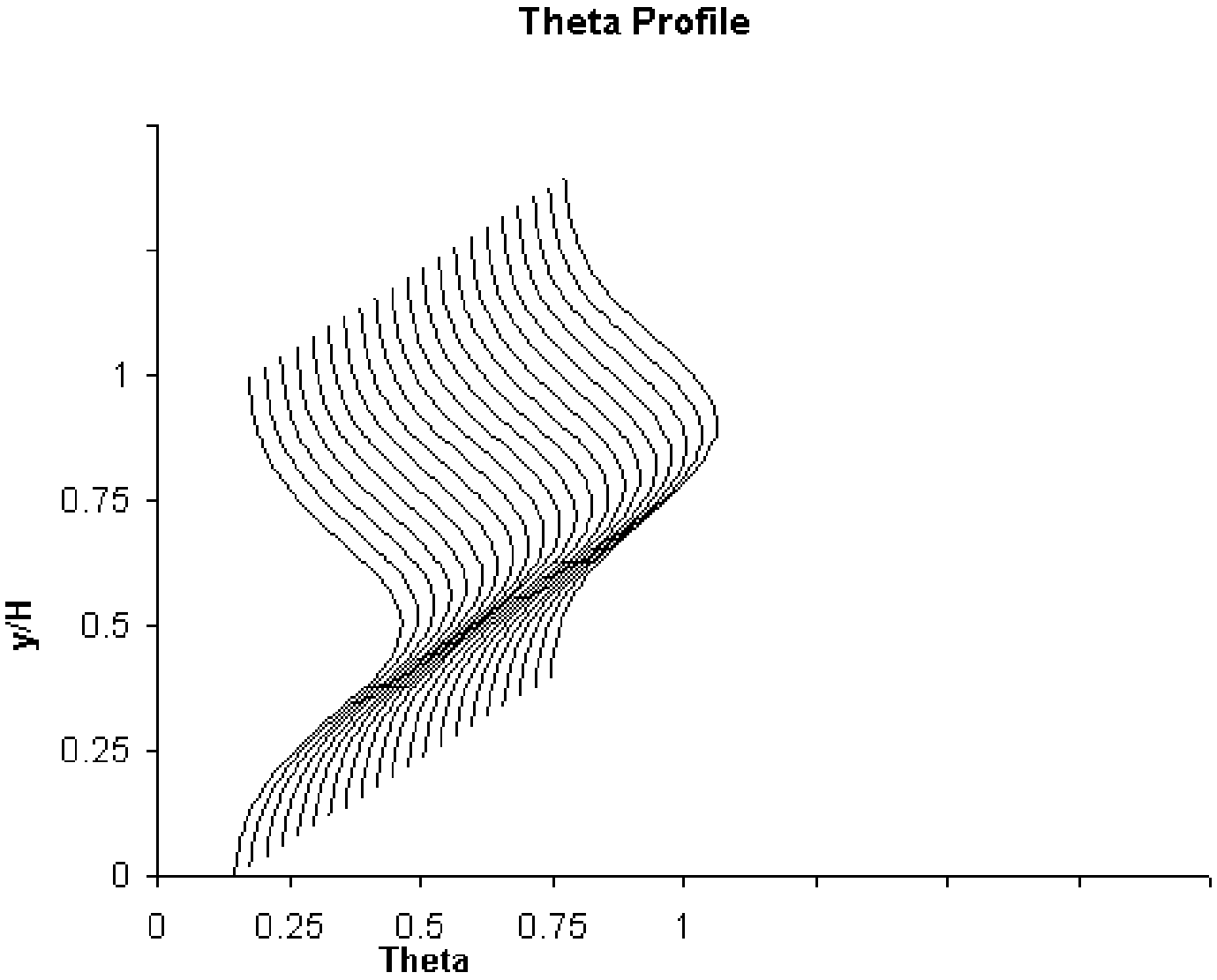


$J|_{top}=105.6$ $J|_{bottom}=0$

$x/H=0.5$, DR=2;2. $S/H=0.25$, $H/d|_{top}=H/d|_{bottom}=8$, $C_d=0.64$

Sequence 18

**Variations in scalar distributions with downstream distance for opposed rows of jets with centerlines staggered**

*x/H=0.25, 0.375 , 0.5, 0.75, 1, 1.5, 2*

*DR=2.2, J=26.4, S/H=1, H/d=8, $C_d$=0.64*

(cf. figure 20(a) in NASA/TM—2005-213137 and figure 17(a) in NASA TM–87294)

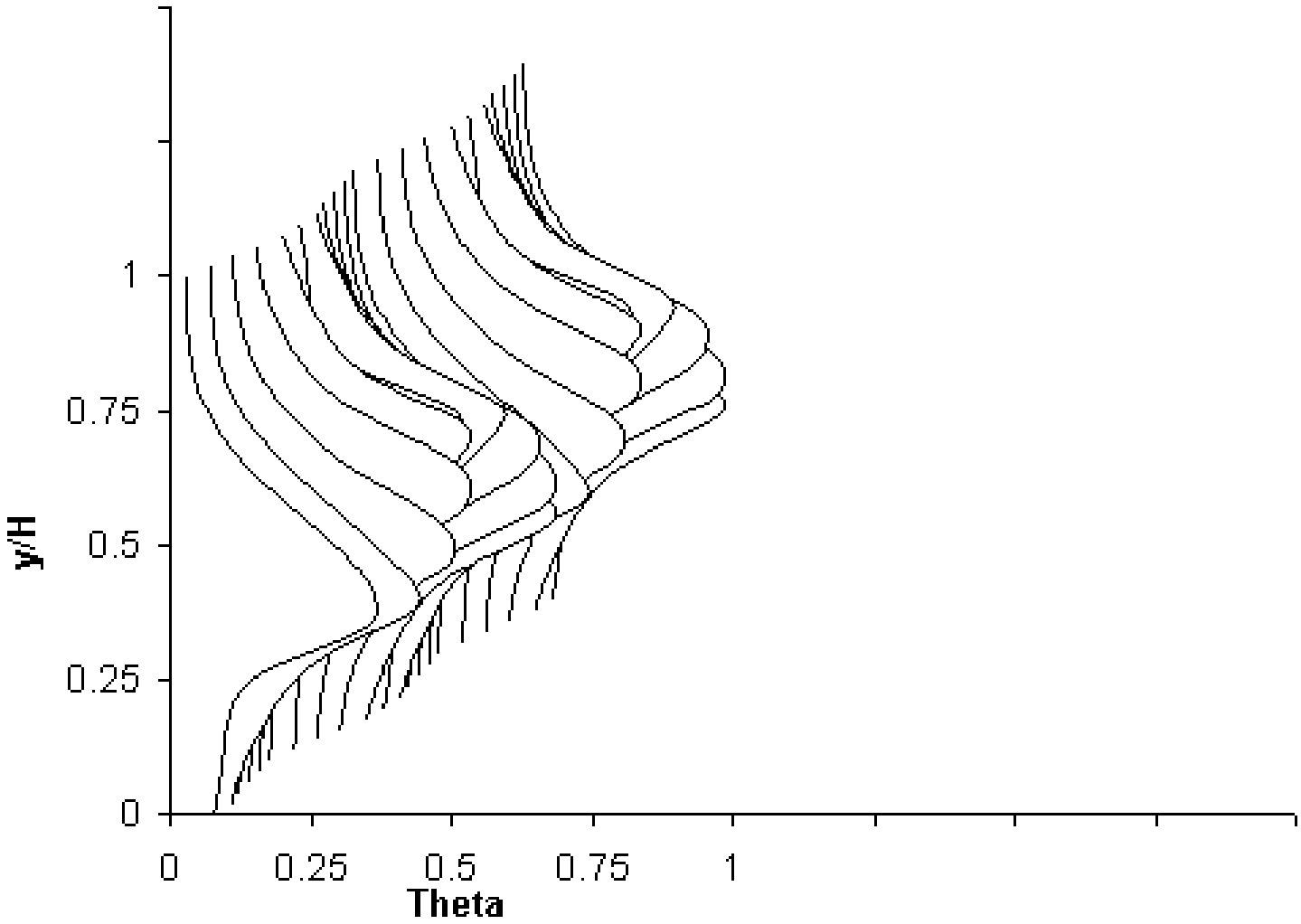


*x/H=0.25 (x/d=2)*

*J=26.4, S/H=1, H/d=8, (S/d=8)*

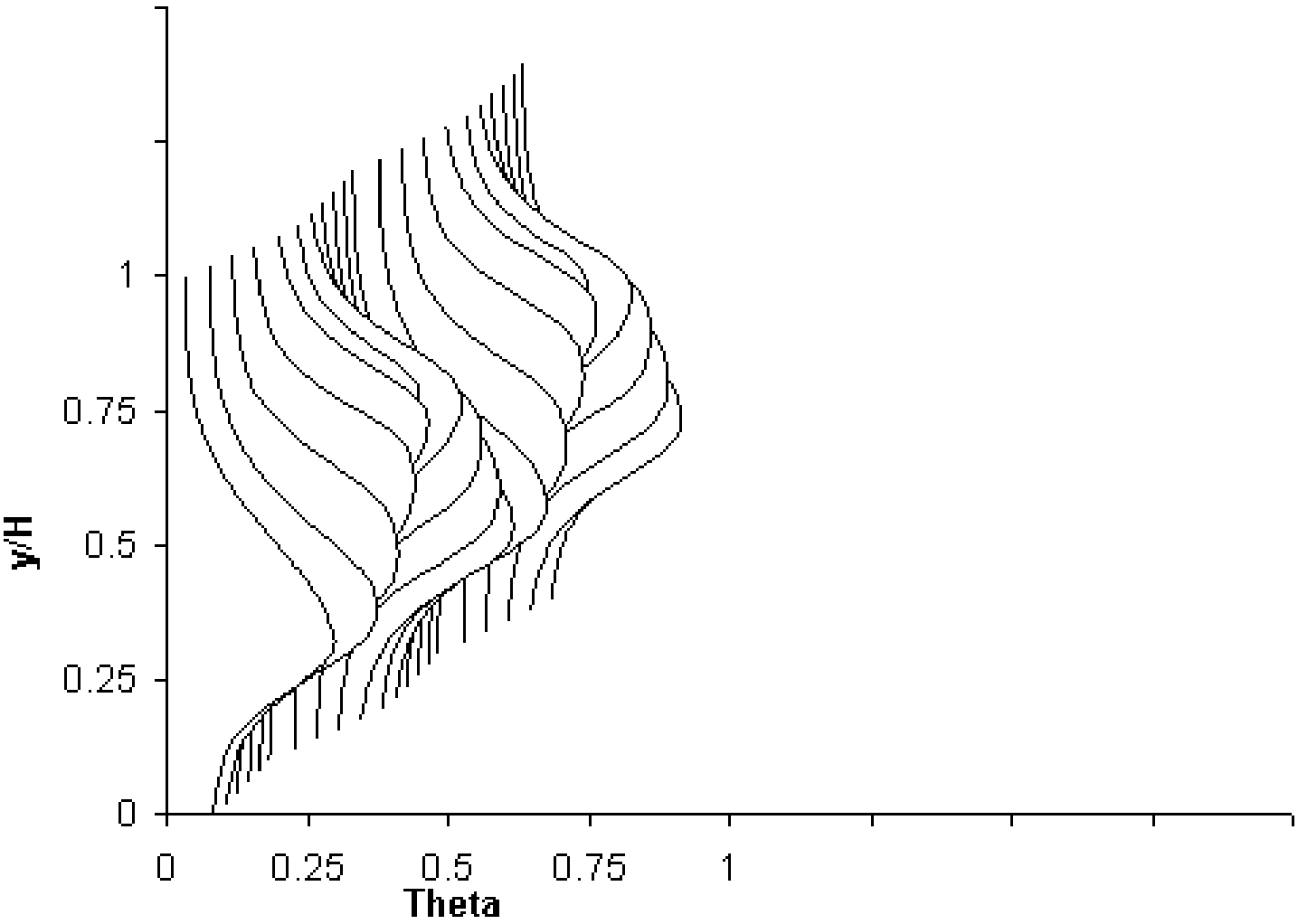


*x/H=0.375 (x/d=3)*

*J=26.4, S/H=1, H/d=8, (S/d=8)*

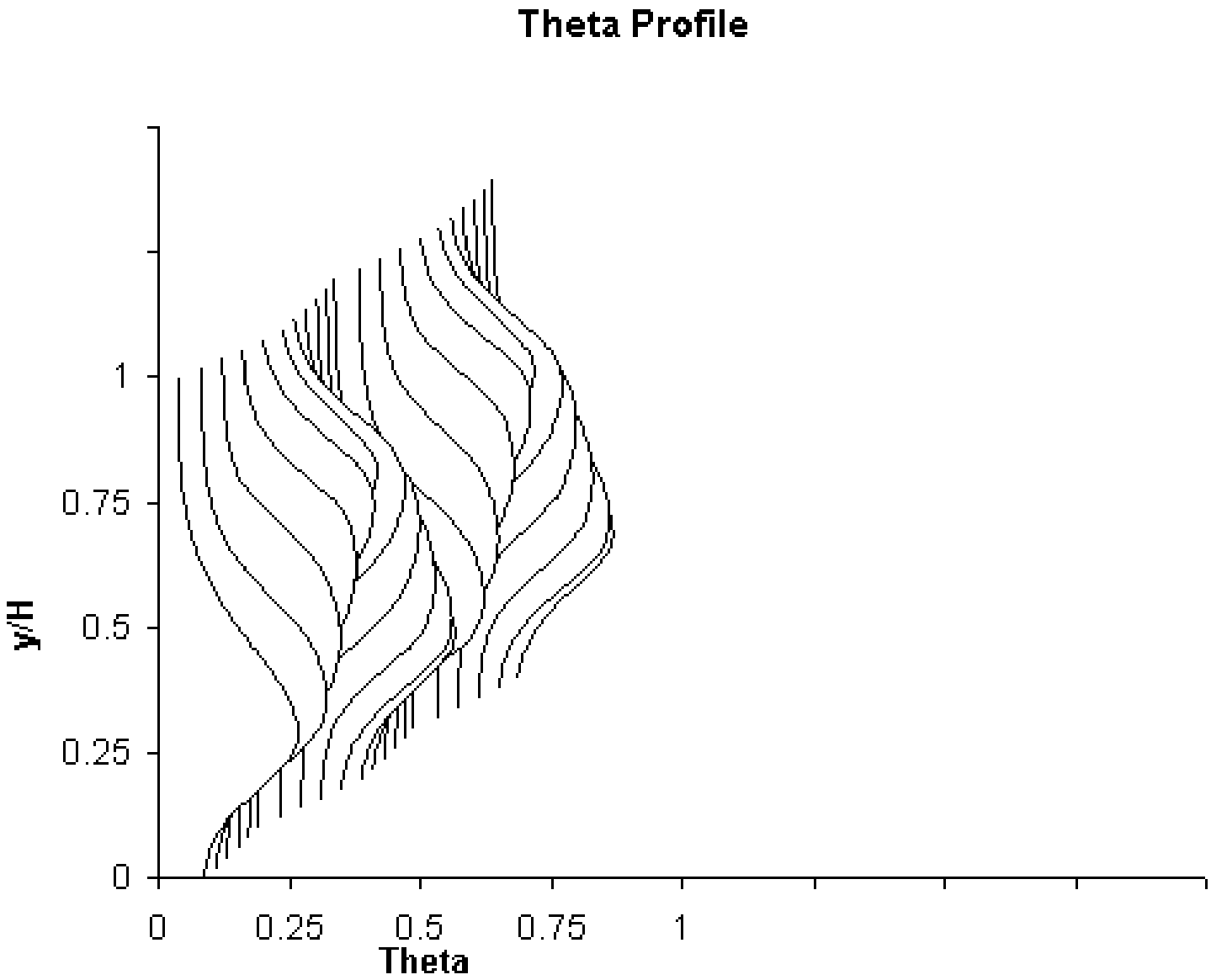


*x/H=0.5 (x/d=4)*

*J=26.4, S/H=1, H/d=8, (S/d=8)*

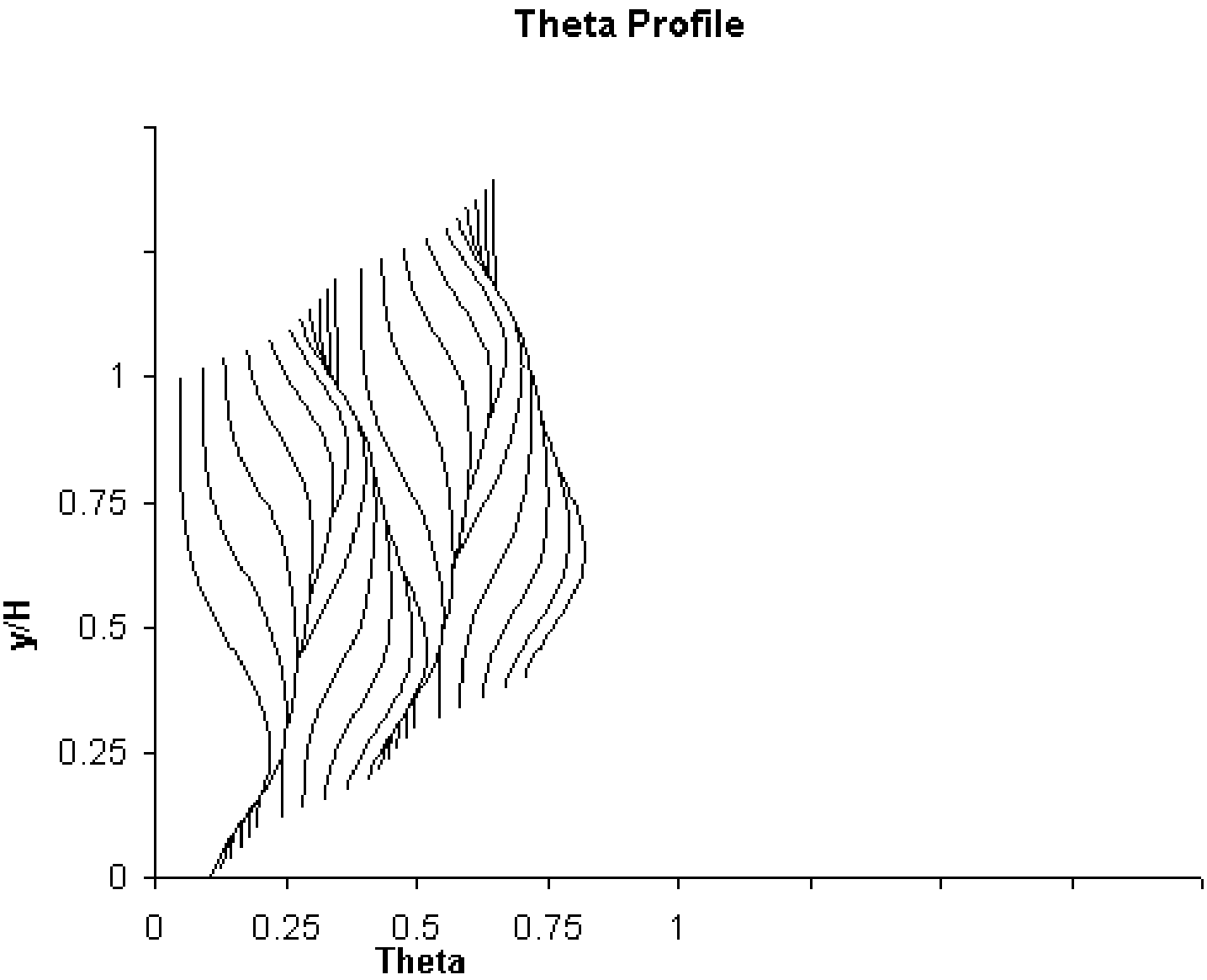


*x/H=0.75 (x/d=6)*

*J=26.4, S/H=1, H/d=8, (S/d=8)*

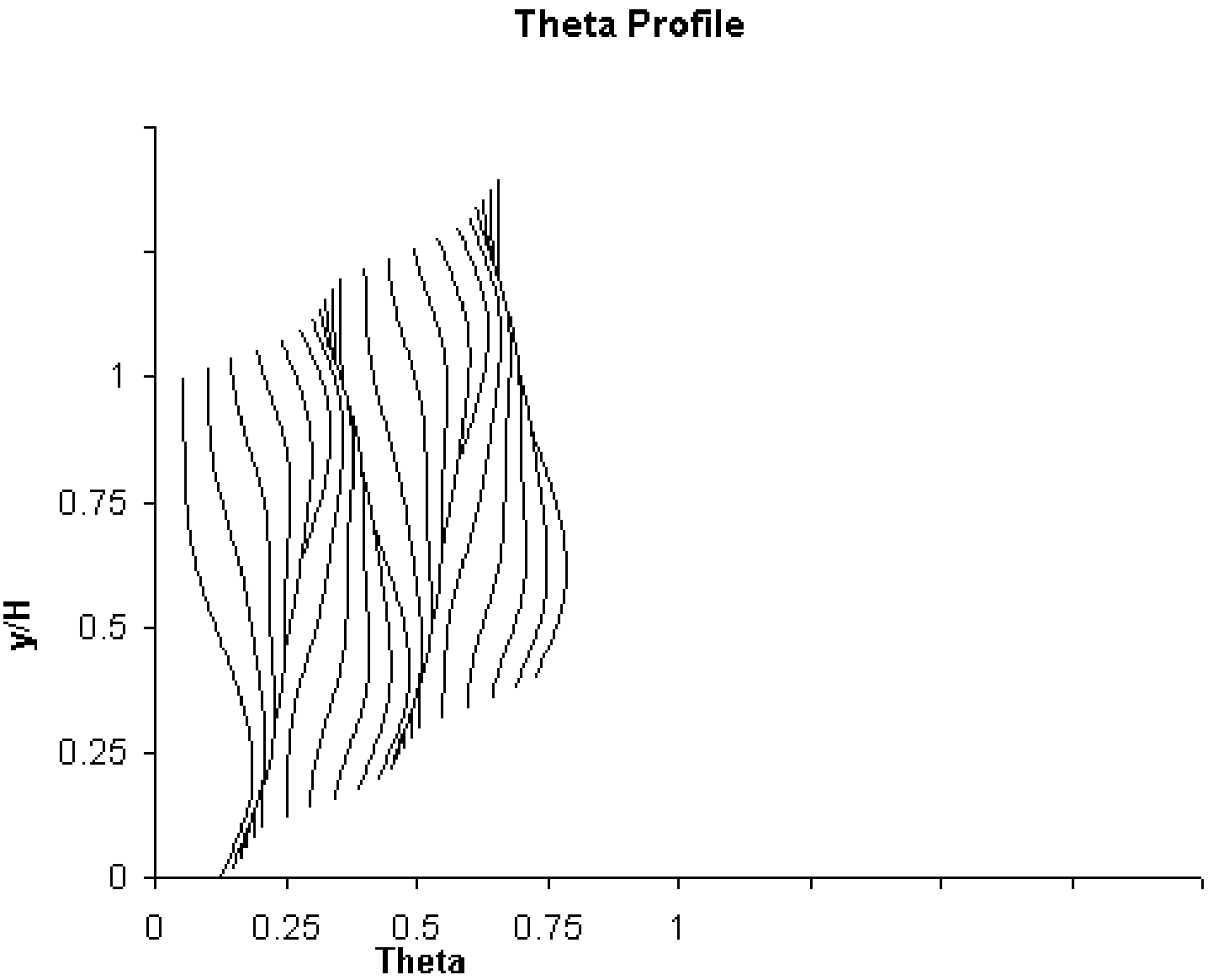


*x/H=1 (x/d=8)*

*J=26.4, S/H=1, H/d=8, (S/d=8)*

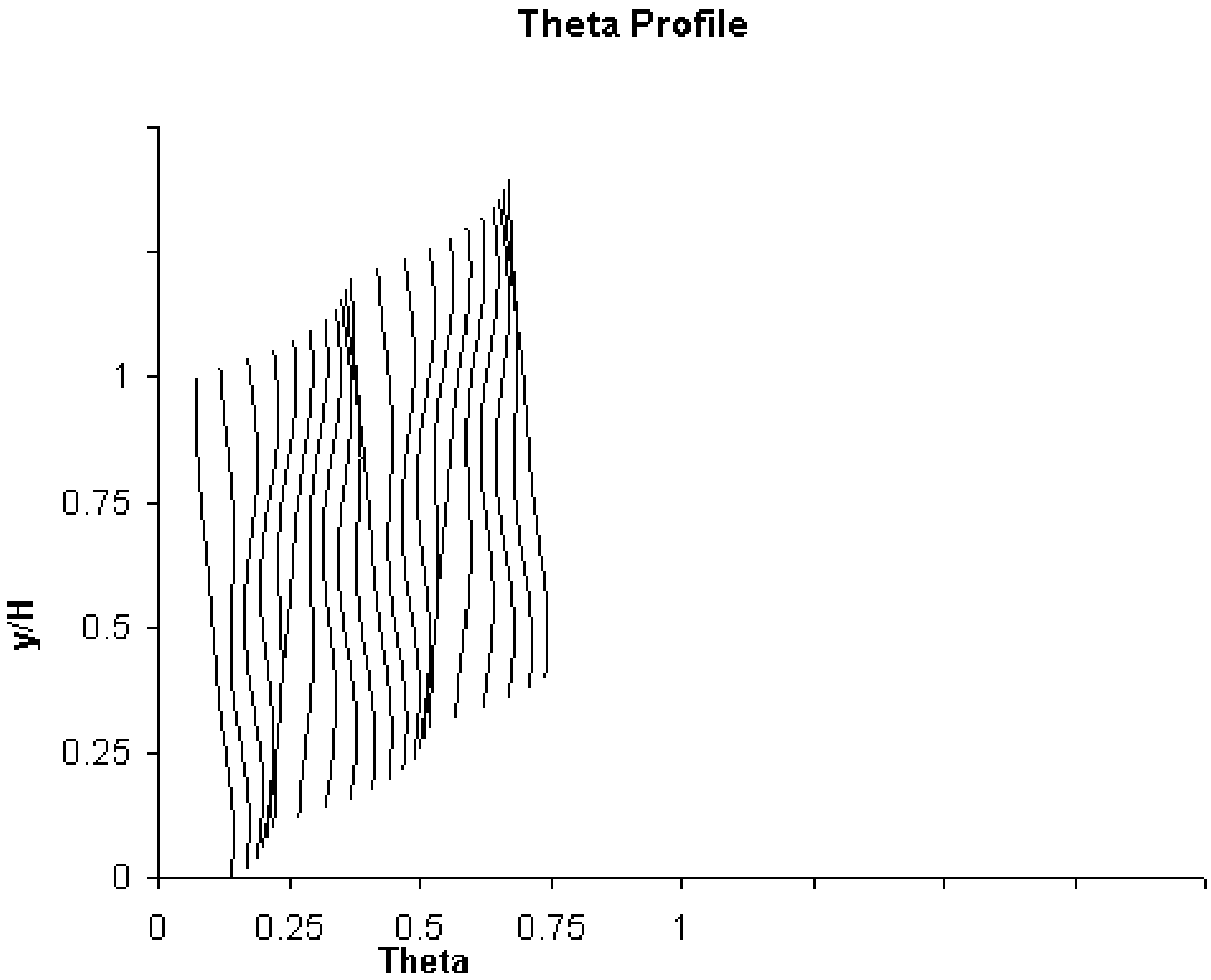


*x/H=1.5 *x/d=12)*

*J=26.4, S/H=1, H/d=8, (S/d=8)*

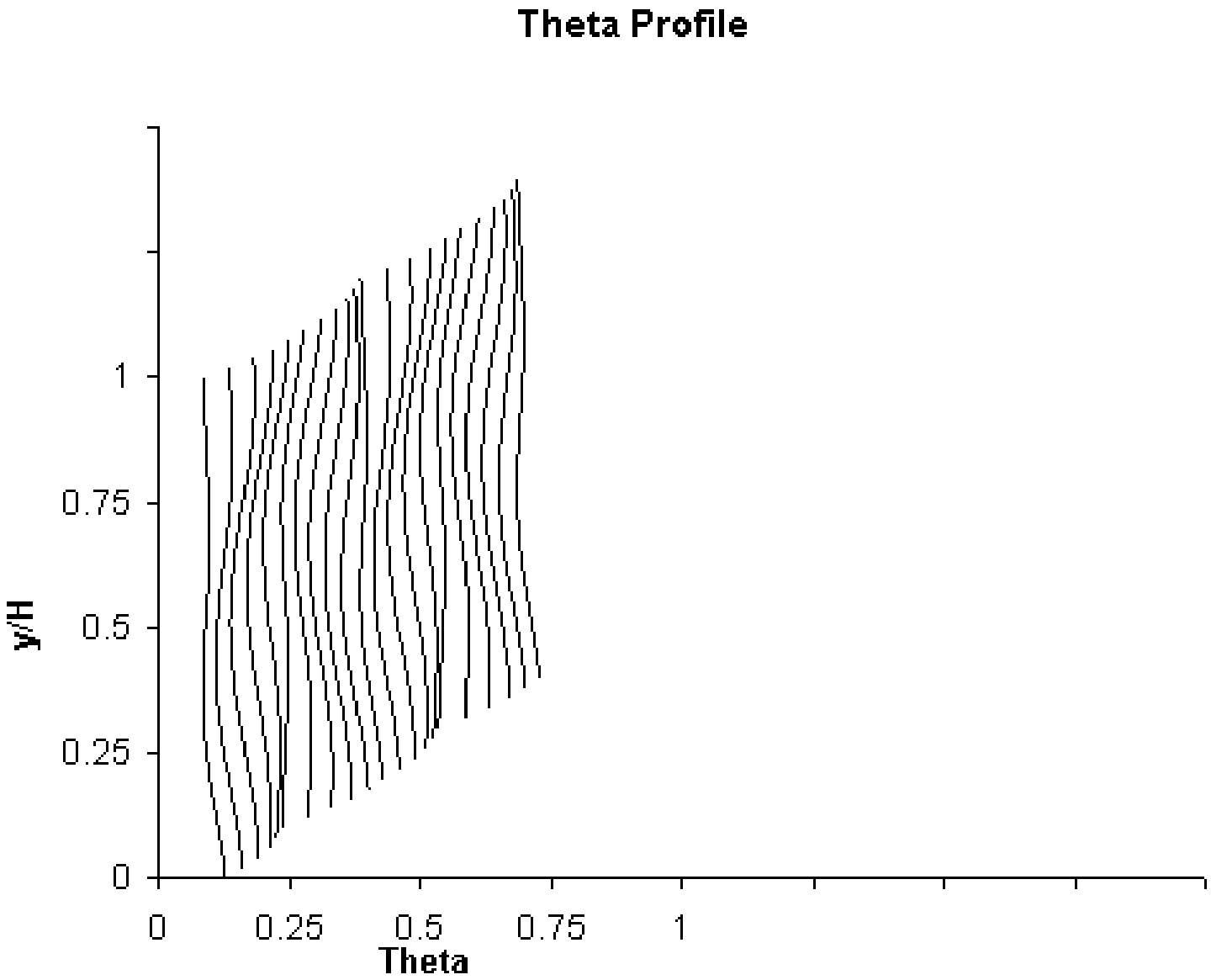


*x/H=2 (x/d=16)*

*J=26.4, S/H=1, H/d=8, (S/d=8)*

Sequence 19

**Variations in scalar distributions for**
**Double rows of jets with centerlines in-line**

*$S_x$/H= 1 (x/H=1.5), 0.75 (x/H=1.375), 0.5 (x/H=1.25), 0.375 (x/H=1.1875), 0.25 (x/H=1.125), 0 (x/H=1), Single row*

Downstream distance = H from midway between rows
(*x/H* is from center of 1st row)

Jet centerplanes in both rows are at same z location,
and all orifices are the same size

*DR=2.2, J=26.4, S/H=0.5, H/d=5.66, $C_d$=0.64*

(cf. figure 21 in NASA/TM—2006-213137 and
figure 18 in NASA TM–87294)

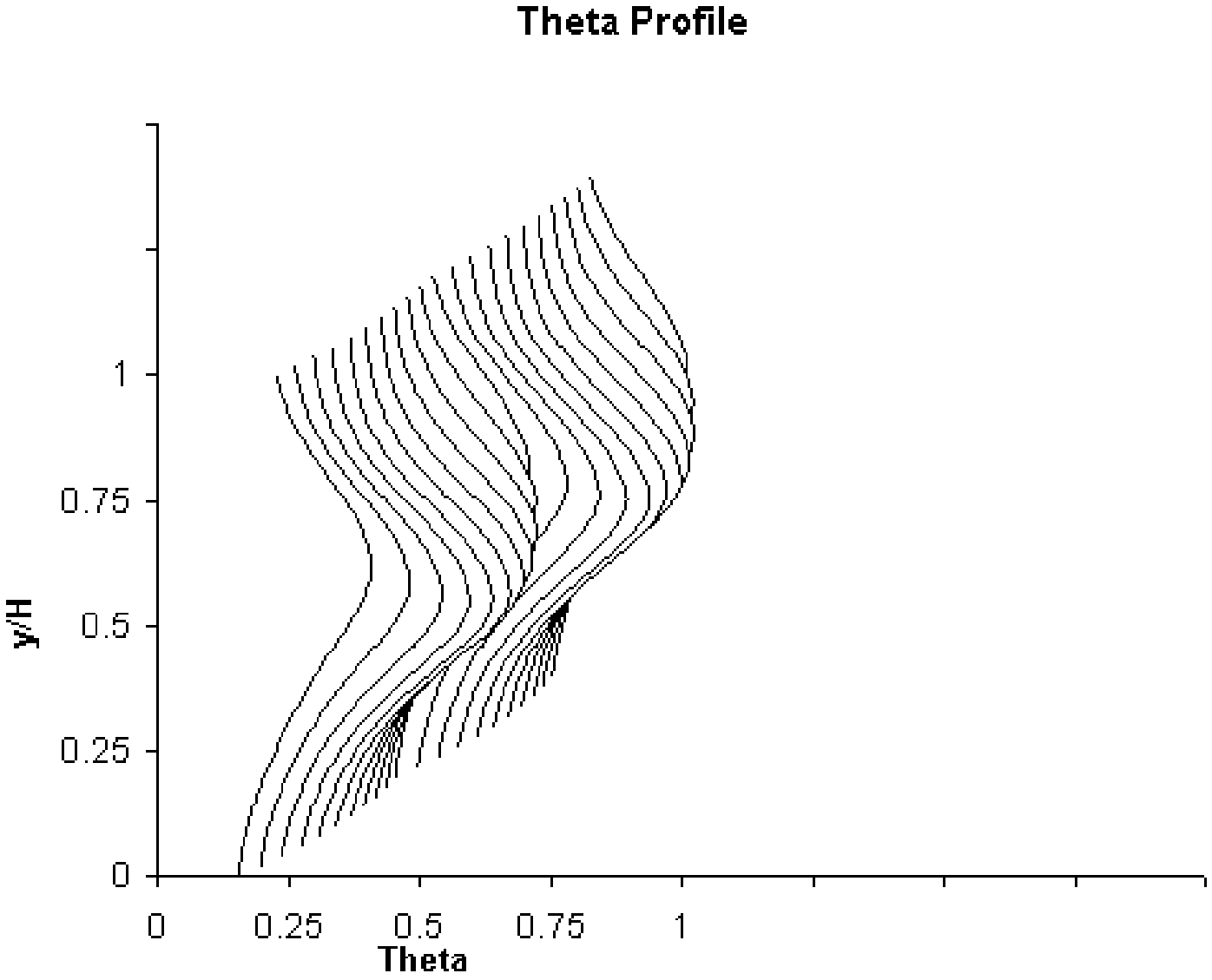


*Sx/H*= 1 *x/H*=1.5

Downstream distance = H from midway between rows

*J*=26.4, *S/H*=0.5; *H/d*=5.66, (S/d=2.83) in both rows

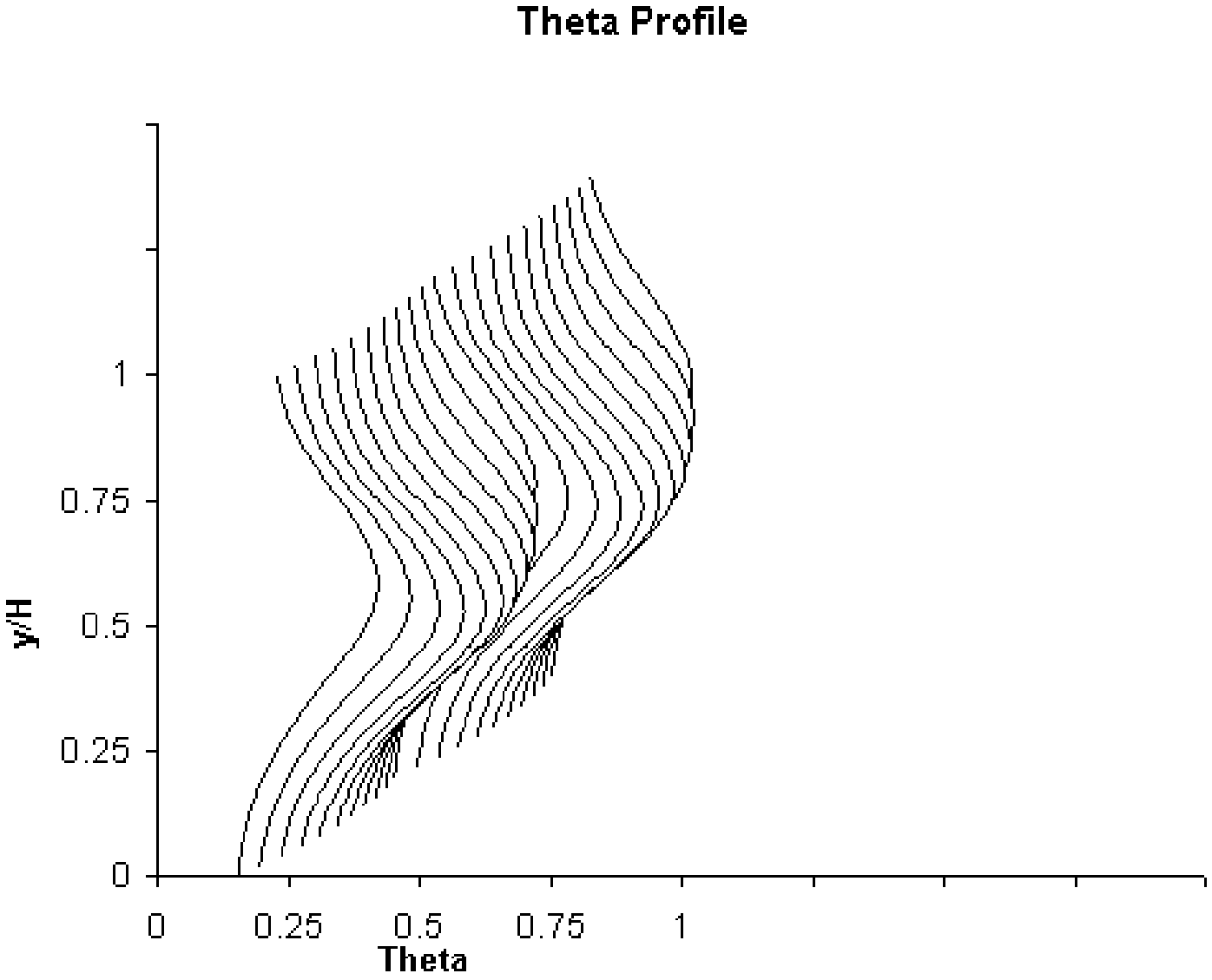


*Sx/H*= 0.75 *x/H*=1.375

Downstream distance = H from midway between rows

*J*=26.4, *S/H*=0.5; *H/d*=5.66, (S/d=2.83) in both rows

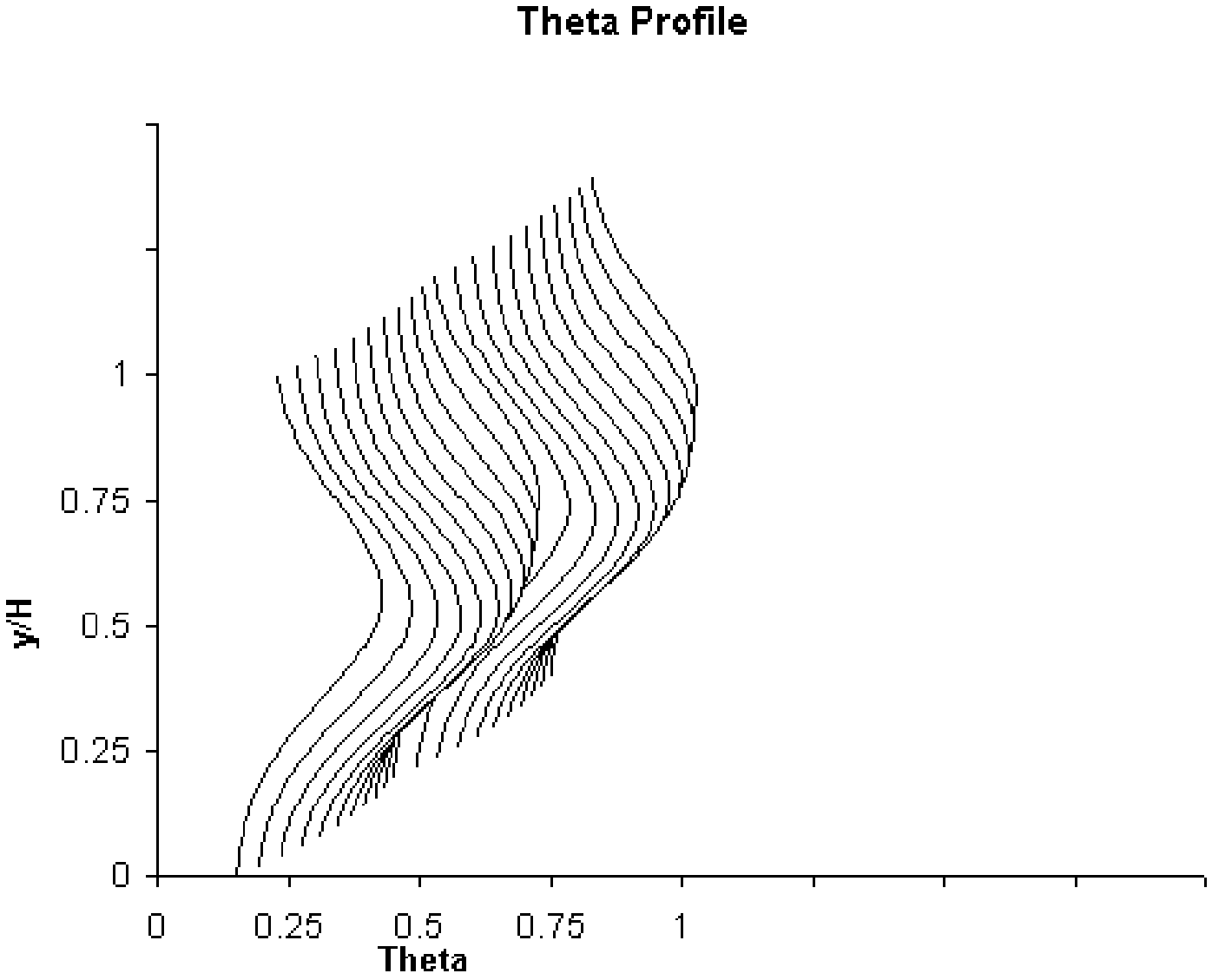


*Sx/H*= 0.5 *x/H*=1.25

Downstream distance = H from midway between rows

*J*=26.4, *S/H*=0.5; *H/d*=5.66, (S/d=2.83) in both rows

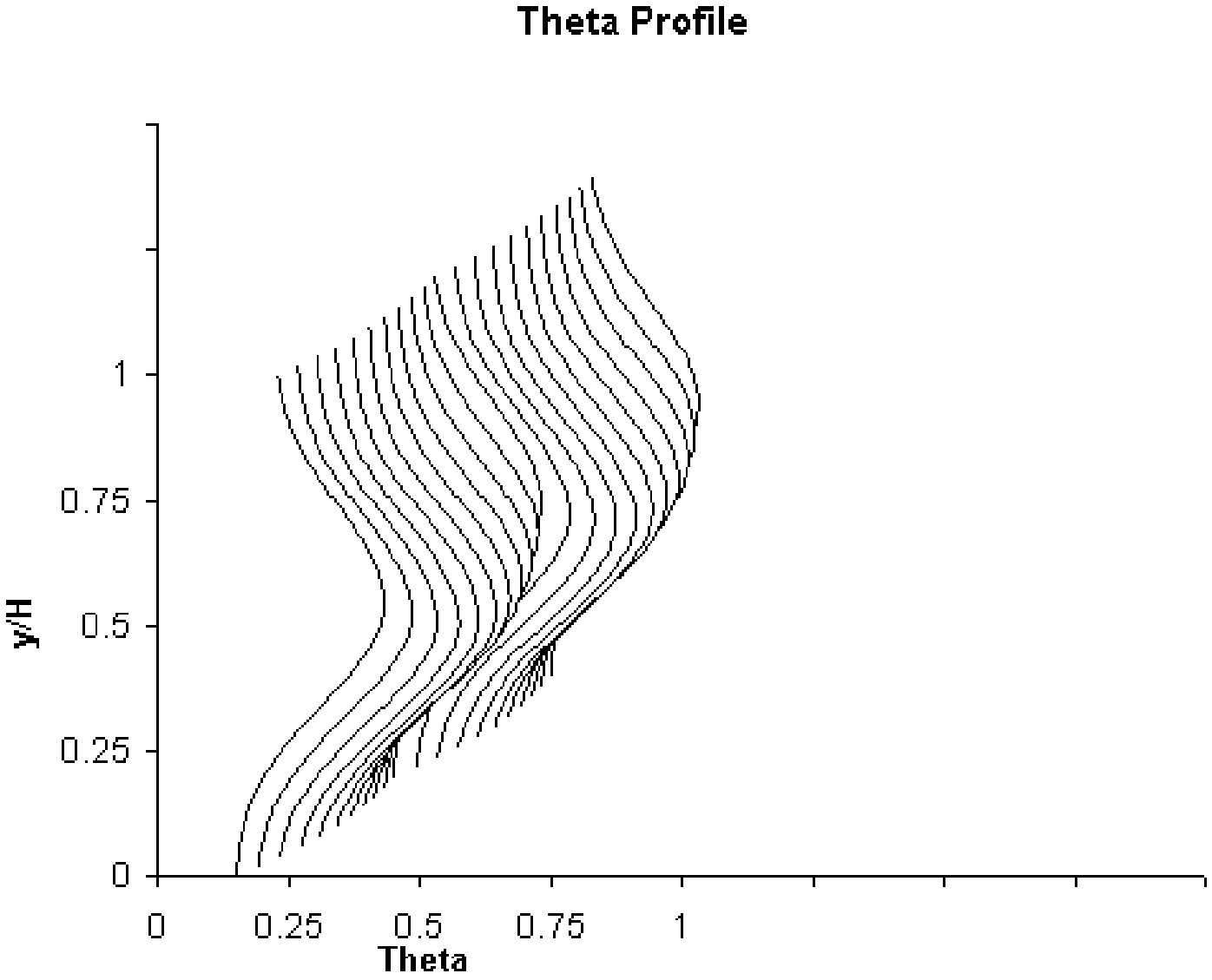


*Sx/H*= 0.25 *x/H*=1.125

Downstream distance = H from midway between rows

*J*=26.4, *S/H*=0.5; *H/d*=5.66, (S/d=2.83) in both rows

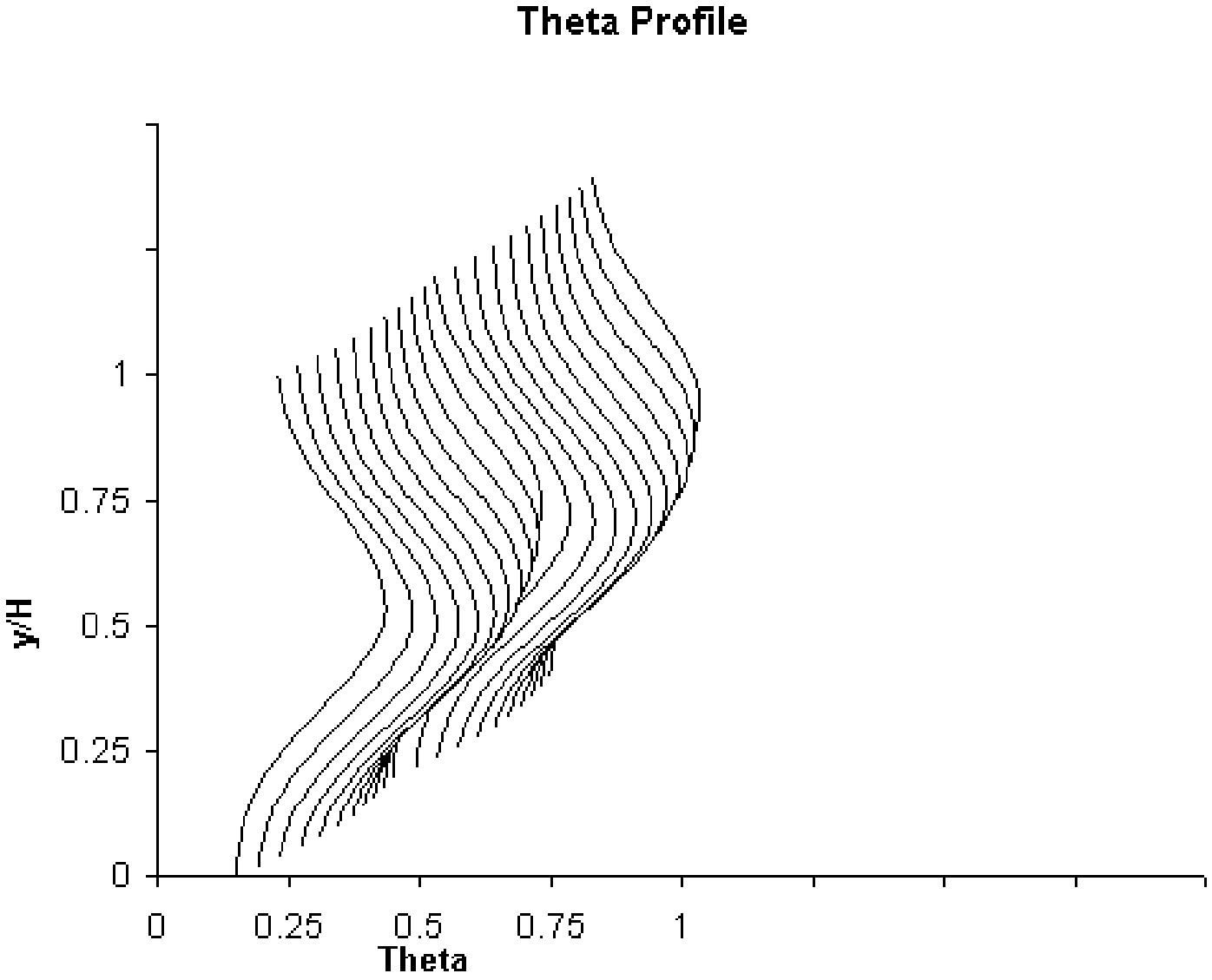


*Sx/H*= 0 *x/H*=1

Downstream distance = H from midway between rows

*J*=26.4, *S/H*=0.5; *H/d*=5.66; (S/d=2.83) in both rows

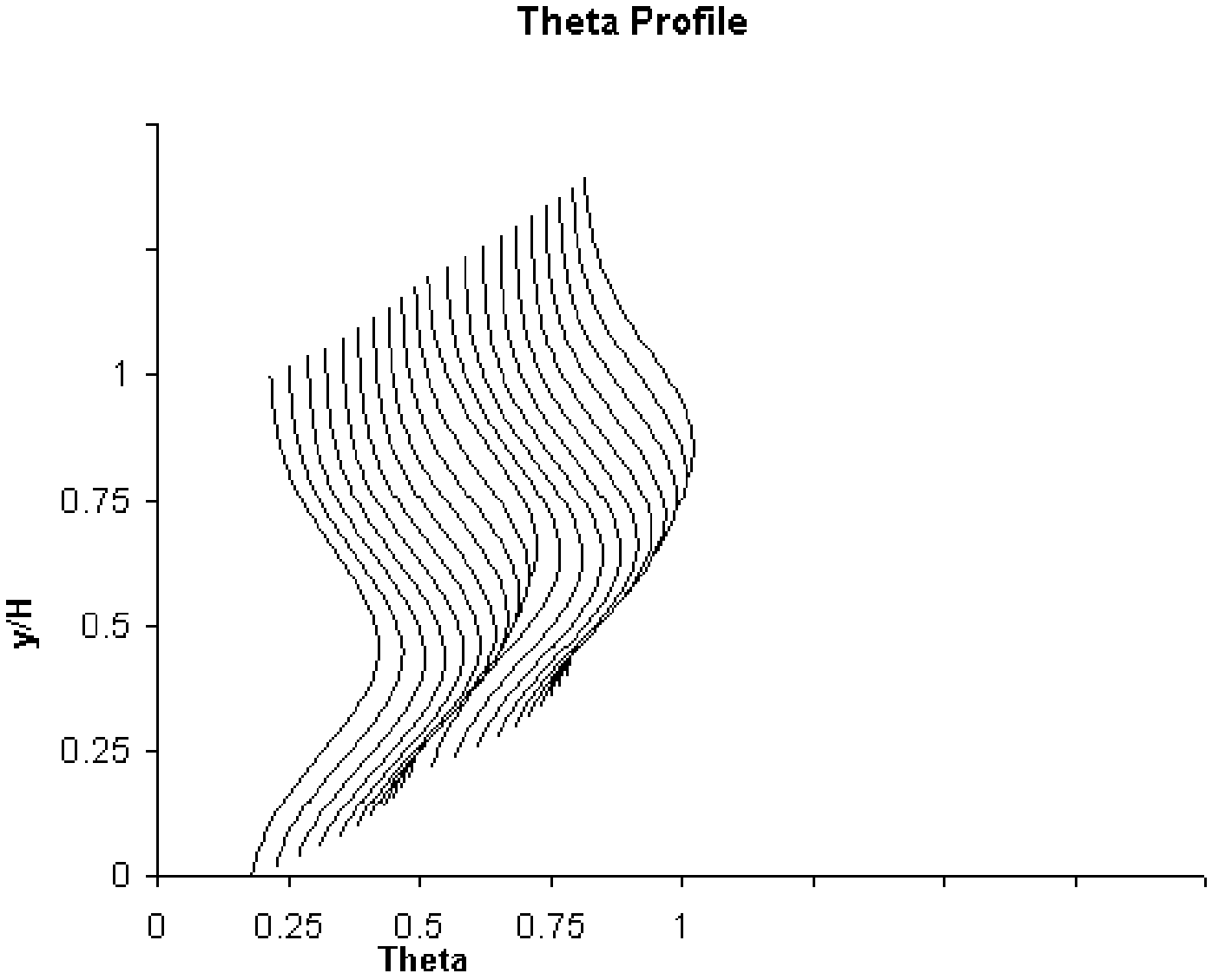


*Single row* *x/H*=1 (x/d=4)

*J*=26.4, *S/H*=0.5; *H/d*=4, (S/d=2)

Sequence 20

**Variations in scalar distributions for**
**Double rows of jets with centerlines staggered**

*$S_{x/}H$= 1 (x/H=1.25), 0.75 (x/H=1), 0.5 (x/H=0.75), 0.375 (x/H=-0.625), 0.25 (x/H=0.5), 0 (x/H=0.25), Single row*

Downstream distance = H/4 from center of 2nd row
(*x/H* is from center of 1st row)

Jet centerplanes in the two rows are staggered in the z direction, but the orifices in both rows have the same size and spacing

*DR=2.2, J=26.4, S/H=1, H/d=4, $C_d$=0.64*

(cf. figure 22(b) in NASA/TM—2006-213137 and figure 19 in NASA TM–87294)

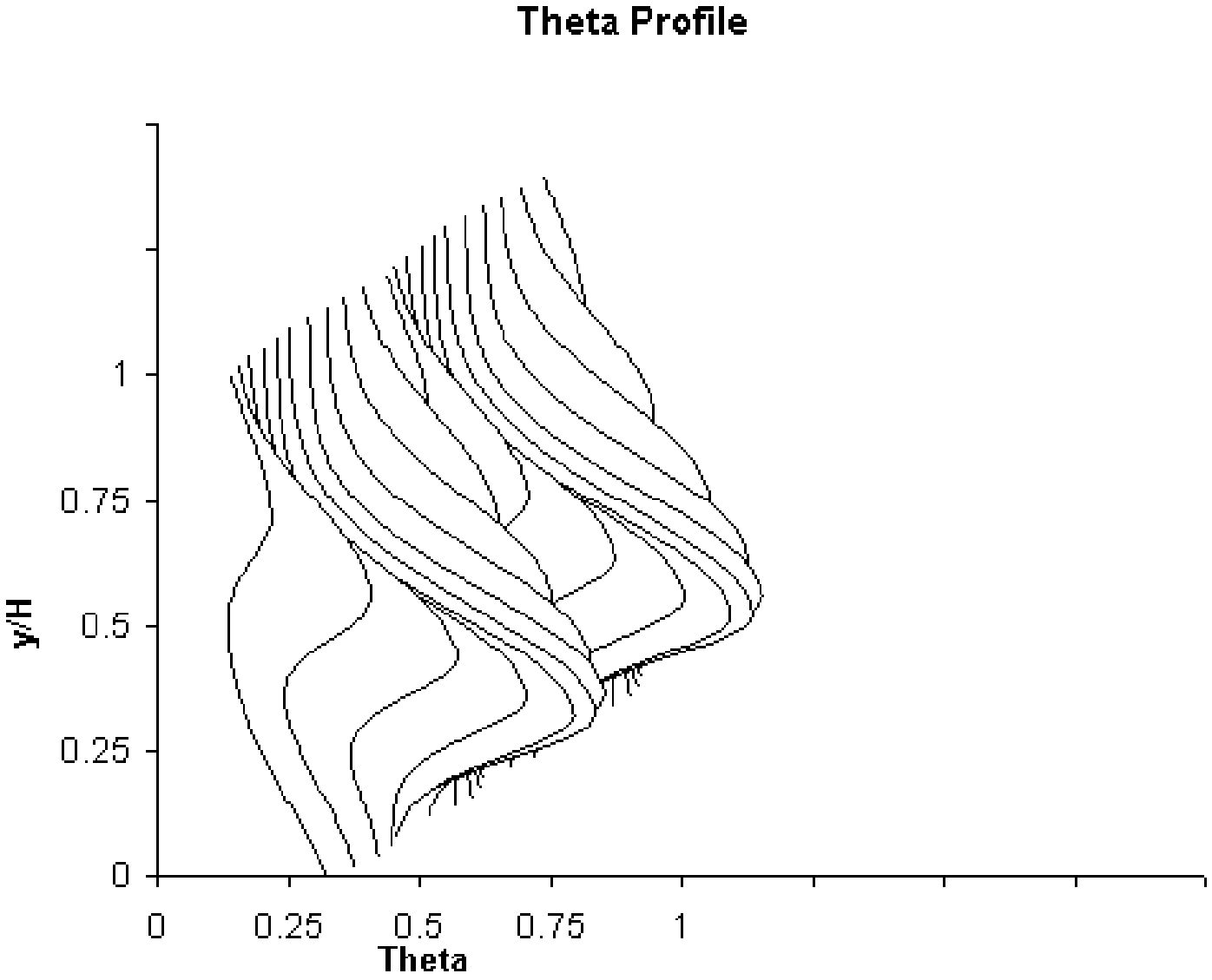


*Sx/H*= 1 *x/H*=1.25

Downstream distance = H/4 from center of 2nd row

*J*=26.4, *S/H*=1; *H/d*=4, *(S/d=4)* in both rows

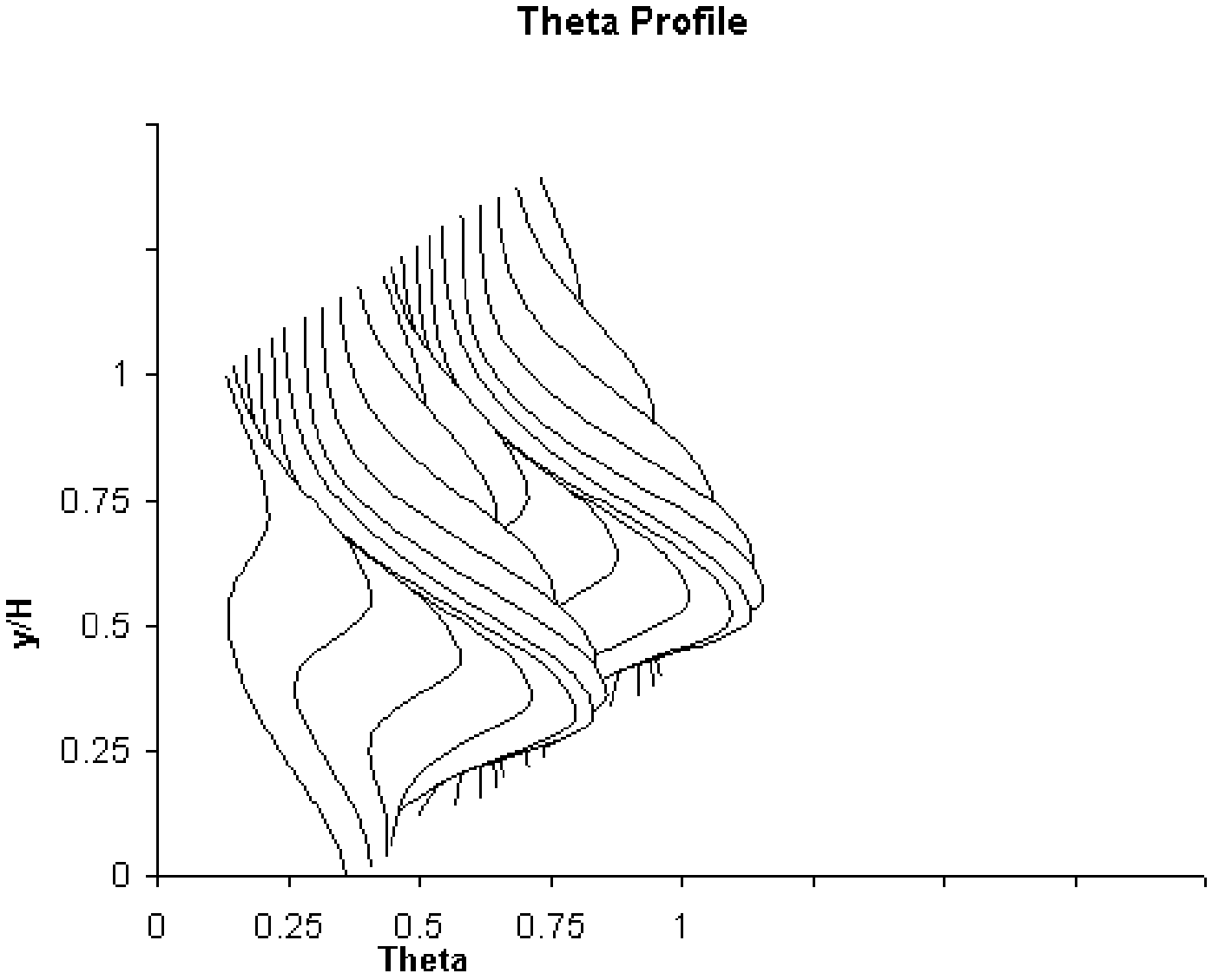


*Sx/H*= .75 *x/H*=1

Downstream distance = H/4 from center of 2nd row

*J*=26.4, *S/H*=1; *H/d*=4, *(S/d=4*) in both rows

## Theta Profile

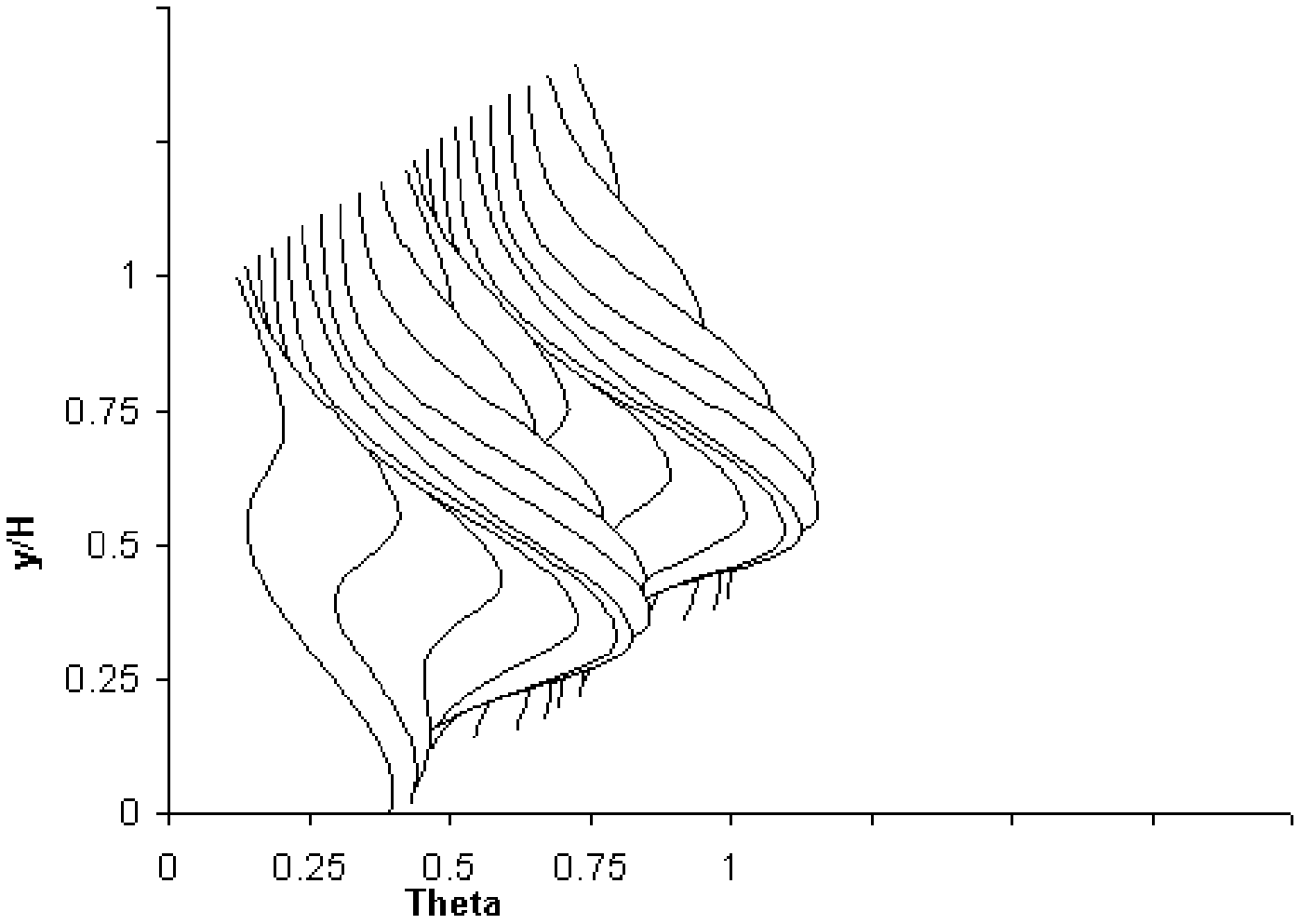


*Sx/H*= 0.5 *x/H*=0.75

Downstream distance = H/4 from center of 2nd row

*J*=26.4, *S/H*=1, *H/d*=4, *(S/d=4)* in both rows

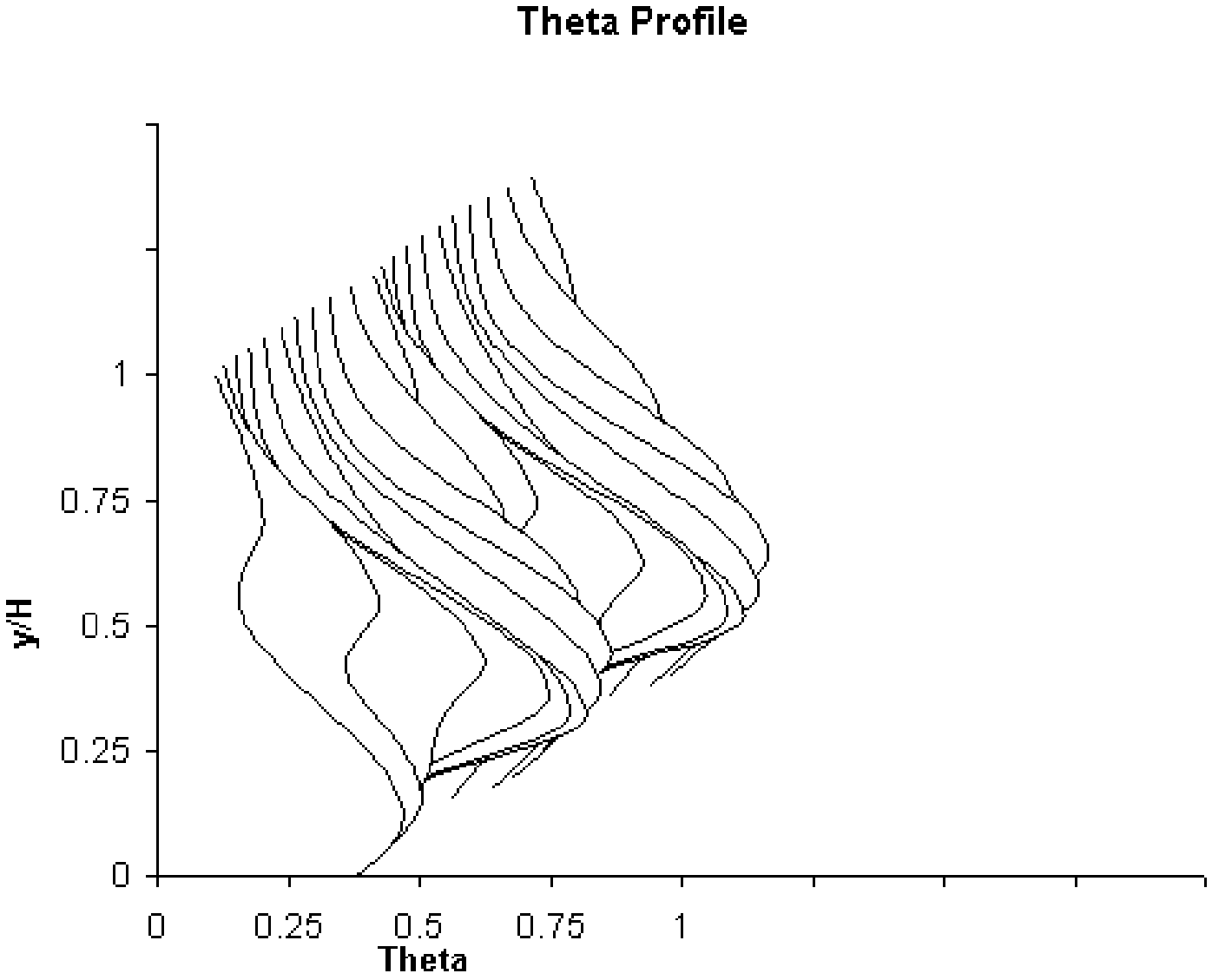


*Sx/H*= 0.25 *x/H*=0.5

Downstream distance = H/4 from center of 2nd row

*J*=26.4, *S/H*=1; *H/d*=4, (*S/d=4)* in both rows

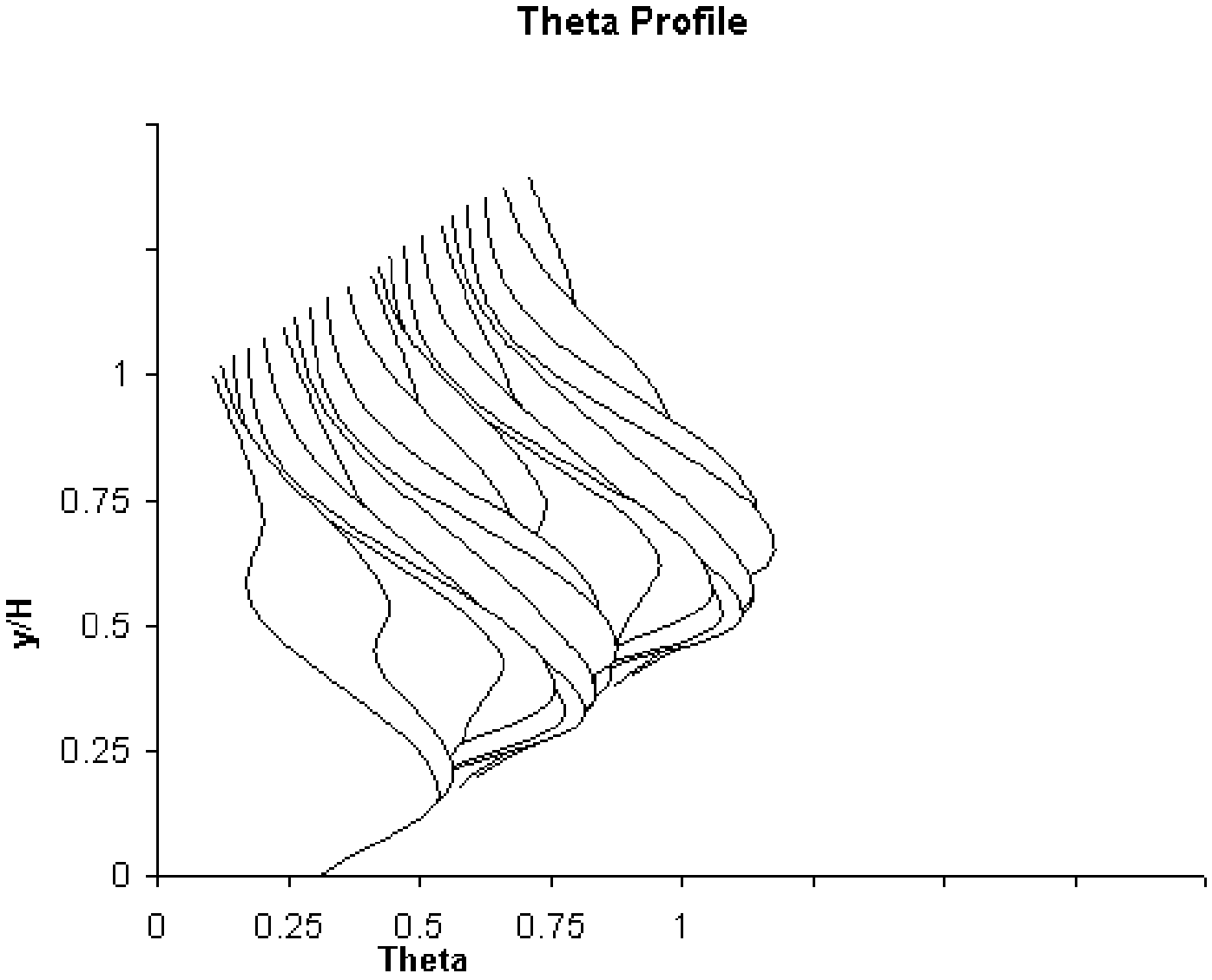


*Sx/H*= 0.125 *x/H*=0.375

Downstream distance = H/4f from center of 2nd row

*J*=26.4, *S/H*=1; *H/d*=4, *(S/d=4)* in both rows

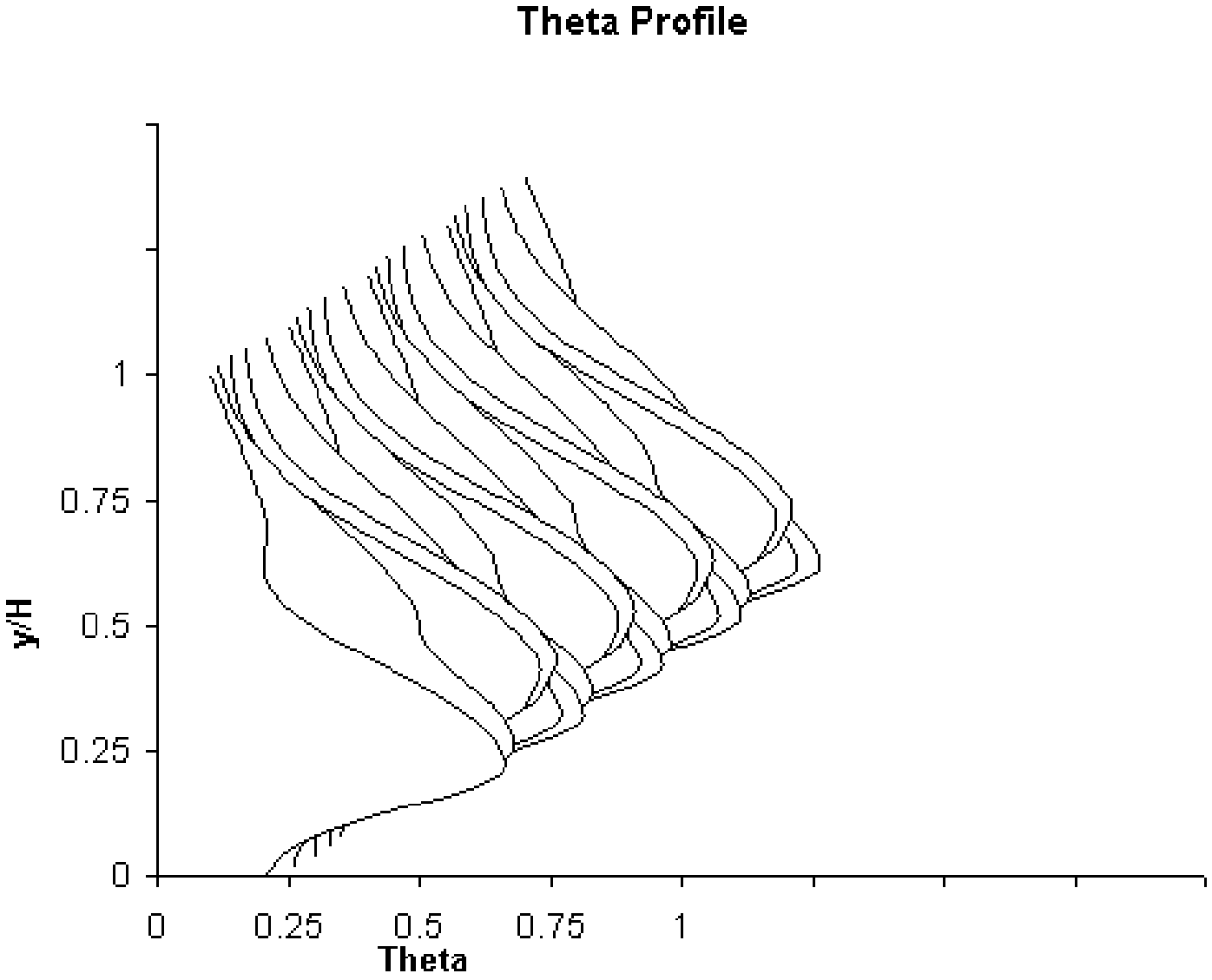


*Sx/H*= 0 *x/H*=0.25

Downstream distance = H/4 from center of 2nd row

*J*=26.4, *S/H*=1; *H/d*=4, *(S/d=4*) in both rows

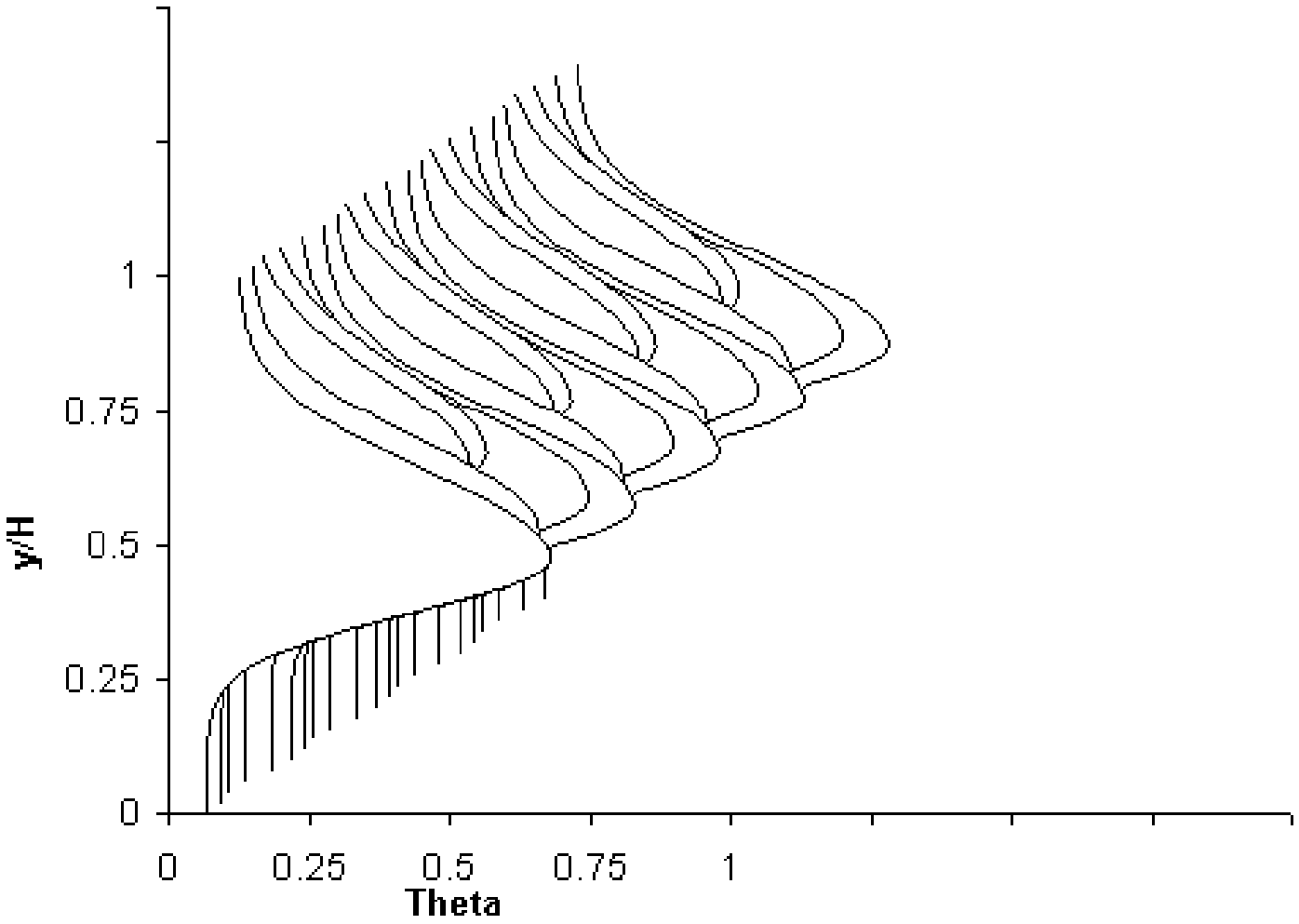


*Single row* *x/H*=0.25 (x/d=1)

*J*=26.4, *S/H*=0.5; *H/d=4, (S/d=2)*

NASA/TM—2006-214226

Sequence 21

## Variations in scalar distributions for double rows of jets with twice as many holes in the 2nd row

*x/H= 0 375, 0.5, 0.75, 1, 1.25, 1.5, 2*
(from center of 1st row)

*$S_x$/H=.25; DR=2.2, J=26.4, $C_d$=0.64*
*Row 1: S/H=.5, H/d=5.66*
*Row 2: S/H=.25, H/d=8*

(cf. figure 20(a) in NASA TM–87294. Note that downstream distances in figure 20 in NASA TM–87294 appear to have been given from the 2nd row

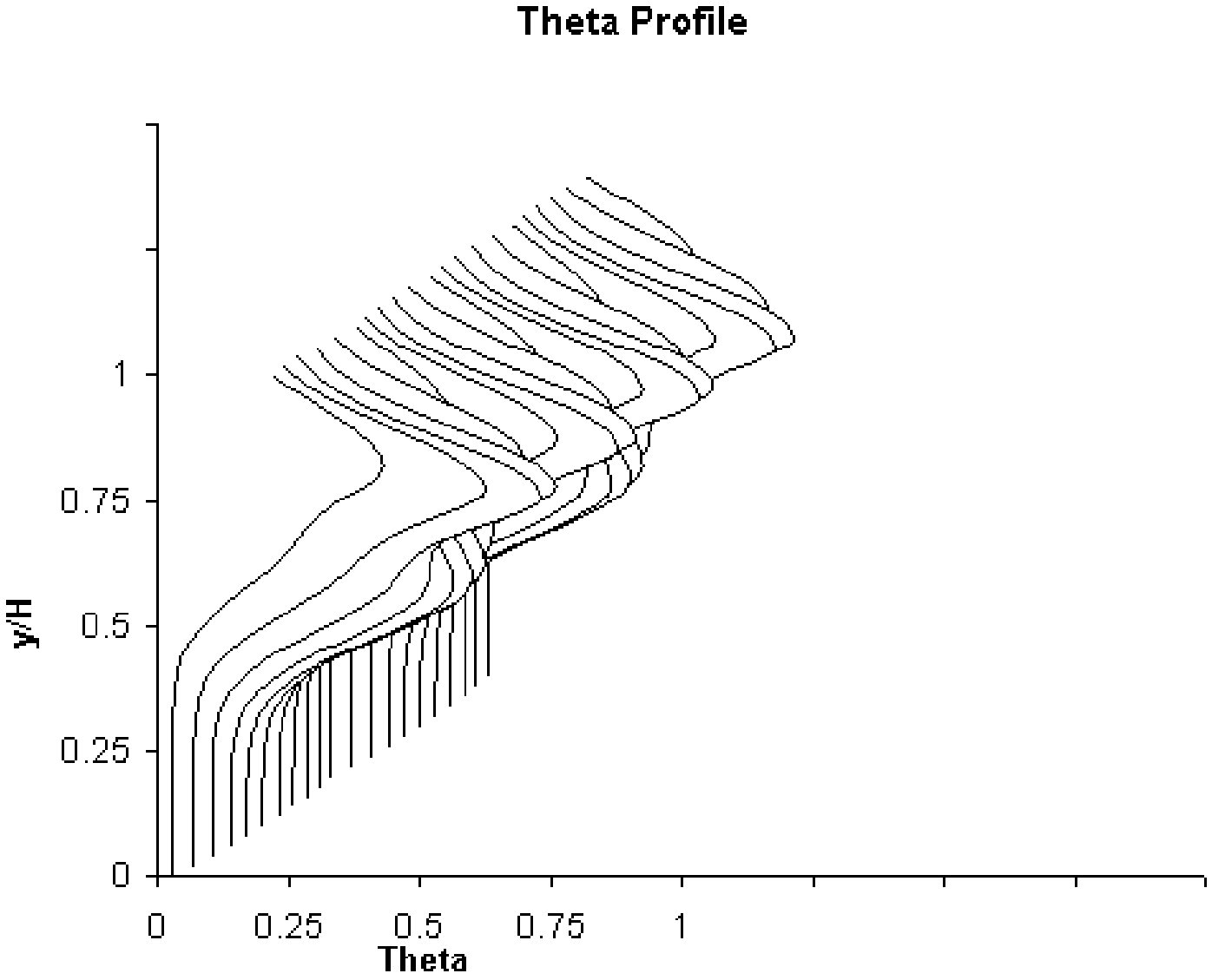


*x/H*=0 375

*$S_x$/H=0.25; DR=2.2, J=26.4, $C_d$=0.64*

*Row 1: S/H=0.5; H/d=5.66* *Row 2: S/H=9.25; H/d=8*

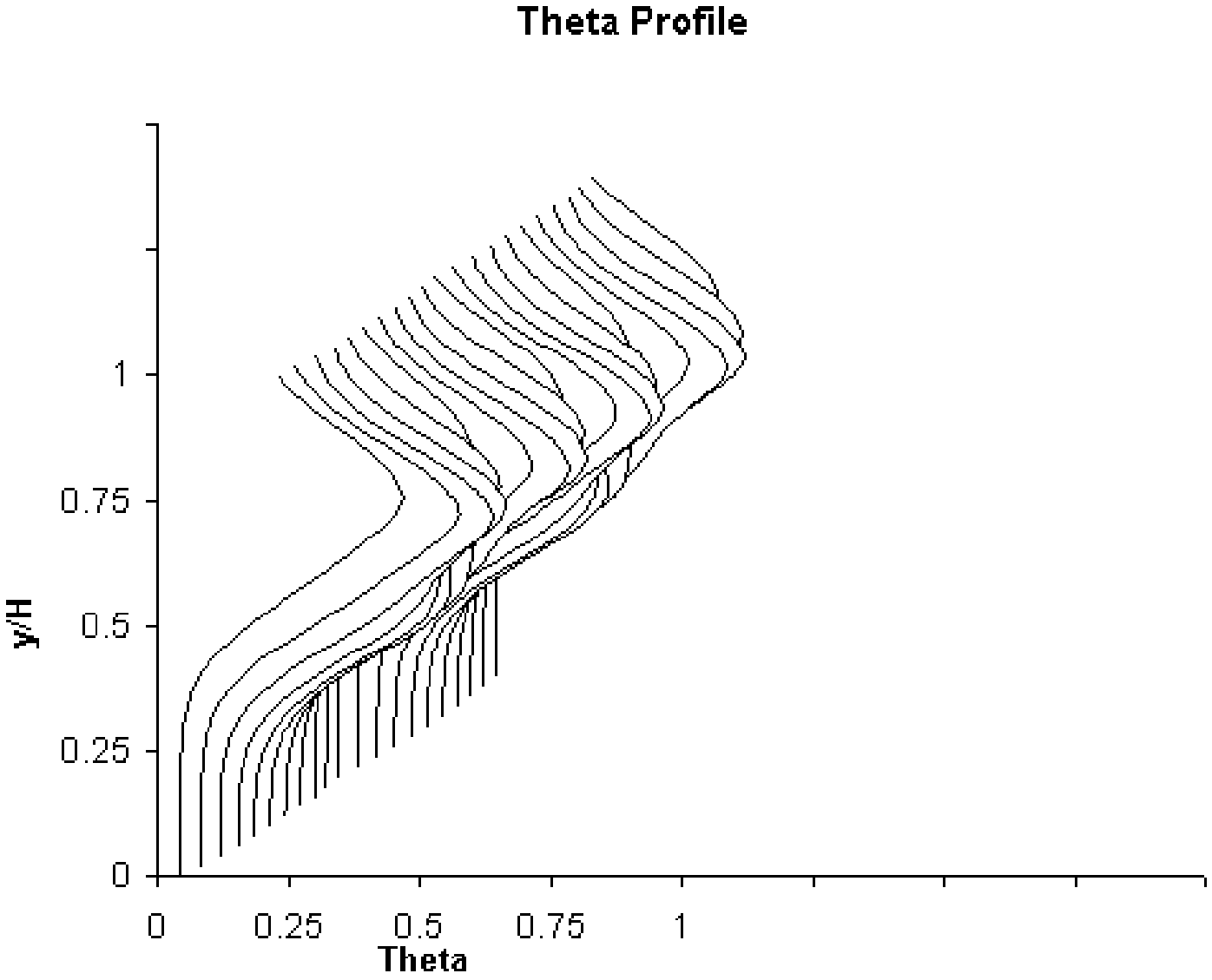


*x/H*=0 5

*$S_x$/H=9.25; DR=2.2, J=26.4, $C_d$=0.64*

*Row 1: S/H=0.5; H/d=5.66* *Row 2: S/H=0.25; H/d=8*

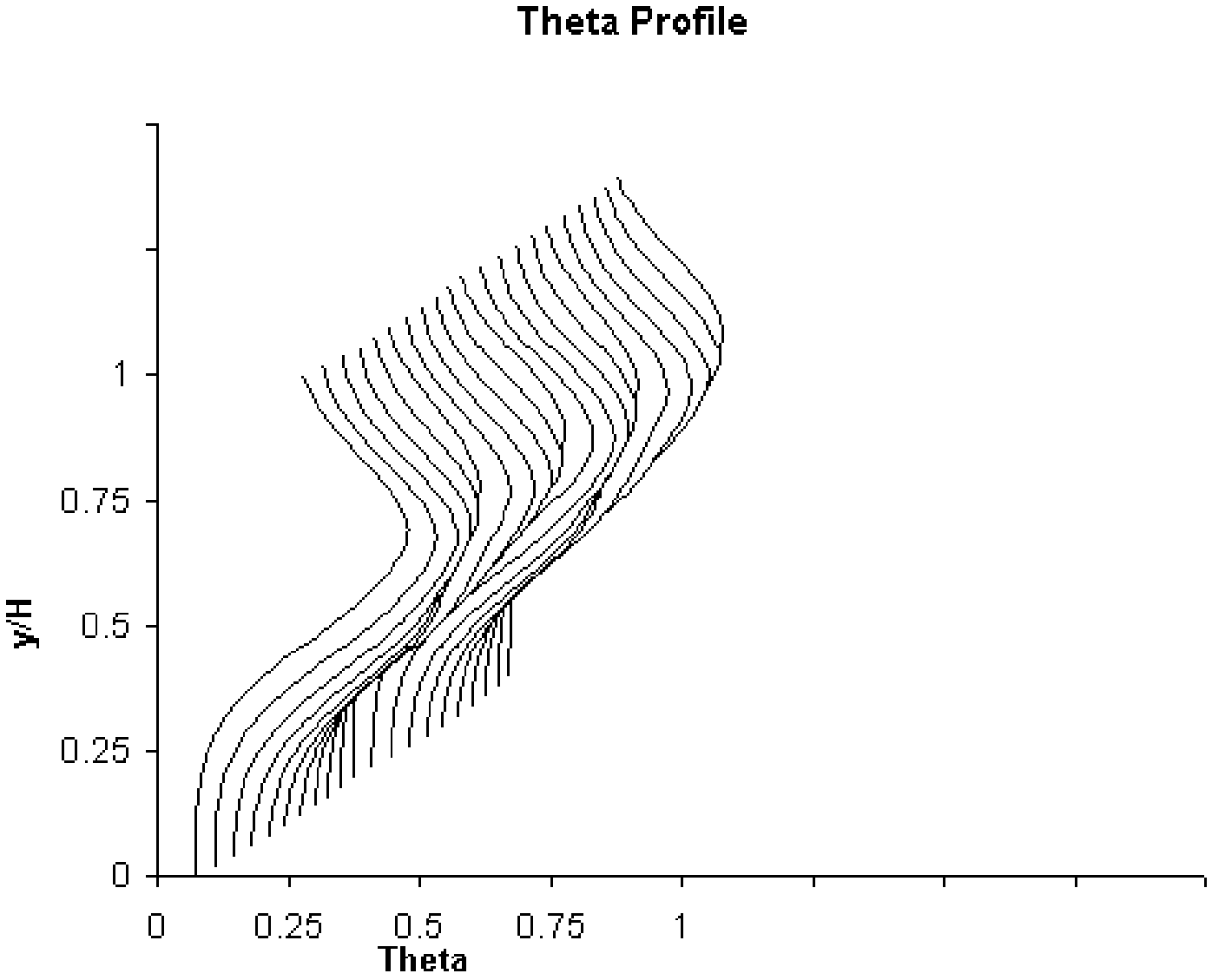


*x/H*=0 75

*$S_x$/H=0.25; DR=2.2, J=26.4, $C_d$=0.64*

*Row 1: S/H=0.5; H/d=5.66* *Row 2: S/H=0.25; H/d=8*

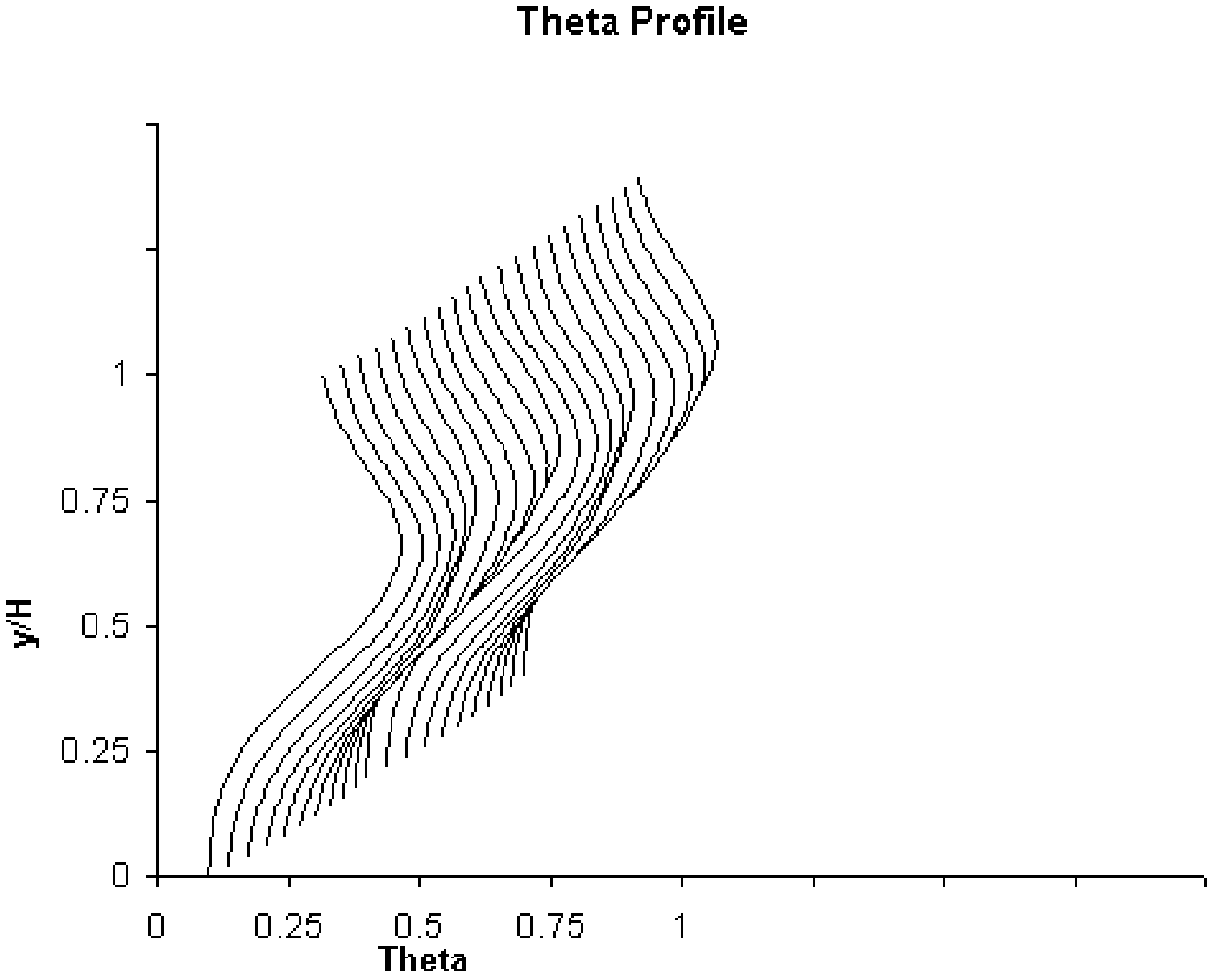


*x/H*=1

*$S_x$/H=0.25; DR=2.2, J=26.4, $C_d$=0.64*

*Row 1: S/H=0.5; H/d=5.66  Row 2: S/H=0.25; H/d=8*

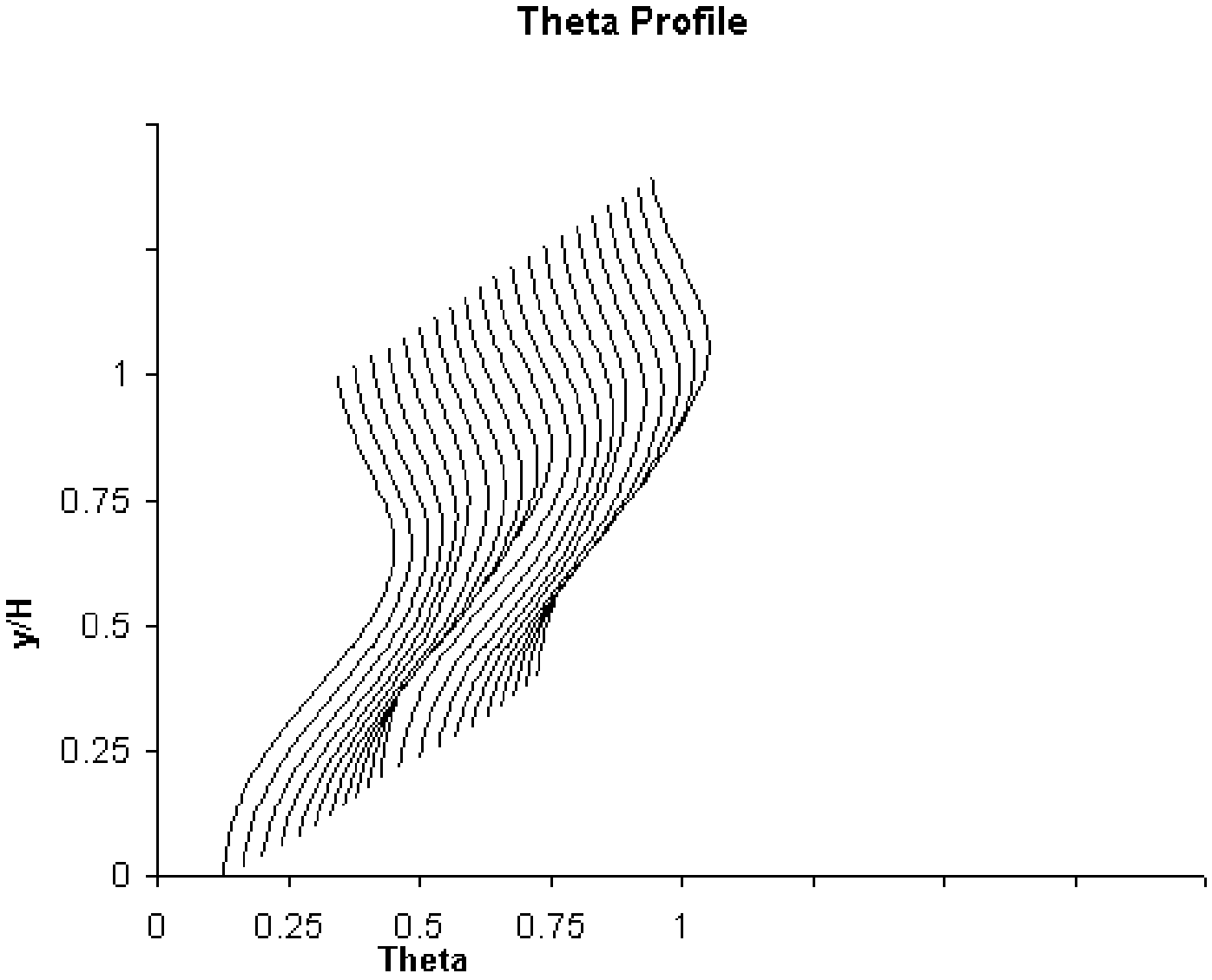


*x/H*=1.25

*$S_x$/H=0.25; DR=2.2, J=26.4, $C_d$=0.64*

*Row 1: S/H=0.5; H/d=5.66* *Row 2: S/H=0.25; H/d=8*

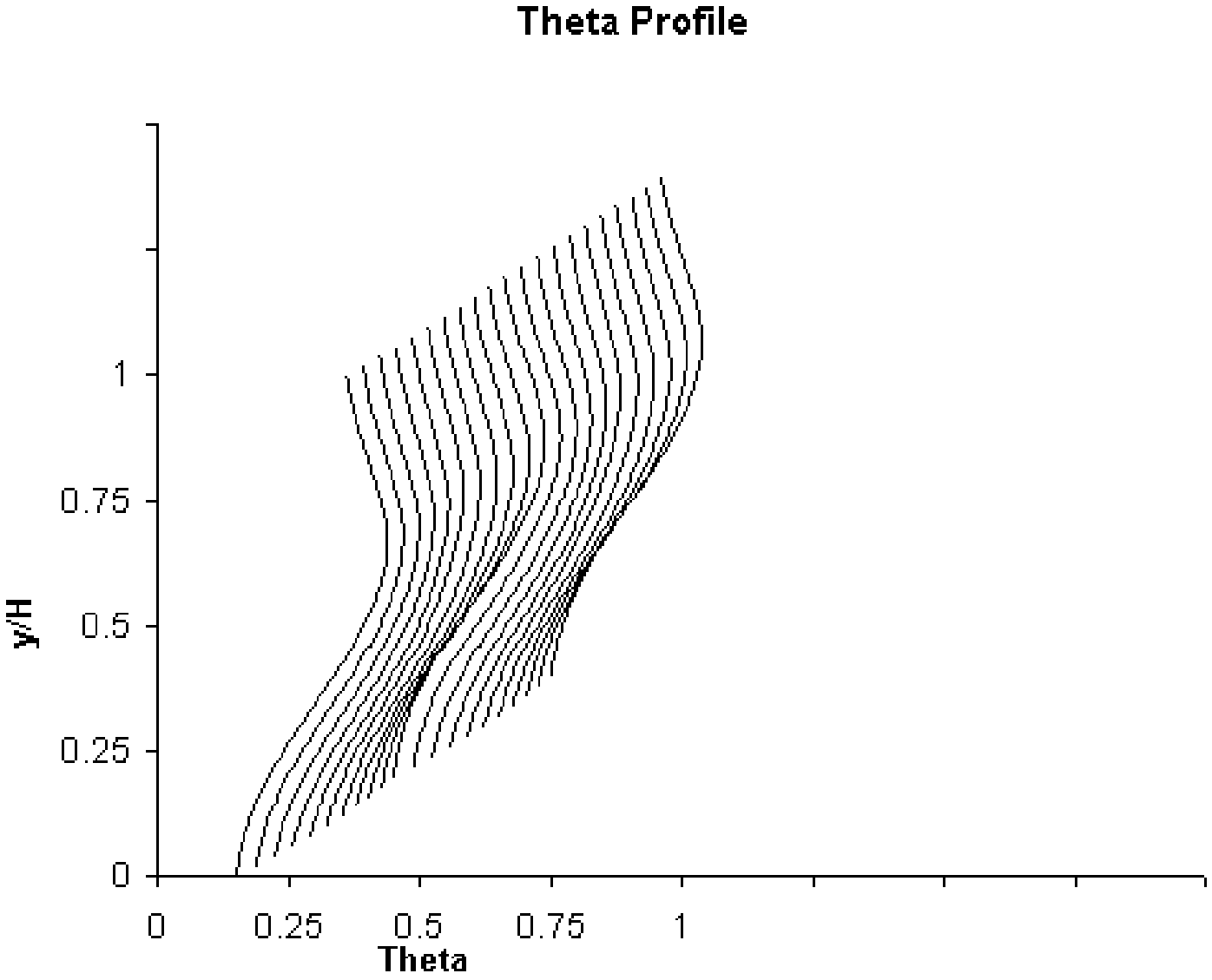


*x/H*=1.5

*$S_x$/H=.925; DR=2.2, J=26.4, $C_d$=0.64*

*Row 1: S/H=0.5; H/d=5.66  Row 2: S/H=0.25; H/d=8*

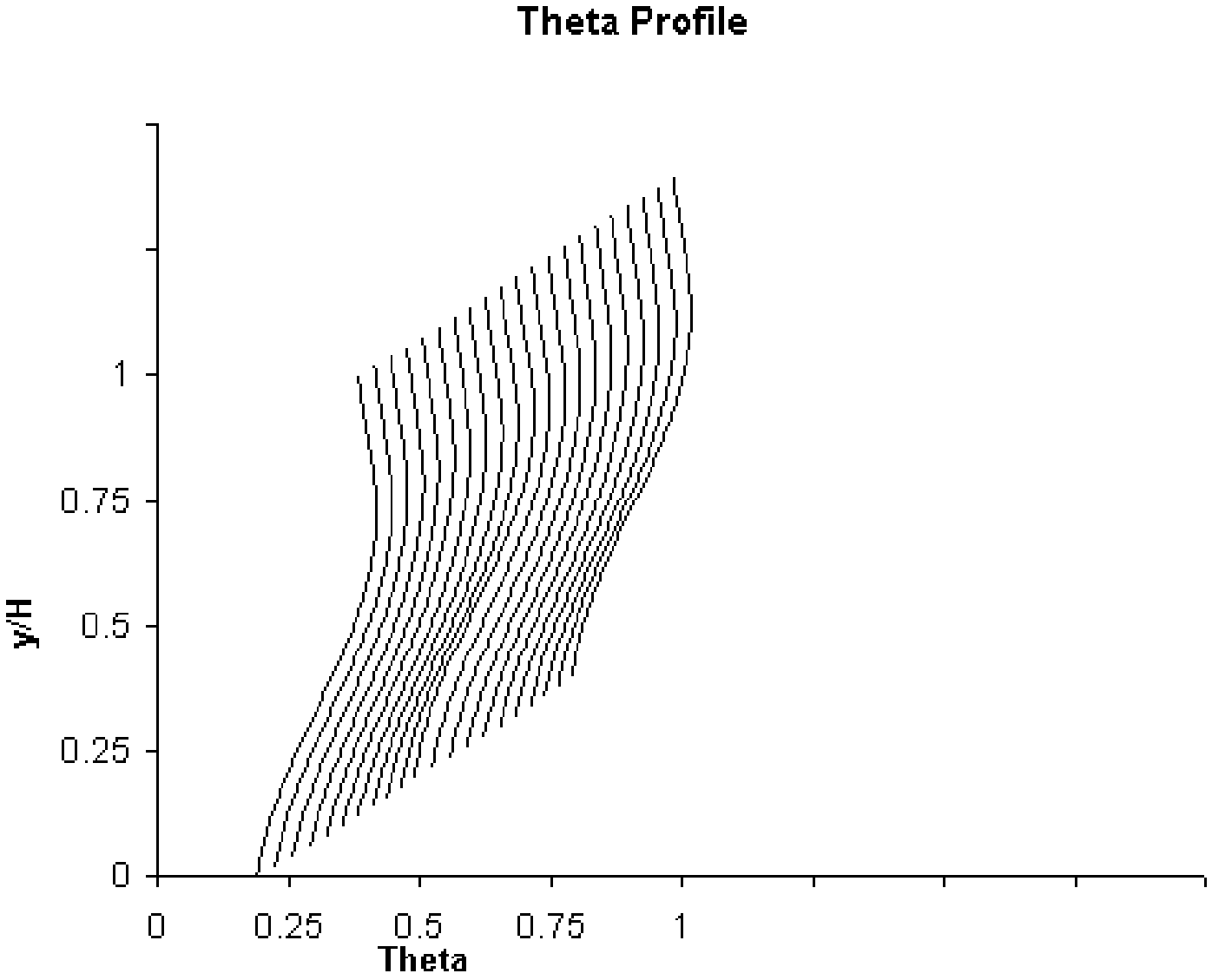


*x/H=2*

*$S_x$/H=0.25; DR=2.2, J=26.4, $C_d$=0.64*

*Row 1: S/H=0.5; H/d=5.66  Row 2: S/H=0.25; H/d=8*

## Summary



Profiles calculated with the Excel JIC spreadsheet, shown in sequences 1 to 21
Illustrate the effects on the mixing that result from varying flow and geometry.

Mixing improves with increasing downstream distance.
(Slides 3-10)

If the velocity ratio is fixed and the density ratio increases, the momentum-flux ratio increases and penetration increases. If the mass-flux ratio is fixed and the density ratio increases, the momentum-flux ratio decreases and the penetration decreases. The effect of density ratio is small if the momentum-flux ratio is constant
(Slides 11-16 – constant R) (Slides 17-22 – constant M) (Slides 23-28 – constant J)

Increasing momentum-flux ratio increases jet penetration and lateral uniformity.
(Slides 29-36)

Increasing orifice spacing increases penetration but decreases lateral uniformity.
(Slides 37-44)

Increasing orifice diameter at a constant spacing increases the magnitude of the scalar difference, but jet penetration and profile shape remain similar.
(Slides 45-50 – x/H=0..5) (Slides 51-56 – x/H=2)

**Summary** (continued)



Similar distributions may be obtained over a range of orifice spacing and momentum-flux ratios, if the orifice spacing is inversely proportional to the square root of the momentum-flux ratio.
(Slides 57-64 – x/H=0.25)  (Slides 65-72 – x/H=2)

The mixing of jets with a non-uniform scalar mainstream distribution can be approximated by superimposing independent calculations of the JIC and upstream profiles. Note that the mainstream profiles do not change with downstream distance.
(Slides 73-81)

Flow area convergence results in slightly increased jet penetration and cross-stream mixing, but the lateral profiles are less uniform than for the non-converging duct case.
(Slides 82-88)

Jets from bluff slots penetrate slightly less and are laterally more uniform, and streamlined slots penetrate slightly farther and are laterally less uniform, than equal-area round holes. The effects of orifice shape are most significant in the region close to the injection plane; farther downstream both slot geometries yield distributions similar to those from equally-spaced, equal-area circular holes.
(Slides 89-96)

**Summary** (continued)



Profiles for jets from 45-degree slanted slots rotate and shift laterally with increasing downstream distance. The rotation is not included in the empirical model; but the lateral is approximated by shifting round hole distributions. (Slide 97-105)

Profiles for opposed rows of jets with their centerlines in-line may be calculated with either a symmetry or superposition method. (Those shown here were calculated using the superposition model.) Three limiting cases of opposed jets are obvious; 1) configurations on opposite sides may be the same, 2) orifices may be of a different size on opposite sides, or 3) the momentum-flux ratios may be different. For the symmetric case, the ratio of orifice spacing to duct height should be **one-half** of the corresponding value for single side injection at the same momentum-flux ratio. (Slides 108-113 – Symmetric) (Slides 114-119 – different H/d's) (Slides 120-127 – different J's)

For opposed rows of jets with their orifice centerlines staggered, the ratio of orifice spacing to duct height should be **double** the corresponding value for single-side injection at the same momentum-flux ratio. This is like an optimum one-side injection case with every other orifice moved to the opposite wall. Note that in an Optimum configuration the jet from opposite sides must pass each other, thus the momentum-flux ratio and orifice spacing must be suitable. If either is too small, a staggered configuration will be similar to an in-line one. (Slides 126-133)

## **Summary** (concluded)



Double (axially-staged) rows of jets with their centerplanes in-line have profile distributions similar to those from a single row of equal-area orifices. at the same momentum-flux ratio and with the same orifice spacing.
(Slides 134-140)

Caution should be exercised when superimposing independent calculations for double rows of jets with their centerplanes staggered, as there may be significant interaction between jets in different rows.
(Slides 141-148)

Superimposing independent calculations of the two rows is used to approximate jets from double rows of orifices of different size and spacing.
(Slides 149-156)

## References


1. Holdeman, J.D., "Mixing of Multiple Jets With a Confined Subsonic Crossflow," *Progress in Energy and Combustion Science*, Vol. 19, pp. 31–70, August 1993 (see also "Mixing of Multiple Jets With a Confined Subsonic Crossflow—Summary of NASA-Supported Experiments and Modeling," AIAA Paper 91–2458 and NASA TM–104412, June 1991).
2. Holdeman, James D., Liscinsky, David S., Oechsle, Victor L., Samuelsen, G. Scott, and Smith, Clifford E., "Mixing of Multiple Jets With a Confined Subsonic Crossflow: Part I—Cylindrical Ducts," *Journal of Engineering for Gas Turbines and Power*, Vol. 119, October 1997 (also ASME Paper 96–GT–482 and NASA TM–107185, June 1996).
3. Holdeman, J.D., Liscinsky, D.S., and Bain, D.B., "Mixing of Multiple Jets With a Confined Crossflow: Part II—Opposed Rows of Orifices in Rectangular Ducts," *Journal of Engineering for Gas Turbines and Power*, Vol. 121, July 1999 (also ASME Paper 97–GT–439 and NASA TM–107461, June 1997).
4. Margason, R.J., "Fifty Years of Jet in Cross Flow Research, Presented at Computational and Experimental Assessment of Jets in Cross Flow," AGARD Conference Proceedings 534, April 1993.
5. Demuren, A.O., "Modeling Jets in Cross Flow," NASA CR–194965 (also ICASE Report No. 94–71). August 1994.
6. Norgren, C.T., and Humenik, F.M., "Dilution Jet Mixing Study for Gas Turbine Combustors," NASA TN D–4695, August 1968.
7. Walker, R.E. and Kors, D.L., "Multiple Jet Study Final Report," NASA CR–121217, June 1973.
8. Holdeman, J.D., Walker, R.E., and Kors, D.L., "Mixing of Multiple Dilution Jets With a Hot Primary Airstream for Gas Turbine Combustors," AIAA Paper 73–1249 (also NASA TM–71426), November 1973.
9. Walker, R.E., Kors, D.L., and Holdeman, J.D., "Mixing of Multiple Jets of Cooling Air With Simulated Combustion Gases," CPIA Publication 243, Proceedings of the 10th JANNAF Combustion Meeting, Vol. II, pp. 377–396, December 1973.
10. Kamotani, Y. and Greber, I. "Experiments on Confined Turbulent Jets in Cross Flow," NASA CR–2392, March 1974.
11. Walker, R.E. and Eberhardt, R.G., "Multiple Jet Study Data Correlations," NASA CR–134795, April 1975.
12. Cox, G.B., Jr., "Multiple Jet Correlations for Gas Turbine Engine Combustor Design," *J. of Engineering for Gas Turbines and Power* (also ASME Paper 75–GT–45), April 1975.
13. Cox, G.B., Jr., "An Analytical Model for Predicting Exit Temperature Profile from Gas Turbine Engine Annular Combustors," AIAA Paper 75–1307. October 1975.
14. Holdeman, J.D., and Walker, R.E., "Mixing of a Row of Jets With a Confined Crossflow," *AIAA Journal*, Vol. 15, No. 2, pp. 243–249, February 1977 (see also "An Empirical Model for the Mixing of a Row of Dilution Jets with a Confined Crossflow," AIAA Paper 76–48 and NASA TM–71821).
15. Srinivasan, R., Berenfeld, A., and Mongia, H.C., "Dilution Jet Mixing Program Phase I Report," NASA CR–168031 (Garrett 21–4302), 1982.
16. Holdeman, J.D., "Perspectives on the Mixing of a Row of Jets With a Confined Crossflow," AIAA Paper 83–1200 (also NASA TM–83457), June 1983.

17. Holdeman, J.D., Srinivasan, R., and Berenfeld, A., "Experiments in Dilution Jet Mixing," *AIAA Journal,* Vol. 22, No. 10, pp. 1436–1443, October 1984 (also, AIAA Paper 83–1201 and NASA TM–83434, June 1983).
18. Srinivasan, R., Coleman, E., and Johnson, K., "Dilution Jet Mixing Program—Phase II Report," NASA CR–174624 (Garret 21–4804), 1984.
19. Srinivasan, R., Meyers, G., Coleman, E., and White, C., "Dilution Jet Mixing Program—Phase III Report," NASA CR–174884 (Garrett 21–5418), 1985.
20. Srinivasan, R. and White, C.D., "Dilution Jet Mixing Program Supplementary Report," NASA CR–175043 (Garrett 21–5705), 1986.
21. Holdeman, J.D., and Srinivasan, R., "Perspectives on Dilution Jet Mixing," AIAA Paper 86–1611 (also NASA TM–87294), June 1986.
22. Srinivasan. R., Reynolds, R., Ball, I., Berry, R., Johnson, K., and Mongia, H., "Aerothermal Modeling Program: Phase I Final Report, Volume II, NASA CR–168243 (Garrett 21–4742–2), August 1983.
23. Holdeman, J.D. and Srinivasan, R., "Modeling Dilution Jet Flowfields," *Journal of Propulsion and Power*, Vol. 2, No. 1, January–February 1986, pp. 4–9 (see also "On Modeling Dilution Jet Flowfields," AIAA Paper 84–1379 and NASA TM–83708, June 1984).
24. Holdeman, J.D., Srinivasan, R., Meyers, G.D., and White, C.D., "Effects of Multiple Rows and Non-circular Orifices on Dilution Jet Mixing," *Journal of Propulsion and Power*, Vol. 3, No. 3, May–June 1987, pp. 219–226 (see also "Experiments in Dilution Jet Mixing—Effects of Multiple Rows and Non-circular Orifices," AIAA Paper 85–1104 and NASA TM–86996, July 1985).
25. Holdeman, J.D., Srinivasan, R., Reynolds, R.S., and White, C.D., "Studies of the Effects of Curvature on Dilution Jet Mixing." *Journal of Propulsion and Power*, Vol. 8, No. 1, January–February 1992, pp. 209–218.
26. Reynolds, R. and White, C., "Transition Mixing Study: Final Report," NASA CR–175062 (Garrett 21–5723), October 1986.
27. Holdeman, J.D., Reynolds, R., and White, C., "A Numerical Study of the Effects of Curvature and Convergence on Dilution Jet Mixing," AIAA Paper 87–1953 (also NASA TM– 89878), June 1987.
28. Srinivasan, R. and White, C., "Transition Mixing Study: Empirical Model Report," NASA CR–182139 (Garrett 21–6689), February 1988.
29. Holdeman, J.D., Srinivasan, R., and White, C.D., "An Empirical Model of the Effects of Curvature and Convergence on Dilution Jet Mixing," AIAA Paper 88–3180 (also NASA TM–100896), July 1988.
30. Holdeman, J.D., Smith, T.D., Clisset, J.R., and Lear, W.E., "A Spreadsheet for the Mixing of a Row of Jets with a Confined Crossflow," NASA/TM—2005-213137, February 2005.
31. Anon., Tecplot User's Manual, Version 10, Amtec Engineering, Inc., Bellvue, Washington, December 2003.
32. Kamotani, Y. and Greber, I., "Experiments on a Turbulent Jet in a Cross Flow," NASA CR–72893 (also FTAS/TR–71–83, Case Western Reserve University), June 1971.
33. Kamotani, Y. and Greber, I., "Experiments on a Turbulent Jet in a Cross Flow," AIAA J. Vol. 10, No. 11, November 1972, pp. 1425–1429 (also AIAA Paper 72–149, January 1972).
34. Holdeman, J.D., "Correlation for Temperature Profiles in the Plane of Symmetry Downstream of a Jet Injected Normal to a Crossflow," NASA TN D–6966, September 1972.

35. Wittig, S.L.K., Elbahar, O.M.F., and Noll, B.E., "Temperature Profile Development in Turbulent Mixing of Coolant Jets with a Confined Hot Cross-Flow," *Journal of Engineering for Gas Turbines and Power*, Vol. 106, January 1984, pp. 193–197 (see also ASME Paper No. 83–GT–39).
36. Liscinsky, D.S., True, B., and Holdeman, J.D., "Effect of Inlet Flow Conditions on Crossflow Jet Mixing," AIAA Paper 96–2881 (also NASA TM–107258), July 1996.
37. Liscinsky. D.S., True, B., and Holdeman, J.D., "Mixing Characteristics of Directly Opposed Rows of Jets Injected Normal to a Crossflow in a Rectangular Duct," AIAA Paper 94–0217 (also NASA TM–106477), January 1994.
38. Lefebvre, Arthur H., *Gas Turbine Combustion, Second Edition,* Taylor and Francis, 1999.

TABLE 1.—RANGE OF FLOW AND GEOMETRIC VARIABLES
ON WHICH THE EMPIRICAL MODEL IS BASED

| Independent Variables | |
|---|---|
| Density ratio, $DR$ | 0.5 to 2.2 |
| Momentum-flux ratio, $J$ | 5 to 105.6 |
| Discharge coefficient, $Cd$ | 0.6 to 1 |
| Downstream distance, $x/H$[a] | 0 to 2 |
| Orifice spacing to duct height ratio, $S/H$[b] | 0 to 1 |
| Orifice size, $H/d$ | 4 to 16 |
| **Dependent Variables** | |
| Downstream distance, $x/d$[a] | 2 to 32 |
| Spacing to orifice diameter ratio, $S/d$[b] | 2 to 6 |
| **Area ratio, $A_J/A_M$** | **0.025 to 0.1** |
| **Jet-to-total mass-flow ratio, $m_J/m_T$** | **0.075 to 0.36** |
| **Jet-to-mainstream mass-flow ratio, $MR$** | **0.08 to 0.6** |
| **Jet-to-mainstream mass-flux ratio, $M$** | **3 to 14** |
| **Jet-to-mainstream velocity ratio, $R$** | **3 to 14** |
| **Equilibrium $\theta$. $\theta_{EB}$** | **0 to 1** |
| **Pattern factor, PF = $(MR)(1 - \theta_{min}/\theta_{EB})$** | **0 to 0.6** |
| **$C = (S/H)(\sqrt{(J)})$** | **0.5 to 10** |

[a]Note that the downstream distance should not be less than the orifice radius.
[b]Note that S/d should not be <1.

TABLE 2.—CONDITIONS FOR CALCULATIONS IN THIS REPORT

| Figure no. | *x*/*H* | *DR* | *J* | *M* (√(*J***DR*)) | *R* (√(*J*/*DR*)) | Configuration (see fig. 3) | *S*/*H* | *H*/*d* | *S*/*d* | *x*/*d* | *MR* | *C* (*S*/*H*)(√(*J*)) |
|---|---|---|---|---|---|---|---|---|---|---|---|---|
| | | | | | | | | | | | | |
| 4(a) | 0.25 | 2.2 | 26.4 | 7.62 | 3.46 | F | 0.5 | 5.66 | 2.83 | 1.42 | 0.239 | 2.57 |
| 4(b) | .5 | 2.2 | 26.4 | 7.62 | 3.46 | F | .5 | 5.66 | 2.83 | 2.83 | .239 | 2.57 |
| 4(c) | 1 | 2.2 | 26.4 | 7.62 | 3.46 | F | .5 | 5.66 | 2.83 | 5.66 | .239 | 2.57 |
| 4(d) | 2 | 2.2 | 26.4 | 7.62 | 3.46 | F | .5 | 5.66 | 2.83 | 11.32 | .239 | 2.57 |
| | | | | | | | | | | | | |
| 5(a) | 0.25 | 2.2 | 26.4 | 7.62 | 3.46 | F | 0.5 | 5.66 | 2.83 | 1.42 | 0.239 | 2.57 |
| 5(b) | .5 | 2.2 | 26.4 | 7.62 | 3.46 | F | .5 | 5.66 | 2.83 | 2.83 | .239 | 2.57 |
| 5(c) | 1 | 2.2 | 26.4 | 7.62 | 3.46 | F | .5 | 5.66 | 2.83 | 5.66 | .239 | 2.57 |
| 5(d) | 2 | 2.2 | 26.4 | 7.62 | 3.46 | F | .5 | 5.66 | 2.83 | 11.32 | .239 | 2.57 |
| | | | | | | | | | | | | |
| 6(a) | 0.25 | 2.2 | 26.4 | 7.62 | 3.46 | F | 0.5 | 5.66 | 2.83 | 1.42 | 0.239 | 2.57 |
| 6(b) | .5 | 2.2 | 26.4 | 7.62 | 3.46 | F | .5 | 5.66 | 2.83 | 2.83 | .239 | 2.57 |
| 6(c) | 1 | 2.2 | 26.4 | 7.62 | 3.46 | F | .5 | 5.66 | 2.83 | 5.66 | .239 | 2.57 |
| 6(d) | 2 | 2.2 | 26.4 | 7.62 | 3.46 | F | .5 | 5.66 | 2.83 | 11.32 | .239 | 2.57 |
| | | | | | | | | | | | | |
| 7(a) | 0.25 | 2.2 | 26.4 | 7.62 | 3.46 | F | 0.5 | 5.66 | 2.83 | 1.42 | 0.239 | 2.57 |
| 7(b) | .5 | 2.2 | 26.4 | 7.62 | 3.46 | F | .5 | 5.66 | 2.83 | 2.83 | .239 | 2.57 |
| 7(c) | 1 | 2.2 | 26.4 | 7.62 | 3.46 | F | .5 | 5.66 | 2.83 | 5.66 | .239 | 2.57 |
| 7(d) | 2 | 2.2 | 26.4 | 7.62 | 3.46 | F | .5 | 5.66 | 2.83 | 11.32 | .239 | 2.57 |
| | | | | | | | | | | | | |
| 8a(a) | 0.25 | 2.2 | 26.4 | 7.62 | 3.46 | C | 0.25 | 8 | 2 | 2 | 0.239 | 1.28 |
| 8a(b) | .5 | 2.2 | 26.4 | 7.62 | 3.46 | C | .25 | 8 | 2 | 4 | .239 | 1.28 |
| 8a(c) | 1 | 2.2 | 26.4 | 7.62 | 3.46 | C | .25 | 8 | 2 | 8 | .239 | 1.28 |
| 8a(d) | 2 | 2.2 | 26.4 | 7.62 | 3.46 | C | .25 | 8 | 2 | 16 | .239 | 1.28 |
| | | | | | | | | | | | | |
| 8b(a) | 0.25 | 2.2 | 26.4 | 7.62 | 3.46 | I | 1 | 4 | 4 | 1 | 0.239 | 5.14 |
| 9b(b) | .5 | 2.2 | 26.4 | 7.62 | 3.46 | I | 1 | 4 | 4 | 2 | .239 | 5.14 |
| 8b(c) | 1 | 2.2 | 26.4 | 7.62 | 3.46 | I | 1 | 4 | 4 | 4 | .239 | 5.14 |
| 8b(d) | 2 | 2.2 | 26.4 | 7.62 | 3.46 | I | 1 | 4 | 4 | 8 | .239 | 5.14 |
| | | | | | | | | | | | | |
| 9(a) | 0.5 | 2.2 | 6.6 | 3.81 | 1.73 | F | 0.5 | 5.66 | 2.83 | 2.83 | 0.1195 | 1.28 |
| 9(b) | .5 | 2.2 | 26.4 | 7.62 | 3.46 | F | .5 | 5.66 | 2.83 | 2.83 | .239 | 2.57 |
| 9(c) | .5 | 2.2 | 105.6 | 15.24 | 6.93 | F | .5 | 5.66 | 2.83 | 2.83 | .478 | 5.14 |
| | | | | | | | | | | | | |
| 10(a) | 0.5 | .5 | 26.4 | 3.83 | 7.27 | F | 0.5 | 5.66 | 2.83 | 2.83 | 0.114 | 2.57 |
| 10(b) | .5 | 1 | 26.4 | 5.14 | 5.14 | F | .5 | 5.66 | 2.83 | 2.83 | .161 | 2.57 |
| 10(c) | .5 | 2 | 26.4 | 7.27 | 3.83 | F | .5 | 5.66 | 2.83 | 2.83 | -.228 | 2.57 |
| | | | | | | | | | | | | |
| 11(a) | 0.5 | 2.2 | 26.4 | 7.62 | 3.46 | E | 1 | 8 | 8 | 4 | 0.06 | 5.14 |
| 11(b) | .5 | 2.2 | 26.4 | 7.62 | 3.46 | D | .5 | 8 | 4 | 4 | .12 | 2.57 |
| 11(c) | .5 | 2.2 | 26.4 | 7.62 | 3.46 | C | .25 | 8 | 2 | 4 | 9.24 | 1.28 |
| | | | | | | | | | | | | |
| 12(a) | 0.5 | 2.2 | 26.4 | 7.62 | 3.46 | A | 0.125 | 16 | 2 | 8 | 0.1195 | 0.64 |
| 12(b) | .5 | 2.2 | 26.4 | 7.62 | 3.46 | C | .25 | 8 | 2 | 4 | .238 | 1.28 |
| 12(c) | .5 | 2.2 | 26.4 | 7.62 | 3.46 | H | .5 | 4 | 2 | 2 | 0.478 | 2.57 |
| | | | | | | | | | | | | |
| 13a(a) | 0.5 | 2.2 | 26.4 | 7.62 | 3.46 | D | .5 | 8 | 4 | 4 | 0.1195 | 2.57 |
| 13a(b) | .5 | 2.2 | 26.4 | 7.62 | 3.46 | F | (~).5 | 6 | 3 | 3 | .213 | 2.57 |
| 13a(c) | .5 | 2.2 | 26.4 | 7.62 | 3.46 | G | .5 | 5 | 2.5 | 2.5 | .307 | 2.57 |
| 13a(d) | .5 | 2.2 | 26.4 | 7.62 | 3.46 | H | .5 | 4 | 2 | 2 | .478 | 2.57 |

TABLE 2.—CONTINUED.

| Figure no. | *x*/*H* | *DR* | *J* | *M* (√(*J***DR*)) | *R* (√(*J*/*DR*)) | Configuration (see fig. 3) | *S*/*H* | *H*/*d* | *S*/*d* | *x*/*d* | *MR* | *C* (*S*/*H*)(√(*J*)) |
|---|---|---|---|---|---|---|---|---|---|---|---|---|
| | | | | | | | | | | | | |
| 13b(a) | 2 | 2.2 | 26.4 | 7.62 | 3.46 | D | 0.5 | 8 | 4 | 16 | 0.1195 | 2.57 |
| 13b(b) | 2 | 2.2 | 26.4 | 7.62 | 3.46 | F | (~).5 | 6 | 3 | !2 | .324 | 2.57 |
| 13b(c) | 2 | 2.2 | 26.4 | 7.62 | 3.46 | G | .5 | 5 | 2.5 | 10 | .307 | 2.57 |
| 13b(d) | 2 | 2.2 | 28.4 | 7.62 | 3.46 | H | .5 | 4 | 2 | 8 | .478 | 2.57 |
| | | | | | | | | | | | | |
| 14a(a) | 0.5 | 2.2 | 6.6 | 3.81 | 1.73 | J | 1 | 2.83 | 2.83 | 1.42 | 0.239 | 2.57 |
| 14a(b) | .5 | 2.2 | 26.4 | 7.62 | 3.46 | F | .5 | 5.66 | 2.83 | 2.83 | .239 | 2.57 |
| 14a(c) | .5 | 2.2 | 105.6 | 15.24 | 6.93 | B | .25 | 11.32 | 2.83 | 5.66 | .239 | 2.57 |
| | | | | | | | | | | | | |
| 14b(a) | 2 | 2.2 | 6.6 | 3.81 | 1.73 | J | 1 | 2.83 | 2.83 | 5.66 | 0.239 | 2.57 |
| 14b(b) | 2 | 2.2 | 26.4 | 7.62 | 3.46 | F | .5 | 5.66 | 2.83 | 11.32 | .239 | 2.57 |
| 14b(c) | 2 | 2.2 | 105.6 | 15.24 | 6.93 | B | .25 | 11.32 | 2.83 | 22.64 | .239 | 2.57 |
| | | | | | | | | | | | | |
| 15a(a) | 0.25 | 2.2 | 6.6 | 3.81 | 1.73 | D | 0.5 | 8 | 4 | 2 | 0.06 | 1.28 |
| | .25 | 2.2 | 6.6 | 3.81 | 1.73 | D | .5 | 8 | 4 | 2 | .06 | 1.28 |
| 15a(b) | .5 | 2.2 | 6.6 | 3.81 | 1.73 | D | .5 | 8 | 4 | 4 | .06 | 1.28 |
| | .5 | 2.2 | 6.6 | 3.81 | 1.73 | D | .5 | 8 | 4 | 4 | .06 | 1.28 |
| 15a(c) | 1 | 2.2 | 6.6 | 3.81 | 1.73 | D | .5 | 8 | 4 | 8 | .06 | 1.28 |
| | 1 | 2.2 | 6.6 | 3.81 | 1.73 | D | .5 | 8 | 4 | 8 | .06 | 1.28 |
| | | | | | | | | | | | | |
| 15b(a) | 0.25 | 2.2 | 6.6 | 3.81 | 1.73 | F | 0.5 | 5.66 | 2.83 | 1.42 | 0.1195 | 1.28 |
| | .25 | 2.2 | 6.6 | 3.81 | 1.73 | F | .5 | 5.66 | 2.83 | 1.42 | .1195 | 1.28 |
| 15b(b) | .5 | 2.2 | 6.6 | 3.81 | 1.73 | F | .5 | 5.66 | 2.83 | 2.83 | .1195 | 1.28 |
| | .5 | 2.2 | 6.6 | 3.81 | 1.73 | F | .5 | 5.66 | 2.83 | 2.83 | .1195 | 1.28 |
| 15b(c) | 1 | 2.2 | 6.6 | 3.81 | 1.73 | F | .5 | 5.66 | 2.83 | 5.66 | .1195 | 1.28 |
| | 1 | 2.2 | 6.6 | 3.81 | 1.73 | F | .5 | 5.66 | 2.83 | 5.66 | .1195 | 1.28 |
| | | | | | | | | | | | | |
| 15c(a) | 0.25 | 2.2 | 6.6 | 3.81 | 1.73 | H | 0.5 | 4 | 2 | 1 | 0.239 | 1.28 |
| | .25 | 2.2 | 6.6 | 3.81 | 1.73 | H | .5 | 4 | 2 | 1 | .239 | 1.28 |
| 15c(b) | .5 | 2.2 | 6.6 | 3.81 | 1.73 | H | .5 | 4 | 2 | 2 | .239 | 1.28 |
| | .5 | 2.2 | 6.6 | 3.81 | 1.73 | H | .5 | 4 | 2 | 2 | .239 | 1.28 |
| 15c(c) | 1 | 2.2 | 6.6 | 3.81 | 1.73 | H | .5 | 4 | 2 | 4 | .239 | 1.28 |
| | 1 | 2.2 | 6.6 | 3.81 | 1.73 | H | .5 | 4 | 2 | 4 | .239 | 1.28 |
| | | | | | | | | | | | | |
| 16a(a) | 0.25 | 2.2 | 26.4 | 7.63 | 3.46 | B | 0.25 | 11.32 | 2.83 | 2.83 | 0.1195 | 1.28 |
| | .25 | 2.2 | 26.4 | 7.63 | 3.46 | B | .25 | 11.32 | 2.83 | 2.83 | .1195 | 1.28 |
| 16a(b) | .5 | 2.2 | 26.4 | 7.63 | 3.46 | B | .25 | 11.32 | 2.83 | 5.66 | .1195 | 1.28 |
| | .5 | 2.2 | 26.4 | 7.63 | 3.46 | B | .25 | 11.32 | 2.83 | 5.66 | .1195 | 1.28 |
| 16a(c) | 1 | 2.2 | 26.4 | 7.63 | 3.46 | B | .25 | 11.32 | 2.83 | 11.32 | .1195 | 1.28 |
| | 1 | 2.2 | 26.4 | 7.63 | 3.46 | B | .25 | 11.32 | 2.83 | 11.32 | .1195 | 1.28 |
| | | | | | | | | | | | | |
| 16b(a) | 0.25 | 2.2 | 26.4 | 7.63 | 3.46 | C | 0.25 | 8 | 2 | 2 | 0.239 | 1.28 |
| | .25 | 2.2 | 26.4 | 7.63 | 3.46 | C | .25 | 8 | 2 | 2 | .239 | 1.28 |
| 16b(b) | .5 | 2.2 | 26.4 | 7.63 | 3.46 | C | .25 | 8 | 2 | 4 | .239 | 1.28 |
| | .5 | 2.2 | 26.4 | 7.63 | 3.46 | C | .25 | 8 | 2 | 4 | .239 | 1.28 |
| 16b(c) | 1 | 2.2 | 26.4 | 7.63 | 3.46 | C | .25 | 8 | 2 | 8 | .239 | 1.28 |
| | | 2.2 | 26.4 | 7.63 | 3.46 | C | .25 | 8 | 2 | 8 | .239 | 1.28 |
| | | | | | | | | | | | | |
| 17(a) | 0.25 | 2.2 | 105.6 | 15.24 | 6.93 | A | 0.125 | 16 | 2 | 4 | 0.239 | 1.28 |
| | .25 | 2.2 | 105.6 | 15.24 | 6.93 | A | .125 | 16 | 2 | 4 | .239 | 1.28 |
| 17(b) | .5 | 2.2 | 105.6 | 15.24 | 6.93 | A | .125 | 16 | 2 | 8 | .239 | 1.28 |
| | .5 | 2.2 | 105.6 | 15.24 | 6.93 | A | .125 | 16 | 2 | 8 | .239 | 1.28 |
| 17(c) | 1 | 2.2 | 105.6 | 15.24 | 6.93 | A | .125 | 16 | 2 | 16 | .239 | 1.28 |
| | 1 | 2.2 | 105.6 | 15.24 | 6.93 | A | .125 | 16 | 2 | 16 | .239 | 1.28 |

TABLE 2.—CONTINUED.

| Figure no. | *x*/*H* | *DR* | *J* | *M* (√(*J***DR*)) | *R* (√(*J*/*DR*)) | Configuration (see fig. 3) | *S*/*H* | *H*/*d* | *S*/*d* | *x*/*d* | *MR* | *C* (*S*/*H*)(√(*J*)) |
|---|---|---|---|---|---|---|---|---|---|---|---|---|
| | | | | | | | | | | | | |
| 18a(a) | 0.25 | 2.2 | 6.6 | 3.81 | 1.73 | B | 0.25 | 11.32 | 2.83 | 2.83 | 0.0598 | 0.64 |
| | .25 | 2.2 | 6.6 | 3.81 | 1.73 | B | .25 | 11.32 | 2.83 | 2.83 | .0598 | .64 |
| 18a(b) | .5 | 2.2 | 6.6 | 3.81 | 1.73 | B | .25 | 11.32 | 2.83 | 5.66 | .0598 | .64 |
| | .5 | 2.2 | 6.6 | 3.81 | 1.73 | B | .25 | 11.32 | 2.83 | 5.66 | .0598 | .64 |
| 18a(c) | 1 | 2.2 | 6.6 | 3.81 | 1.73 | B | .25 | 11.32 | 2.83 | 11.43 | .0598 | .64 |
| | 1 | 2.2 | 6.6 | 3.81 | 1.73 | B | .25 | 11.32 | 2.83 | 11.32 | .0598 | .64 |
| | | | | | | | | | | | | |
| 18b(a) | 0.25 | 2.2 | 6.6 | 3.81 | 1.73 | C | 0.25 | 8 | 2 | 2 | 0.1195 | 0.64 |
| | .25 | 2.2 | 6.6 | 3.81 | 1.73 | C | .25 | 8 | 2 | 2 | .1195 | .64 |
| 18b(b) | .5 | 2.2 | 6.6 | 3.81 | 1.73 | C | .25 | 8 | 2 | 4 | .1195 | .64 |
| | .5 | 2.2 | 6.6 | 3.81 | 1.73 | C | .25 | 8 | 2 | 4 | .1195 | .64 |
| 18b(c) | 1 | 2.2 | 6.6 | 3.81 | 1.73 | C | .25 | 8 | 2 | 8 | .1195 | .65 |
| | 1 | 2.2 | 6.6 | 3.81 | 1.73 | C | .25 | 8 | 2 | 8 | .1195 | .64 |
| | | | | | | | | | | | | |
| 19(a) | 0.25 | 2.2 | 26.4 | 7.63 | 3.46 | A | 0.125 | 16 | 2 | 4 | 0.1195 | 0.64 |
| | .25 | 2.2 | 26.4 | 7.63 | 3.46 | A | .125 | 16 | 2 | 4 | .1195 | .64 |
| 19(b) | .5 | 2.2 | 26.4 | 7.63 | 3.46 | A | .125 | 16 | 2 | 8 | .1195 | .64 |
| | .5 | 2.2 | 26.4 | 7.63 | 3.46 | A | .125 | 16 | 2 | 8 | .1195 | .64 |
| 19(c) | 1 | 2.2 | 26.4 | 7.63 | 3.46 | A | .125 | 16 | 2 | 16 | .1195 | .64 |
| | 1 | 2.2 | 26.4 | 7.63 | 3.46 | A | .125 | 16 | 2 | 16 | .1195 | .64 |
| | | | | | | | | | | | | |
| 20a(a) | 0.5 | 2.2 | 6.6 | 3.81 | 1.73 | D | 0.5 | 8 | 4 | 4 | 0.06 | 1.28 |
| | | 2.2 | 6.6 | 3.81 | 1.73 | D | .5 | 8 | 4 | 4 | .06 | 1.28 |
| 20a(b) | .5 | 2.2 | 6.6 | 3.81 | 1.73 | -- | .5 | 11.32 | 5.66 | 5.66 | .03 | 1.28 |
| | | 2.2 | 6.6 | 3.81 | 1.73 | -- | .5 | 6.54 | 3.17 | 3.17 | .0895 | 1.28 |
| 20a(c) | .5 | 2.2 | 6.6 | 3.81 | 1.73 | F | .5 | 5.66 | 2.83 | 2.83 | .1195 | 1.28 |
| | | | | | | | | | | | | |
| 20b(a) | 0.52 | 2,2 | 6.6 | 3.81 | 1.73 | F | 0.5 | 5.66 | 2.83 | 2.83 | 0.1195 | 1.28 |
| | | 2,2 | 6.6 | 3.81 | 1.73 | F | .5 | 5.66 | 2.83 | 2.83 | .1195 | 1.28 |
| 20b(b) | .52 | 2.2 | 6.6 | 3.81 | 1.73 | D | .5 | 8 | 4 | 4 | .06 | 1.28 |
| | | 2.2 | 6.6 | 3.81 | 1.73 | -- | .5 | 4.62 | 2.31 | 2.31 | .179 | 1.28 |
| 20b(c) | 9.52 | 2.2 | 6.6 | 3.81 | 1.73 | H | .5 | 4 | 2 | 8 | .239 | 1.28 |
| | | | | | | | | | | | | |
| 21(a) | 0.5 | 2.2 | 26.4 | 7.63 | 3.46 | B | 0.25 | 11.32 | 2.83 | 5.66 | 0.1195 | 1.28 |
| | | 2.2 | 26.4 | 7.63 | 3.46 | B | .25 | 11.32 | 2.83 | 5.66 | .1195 | 1.28 |
| 21(b) | .5 | 2.2 | 26.4 | 7.62 | 3.46 | -- | .25 | 16 | 4 | 8 | .06 | 1.28 |
| | | 2.2 | 26.4 | 7.62 | 3.46 | -- | .25 | 9.25 | 2.31 | 4.62 | .179 | 1.28 |
| 21(c) | .5 | 2.2 | 26.4 | 7.63 | 3.46 | C | .25 | 8 | 2 | 4 | .239 | 0.64 |
| | | | | | | | | | | | | |
| Column 1 | | | | | | | | | | | | |
| 22(a) | 0.25 | 2.2 | 6.6 | 3.81 | 1.73 | I | 1 | 4 | 4 | 1 | 0.239 | 2.57 |
| 22(b) | .5 | 2,2 | 6.6 | 3.81 | 1.73 | I | 1 | 4 | 4 | 1 | .239 | 2.57 |
| 22(c) | 1 | 2.2 | 6.6 | 3.81 | 1.73 | I | 1 | 4 | 4 | 1 | .239 | 2.57 |
| | | | | | | | | | | | | |
| Column 2 | | | | | | | | | | | | |
| 22(a) | 0.25 | 2.2 | 26.4 | 7.63 | 3.46 | F | 0.5 | 5.66 | 2.83 | 1.42 | 0.239 | 2.57 |
| 22(b) | .5 | 2.2 | 26.4 | 7.63 | 3.46 | F | .5 | 5.66 | 2.83 | 1.42 | .239 | 2.57 |
| 22(c) | 1 | 2.2 | 26.4 | 7.63 | 3.46 | F | .5 | 5.66 | 2.83 | 1.42 | .239 | 2.57 |
| | | | | | | | | | | | | |
| 23a(a) | 0.25 | 2.2 | 6.6 | 3.81 | 2.73 | B | 0.25 | 11.32 | 2.83 | 2.83 | 0.0598 | 0.64 |
| | | 2.2 | 59.4 | 11.43 | 5.20 | B | .25 | 11.32 | 2.83 | 2.83 | .1796 | 1.93 |
| 23a(b) | .5 | 2.2 | 6.6 | 3.81 | 2.73 | B | .25 | 11.32 | 2.83 | 5.66 | .0598 | .64 |
| | | 2.2 | 59.4 | 11.43 | 5.20 | B | .25 | 11.32 | 2.83 | 5.66 | .1796 | 1.93 |
| 23a(c) | 1 | 2.2 | 6.6 | 3.81 | 2.73 | B | .25 | 11.32 | 2.83 | 11.32 | .0598 | .64 |
| | | 2.2 | 59.4 | 11.43 | 5.20 | B | .25 | 11.32 | 2.83 | 11.32 | .1796 | 1.93 |

TABLE 2.—CONCLUDED.

| Figure no. | *x*/*H* | *DR* | *J* | *M* (√(*J***DR*)) | *R* (√(*J*/*DR*)) | Configuration (see fig. 3) | *S*/*H* | *H*/*d* | *S*/*d* | *x*/*d* | *MR* | *C* (*S*/*H*)(√(*J*)) |
|---|---|---|---|---|---|---|---|---|---|---|---|---|
| | | | | | | | | | | | | |
| 23b(a) | 0.25 | 2.2 | 6.6 | 3.81 | 2.73 | C | 0.25 | 8 | 2 | 2 | 0.1195 | 0.64 |
| | | 2.2 | 59.4 | 11.43 | 5.20 | C | .25 | 8 | 2 | 2 | .3592 | 1.93 |
| 23b(b) | .5 | 2.2 | 6.6 | 3.81 | 2.73 | C | .25 | 8 | 2 | 4 | .1195 | 0.64 |
| | | 2.2 | 59.4 | 11.43 | 5.20 | C | .25 | 8 | 2 | 4 | .3592 | 1.93 |
| 23b(c) | 1 | 2.2 | 6.6 | 3.81 | 2.73 | C | .25 | 8 | 2 | 8 | .1195 | 0.64 |
| | | 2.2 | 59.4 | 11.43 | 5.20 | C | .25 | 8 | 2 | 8 | .3592 | 1.93 |
| | | | | | | | | | | | | |
| 24a(a) | 0.5 | 2.2 | 26.4 | 7.63 | 3.46 | C | 0.25 | 8 | 2 | 4 | 0.239 | 1.28 |
| | .5 | 2,2 | 26.4 | 7.63 | 3.46 | C | .25 | 8 | 2 | 4 | .239 | 1.28 |
| 24a(b) | .5 | 2.2 | 38.8 | 9.24 | 4.40 | C | .25 | 8 | 2 | 4 | .29 | 1.55 |
| | .5 | 2.2 | 16.9 | 6.10 | 2.70 | C | .25 | 8 | 2 | 4 | .19 | 1.02 |
| 24a(c) | .5 | 2.2 | 51.7 | 10.66 | 4.85 | C | .25 | 8 | 2 | 4 | .335 | 1.80 |
| | .5 | 2.2 | 9.5 | 4.57 | 2.08 | C | .25 | 8 | 2 | 4 | .144 | 0.77 |
| 24a(d) | .5 | 2.2 | 67.6 | 12.20 | 5.54 | C | .25 | 8 | 2 | 4 | .383 | 2.06 |
| | .5 | 2.2 | 4.2 | 3.03 | 1.38 | C | .25 | 8 | 2 | 4 | .096 | 0.51 |
| 24a(e) | .5 | 2.2 | 105.6 | 15.24 | 6.93 | C | .25 | 8 | 2 | 4 | .479 | 2.57 |
| | .5 | 2,2 | 0 | 0 | 0 | C | .25 | 8 | 2 | 4 | 0 | |
| | | | | | | | | | | | | |
| 24b(a) | 0.5 | 2.2 | 26.4 | 7.63 | 3.46 | C | 0.25 | 8 | 2 | 4 | 0.239 | 1.28 |
| | .5 | 2,2 | 26.4 | 7.63 | 3.46 | C | .25 | 8 | 2 | 4 | .239 | 1.28 |
| 24b(b) | .5 | 2.2 | 38.8 | 9.24 | 4.40 | C | .25 | 8 | 2 | 4 | .29 | 1.55 |
| | .5 | 2.2 | 16.9 | 6.10 | 2.70 | C | .25 | 8 | 2 | 4 | .19 | 1.02 |
| 24b(c) | .5 | 2.2 | 51.7 | 10.66 | 4.85 | C | .25 | 8 | 2 | 4 | .335 | 1.80 |
| | .5 | 2.2 | 9.5 | 4.57 | 2.08 | C | .25 | 8 | 2 | 4 | .144 | 0.77 |
| 24b(d) | .5 | 2.2 | 67.6 | 12.20 | 5.54 | C | .25 | 8 | 2 | 4 | .383 | 2.06 |
| | .5 | 2.2 | 4.2 | 3.03 | 1.38 | C | .25 | 8 | 2 | 4 | .096 | 0.51 |
| 24b(e) | .5 | 2.2 | 105.6 | 15.24 | 6.93 | C | .25 | 8 | 2 | 4 | .479 | 2.57 |
| | .5S | 2,2 | 0 | 0 | 0 | C | .25 | 8 | 2 | 4 | 0 | |

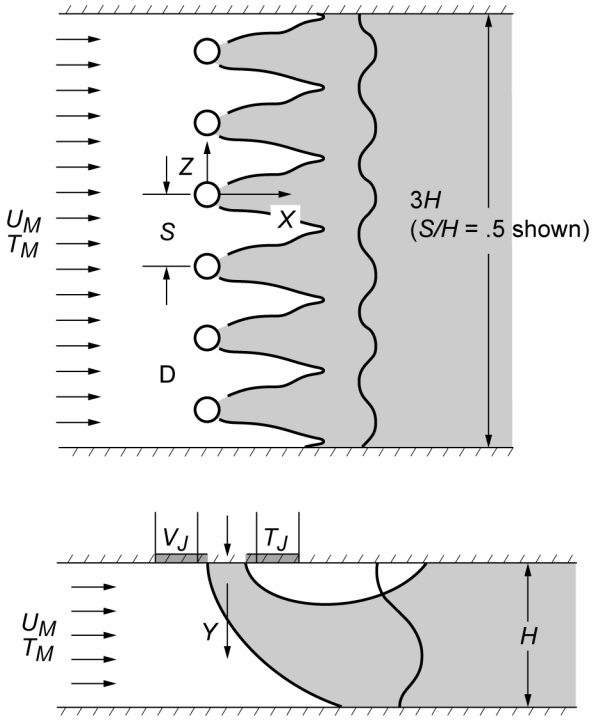


Figure 1.—Schematic of flow field for one side injection of a row of jets in a confined cross flow. (Shown for injection from the top duct wall).

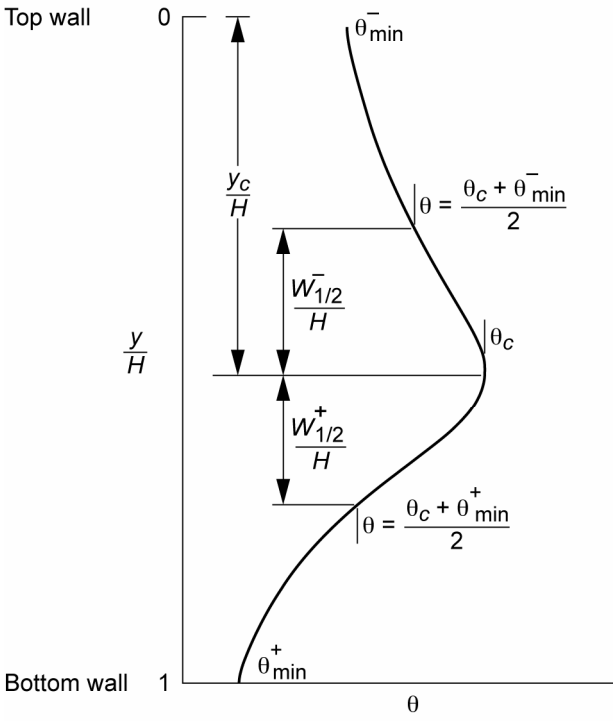


Figure 2.—Schematic of a typical vertical scalar profile showing scaling parameters in empirical model (shown for one-side jet injection from the top duct wall).

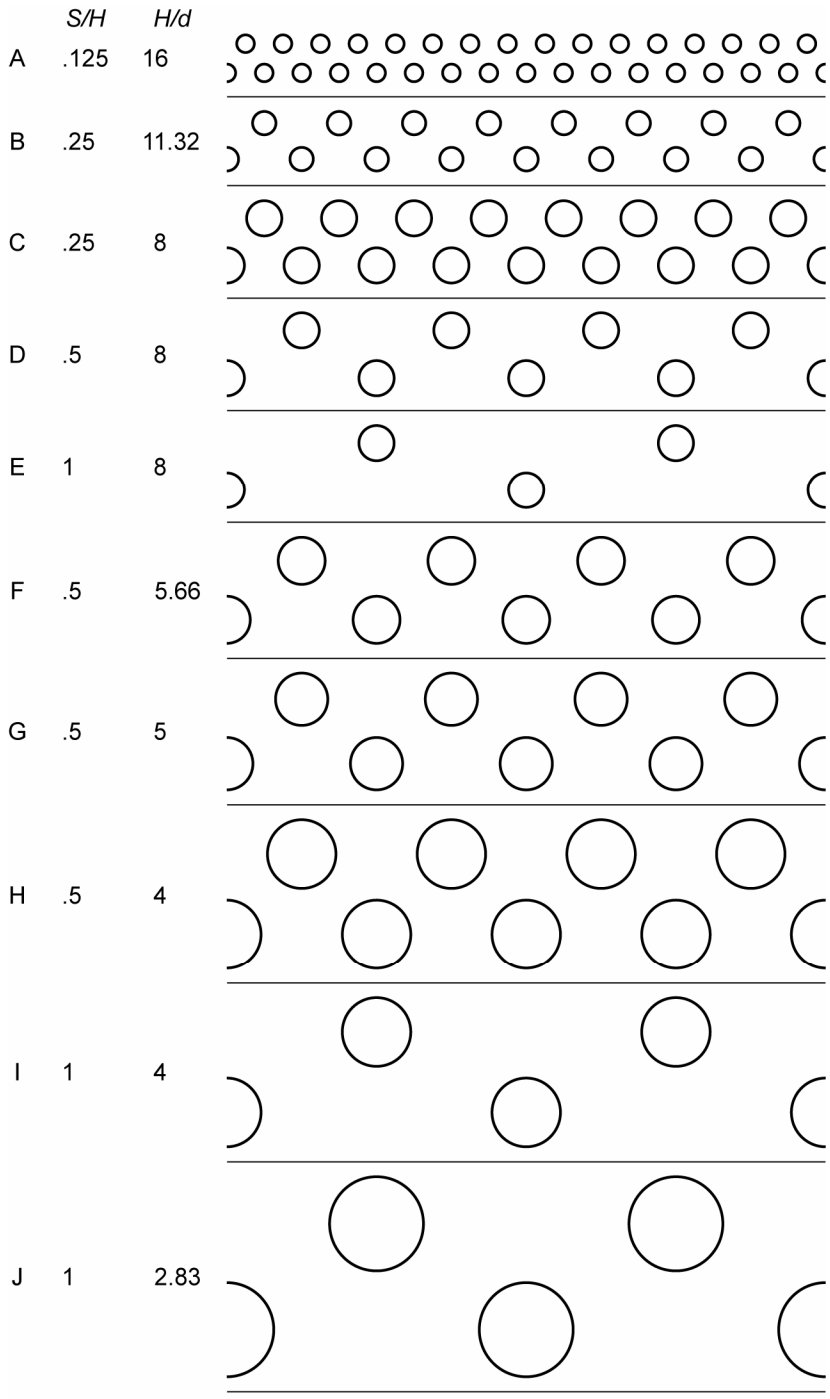


Figure 3.—Round hole orifice configuration.

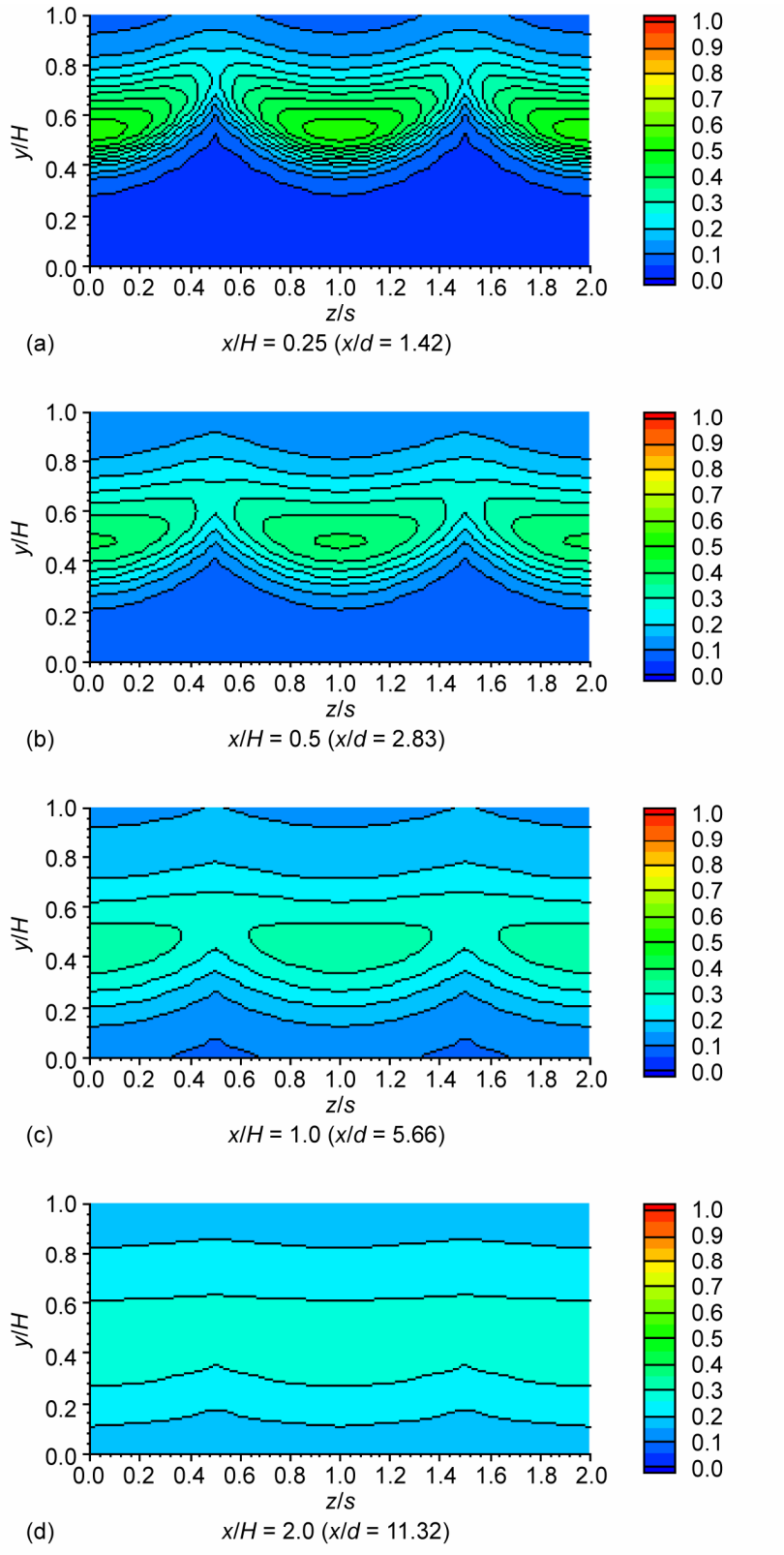


Figure 4.—Variation of scalar distributions with increasing downstream distance: orifice configuration F in figure 3 (centerplane at edge [)-0-( in spreadsheet]) for $S/H$ = 0.5, $H/d$ = 5.66, $DR$ = 2.2, $J$ = 26.4, and $C_d$ = 0.64.

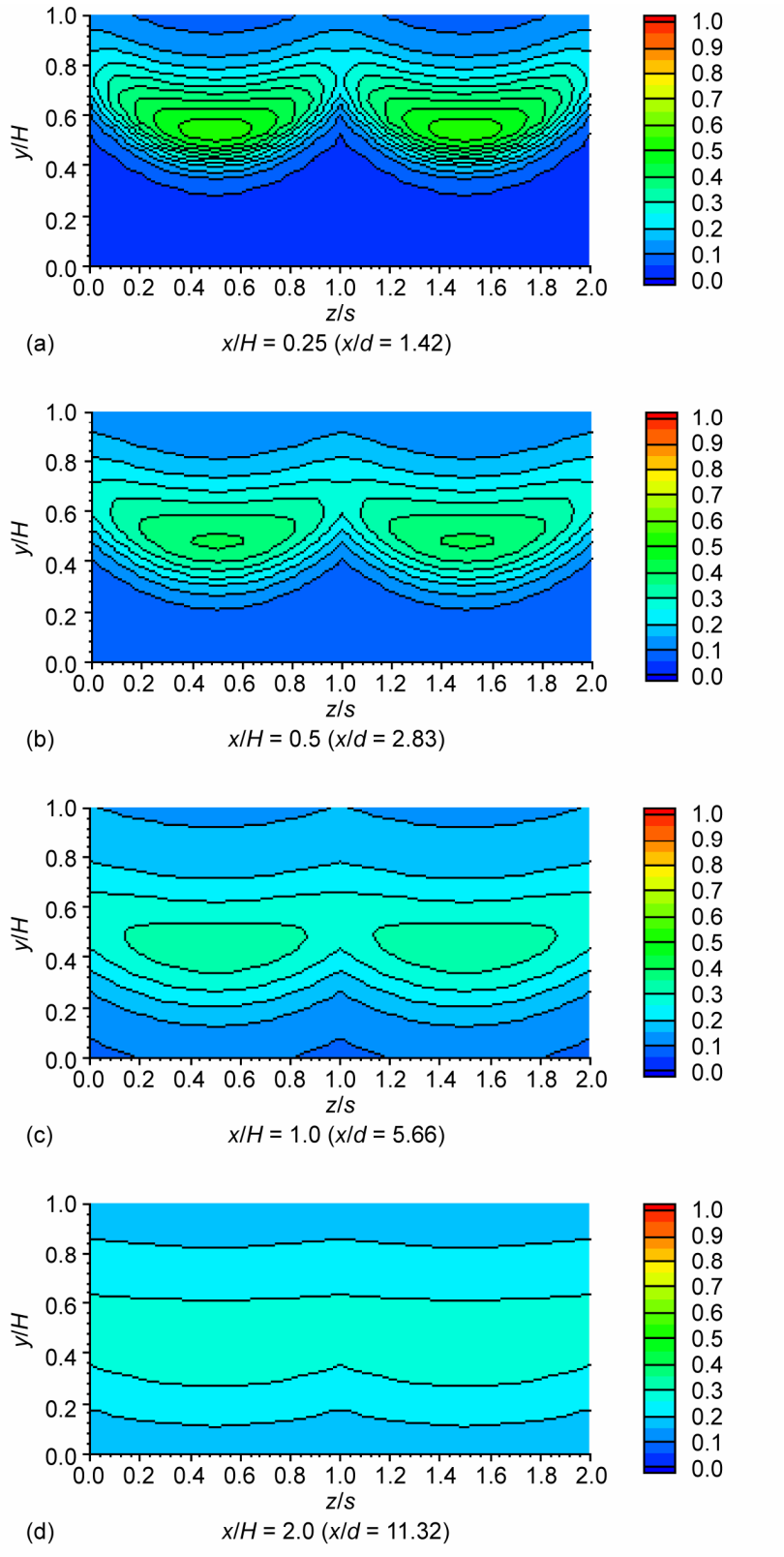


Figure 5.—Variation of scalar distributions with increasing downstream distance: orifice configuration F in figure 3 (midplane at edge [-0-0- in spreadsheet]) for $S/H$ = 0.5, $H/d$ = 5.66, $DR$ = 2.2, $J$ = 26.4, and $C_d$ = 0.64.

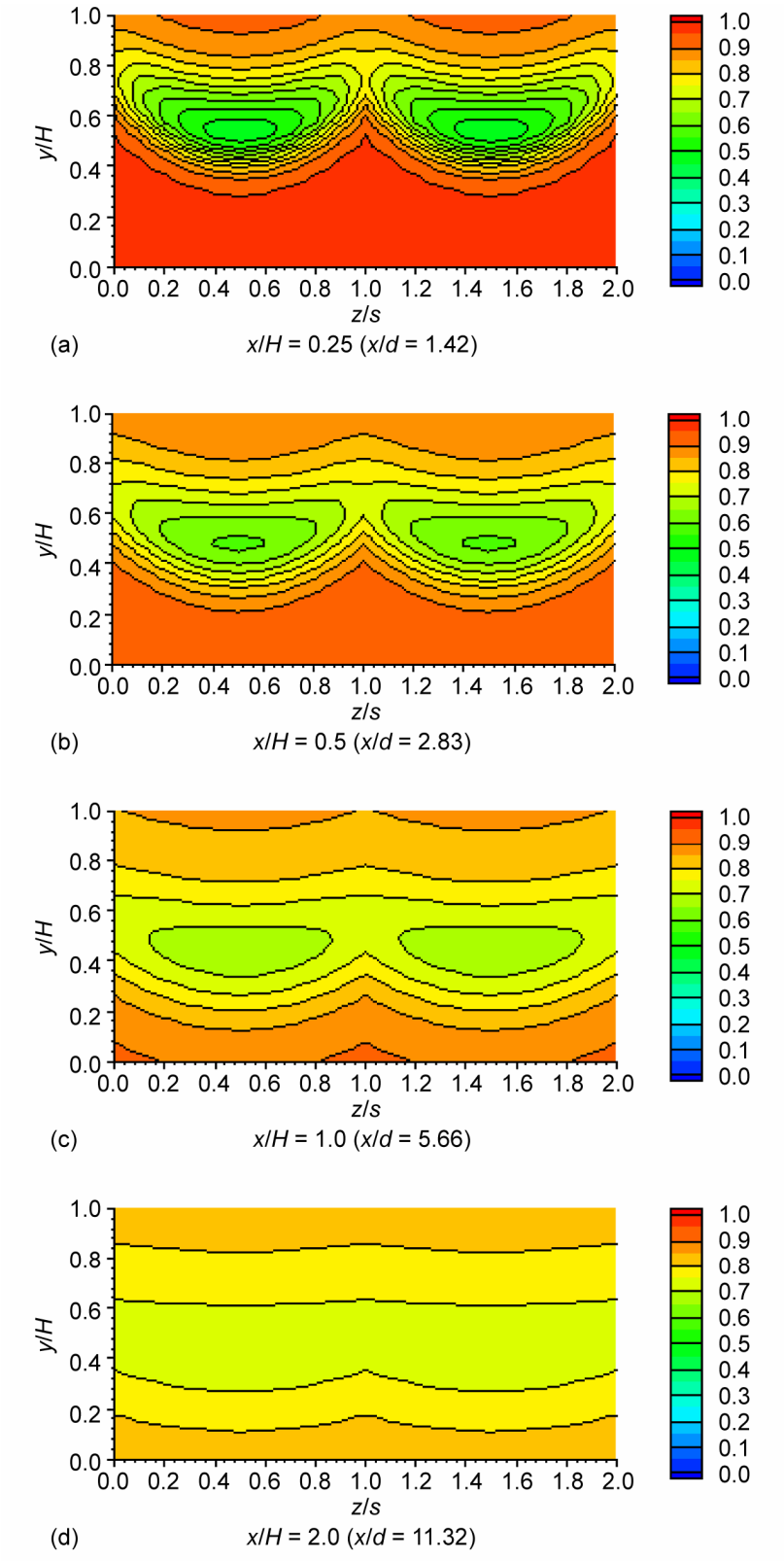


Figure 6.—Variation of “hot” scalar distributions with increasing downstream distance: orifice configuration F in figure 3 (midplane at edge [-0-0- in spreadsheet]) for $S/H$ = 0.5, $H/d$ = 5.66, $DR$ = 2.2, $J$ = 26, and $C_d$ = 0.64.

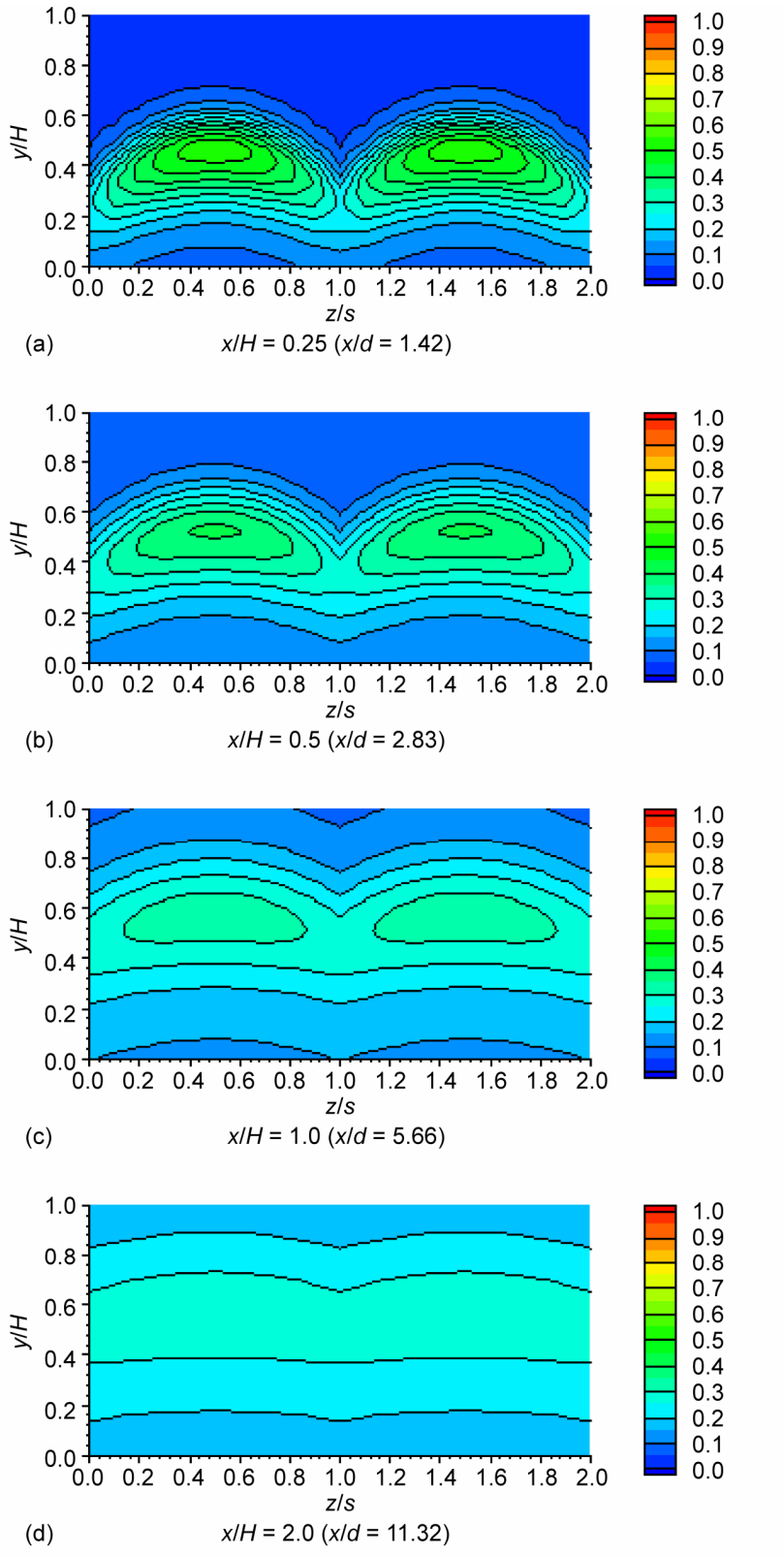


Figure 7.—Variation of bottom injection scalar distributions with increasing downstream distance: orifice configuration F in figure 3 (midplane at edge [-0-0- in spreadsheet]) for $S/H$ = 0.5, $H/d$ = 5.66, $DR$ = 2.2, $J$ = 26.4, and $C_d$ = 0.64.

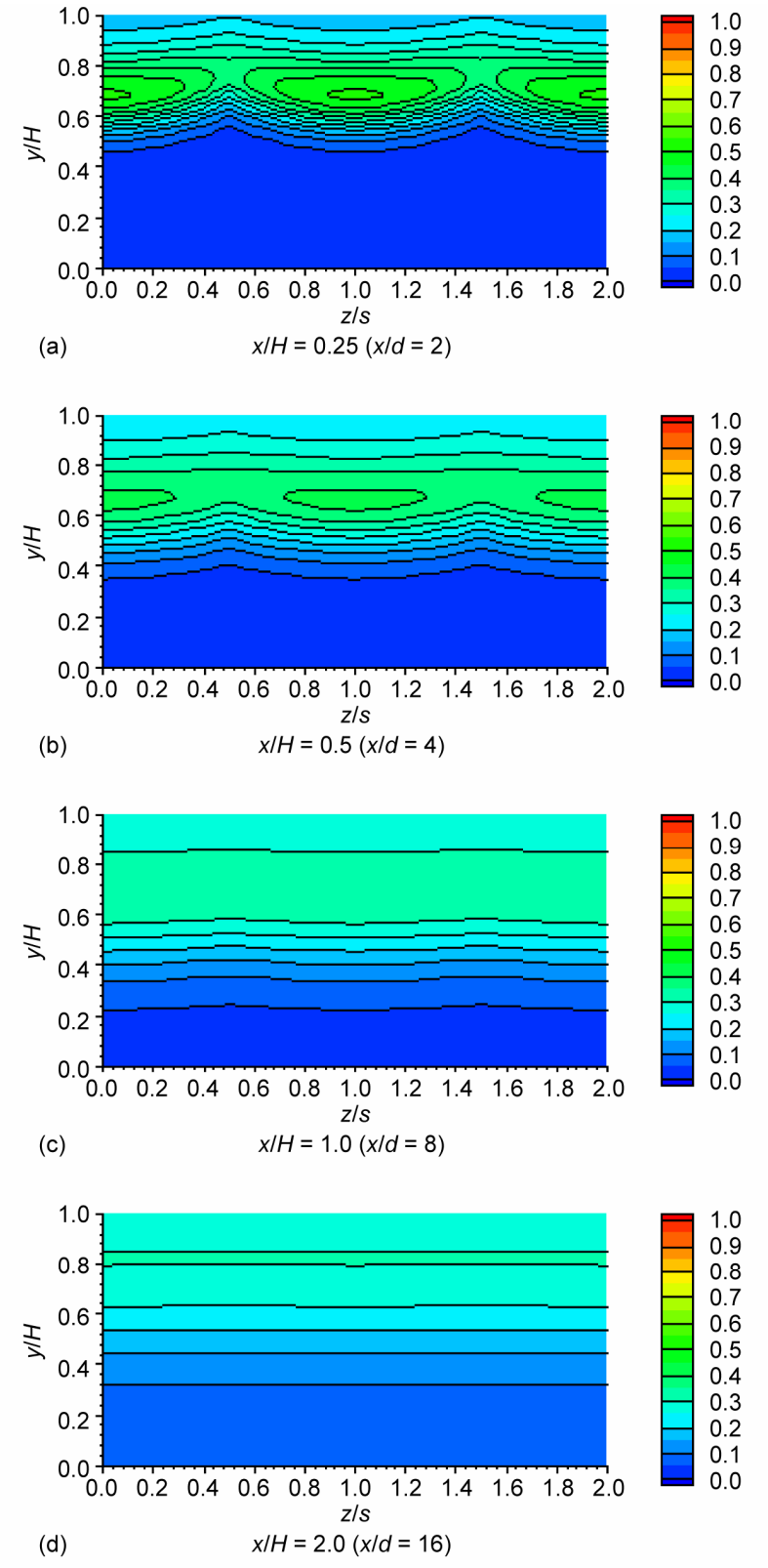


Figure 8(a).—Variation of scalar distributions with increasing downstream distance: orifice configuration C in figure 3 (centerplane at edge [)-0-( in spreadsheet]) for $S/H$ = 0.25, $H/d$ = 8, $DR$ = 2.2, $J$ = 26.4, and $C_d$ = 0.64.

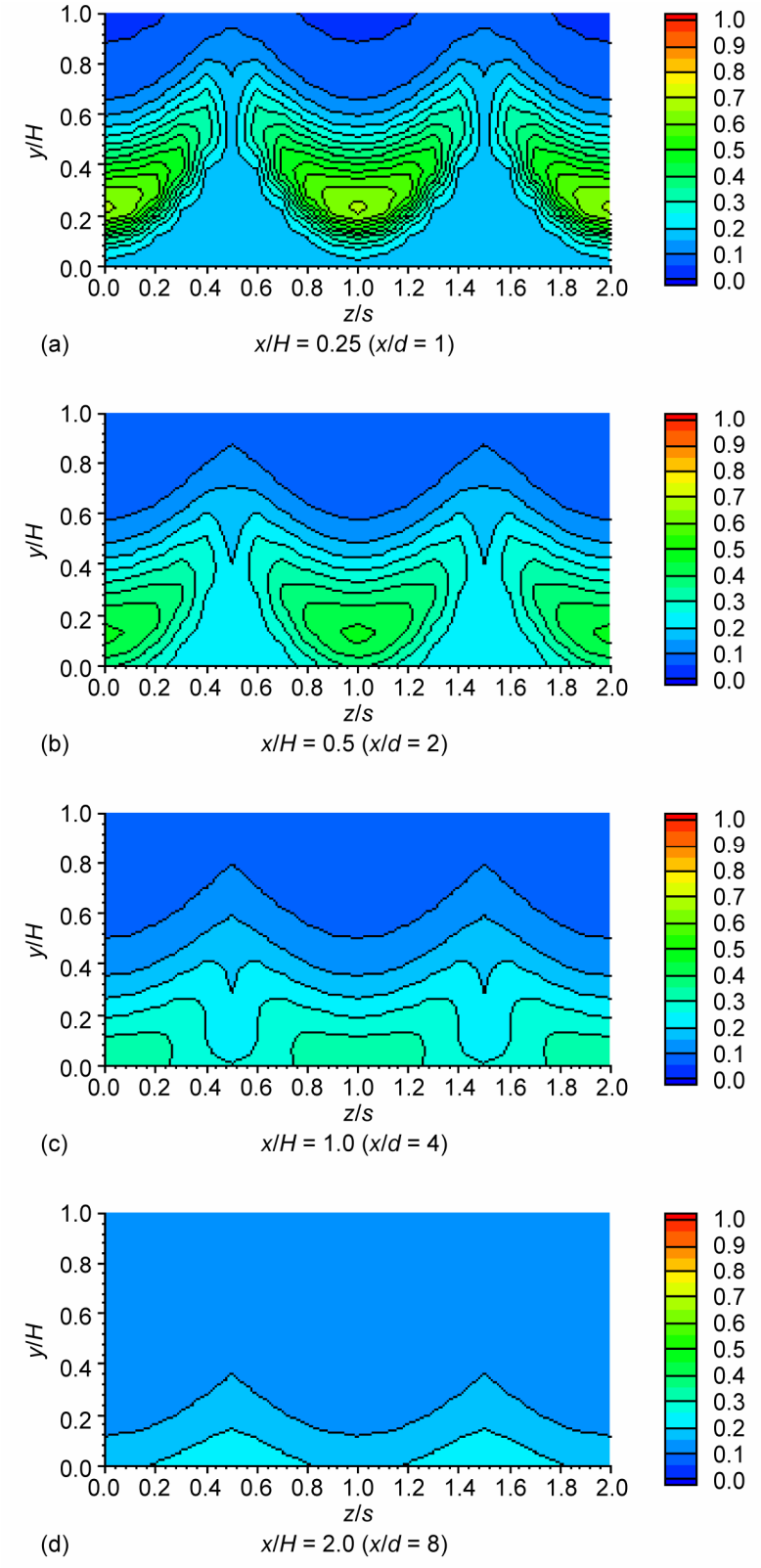


Figure 8(b).—Variation of scalar distributions with increasing downstream distance: orifice configuration I in figure 3 (centerplane at edge [)-0-( in spreadsheet]) for $S/H$ = 1, $H/d$ = 4, $DR$ = 2.2, $J$ = 26.4, and $C_d$ = 0.64.

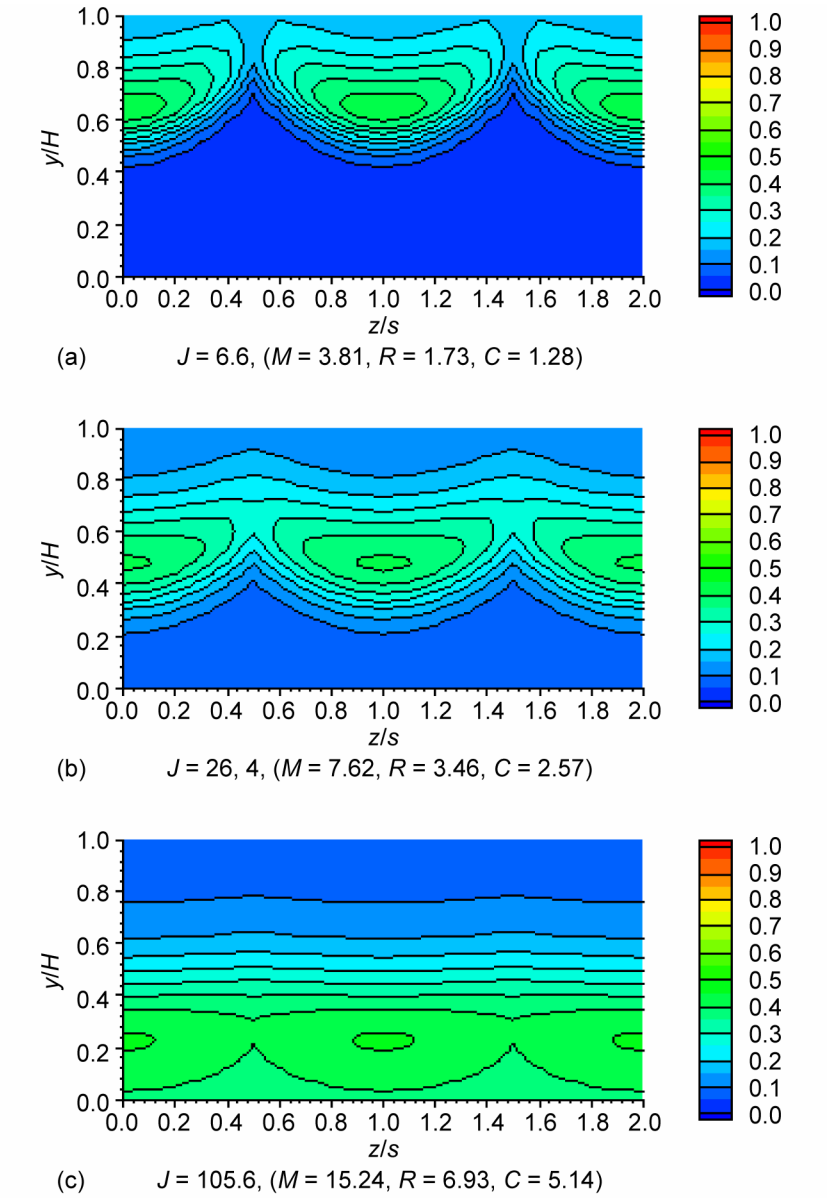


(a) $J$ = 6.6, ($M$ = 3.81, $R$ = 1.73, $C$ = 1.28)

(b) $J$ = 26, 4, ($M$ = 7.62, $R$ = 3.46, $C$ = 2.57)

(c) $J$ = 105.6, ($M$ = 15.24, $R$ = 6.93, $C$ = 5.14)

Figure 9.—Variation of scalar distributions with increasing momentum-flux ratio: orifice configuration F in figure 3 (centerplane at edge [)-0-( in spreadsheet]) for $S/H$ = 0.5, $H/d$ = 5.66, $DR$ = 2.2, and $C_d$ = 0.64 at $x/H$ = 0.5.

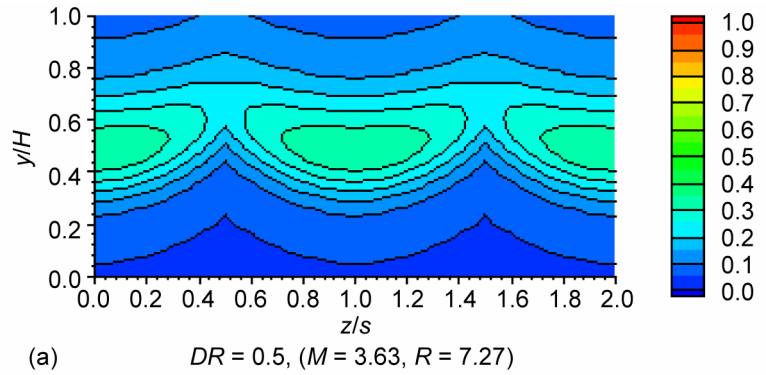


(a) $DR$ = 0.5, ($M$ = 3.63, $R$ = 7.27)

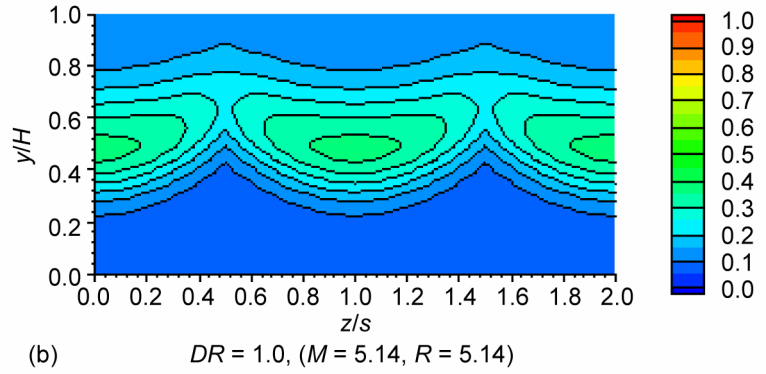


(b) $DR$ = 1.0, ($M$ = 5.14, $R$ = 5.14)

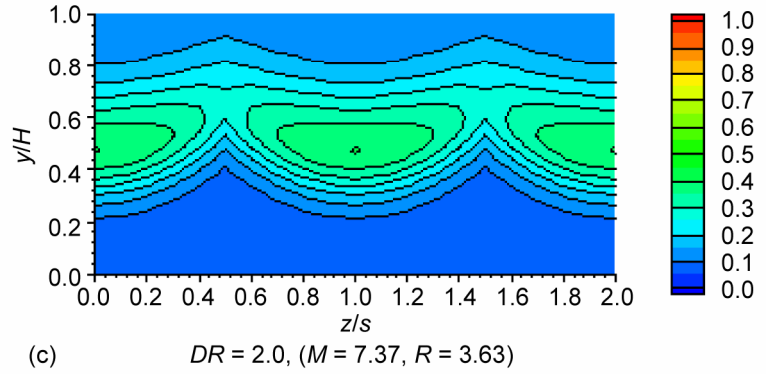


(c) $DR$ = 2.0, ($M$ = 7.37, $R$ = 3.63)

Figure 10.—Variation of scalar distributions with increasing density ratio: orifice configuration F in figure 3 (centerplane at edge [)-0-( in spreadsheet]) for $S/H$ = 0.5, $H/d$ = 5.66, $J$ = 26.4, and $C_d$ = 0.64 at $x/H$ = 0.5.

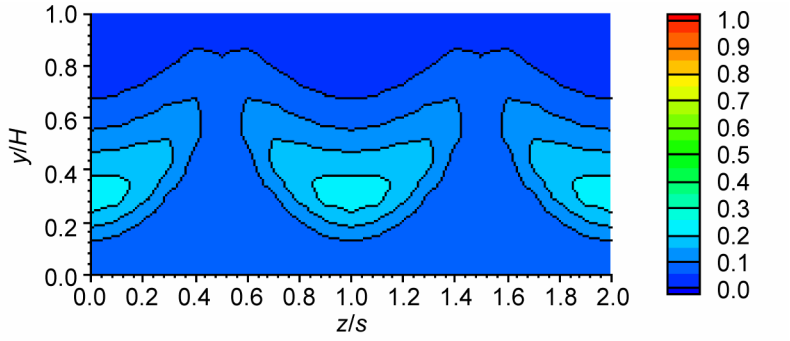


(a) Configuration E: $S/H$ = 1.0, ($S/d$ = 8, $C$ = 5.14)

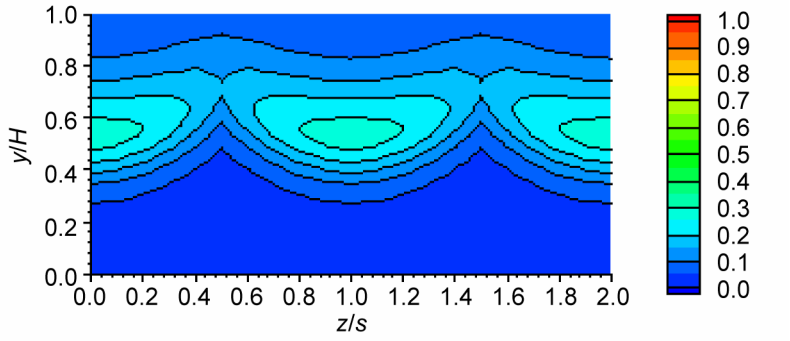


(b) Configuration C: $S/H$ = 0.5, ($S/d$ = 4, $C$ = 2.57)

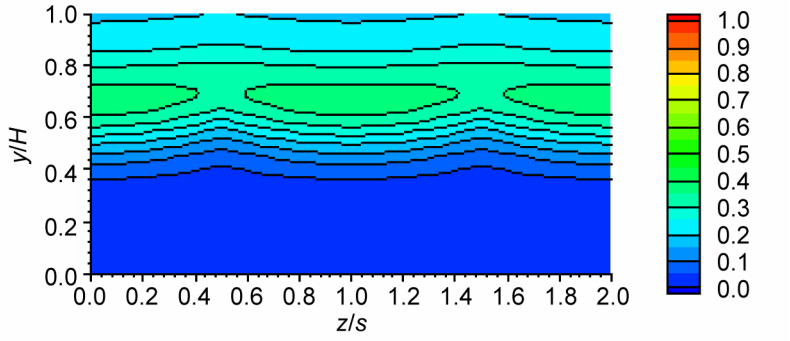


(c) Configuration C: $S/H$ = 0.25, ($S/d$ = 2, $C$ = 1.28)

Figure 11.—Variation of scalar distributions with decreasing orifice spacing at constant round hole diameter (constant ($H/d$): centerplane at edge [)-0-( in spreadsheet] for $H/d$ = 8, $DR$ = 2.2, $J$ = 26.4, and $C_d$ = 0.64 at $x/H$ = 0.5.

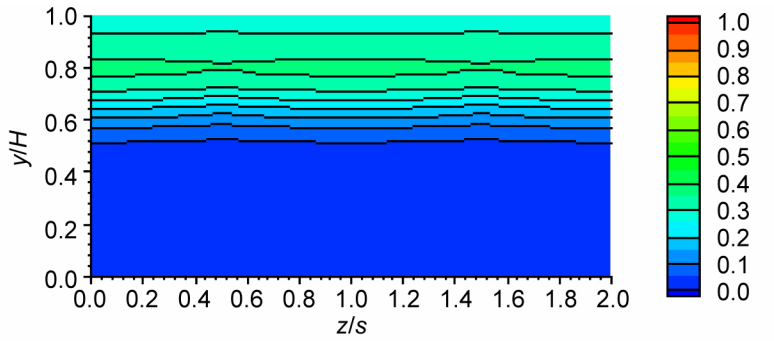


(a) Configuration A: $H/d$ = 16, $S/H$ = 0.125, ($x/d$ = 8, $C$ = 0.64)

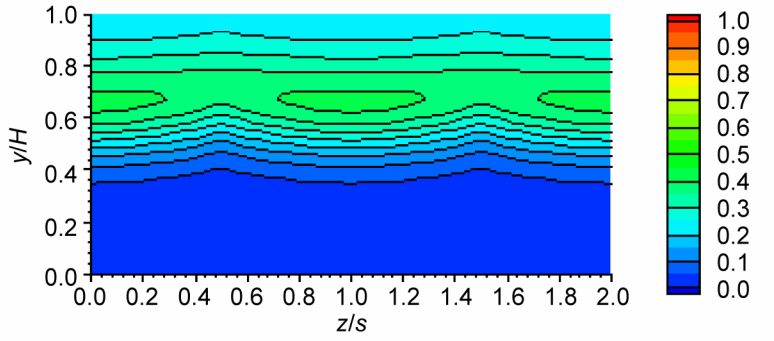


(b) Configuration C: $H/d$ = 8, $S/H$ = 0.25, ($x/d$ = 4, $C$ = 1.28)

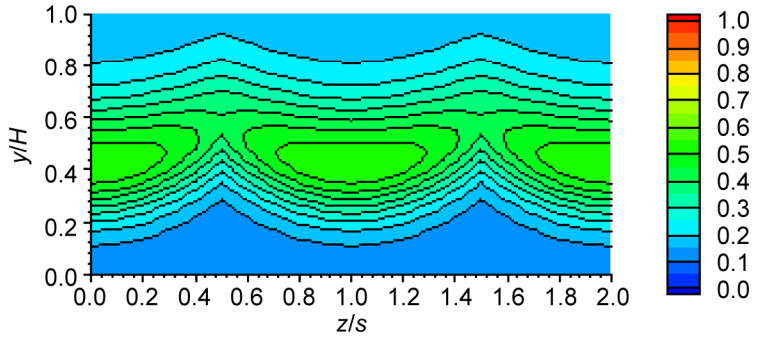


(c) Configuration H: $H/d$ = 4, $S/H$ = 0.5, ($x/d$ = 2, $C$ = 2.57)

Figure 12.—Variation of scalar distributions with increasing orifice diameter (decreasing $H/d$) at constant $S/d$: centerplane at edge [)-0-( in spread-sheet] for $S/d$ = 2, $DR$ = 2.2, $J$ = 26.4, and $C_d$ = 0.64 at $x/H$ = 0.5.

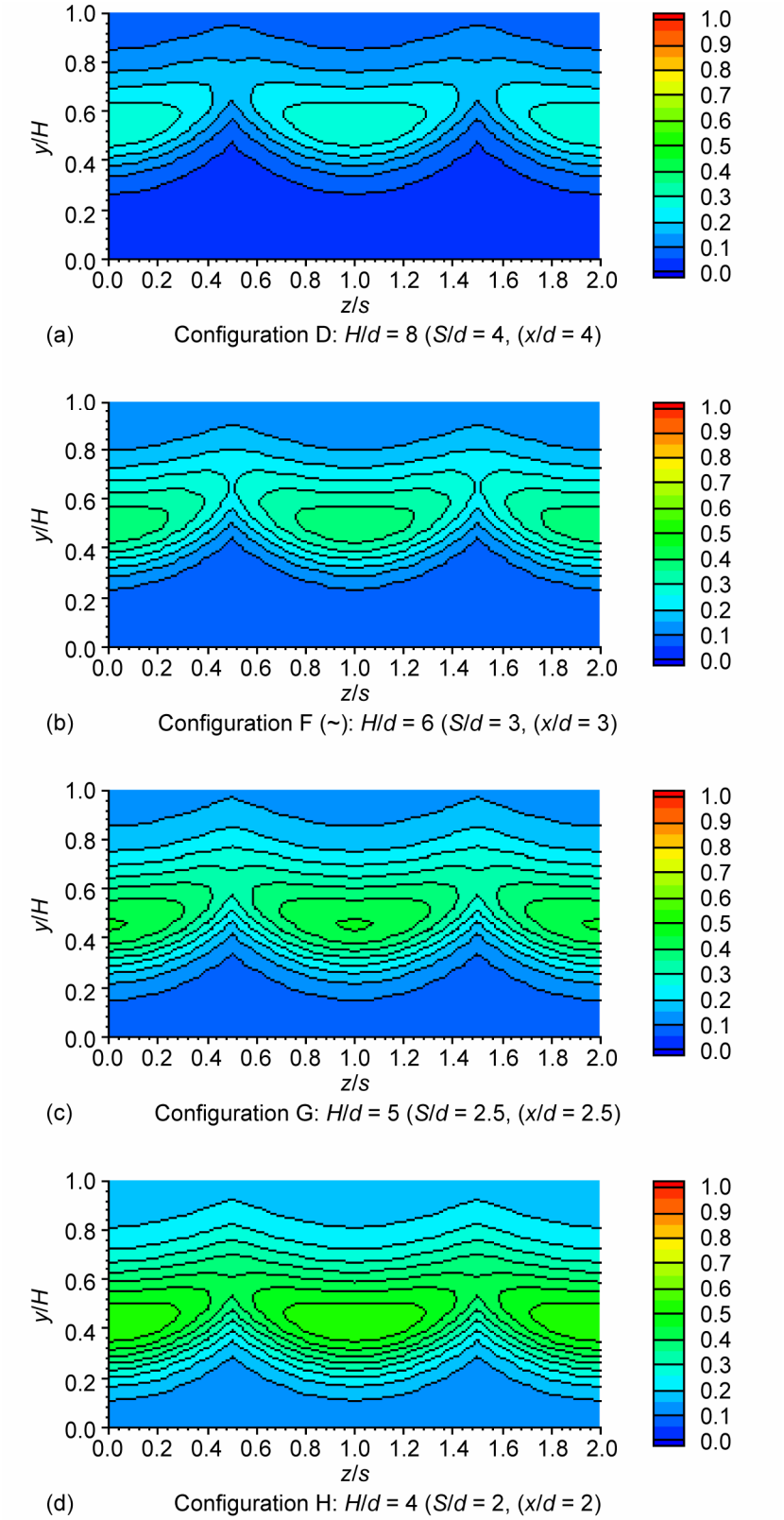


(a) Configuration D: $H/d$ = 8 ($S/d$ = 4, ($x/d$ = 4)

(b) Configuration F (~): $H/d$ = 6 ($S/d$ = 3, ($x/d$ = 3)

(c) Configuration G: $H/d$ = 5 ($S/d$ = 2.5, ($x/d$ = 2.5)

(d) Configuration H: $H/d$ = 4 ($S/d$ = 2, ($x/d$ = 2)

Figure 13(a).—Variation of scalar distributions with increasing orifice diameter (decreasing $H/d$) at constant $S/H$: centerplane at edge [)-0-( in spreadsheet] for $S/H$ = 0.5, $DR$ = 2.2, $J$ = 26.4, and $C_d$ = 0.64 at $x/H$ = 0.5.

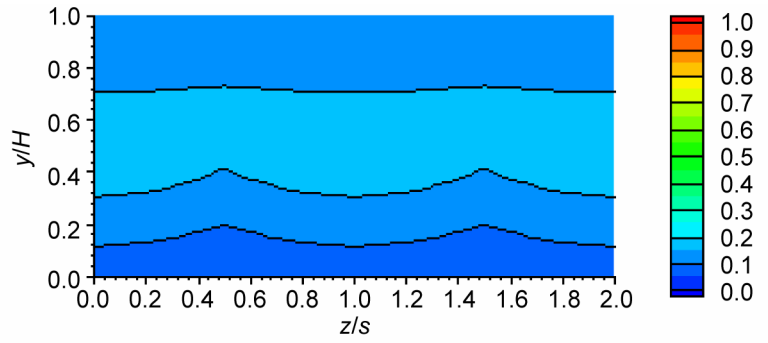


(a) Configuration D: $H/d$ = 8 ($S/d$ = 4, ($x/d$ = 16)

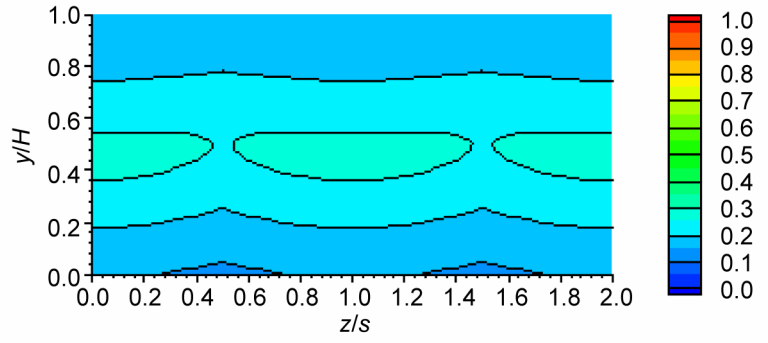


(b) Configuration F (~): $H/d$ = 6 ($S/d$ = 3, ($x/d$ = 12)

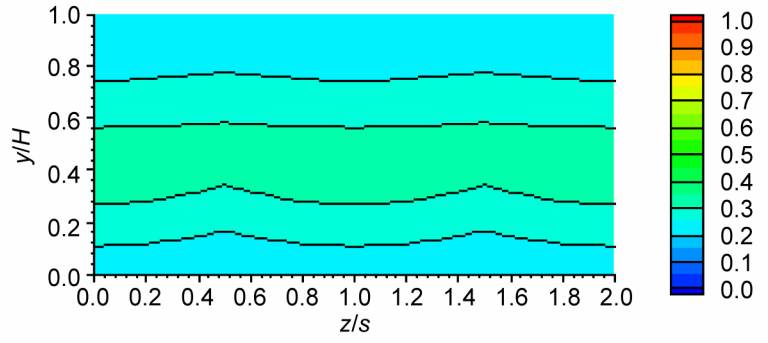


(c) Configuration G: $H/d$ = 5 ($S/d$ = 2.5, ($x/d$ = 10)

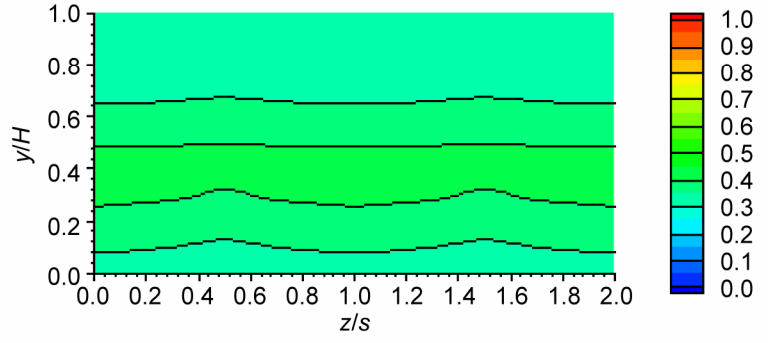


(d) Configuration H: $H/d$ = 4 ($S/d$ = 2, ($x/d$ = 2)

Figure 13b.—Variation of scalar distributions with increasing orifice diameter (decreasing $H/d$) at constant $S/H$: centerplane at edge [)-0-( in spreadsheet] for $S/H$ = 0.5, $DR$ = 2.2, $J$ = 26.4, and $C_d$ = 0.64 at $x/H$ = 2.

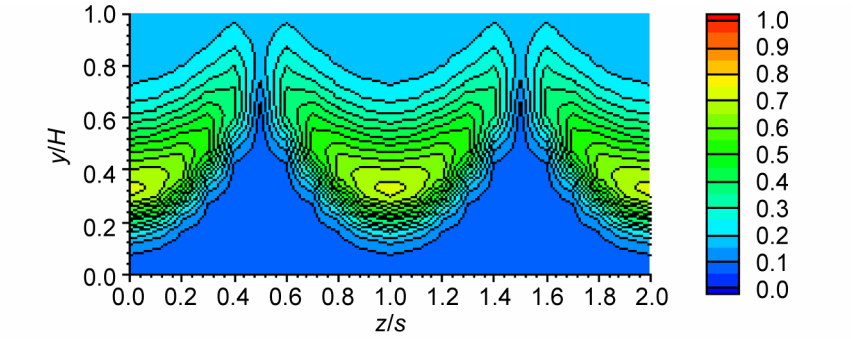


(a) $J$ = 6.6, Configuration J: $S/H$ = 1, $H/d$ = 2.83, ($C$ = 2.57, ($x/d$ = 1.42)

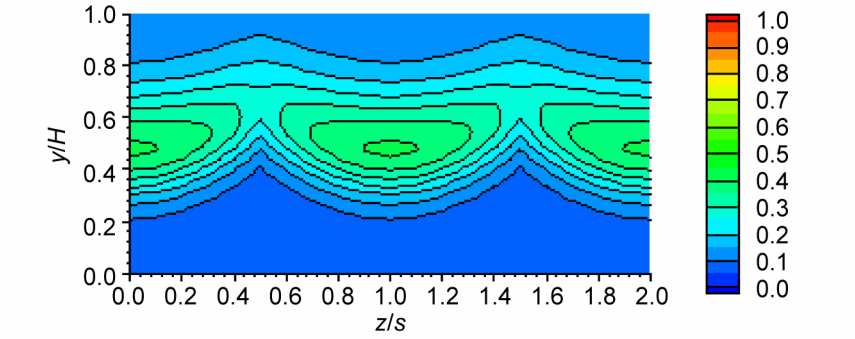


(b) $J$ = 26.4, Configuration F: $S/H$ = 0.5, $H/d$ = 5.66, ($C$ = 2.57, ($x/d$ = 2.83)

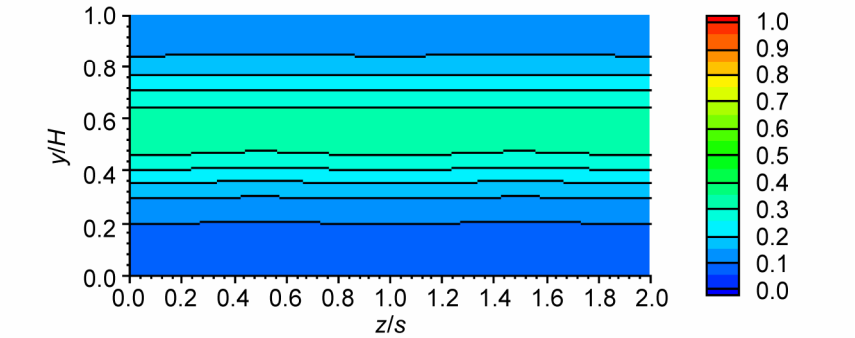


(c) $J$ = 105.6, Configuration B: $S/H$ = 0.25, $H/d$ = 11.32, ($C$ = 2.57, ($x/d$ = 5.66)

Figure 14(a).—Variation of scalar distributions with coupled momentum-flux ratio (J) and orifice spacing ($S/H$): centerplane at edge [)-0-( in spreadsheet] for $DR$ = 2.2 and $C_d$ = 0.64 at $x/H$ = 0.5.

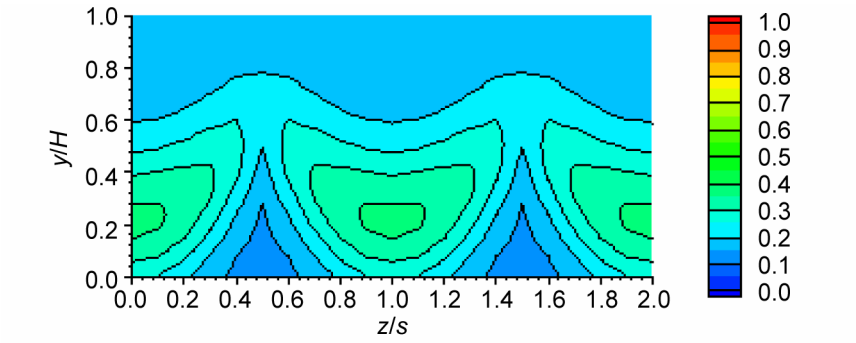


(a) $J$ = 6.6, Configuration J: $S/H$ = 1, $H/d$ = 2.83, ($C$ = 2.57, ($x/d$ = 5.66)

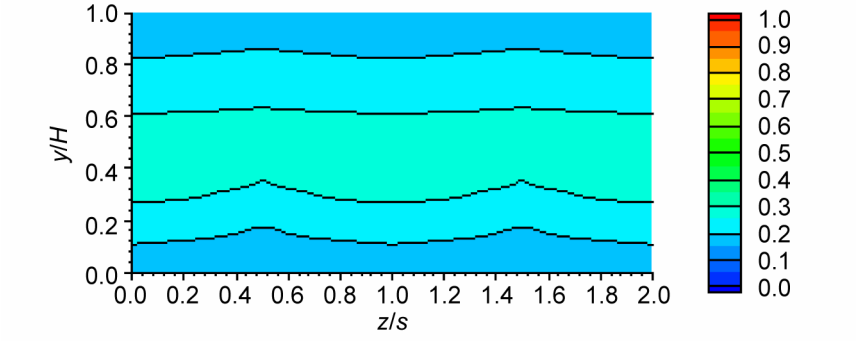


(b) $J$ = 26.4, Configuration F: $S/H$ = 0.5, $H/d$ = 5.66, ($C$ = 2.57, ($x/d$ = 11.32)

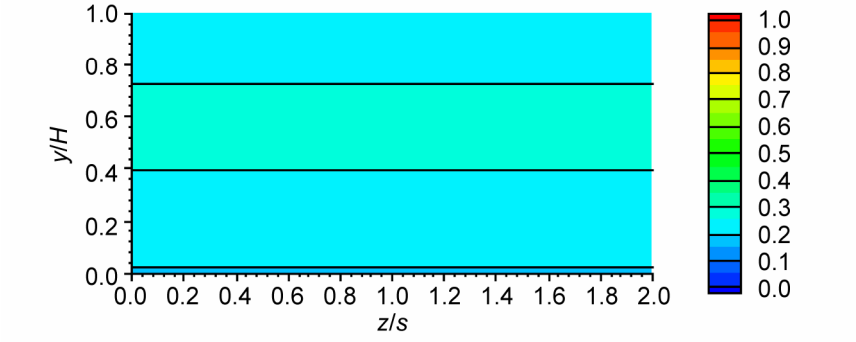


(c) $J$ = 105.6, Configuration B: $S/H$ = 0.25, $H/d$ = 11.32, ($C$ = 2.57, ($x/d$ = 22.64)

Figure 14(b).—Variation of scalar distributions with coupled momentum-flux ratio (J) and orifice spacing ($S/H$): centerplane at edge [)-0-( in spreadsheet] for $DR$ = 2.2 and $C_d$ = 0.64 at $x/H$ = 2.

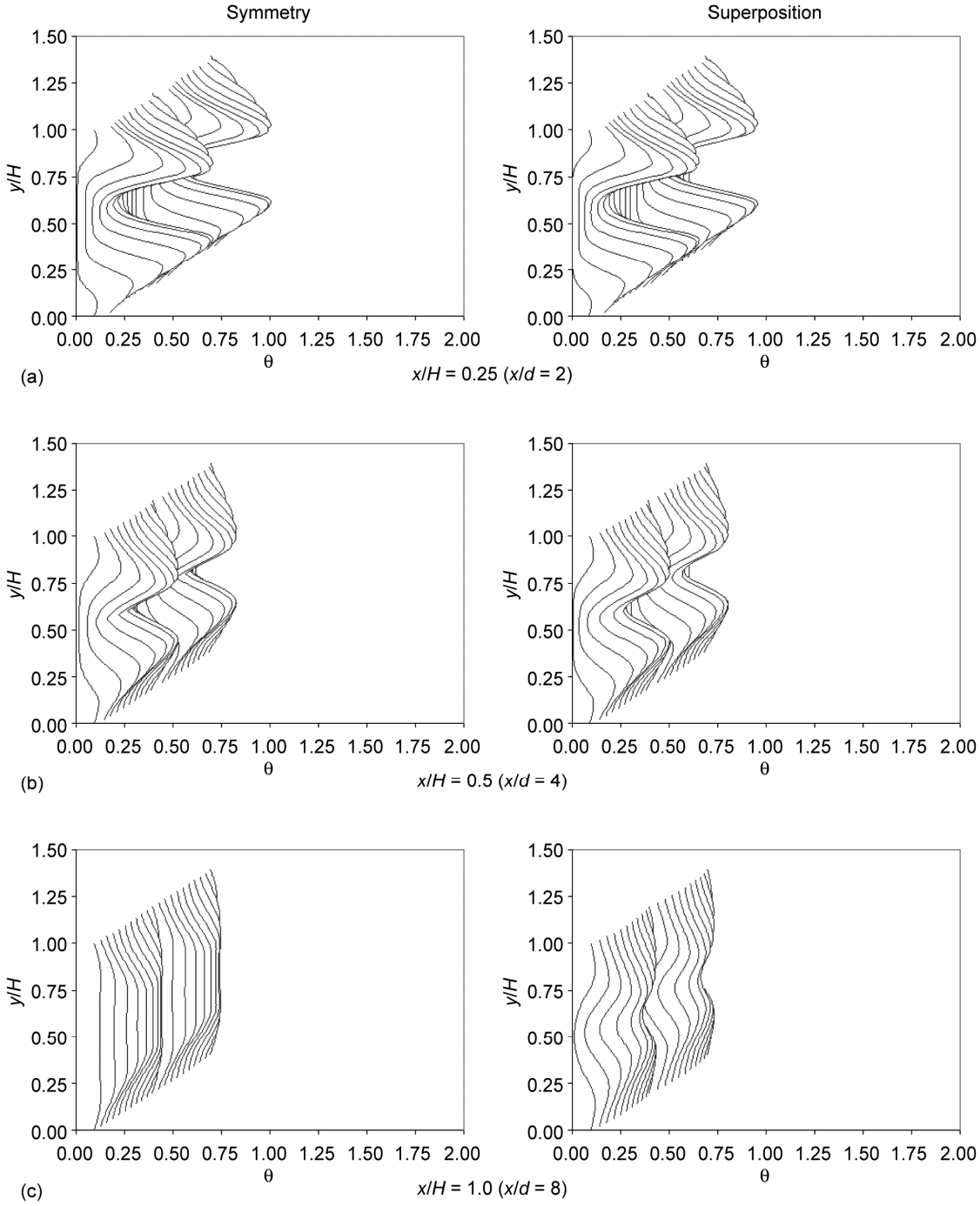


Figure 15(a).—Symmetry and superposition calculations of scalar distributions for opposed rows of jets with centerlines inline-orifice configuration D: $S/H$ = 0.5, $H/d$ = 8, ($S/d$ = 4); $DR$ = 2.2, $J$ = 6.6, ($C$ = 1.28), and $C_d$ = 0.64.

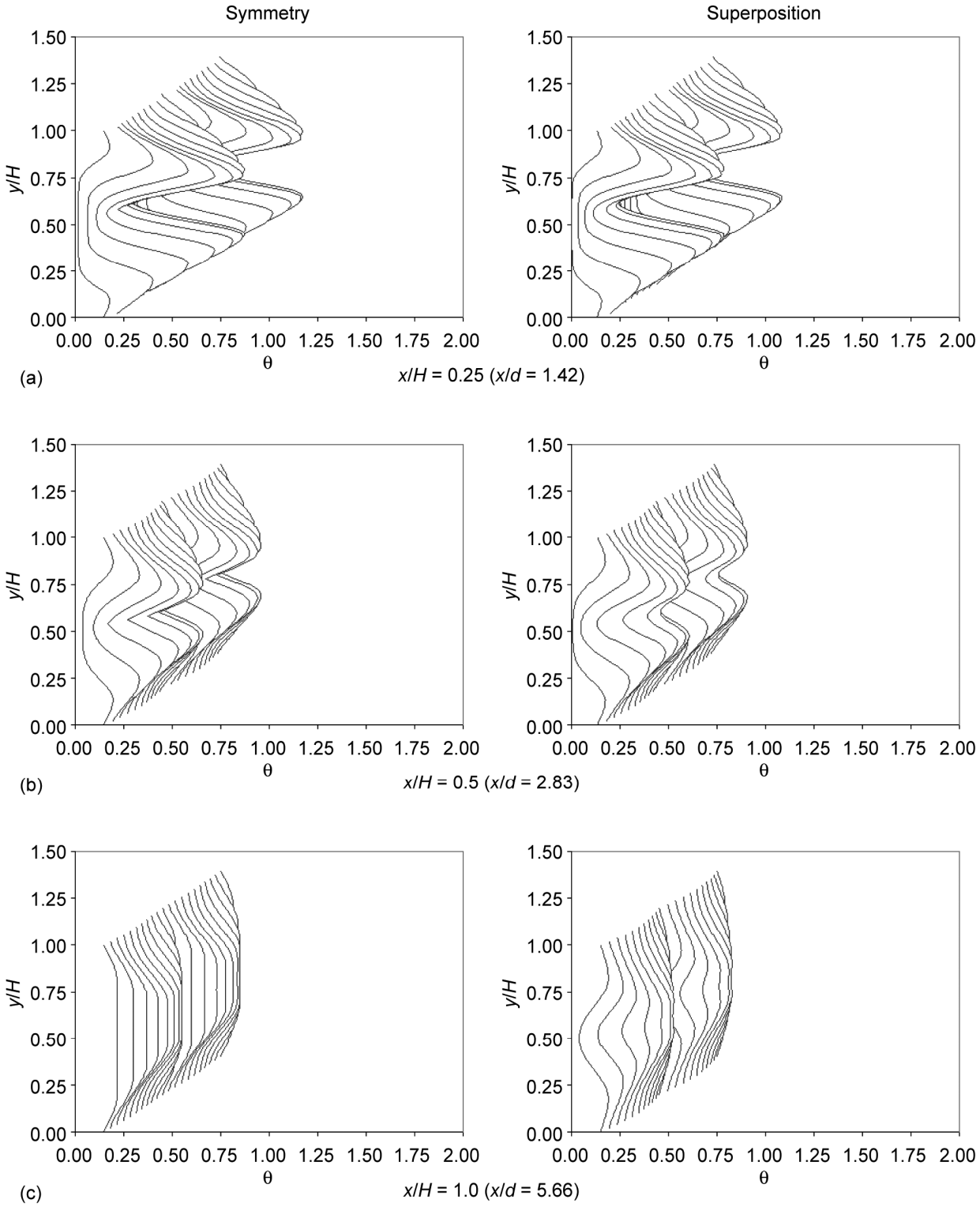


Figure 15(b).—Symmetry and superposition calculations of scalar distributions for opposed rows of jets with centerlines inline-orifice configuration F: $S/H$ = 0.5, $H/d$ = 5.66, ($S/d$ = 2.83); $DR$ = 2.2, $J$ = 6.6, ($C$ = 1.28), and $C_d$ = 0.64.

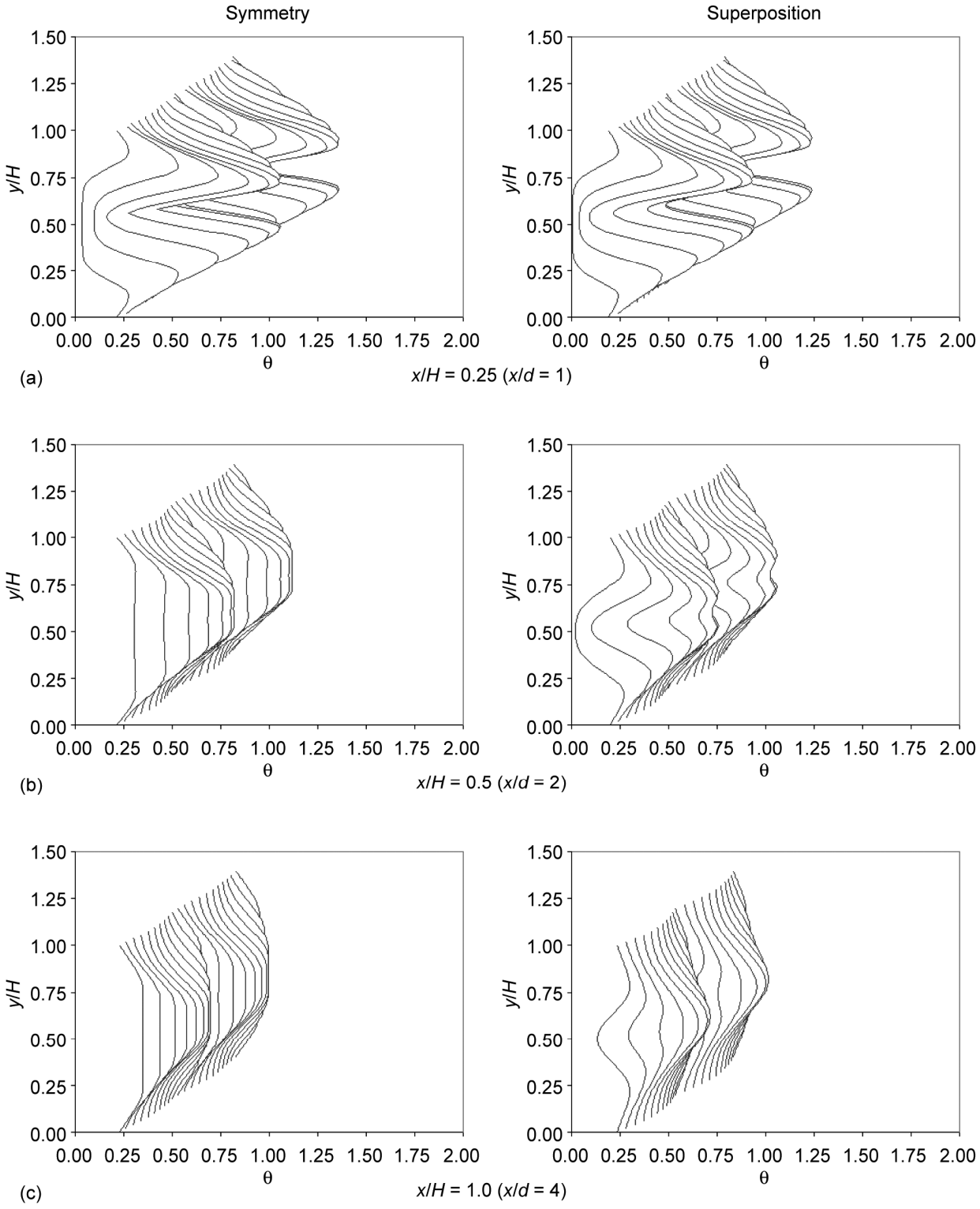


Figure 15(c).—Symmetry and superposition calculations of scalar distributions for opposed rows of jets with centerlines inline-orifice configuration H: $S/H$ = 0.5, $H/d$ = 4, ($S/d$ = 2); $DR$ = 2.2, $J$ = 6.6, ($C$ = 1.28), and $C_d$ = 0.64.

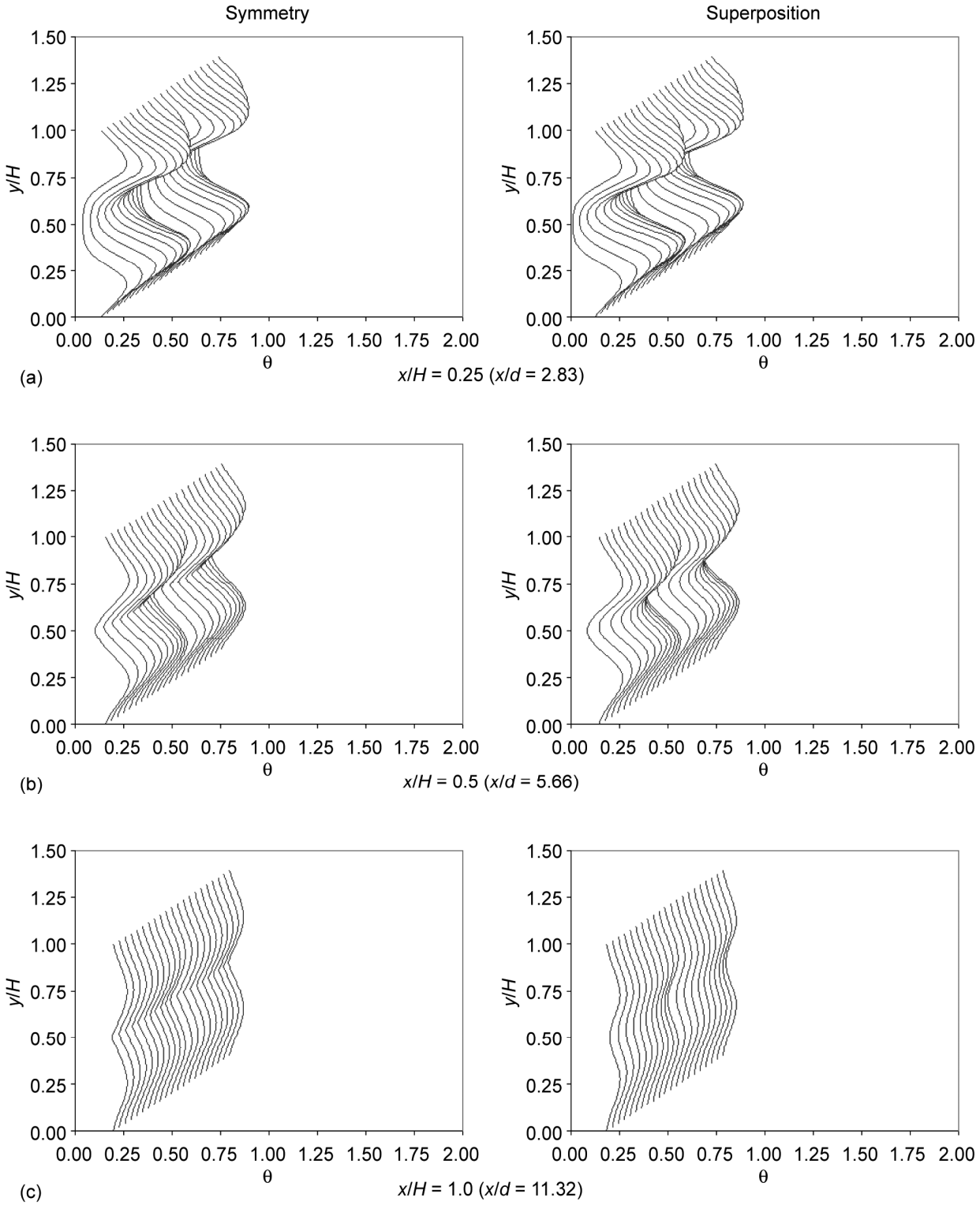


Figure 16(a).—Symmetry and superposition calculations of scalar distributions for opposed rows of jets with centerlines inline-orifice configuration B: $S/H$ = 0.25, $H/d$ = 11.32, ($S/d$ = 2.83); $DR$ = 2.2, $J$ = 26.4, ($C$ = 1.28), and $C_d$ = 0.64.

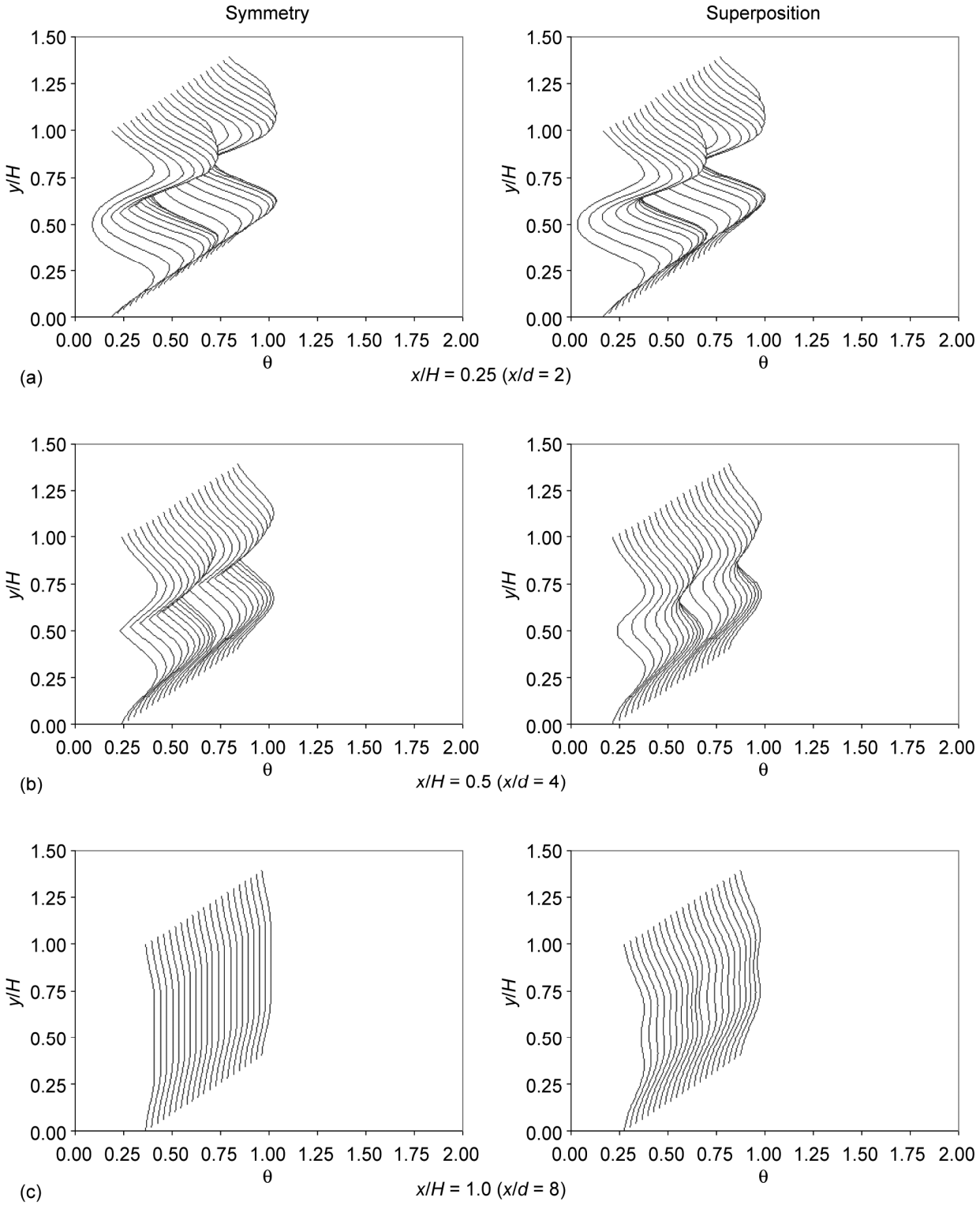


Figure 16(b).—Symmetry and superposition calculations of scalar distributions for opposed rows of jets with centerlines inline-orifice configuration C: $S/H$ = 0.25, $H/d$ = 8, ($S/d$ = 4); $DR$ = 2.2, $J$ = 26.4, ($C$ = 1.28), and $C_d$ = 0.64.

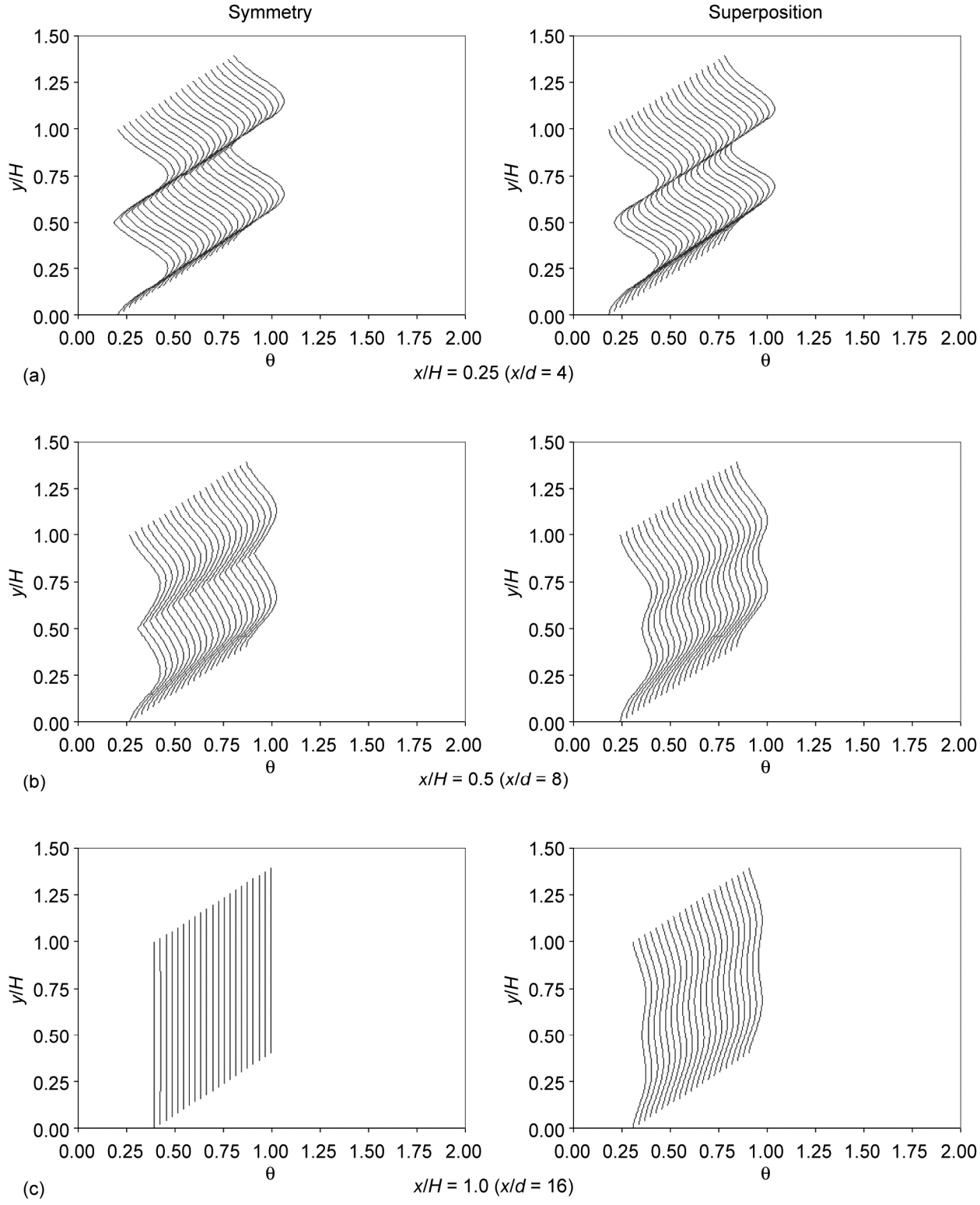


Figure 17.—Symmetry and superposition calculations of scalar distributions for opposed rows of jets with centerlines inline-orifice configuration A: $S/H$ = 0.125, $H/d$ = 16, ($S/d$ = 2); $DR$ = 2.2, $J$ = 105.6, ($C$ = 1.28), and $C_d$ = 0.64.

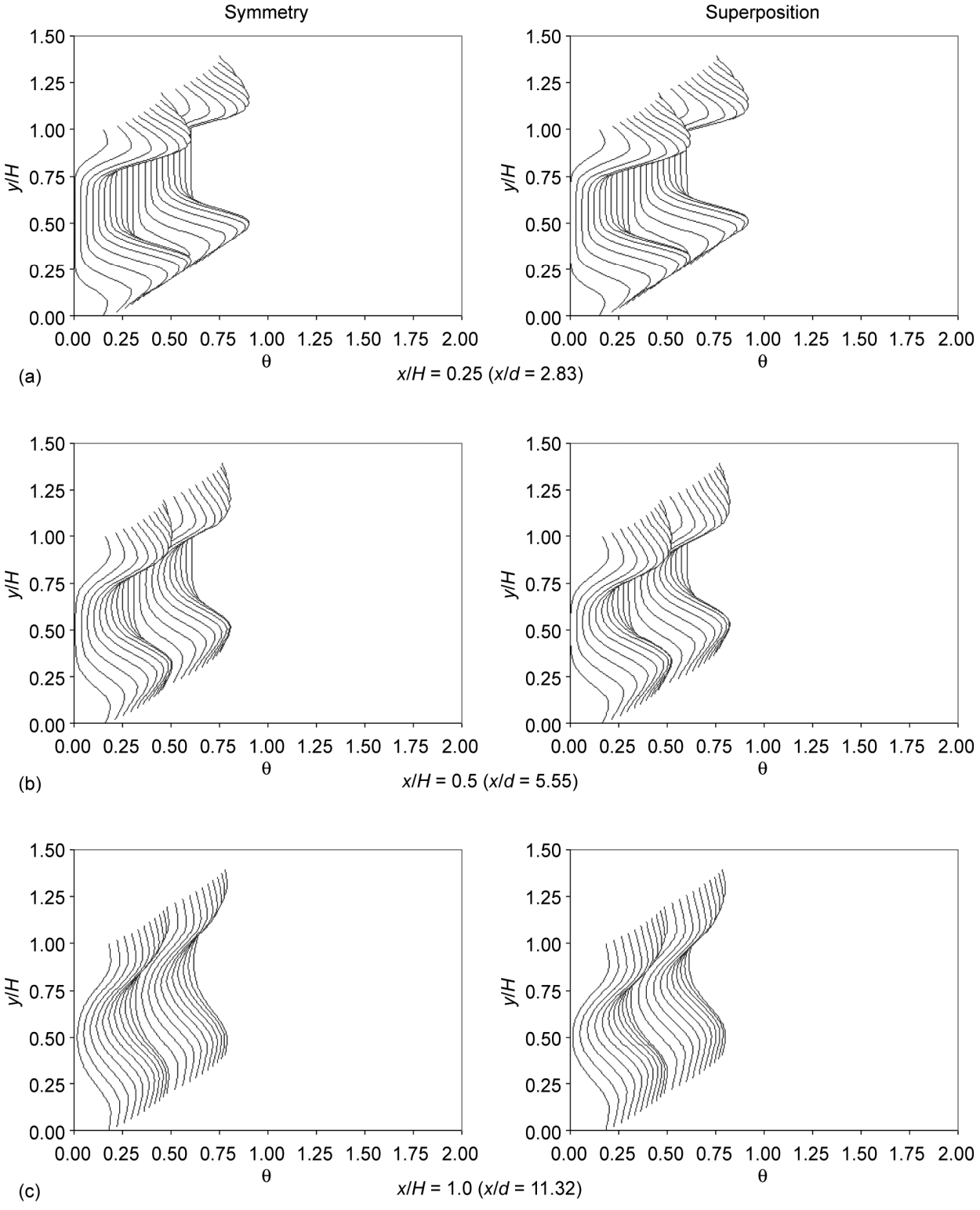


Figure 18(a).—Symmetry and superposition calculation of scalar distributions for under-penetrating jets from opposed rows with centerlines inline-orifice configuration B: $S/H$ = 0.25, $H/d$ = 11.32, ($S/d$ = 2.83); $DR$ = 2.2, $J$ = 6.6, ($C$ = 0.64), and $C_d$ = 0.64.

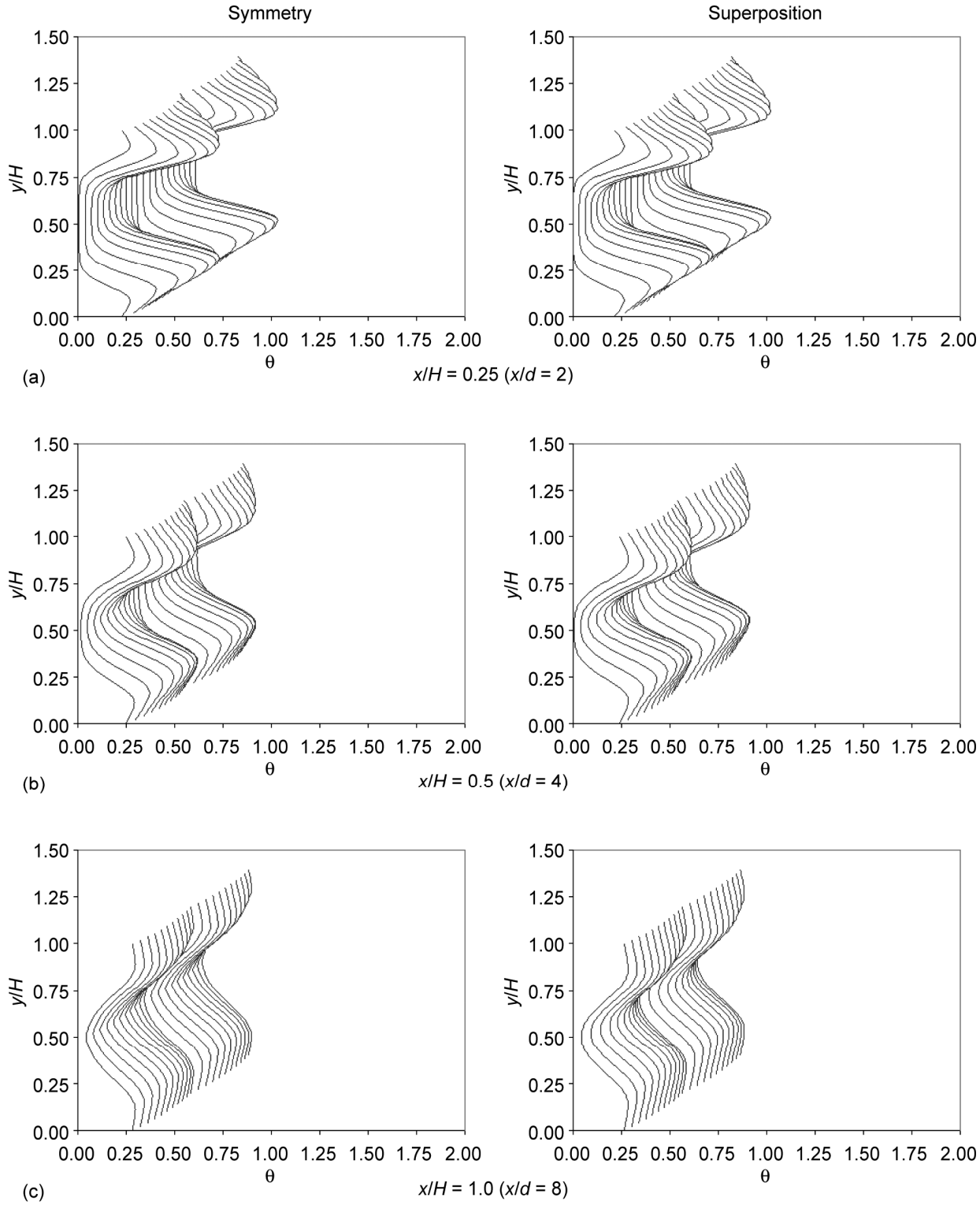


Figure 18(b).—Symmetry and superposition calculations of scalar distributions for under-penetrating jets from opposed rows with centerlines inline-orifice configuration C: $S/H$ = 0.25, $H/d$ = 8, ($S/d$ = 2); $DR$ = 2.2, $J$ = 6.6, ($C$ = 0.64), and $C_d$ = 0.64.

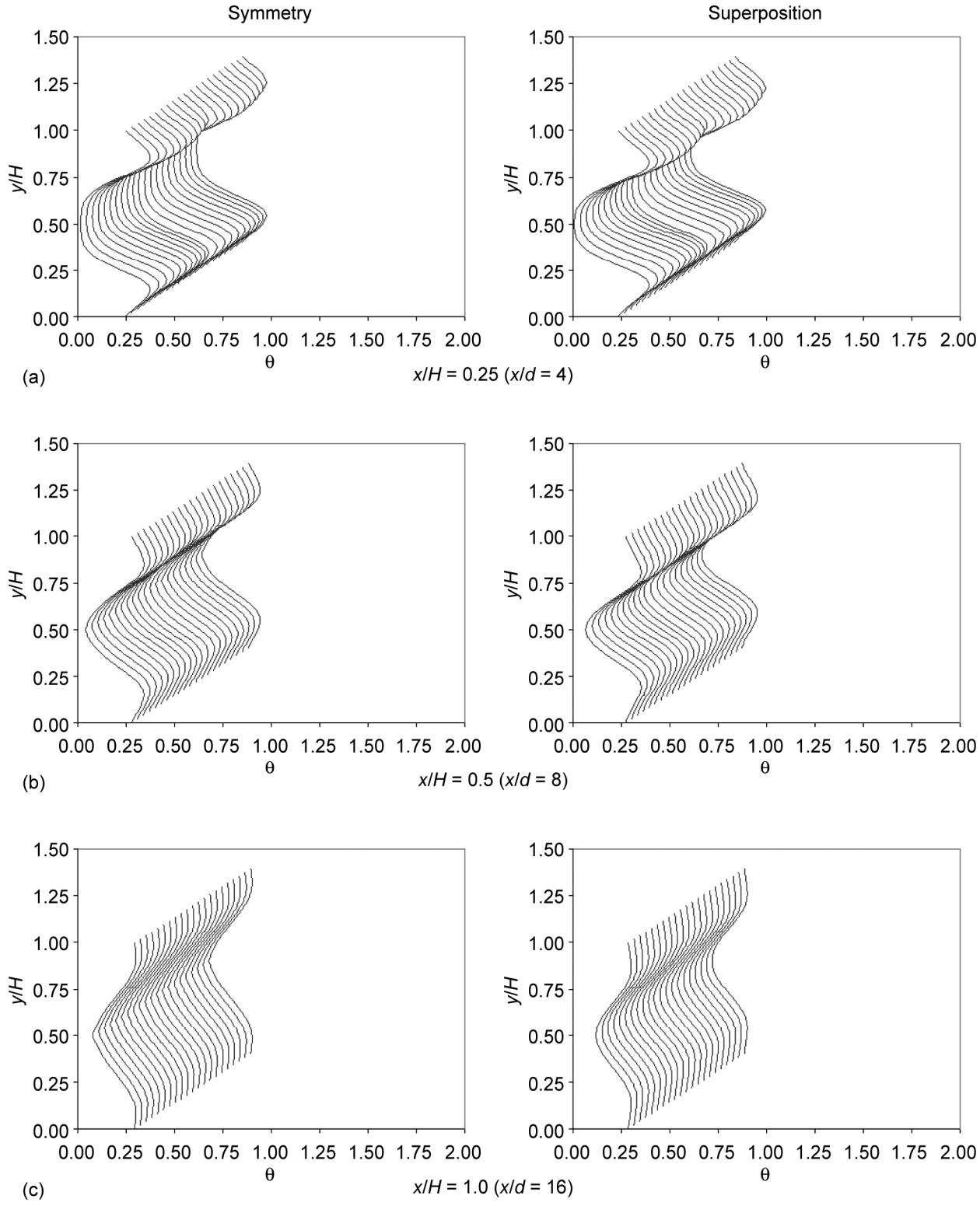


Figure 19.—Symmetry and superposition calculations for under-penetrating jets from opposed rows with centerlines inline-orifice configuration A: $S/H$ = 0.125, $H/d$ = 16, ($S/d$ = 2); $DR$ = 2.2, $J$ = 26.4, ($C$ = 0.64), and $C_d$ = 0.64.

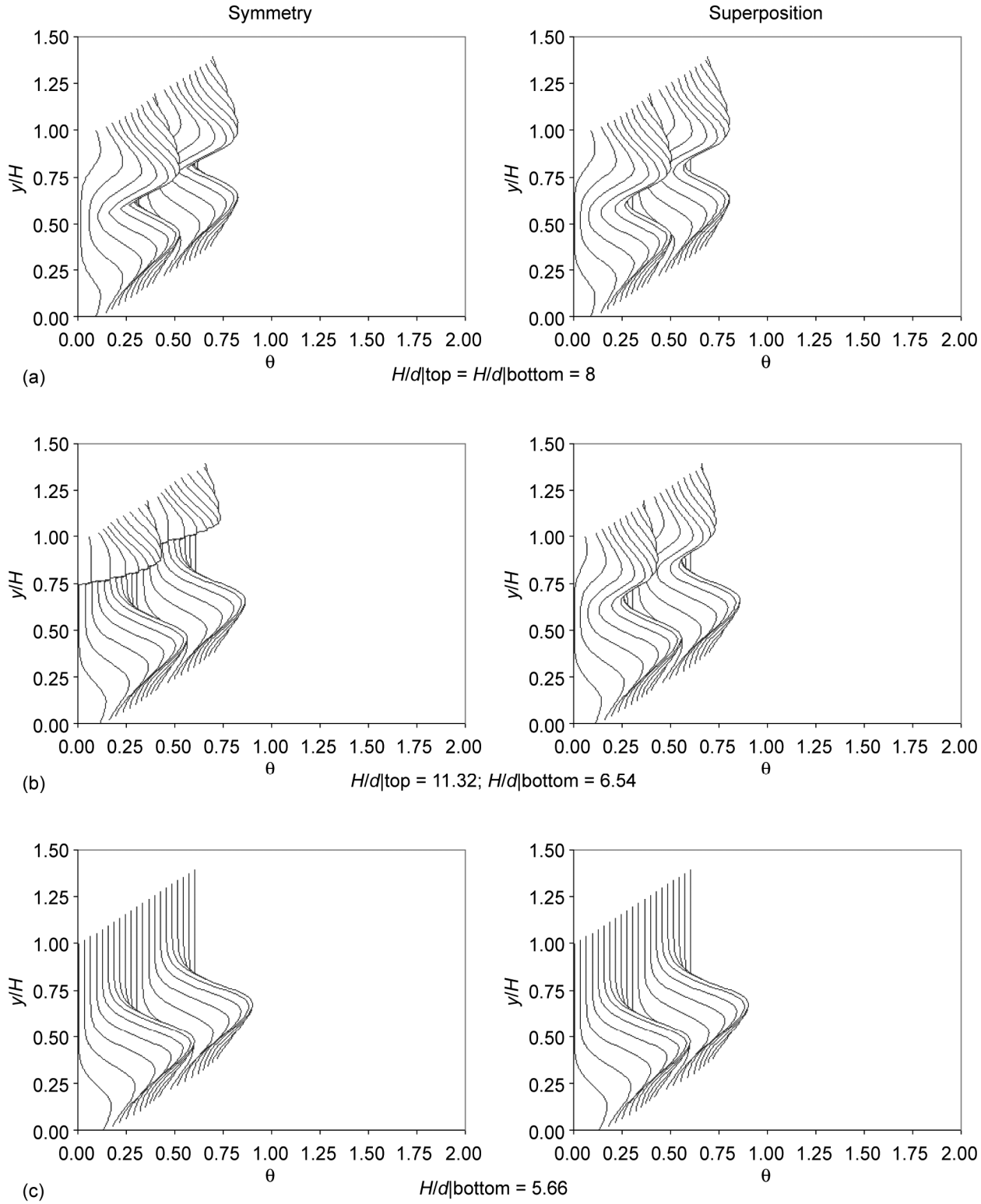


Figure 20(a).—Symmetry and superposition calculations of scalar distributions at $x/H$ = 0.5 orifice configuration D: $S/H$ = 0.5, $H/d$ = 8, ($S/d$ = 4); $DR$ = 2.2, $J$ = 6.6, ($C$ = 1.28), and $C_d$ = 0.64 for opposed jets; and orifice configuration F: $S/H$ = 0.5, $H/d$ = 5.66, ($S/d$ = 2.83); $DR$ = 2.2, $J$ = 6.6, ($C$ = 1.28), and $C_d$ = 0.64 for single side injection.

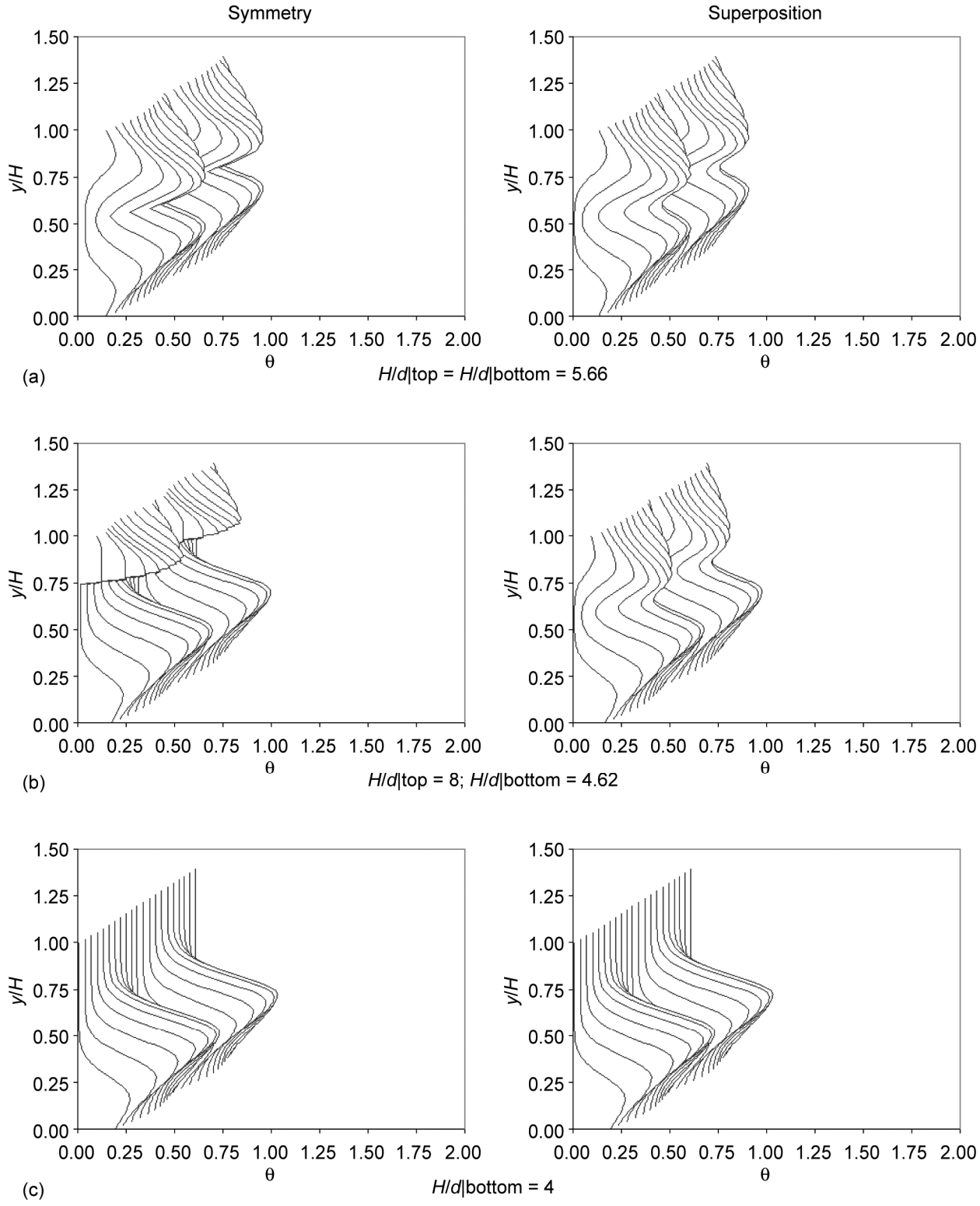


Figure 20(b).—Symmetry and superposition calculations of scalar distributions at $x/H$ = 0.5 orifice configuration F: $S/H$ = 0.5, $H/d$ = 5.66, ($S/d$ = 2.83); $DR$ = 2.2, $J$ = 26.4, ($C$ = 1.28), and $C_d$ = 0.64 for opposed jets; and orifice configuration H: $S/H$ = 0.5, $H/d$ = 4, ($S/d$ = 2); $DR$ = 2.2, $J$ = 6.6, ($C$ = 1.28), and $C_d$ = 0.64 for single side injection.

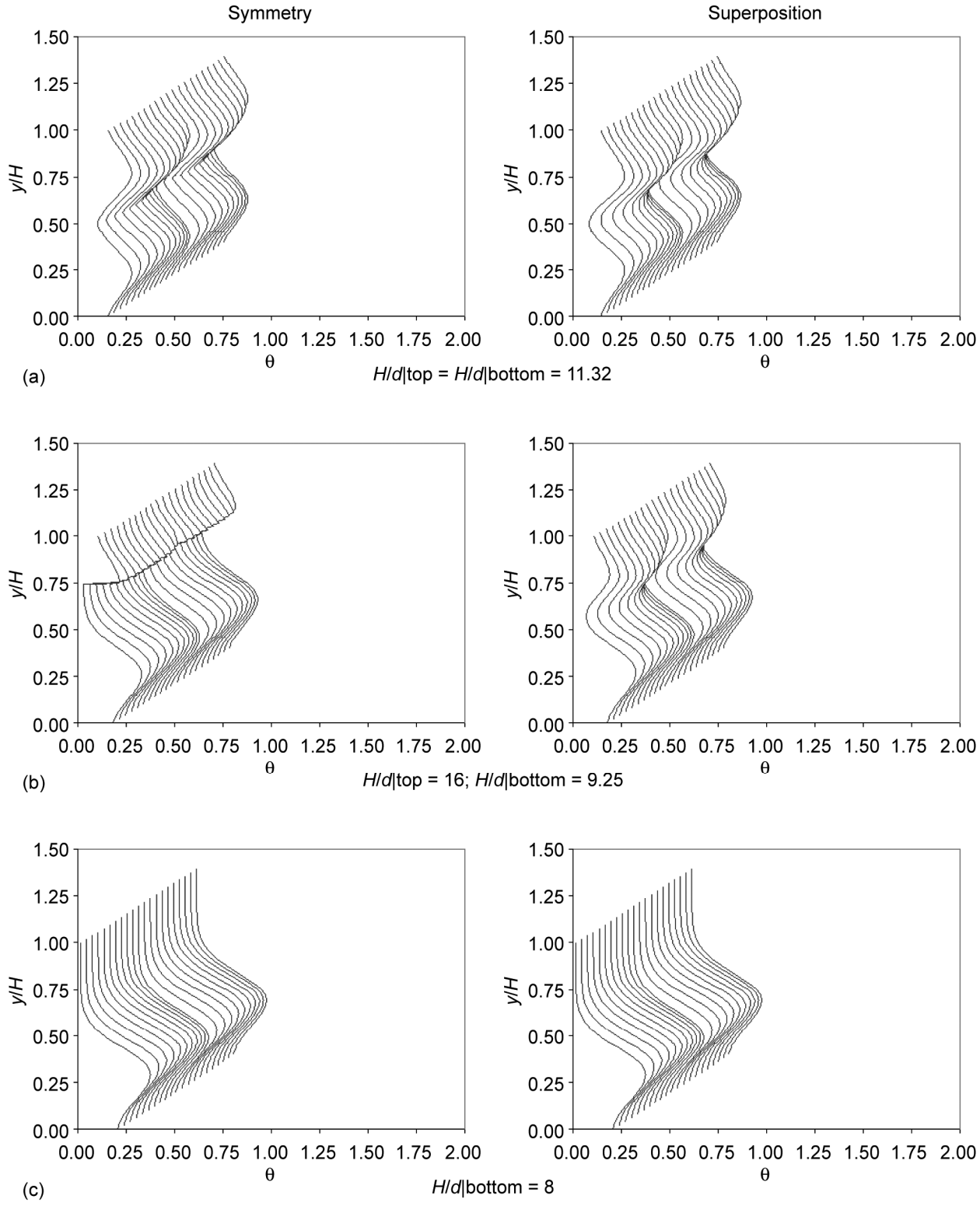


Figure 21.—Symmetry and superposition calculations of scalar distributions at $x/H$ = 0.5 orifice configuration B: $S/H$ = 0.25, $H/d$ = 11.32, ($S/d$ = 2.83); $DR$ = 2.2, $J$ = 26.4, ($C$ = 1.28), and $C_d$ = 0.64 for opposed jets; and orifice configuration C: $S/H$ = 0.25, $H/d$ = 8, ($S/d$ = 2); $DR$ = 2.2, $J$ = 26.4, ($C$ = 1.28), and $C_d$ = 0.64 for single side injection.

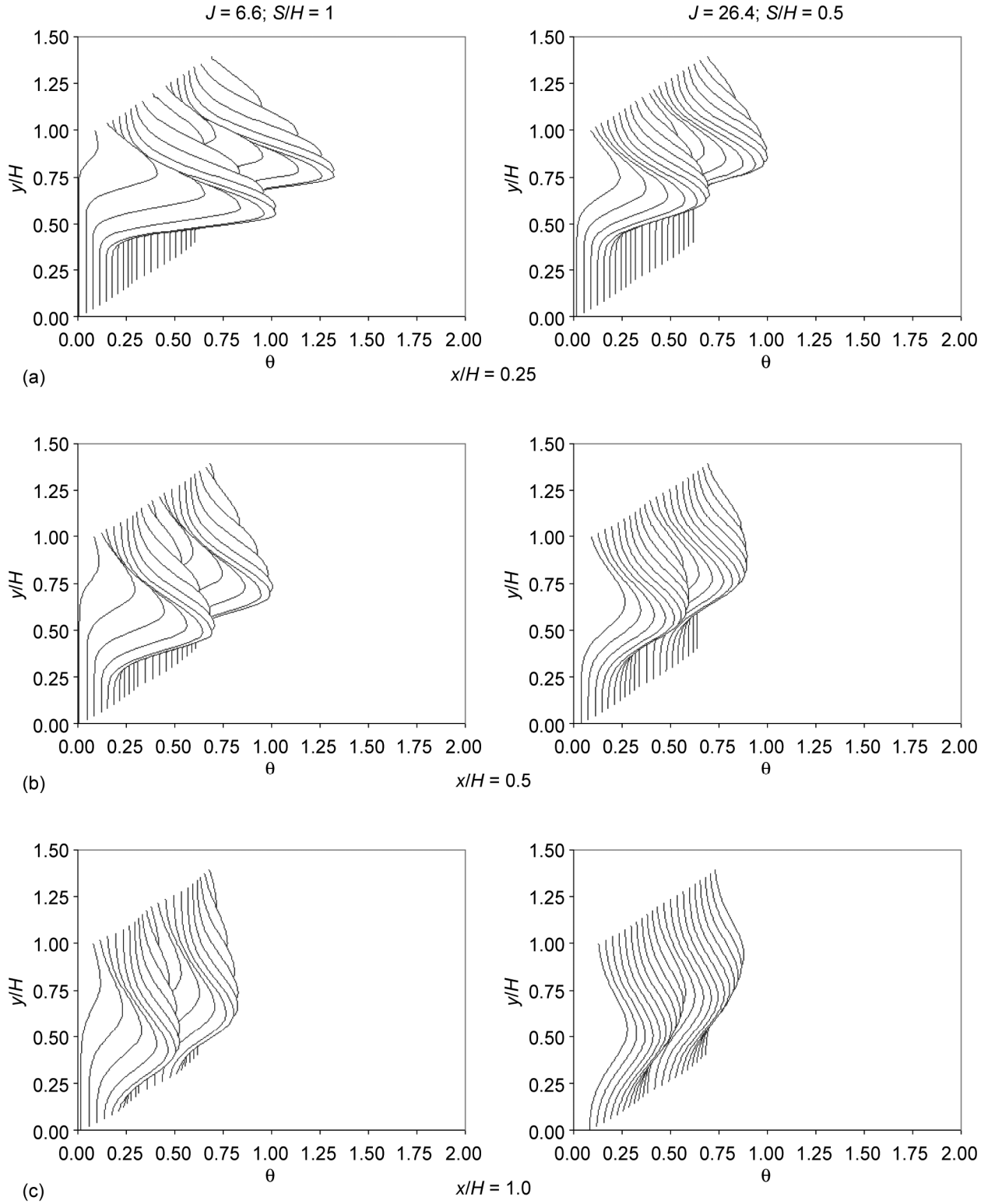


Figure 22.—Calculations of scalar distributions for single side injection: Column 1–orifice configuration I: $S/H$ = 1, $H/d$ = 4, ($S/d$ = 4); $DR$ = 2.2, $J$ = 6.6, ($C$ = 2.57), and $C_d$ = 0.64; Column 2–orifice configuration F: $S/H$ = 0.5, $H/d$ = 5.66, ($S/d$ = 2.83), $DR$ = 2.2, $J$ = 26.4, ($C$ = 2.57), and $C_d$ = 0.64.

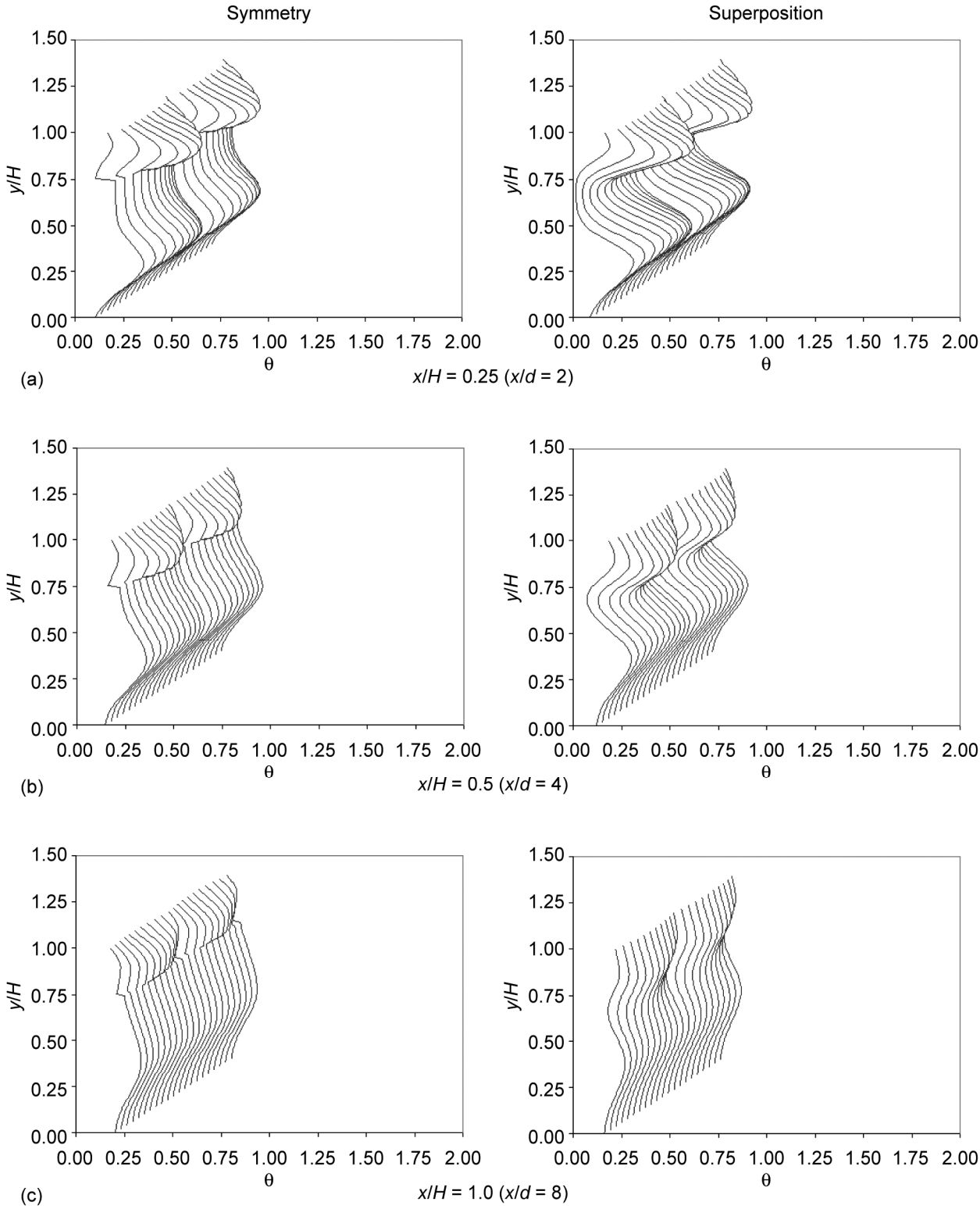


Figure 23(a).—Symmetry and superposition calculation of scalar distributions for opposed rows of jets with centerlines inline for $Jt_{op}$ = 6.6 and $J_{botttom}$ = 59.4: orifice configuration B: $S/H$ = 0.25, $H/d$ = 11.32, ($S/d$ = 2.83), $DR$ = 2.2, and $C_d$ = 0.64.

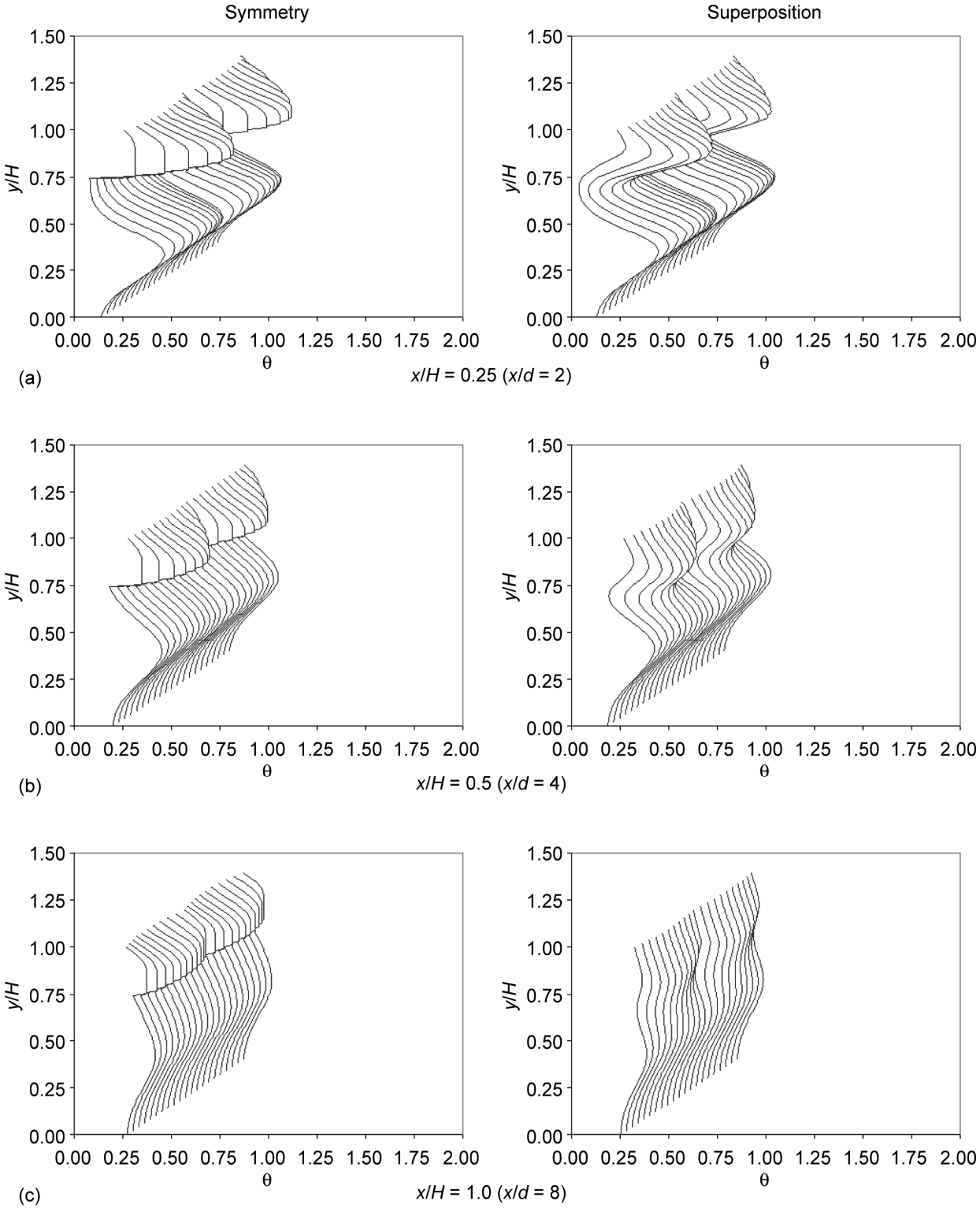


Figure 23(b).—Symmetry and superposition calculation of scalar distributions for opposed rows of jets with centerlines inline for $J_{top}$ = 6.6 and $J_{botttom}$ = 59.4: orifice configuration C: $S/H$ = 0.25, $H/d$ = 8, ($S/d$ = 2), $DR$ = 2.2, and $C_d$ = 0.64. (Note that experimental data for this case in shown in test 34 in reference 17.)

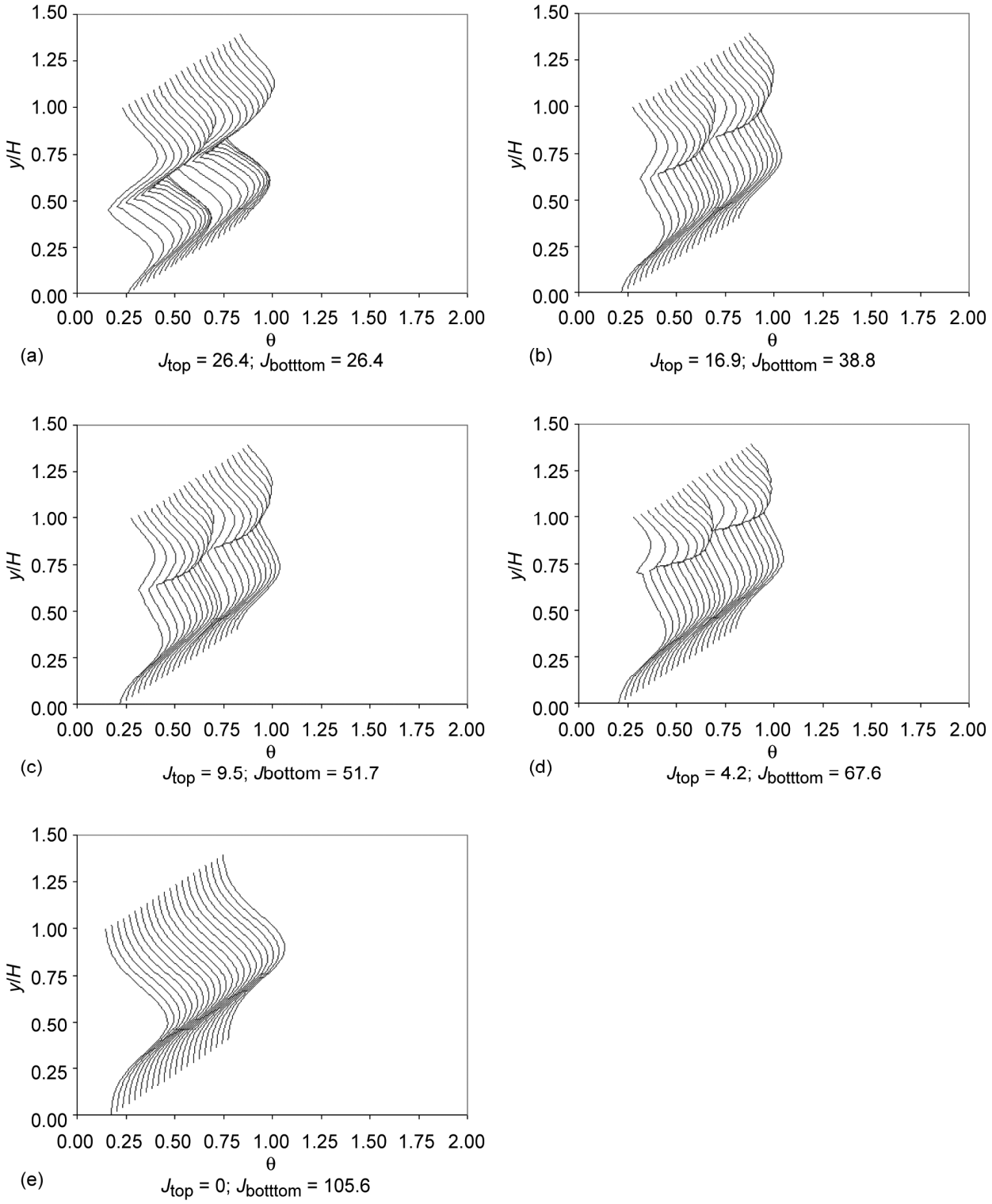


Figure 24(a).—Symmetry calculation of scalar distributions for opposed rows of jets with centerlines inline for different momentum-flux ratios on opposite sides: orifice configuration C: $S/H$ = 0.25, $H/d$ = 8, ($S/d$ = 2), $DR$ = 2.2, and $C_d$ = 0.64. at $x/H$ = 0.5 ($x/d$ = 4).

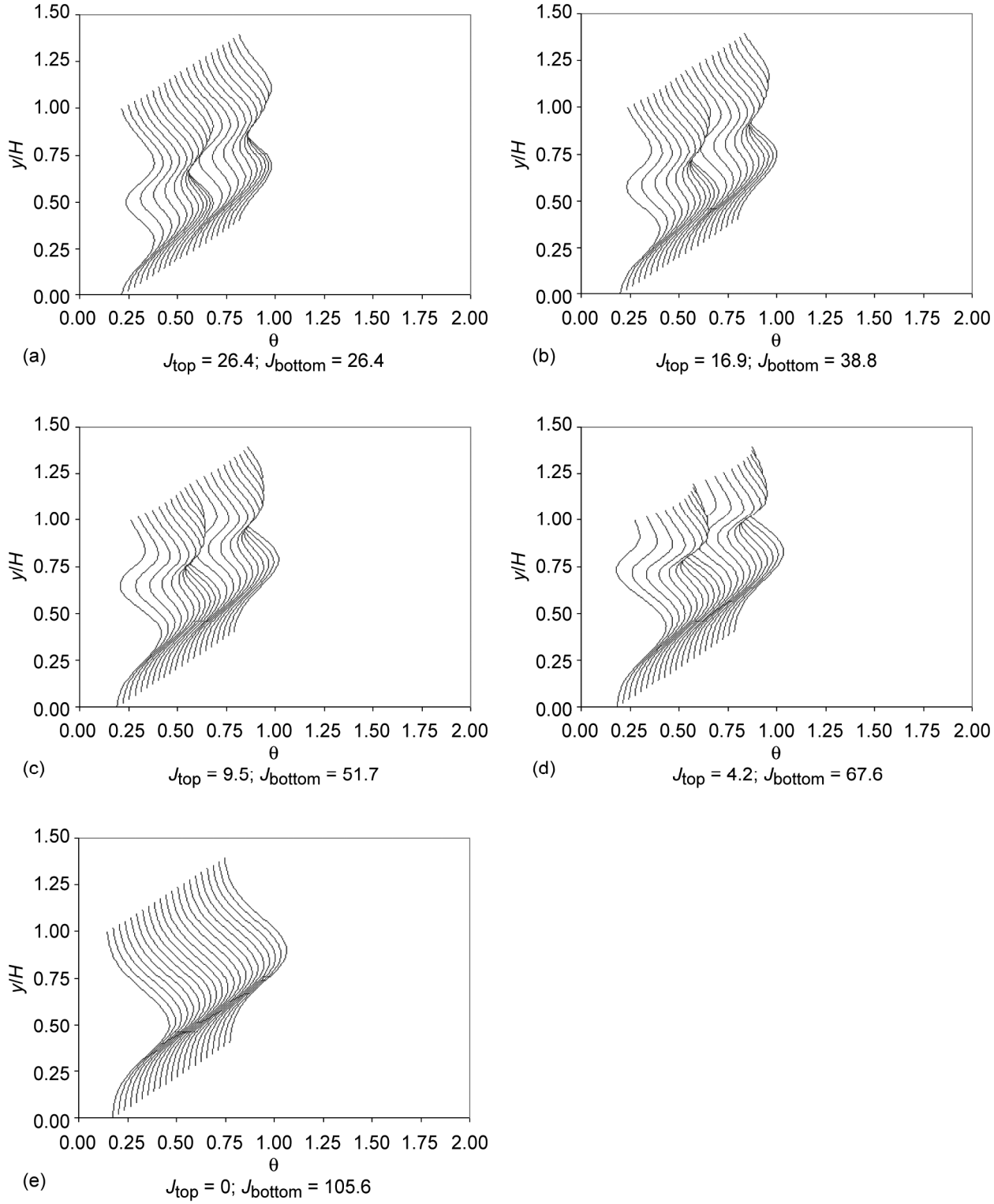


Figure 24(b).—Superposition calculation of scalar distributions for opposed rows of jets with centerlines inline for different momentum-flux ratios on opposite sides: orifice configuration C: $S/H$ = 0.25, $H/d$ = 8, ($S/d$ = 2), $DR$ = 2.2, and $C_d$ = 0.64. at $x/H$ = 0.5 ($x/d$ = 4).

# REPORT DOCUMENTATION PAGE

*Form Approved*
*OMB No. 0704-0188*



| 1. AGENCY USE ONLY (*Leave blank*) | 2. REPORT DATE | 3. REPORT TYPE AND DATES COVERED |
|---|---|---|
| | October 2006 | Technical Memorandum |

**4. TITLE AND SUBTITLE**

On the Mixing of Single and Opposed Rows of Jets With a Confined Crossflow

**5. FUNDING NUMBERS**

WU–22–066–10–12

**6. AUTHOR(S)**

James D. Holdeman, James R. Clisset, Jeffrey P. Moder, and William E. Lear

**7. PERFORMING ORGANIZATION NAME(S) AND ADDRESS(ES)**

National Aeronautics and Space Administration
John H. Glenn Research Center at Lewis Field
Cleveland, Ohio 44135–3191

**8. PERFORMING ORGANIZATION REPORT NUMBER**

E–15473

**9. SPONSORING/MONITORING AGENCY NAME(S) AND ADDRESS(ES)**

National Aeronautics and Space Administration
Washington, DC 20546–0001

**10. SPONSORING/MONITORING AGENCY REPORT NUMBER**

NASA TM—2006-214226

**11. SUPPLEMENTARY NOTES**

J.D. Holdeman and J.P. Moder, NASA Glenn Research Center; J.R. Clisset and W.E. Lear, University of Florida, College of Engineering, Department of Mechanical Engineering, Gainesville, Florida 32611. Responsible person, Jeffrey P. Moder, organization code RTB, 216–433–8254, e-mail: Jeffrey.P.Moder@nasa.gov. A supplemental Microsoft Excel (Microsoft Corporation) spreadsheet (TM-2006-214226-SUPPL.xls) is included on the CD-ROM and can be viewed on the Web at http://gltrs.grc.nasa.gov.

**12a. DISTRIBUTION/AVAILABILITY STATEMENT**

Unclassified - Unlimited
Subject Category: 07

Available electronically at http://gltrs.grc.nasa.gov

This publication is available from the NASA Center for AeroSpace Information, 301–621–0390.

**12b. DISTRIBUTION CODE**

**13. ABSTRACT** ***(Maximum 200 words)***

The primary objectives of this study were 1) to demonstrate that contour plots could be made using the data interface in the NASA GRC jet-in-crossflow (JIC) spreadsheet, and 2) to investigate the suitability of using superposition for the case of opposed rows of jets with their centerlines in-line. The current report is similar to NASA/TM—2005-213137 but the "basic" effects of a confined JIC that are shown in profile plots there are shown as contour plots in this report, and profile plots for opposed rows of aligned jets are presented here using both symmetry and superposition models. Although superposition was found to be suitable for most cases of opposed rows of jets with jet centerlines in-line, the calculation procedure in the JIC spreadsheet was not changed and it still uses the symmetry method for this case, as did all previous publications of the NASA empirical model. The spreadsheet that is included on the CD-ROM and posted with the current report on the Web at http://gltrs.grc.nasa.gov supercedes the spreadsheet previously posted in NASA/TM—2005-213137.

**14. SUBJECT TERMS**

Dilution jets; Jet in crossflow; Gas turbine combustor; Empirical model; Correlations; Multiple jets; RQL; Conserved scalar; Pattern factor; Temperature distribution

**15. NUMBER OF PAGES**

223

**16. PRICE CODE**

| 17. SECURITY CLASSIFICATION OF REPORT | 18. SECURITY CLASSIFICATION OF THIS PAGE | 19. SECURITY CLASSIFICATION OF ABSTRACT | 20. LIMITATION OF ABSTRACT |
|---|---|---|---|
| Unclassified | Unclassified | Unclassified | |